

Dissertation zur Erlangung des Doktorgrades
der Fakultät für Chemie und Pharmazie
der Ludwig-Maximilians-Universität München

Theoretical Investigations in Nucleophilic Organocatalysis

von

Boris Maryasin

aus

Nizhny Novgorod, Russland

2011

Erklärung

Diese Dissertation wurde im Sinne von § 13 Abs. 3 bzw. 4 der Promotionsordnung vom 29. Januar 1998 (in der Fassung der sechsten Änderungssatzung vom 16. August 2010) von Prof. Dr. Hendrik Zipse betreut.

Ehrenwörtliche Versicherung

Diese Dissertation wurde selbständig, ohne unerlaubte Hilfe erarbeitet.

München, 09.05.2011

Boris Maryasin

Dissertation eingereicht am 09.05.2011

- | | |
|---------------|--------------------------------|
| 1. Gutachter: | Prof. Dr. Hendrik Zipse |
| 2. Gutachter: | Prof. Dr. Christian Ochsenfeld |

Mündliche Prüfung am 10.06.2011

Die vorliegende Arbeit wurde in der Zeit von Juli 2007 bis Januar 2011 am Department Chemie und Biochemie der Ludwig-Maximilians-Universität München unter der Anleitung von Herrn Prof. Dr. Hendrik Zipse durchgeführt.

To my family

Acknowledgments

My first “thank you very very much!” goes to Prof. Dr. Hendrik Zipse for the interesting and beautiful time in his research group, for support and for inspiration! Critical way of thinking, ideas, questions, comments, constructive discussions from Professor Zipse do help! I do appreciate everything that I have got from my Teacher and I will never forget. Vielen herzlichen Dank!

I thank Prof. Dr. Christian Ochsenfeld for agreeing to be my “Zweitgutachter”! I would like to thank also Prof. Dr. Konstantin Karaghiosoff, Prof. Dr. Manfred Heuschmann, Prof. Dr. Paul Knochel and Prof. Dr. Andreas Kornath for the interest to the present work and for accepting to be my examiners.

I am very indebted to Prof. Yitzhak Apeloig, for giving me the opportunity to spend several months in his group at the Technion – Israel Institute of Technology (Haifa, Israel) during my master study – this was my first serious meeting with my beloved computational chemistry! And I say “thank you” to my advisors from bachelor and master studies in Nizhny Novgorod State University (Nizhny Novgorod, Russia) – to Prof. Sergey Zelentsov and Prof. Alexey Fedorov. During my PhD study I was happy to visit group of Prof. Shi Min from Shanghai Institute of Organic Chemistry (China, Shanghai), thank you very much, Prof. Shi, for fruitful discussions and kind help!

Thank you, my dear friends and colleagues Johnny Hioe and Elija Wiedemann for careful reading and correcting of the present manuscript! My thanks come to all present as well as former members of our research group, especially to Dr. Yin Wei, Dr. Ingmar Held, Dr. Yinghao Liu, Johnny Hioe, Sven Österling, Evgeny Larionov, Florian Achrainger, Christoph Lindner, Raman Tandon, Dr. Valerio D’Elia, Elija Wiedemann, Regina Bleichner, Jowita Humin, Florian Barth, Michael Miserok, Cong Zhang and to all my friends in Germany!

I thank Ludwig-Maximilians-Universität München for financial support and Leibniz-Rechenzentrum München for providing computational facilities.

And the huge “Thank You” I give to my family. My parents and sister are indeed “holding” me like atlantes, even via Skype from Russia. I do not really want to generate words now – it will be always too small and weak as compared to what I feel, thinking about you. My destiny was so kind to bring me “additional” present – another “atlant” – or, strictly speaking, – “caryatid” – Veronika, my love! Dear papa and mama, Irka&Mashka and my Nika, this work is dedicated to you! Thank you very much for your love!

List of Abbreviations and Symbols

°C	Degree Celsius
‡	transition state
Å	Ångström
a.u.	atomic units
Ac	acetyl
Ar	aryl
aug-cc-pVXZ	Dunning's correlation consistent basis set (X = D (double), X = T (triple), X = Q (quadruple)) augmented (aug) with diffuse functions
aza-MBH	aza-Morita-Baylis-Hillman reaction
B2K-PLYP	double-hybrid density functional for thermochemical kinetics developed by Martin
B2-PLYP	double-hybrid density functional by Grimme
B3LYP	the hybrid density functional including Becke's three-parameter exchange functional and Lee-Yang-Parr's correlation functional
B97-D	Grimme's density functional including dispersion
B98	Becke's 1998 revisions to Becke's 1997 hybrid density functional (B97)
BP	Becke-Perdew density functional
BP86	combination of the local Slater-Dirac exchange functional, the correlation functional by Vosko, Wilk, and Nusair (VWN (V)), Becke's gradient corrected exchange functional B88, and the gradient corrected correlation functional by Perdew (P86)
BPC	bifunctional phosphane catalyst
BSSE	basis set superposition error
cal	calorie
calc.	calculated
CBS	complete basis set
CCSD(T)	coupled-cluster with single and double and perturbative triple excitations
conv.	convergence
d	day
DABCO	1,4-diazabicyclo[2.2.2]octan
def2-QZVPP	second-generation default (def2) valence quadruple zeta (QZV) heavily polarized (PP) basis set by Ahlrichs
DFT	density functional theory
DMAP	4-dimethylaminopyridine
DMSO	dimethyl sulfoxide
E_{FLP}	frustration energy
EPR	electron paramagnetic resonance
eqn.	equation
Et	ethyl
E_{tot}	total energy
EWG	electron withdrawing group
exp.	experimental
FLP	frustrated Lewis pair
G2	gaussian-2 theory
G2(MP2)	cheaper variation of G2
G3	gaussian-3 theory
G3(MP2)MPW1K(+)	adaptation of G3(MP2) theory (cheaper variant of G3) based on geometries and zero point vibrational energies calculated at the

G3B3	MPW1K/6-31+G(d) level of theory G3 with geometries and zero-point vibrational energies calculated at B3LYP/6-31G(d) level of theory
G3large	an extension of 6-311G(d,p) basis set with more flexible polarization functions (2df) and polarization of the core electrons (3d2f on Na-Ar). This basis set is used as the ‘limiting HF’ basis set in the G3 method.
G3MP2large	G3large basis set excluding core polarization functions.
G3MPW1K(+)	G3B3 using MPW1K/6-31+G(d) instead of B3LYP/6-31G(d)
GIAO	gauge including (invariant) atomic orbitals
<i>h</i>	Planck constant (6.62×10^{-34} J s)
h	Hour
HOMO	highest occupied molecular orbital
IGLO	individual gauge for localized orbitals
Int	intermediate
J	Joule
K	Kelvin
<i>k</i>	rate constant
k	kilo
<i>k_B</i>	Boltzmann constant (1.38×10^{-23} J K ⁻¹)
LA	Lewis acid
LB	Lewis base
LP	Lewis pair
LUMO	lowest unoccupied molecular orbital
M05-2X	the hybrid functional of Truhlar and Zhao
MA	Michael acceptor
MAD	mean absolute deviation
MBH	Morita-Baylis-Hillman reaction
MCA	methyl cation affinity
Me	methyl
min.	minute
MM3	molecular mechanics developed by Allinger
MO	molecular orbital
mol	mole
MP2(FC)	second-order Møller–Plesset perturbation theory with frozen core approximation
MP2(FULL)	second-order Møller–Plesset perturbation theory; inner-core electrons are included
MP2-5	MP2(FC)/6-31+G(2d,p)//B98/6-31G(d)
MPW1K	modified Perdew-Wang one parameter hybrid density functional for kinetics
MVK	methyl vinyl ketone
MVKA	methyl vinyl ketone affinity
MVKA-c	methyl vinyl ketone affinity (cyclic complex)
NBO	natural bond orbital
NMR	nuclear magnetic resonance
NPA	natural population analysis
Nu	nucleophile
OPLS-AA	optimized potentials for liquid simulations in the all-atom version – force field developed by Jorgensen
PCM	polarizable continuum model
PDLB2	pyridine-derived Lewis base catalyst

Ph	phenyl
pK_a	negative lg of acid dissociation constant (K_a)
PNP	<i>p</i> -nitrophenol
ppm	parts per million
R	common organic substituent or (R)-configured enantiomer
R	universal gas constant ($8.314510 \text{ J mol}^{-1} \text{ K}^{-1}$)
RDS	rate-determining state
RHF	restricted Hartree-Fock
RT	room temperature
S	(S)-configured enantiomer
S	Entropy
SCF	self-consistent field
SCS-MP2	spin-component scaled second-order Møller–Plesset perturbation theory
T	Temperature
t_{1/2}	half-life time
THF	Tetrahydrofuran
TS	transition state
TZVP	the Ahlrichs' type triple- ζ basis sets with one set of polarization functions
TZVPP	the Ahlrichs' type triple- ζ basis sets with two sets of polarization functions
UAHF	united Atom for Hartree-Fock
UAKS	united atom Kohn-Sham
vs.	<i>Versus</i>
XKA	“X” ketone affinity
X-YZ+G(ndf,mpd)	valence-double- ζ basis set by Pople and coworkers supplemented by polarization (df,pd) and diffuse (+ or ++) functions, <i>e.g.</i> 6-31+G(2d,p)
X-YZW+G(ndf,mpd)	valence-triple- ζ basis set by Pople and coworkers supplemented by polarization (df,pd) and diffuse (+ or ++) functions, <i>e.g.</i> 6-311++G(2d,2p)
ZPE	zero-point energy
δ	chemical shift
ΔG_{298}	Gibbs free energy at 298K
ΔH_{298}	enthalpy at 298K
σ	shielding

Parts of this Ph.D. Thesis have been published

1. Theoretical Studies of ^{31}P NMR Spectral Properties of Phosphanes and Related Compounds in Solution
B. Maryasin and H. Zipse, *Phys. Chem. Chem. Phys.*, **2011**, 13, 5150-5158
2. Methyl cation affinity (MCA) values for phosphanes
C. Lindner, B. Maryasin, F. Richter and H. Zipse, *J. Phys. Org. Chem.*, **2010**, 23, 1036-1042
3. The Performance of Computational Techniques in Locating the Charge Separated Intermediates in Organocatalytic Transformations
Y. Wei, B. Sateesh, B. Maryasin, G. N. Sastry, H. Zipse, *J. Comput. Chem.*, **2009**, Vol. 30, No. 16, 2617-2624

Table of Contents

1. General Introduction	1
1.1. Morita-Baylis-Hillman Reaction	1
1.2. Frustratedness of Lewis Acid – Lewis Base Pairs	3
1.3. Acylation Reactions Catalyzed by DMAP Derivatives	3
1.4. References	5
2. Theoretical Studies of ³¹P NMR Spectral Properties of Phosphanes and Related Compounds Relevant in Organocatalytic Processes	
2.1. Development of a New Approach for ³¹ P NMR Shift Predictions	6
2.1.1. Introduction	6
2.1.2. Results and Discussion	7
2.1.3. Conclusions	23
2.2. Application of the Proposed Approach to the MBH Reaction	24
2.2.1. Introduction	24
2.2.2. Results and discussions	26
2.2.3. Conclusions	38
2.3. References	39
3. The Catalytic Cycle of the Morita-Baylis-Hillman Reaction	43
3.1. Introduction	43
3.2. Choice of the Methods	45
3.3. Results and Discussion	46
3.3.1. Michael Addition of MVK to PPh ₃	50
3.3.2. Addition of the Aldehyde: C-C Bond Formation	52
3.3.3. The Proton Transfer	54
3.3.4. The Product Elimination Step	56
3.3.5. The Diastereomeric Pathways	57
3.3.6. Calculated Results and Literature Kinetic Data in Comparison	57
3.4. References	60
4. Protonation/Deprotonation Equilibria in the Morita-Baylis-Hillman Reaction	61
4.1. Introduction	61
4.2. The Acidity of Enolate Intermediates	62
4.3. Benchmarking Calculations and Extension to Different Nucleophiles and Substrates	65
4.4. Conclusions	70
4.5. References	71
5. Description of Organocatalytic Reactivity	72
5.1. Introduction	72
5.2. MCA. Choice of the Systems and Methods	73
5.2.1. Systems	73
5.2.2. Methods	73
5.2.3. Development of MM3 Force Field Parameters for Phosphonium Derivatives and a Scheme for Accurate Conformational Search	73
5.3. MCA Values for Phosphanes	80
5.3.1. Phosphanes With Unbranched and Branched Acyclic Substituents and Cyclic Substituents	80

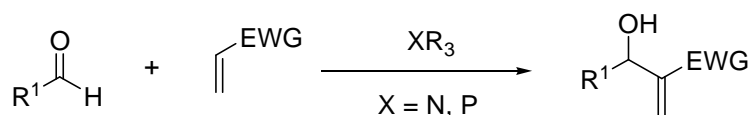
5.3.2. Cyclophane-substituted and Cyclic Phosphanes	85
5.4. MVKA and XKA	90
5.4.1. MVKA of Recently Synthesized Bifunctional Phosphane Catalysts	91
5.4.2. Correlation of MVKA and Experimentally Measured Kinetic Data for BPC Catalysts	96
5.4.3. XKA of Triphenylphosphane and Pyridine-derived Lewis Base Catalysts using Three Different Michael Acceptors. Experiment and theory in Comparison	97
5.5. Conclusions	103
5.6. References	104
6. The Frustratedness of Lewis acid – Lewis Base Pairs	105
6.1. Introduction	105
6.2. Results and Discussion	107
6.2.1. Geometry Optimization	107
6.2.2. Energies	115
6.3. Conclusions	122
6.4. References	123
7. Theoretical Studies of the Acylation Reaction Catalyzed by DMAP with Participation of Aryl Derivatives	124
7.1. Introduction	122
7.2. The Background Reaction	125
7.3. Nucleophilic Catalysis vs. Base Catalysis	127
7.4. The Influence of Donor and Acceptor Substituents in the Aromatic Ring of the Alcohol	129
7.5. Conclusions	133
7.6. References	134
8. General Conclusions	135
9. Appendix	140
9.1. General Details	140
9.2. Calculated Data for Chapter 2: Shielding Values, Total Energies, Free Energies	140
9.3. Calculated Data for Chapter 3	156
9.4. Calculated Data for Chapter 4	158
9.5. Calculated Data for Chapter 5	163
9.5.1. Energies of Scan Calculations Performed During Development of MM3 Force Field Parameters for Phosponium Derivatives	163
9.5.2. Phosphanes With Unbranched and Branched Acyclic Substituents and Cyclic Substituents	177
9.5.3. Cyclophane-Substituted Phosphanes	185
9.5.4. Cyclic Phosphanes	188
9.5.5. MVKA of Recently Synthesized Bifunctional Phosphane Catalysts	190
9.5.6. XKA of Triphenylphosphane and Pyridine-derived Lewis Base Catalyst Using Three Different Michael Acceptors. Experiment and Theory in Comparison	192
9.6. Calculated Data for Chapter 6	194
9.7. Calculated Data for Chapter 7	198

1. General Introduction

Organocatalysis has a long history, but at the same time it is a currently rapidly growing field. The first example of organocatalysis in the variant of benzoin condensation under cyanide catalysis was shown by Justus von Liebig und Friedrich Wöhler in 1832,^[1] but the term “organocatalysis” was introduced by MacMillan only in 2000 for highly enantioselective organocatalytic Diels-Alder reactions,^[2] and nowadays the development of organocatalysis proceeds briskly.^[3] Obviously the pace will increase in the future, since the main goal of organocatalysis is synchronized with “green chemistry” – to develop environmentally friendly methods obviating the use of toxic metal-based catalysts. Since organocatalysis has become popular in modern organic chemistry, immediately a lot of mechanistically related questions arise, *e.g.*: What is the mechanism of a particular transformation? How to investigate the mechanism? What kind of molecule can serve as the most efficient and selective catalyst for a given reaction? In spite of a large amount of studies such questions stay topical due to the complexity and ambiguity of organocatalytic transformations. The main goal of the present work is to make a step in the direction of organocatalysis mechanisms understanding. As the major topic to study the Morita-Baylis-Hillman (MBH) reaction catalyzed by phosphorus- and nitrogen-containing organocatalysts has been chosen. Two additional topics: the frustratedness of Lewis acid – Lewis base pairs and acylation reactions catalyzed by 4-dimethylaminopyridine (DMAP) are considered. These three subareas will be now briefly reviewed and the motives and scopes of this thesis will be introduced.

1.1. Morita-Baylis-Hillman Reaction

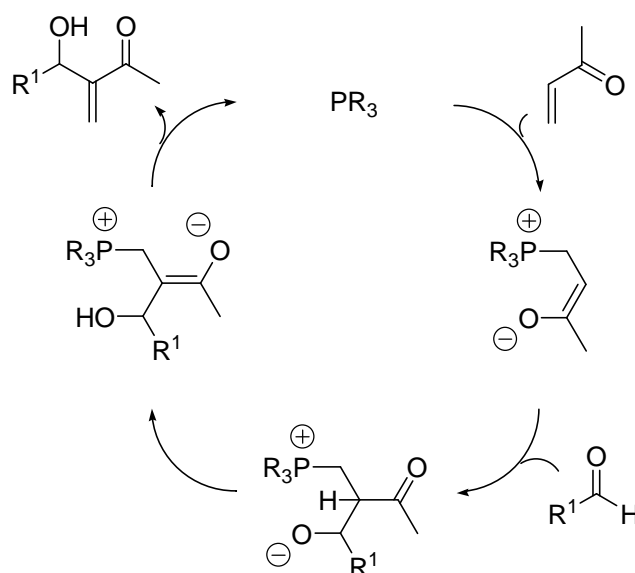
The Morita-Baylis-Hillman (MBH) reaction is a reaction of aldehydes with electron-deficient alkenes catalyzed by Lewis bases (phosphines or amines).^[4]



Scheme 1.1 MBH reaction.

The MBH reaction has a series of advantages (*e.g.* atom economy), but also the big problem of a notoriously low reaction rate. Any attempt to improve the MBH reaction efficiency leads to the necessity of a better understanding of the reaction mechanism. In spite

of numerous studies in the field of MBH reaction mechanisms, there is still no agreement between different hypotheses. Currently it is accepted that the reaction involves a sequence of Michael addition, aldol reaction and β -elimination steps. The respective catalytic cycle is shown in Scheme. 1.2

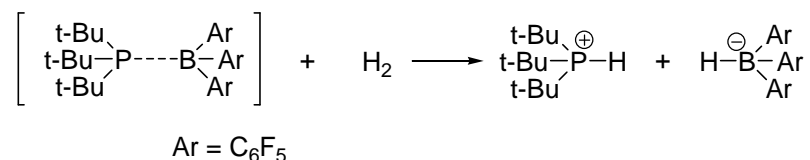


Scheme 1.2 Proposed mechanism of the MBH reaction.

Topical questions are related to the zwitterionic intermediates, since their experimental detection is complicated,^[5] also to transition states and the nature of the rate-limiting steps.^[6] In the present study attempts to reinvestigate the mechanism for a “real-life” system will be shown – the major aim was to reject small model systems, which are often used in computational studies, but they are practically far away from experiment. First of all a way of interplay between experimental and theoretical mechanistically related studies is suggested: development and testing of a reliable approach for ³¹P NMR chemical shift calculations in solution will be shown in chapter 2. This point can be helpful for assigning ³¹P NMR chemical shifts obtained in phosphane-catalyzed MBH reactions. Chapter 3 is devoted to a detailed investigation of the MBH catalytic cycle and possible side reactions. The latter are often ignored in mechanistical studies. It will be shown how important can be the consideration of side reactions, in particular the protonation of zwitterionic intermediates – this will be addressed in chapter 3 and then in detail studied in chapter 4. Finally in chapter 5 a *Methyl Cation Affinity* approach (MCA) as a descriptor of catalytic activity will be tested and a new descriptor of catalytic activity – “X ketone affinity” (XKA) that can easily and quickly bring important preliminary information on the efficiency and selectivity of any MBH catalyst will be suggested.

1.2. Frustratedness of Lewis Acid – Lewis Base Pairs

A peculiar type of organocatalysts are so called *Frustrated Lewis Pairs* (FLP). FLP is a compound or mixture containing a Lewis acid and a Lewis base that, because of steric hindrance, cannot combine to form an adduct.^[7] Due to their “unslaked” reactivity, these systems are very active and can split dihydrogen heterolytically (Scheme 1.3), thus they promise to be efficient for hydrogenation processes.

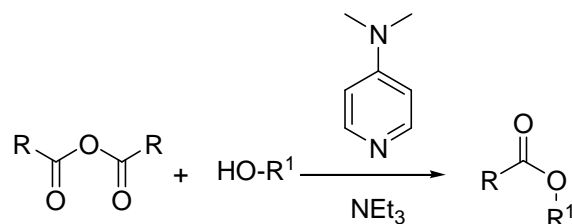


Scheme 1.3 Activation of dihydrogen H₂ through reaction with a frustrated Lewis pair.

FLP chemistry is currently a “hot” topic in organic chemistry and obviously it needs theoretical support as a guide line. The mechanism of the FLP formation and the subsequent splitting reaction, the structural properties of FLP, the interplay between the structure and reactivity – all these aspects and many others are not well understood today. The term “Frustratedness” of FLP by itself is not clearly defined and it is arguable. Moreover the literature data for even small (“unfrustrated”) LA-LB pairs are scarce. In chapter 6 a development of a computational approach which can accurately describe the LA-LB pairs geometrical and energetic characteristics will be presented.

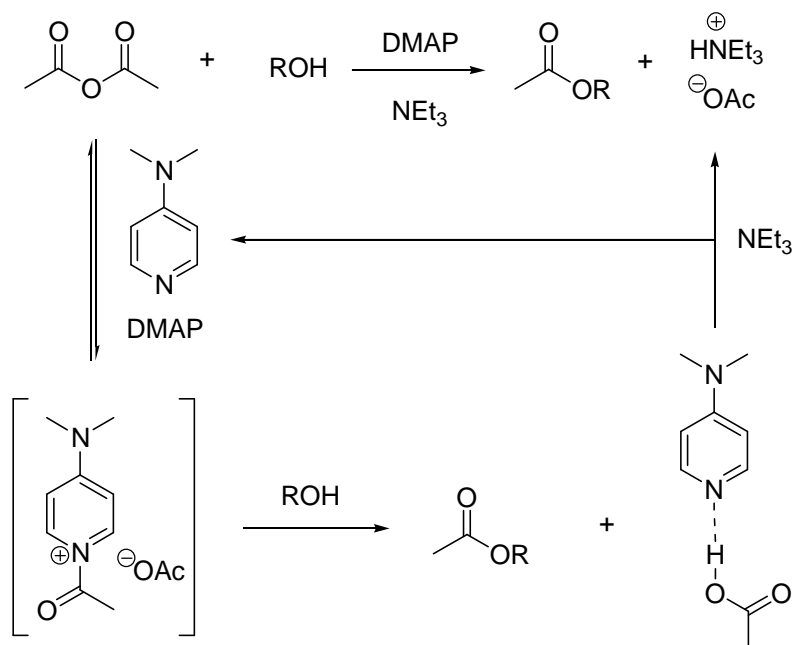
1.3. Acylation Reactions Catalyzed by DMAP Derivatives

The acylation of alcohols and amines is a common transformation and it can be promoted by a variety of catalysts.^[8] Special attention has to be drawn to DMAP and its derivatives, which have been extensively applied as esterification catalysts since the pioneering reports made by Steglich and Höfle^[9] and by Litvinenko and Kirichenko^[10] almost simultaneously in the 1960s. Today the field is still developing in the direction of new, more active and also enantioselective catalysts.^[11]



Scheme 1.4 DMAP-catalyzed esterification.

The development of new catalysts obviously needs understanding of mechanism and therefore recently high quality mechanistic studies have been performed.^[8, 12] The accepted mechanism involves the acylpyridinium intermediate (Scheme 1.5, on example of acetylation by acetic anhydride)



Scheme 1.5 Proposed mechanism for DMAP-catalyzed acylation reaction.

It has been shown, that this mechanism can be in competition with a concerted base catalysis pathway, avoiding formation of acylpyridinium intermediates. For many cases the latter pathway is less favorable, however, the difference between these mechanisms depends on the system. DFT calculations that continue a series of studies in esterification mechanisms of the Zipse group are presented in chapter 7. Some subjects that have not been discussed before are considered now – the acylation reagent contains a benzoic acid moiety and the aromatic ring of the alcohol is substituted by donor or acceptor substituents in order to explore their effects. Different catalyzed pathways are compared with background reaction calculated on the same level of theory.

1.4. References

- [1] F. Wöhler, J. Liebig, *Ann. Pharm.* **1832**, 3, 249.
- [2] K. A. Ahrendt, C. J. Borths, D. W. C. MacMillan, *J. Am. Chem. Soc.* **2000**, 122, 4243-4244.
- [3] A. Berkessel, H. Groeger, *Asymmetric Organocatalysis: from Biomimetic Concepts to Applications in Asymmetric Synthesis*, Wiley-VCH, **2005**.
- [4] a) A. B. Baylis, M. E. D. Hillman, *Vol. 2155113*, Germany, **1972**; b) K. Morita, Z. Suzuki, H. Hirose, *Bull. Chem. Soc. Jpn.* **1968**, 41, 2815-2820.
- [5] a) M. E. Kraft, T. F. N. Haxell, K. A. Seibert, K. A. Abboud, *J. Am. Chem. Soc.* **2006**, 128, 4174-4175; b) M. Shi, L. H. Chen, C.-Q. Li, *J. Am. Chem. Soc.* **2005**, 127, 3790-3800; c) L. S. Santos, C. H. Pavam, W. P. Almeida, F. Coelho, M. N. Eberlin, *Angew. Chem. Int. Ed.* **2004**, 43, 4330-4333.
- [6] a) R. Robiette, V. K. Aggarwal, H. J. N., *J. Am. Chem. Soc.* **2007**, 129, 15513-15525; b) D. Roy, R. B. Sunoj, *Org. Lett.* **2007**, 9, 4873-4876; c) J. Xu, *Journal of Molecular Structure: THEOCHEM* **2006**, 767, 61-66; d) D. Cantillo, C. O. Kappe, *J. Org. Chem* **2010**, 75, 8615-8626.
- [7] D. W. Stephan, *Org. Biomol. Chem.* **2008**, 6, 1535-1539.
- [8] Y. Wei, PhD thesis, Ludwig-Maximilians-Universität München (München), **2008**.
- [9] a) G. Höfle, W. Steglich, *Synthesis* **1972**, 619-621; b) W. Steglich, G. Höfle, *Angew. Chem. Int. Ed.* **1969**, 8, 981.
- [10] L. M. Litvinenko, A. I. Kirichenko, *Dokl. Akad. Nauk. SSSR* **1967**, 167, 97.
- [11] a) A. C. Spivey, S. Arseniyadis, *Angew. Chem. Int. Ed.* **2004**, 43, 5436-5441; b) G. Höfle, W. Steglich, H. Vorbrüggen, *Angew. Chem. Int. Ed.* **1978**, 90, 569-583; c) G. C. Fu, *Acc. Chem. Res.* **2004**, 37, 542-547.
- [12] a) C. B. Fischer, S. Xu, H. Zipse, *Chem. - Eur. J.* **2006**, 12, 5779-5784; b) S. Xu, I. Held, B. Kempf, H. Mayr, W. Steglich, H. Zipse, *Chem. Eur. J.* **2005**, 11, 4751-4757.

2. Theoretical Studies of ^{31}P NMR Spectral Properties of Phosphanes and Related Compounds Relevant in Organocatalytic Processes

2.1. Development of a New Approach for ^{31}P NMR Shift Predictions

2.1.1. Introduction

Phosphanes are of outstanding relevance as ligands in transition metal mediated catalytic processes, but also as reagents in a series of named reactions such as the Wittig, the Appel, and the Staudinger reaction. The Lewis base properties relevant in these reactions have recently led to the highly successful development of phosphanes as catalysts in organocatalytic processes. This includes applications in C–C bond forming reactions such as the Morita–Baylis–Hillman^[1] and the Rauhut–Currier reaction,^[2] in the addition of weak nucleophiles to Michael acceptors,^[3] in the acylation of weak nucleophiles with carboxylic acid derivatives,^[4] just to name a few. The Lewis basicity of catalytically active phosphanes can be characterized by their respective affinities towards cationic or neutral carbon electrophiles such as methyl cation or methyl vinyl ketone (MVK).^[5] These thermodynamic properties can be complemented with kinetic data towards model electrophiles^[6] in a way to allow for quantitative predictions of new phosphane-based organocatalysts. Experimental studies of organocatalytic reactions highly profit from ^{31}P NMR measurements as these allow for a direct detection of catalyst-derived species under catalytic conditions. The phosphonium intermediates expected after nucleophilic attack of phosphanes on C-electrophiles have, for example, been detected in a number of studies.^[3b, 7] The assignment of experimentally observed signals can greatly be supported by comparison to theoretically calculated ^{31}P chemical shifts. Highly accurate shift calculations have been executed at correlated levels for a series of smaller systems.^[8] For intermediates in organocatalytic processes, however, these methods are usually not applicable and calculations at either the Hartree–Fock (HF) or the density functional theory (DFT) level appear as the only practical option. Despite the fact that the application of DFT methods in NMR shift calculations meets with some fundamental concerns, there have nevertheless been numerous successful studies in this area in recent years.^[9] One additional technical point concerns the treatment of solvation effects, which are known to be quite significant for some phosphane-derived species such as triarylphosphane oxides.^[10] In order to identify computational schemes suitable for the reliable calculation of ^{31}P shifts for phosphorous-containing molecular systems we compare here the performance of

a series of DFT methods such as MPW1K, B98 and B3LYP with the *ab initio* methods HF and MP2 using the GIAO scheme. These studies will be combined with various approaches to account for solvent effects.

2.1.2. Results and Discussion

Triphenylphosphane (PPh₃, **1**) is a frequently used organocatalyst and will therefore be used as a first model system for ³¹P shift calculations on large systems. Under catalytic reaction conditions this catalyst is often degraded to the respective oxide (OPPh₃, **2**), either through reaction with residual atmospheric oxygen or through side reactions along a Wittig-type pathway. The ³¹P NMR chemical shift measured for **1** (relative to the ³¹P NMR standard of 85% aqueous phosphoric acid) is quite insensitive to solvent polarity with $\delta(^{31}\text{P}, \mathbf{1}) = -4.7$ ppm in benzene-d₆^[11] and $\delta(^{31}\text{P}, \mathbf{1}) = -4.7$ ppm in chloroform-d₁.^[12] As the use of aqueous phosphoric acid as the reference compound in NMR shift calculations is clearly impractical, we will in the following use the experimentally determined value of **1** as the reference for gas phase calculations. ³¹P NMR shifts determined for phosphaneoxide **2** are significantly more solvent dependent with measured values of $\delta(^{31}\text{P}, \mathbf{2}) = +24.7$ ppm in benzene-d₆^[13] and $\delta(^{31}\text{P}, \mathbf{2}) = +29.7$ ppm in chloroform-d₁.^[12] Assuming the values determined in benzene to be representative also for the gas phase, NMR calculations must reproduce a shift difference of $\Delta\delta(\mathbf{2} - \mathbf{1}) = +29.4$ ppm. In more general terms the direct result of NMR shift calculations is the absolute magnetic shielding σ , which reflects the NMR chemical shift relative to the free nucleus. Relative ³¹P chemical shifts of phosphorous-containing compounds **X** compared to phosphane **1** as the reference can then be derived from differences in shieldings as expressed in eqn (2.1).

$$\delta(\mathbf{X}) = \sigma(\mathbf{1}) - \sigma(\mathbf{X}) + \delta(\mathbf{1}) \quad (2.1)$$

As a first step in identifying a computational protocol for reliable shift calculations we have calculated ³¹P absolute shieldings for compounds **1** and **2** using selected density functional theory (DFT) methods, the restricted Hartree–Fock theory (RHF), and the 2nd order Møller–Plesset (MP2) perturbation theory in combination with the GIAO model. All of these calculations employ the same 6-311+G(d,p) basis set and use the same geometries obtained at the MPW1K/6-31G(d) level of theory. The MPW1K functional^[14] is used here due to its good performance in calculations of zwitterionic structures, whose occurrence in organocatalytic reactions is quite frequent.^[5c, 15] At this level of theory two different minima are identified for

phosphane oxide **2** (C_3 vs. C_1 symmetry; the latter structure is also found in solid-state X-ray studies).^[16] Only a single minimum with C_3 symmetry can be found for phosphane **1**. This is in agreement with results from solid state X-ray studies, gas phase electron diffraction measurements and earlier *ab initio* calculations.^[17] Fig. 2.1 shows the structures obtained at the MPW1K/6-31G(d) level and Fig. 2.2 collects all results obtained for these systems.

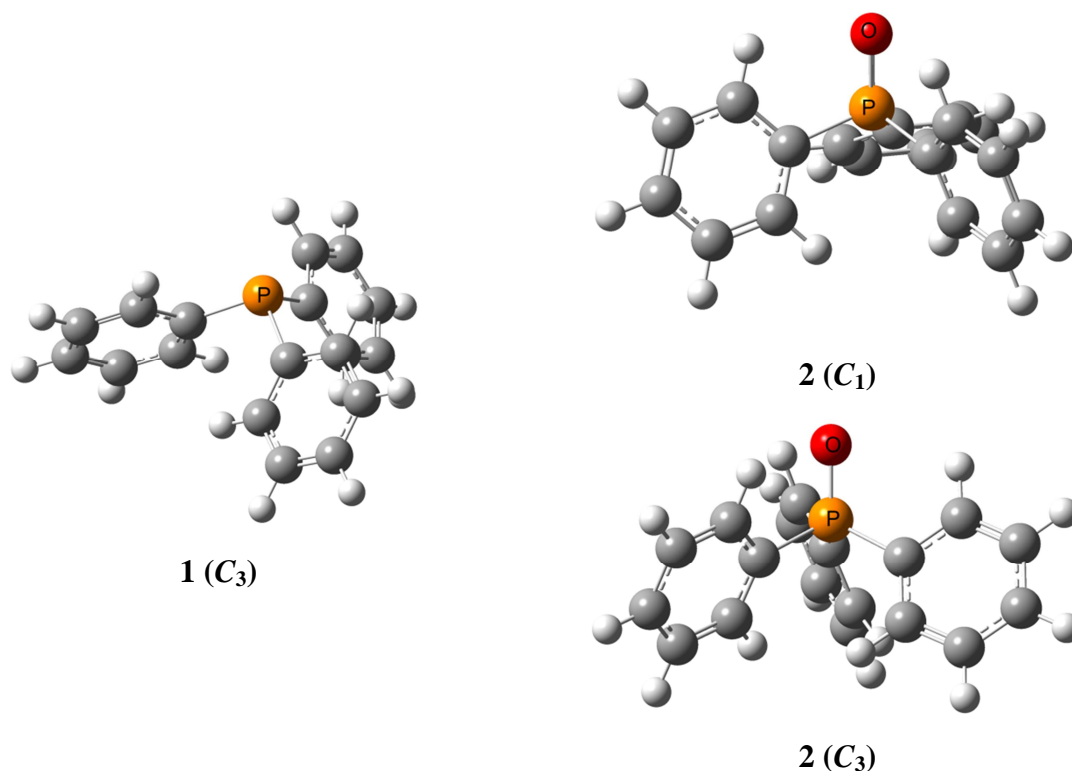


Fig. 2.1 Structures of PPh_3 (**1**) and OPPh_3 (**2**) as optimized at the MPW1K/6-31G(d) level of theory.

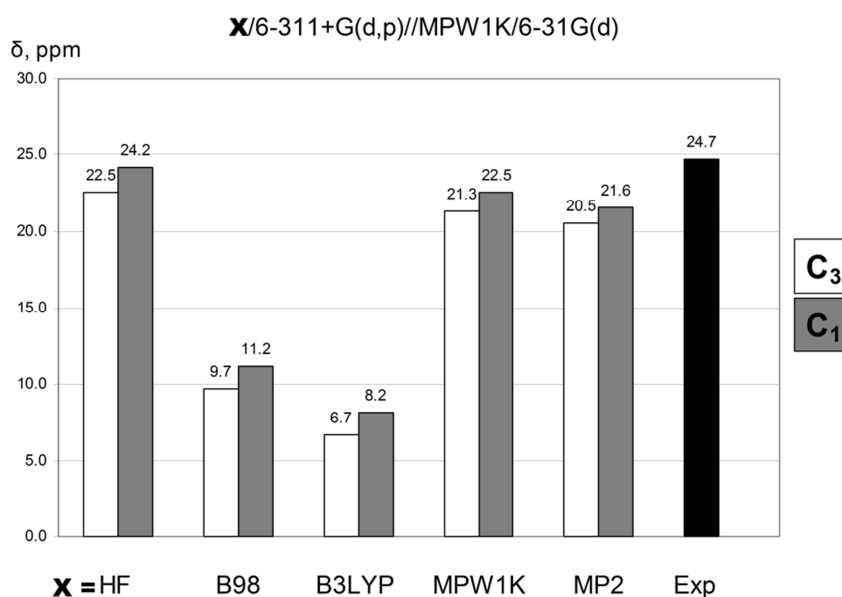


Fig. 2.2 Theoretically calculated and experimentally measured values for the ^{31}P resonance in OPPh_3 (**2**) using selected theoretical methods in combination with the 6-311+G(d,p) basis set.

Predictions made at MP2, RHF and MPW1K levels are in close to quantitative agreement with experiment, while the hybrid functionals B98 and B3LYP predict the ^{31}P shift in phosphane oxide **2** to be too low. Given the slightly better predictive value of DFT methods over RHF in previous studies^[9n] and taking into account the high price of MP2 calculations we will continue with MPW1K as the preferred choice for further studies. We also note that predicted shifts for the C_3 conformer are systematically lower (and thus inferior) than those predicted for the C_1 conformer. The triple zeta 6-311+G(d,p) basis set used in the shift calculations in Fig. 2.2 is known to provide good results for structural and energetic data of molecular systems,^[18] but may not be the ideal choice for the prediction of NMR chemical shifts. The dependence of the ^{31}P chemical shifts calculated for phosphane oxide **2** with the MPW1K hybrid functional has therefore been analyzed using additional basis set variations. This includes on the smaller side the 3-21G and 6-31G(d) split valence basis sets often used for calculations on very large molecular systems, and on the larger side the 6-311++G(2d,2p) and IGLO-III basis sets. The members of the IGLO basis set family have been optimized for application in NMR and EPR calculations.^[9h] The results obtained for all basis sets are shown in Fig. 2.3.

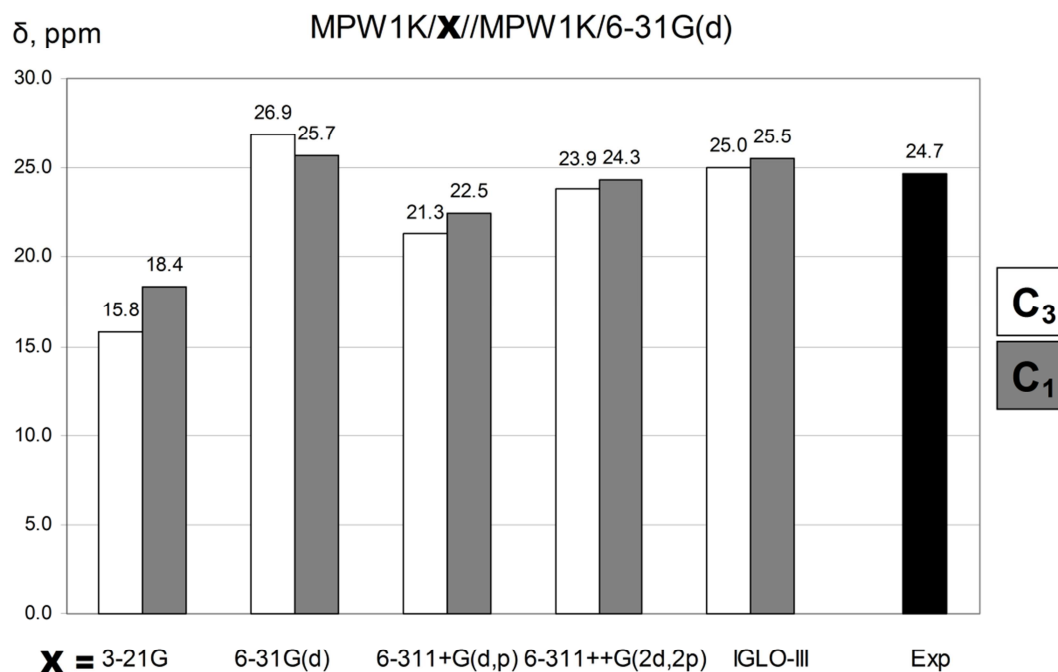


Fig. 2.3 Theoretically calculated and experimentally measured values for the ^{31}P resonance in OPPh_3 (**2**) using selected basis sets in combination with the MPW1K density functional method.

The predictive value of the small basis set 3-21G is quite low. The basis set 6-31G(d), which has been used for geometry optimization, yields a surprisingly good prediction of the ^{31}P shift in OPPh_3 , most likely due to adventitious error cancellation. Predictions made with the 6-311+G(d,p) basis set can indeed be improved somewhat through inclusion of additional polarization functions (as in 6-311++G(2d,2p)) or the use of a specifically designed basis set such as IGLO-III. It can clearly be seen that the IGLO-III and 6-311++G(2d,2p) basis sets provide almost the same results for the systems under study. The wall-clock time for calculations with the IGLO-III basis set is twice as long as with the 6-311++G(2d,2p) basis and the 6-311++G(2d,2p) basis set will therefore be used as the preferred choice in all further calculations reported here (as has also been done in other recent studies).^[9t, 9v] The basis set quality as probed through relative shift calculations for the exceedingly similar systems **1** and **2** may not necessarily be the same if two structurally rather different compounds of different sizes are compared. In order to analyze this point more clearly we have recalculated the shift of phosphane oxide **2** (C_1 conformation) using the reference compounds **3** and **6**. Trimethylphosphane (PMe_3 , **6**) is significantly smaller than phosphane **1**, but preserves the structural feature of three P–C bonds. Moreover, ^{31}P NMR shifts measured for **6** give rather similar values of $\delta(^{31}\text{P}, \mathbf{6}) = -61.0$ ppm in benzene- d_6 ^[19] and $\delta(^{31}\text{P}, \mathbf{6}) = -61.6$ ppm in chloroform- d_1 .^[20] The second reference compound phosphane (PH_3 , **3**) is even smaller than **6** and structurally even more dissimilar to **1**. In contrast to these other reference compounds the ^{31}P NMR chemical shifts measured for **3** in solution depend on a number of experimental factors (temperature and concentration) as well as on the solvent. The value reported for **3** in benzene at 29 °C of $\delta(^{31}\text{P}, \mathbf{3}) = -242$ ppm^[21] most closely approaches the conditions chosen for all other compounds used here, but we note that this value is distinctly different from the two values reported from gas phase measurements of $\delta(^{31}\text{P}, \mathbf{3}) = -254.2$ ppm^[21] and -266.1 ppm.^[22] The ^{31}P chemical shift for phosphane oxide **2** calculated with reference to compounds **1**, **3**, and **6** is graphically shown in Fig. 2.4 for the three larger basis sets used before in combination with the MPW1K functional. Using PMe_3 (**6**) as the reference compound essentially identical ^{31}P NMR shifts are calculated for **2** when using the 6-311+G(d,p), 6-311++G(2d,2p) and IGLO-III basis sets. In contrast, when using PH_3 (**3**) as the reference compound, significantly different ^{31}P NMR shifts are calculated for **2** when using the smaller 6-311+G(d,p) basis set as compared to the results obtained with the 6-311++G(2d,2p) and IGLO-III basis sets. This implies that relative shift calculations of compounds of exceedingly different sizes and structures may require more sophisticated theoretical methods as the comparison of two compounds as similar as **1** and **2**.

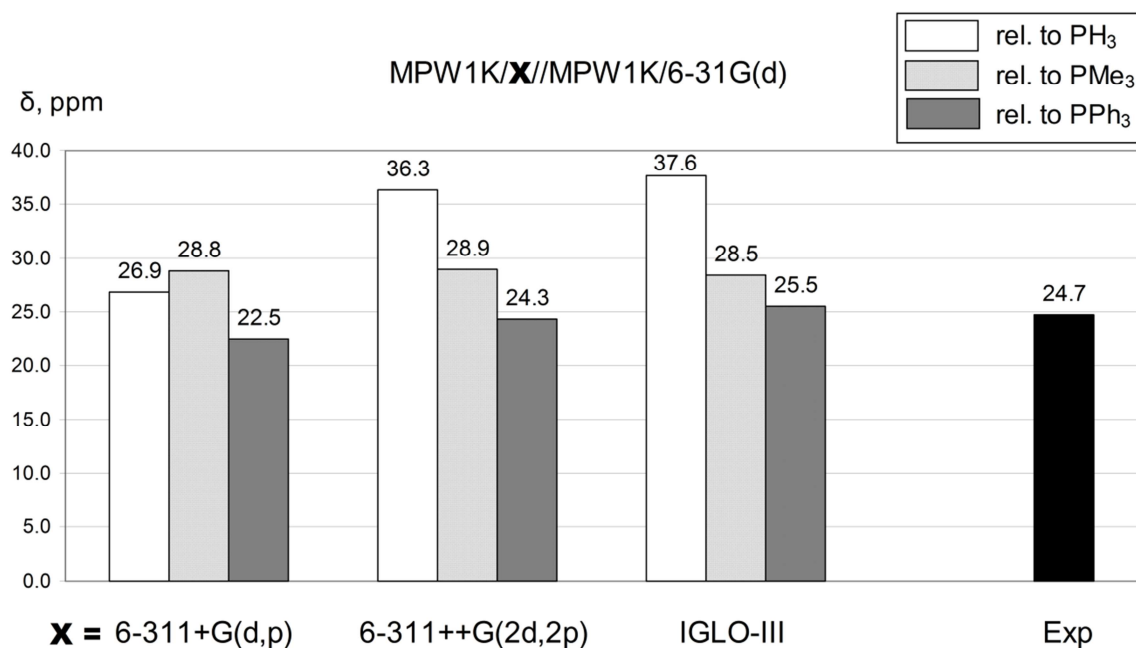


Fig. 2.4 Theoretically calculated and experimentally measured values for the ^{31}P resonance in OPPh_3 (**2**, C_1) using selected basis sets and three different reference compounds in combination with the MPW1K density functional method.

We conclude at this point that from the methods surveyed here the GIAO-MPW1K/6-311++G(2d,2p)//MPW1K/6-31G(d) is the most appropriate for ^{31}P shift predictions in large molecular systems. This approach was subsequently tested for a larger set of systems included in a previous methodological survey by van Wüllen^[9n] (Table 2.1). To be consistent with this study PH_3 (**3**) was selected as the reference compound. From this latter study we include in Table 2.1 only those methods with the best error statistics as quantified by the squared correlation coefficient (R^2) and the mean absolute deviation ($\text{MAD} = 1/n \sum |\delta_{\text{exp}} - \delta_{\text{calc}}|$) with respect to experimental values. In terms of these two error metrics the GIAO-MPW1K/6-311++G(2d,2p) method employed here gives slightly better (slightly better R^2 , while MAD is 0.7 ppm larger) results as compared to the GIAO-MP2/IGLO-II//BP/IGLO-II approach considered to be the most accurate in the van Wüllen study. As in this previous study we exclude the PN system from the error analysis. The correlation between ^{31}P shifts measured experimentally and those calculated at the GIAO-MPW1K/6-311++G(2d,2p) level is shown graphically in Fig. 2.5. Larger molecular systems are often conformationally quite flexible and the question naturally arises how to deal with this point in ^{31}P NMR shift calculations. Assuming rapid interconversion between individual conformers (on the NMR time scale) it would seem obvious to calculate ^{31}P NMR shifts as the Boltzmann-weighted average over all conformations. The shifts reported in Table 2.1 at the GIAO-MPW1K level were actually obtained by Boltzmann-averaging at 298.15 K using free energies obtained at the MP2(FC)/6-

31+G(2d,p)//MPW1K/6-31G(d) level of theory. This latter method has been used recently in the accurate prediction of thermochemical data of a large set of N- and P-based Lewis bases.^[5] To illustrate the importance of conformational averaging already in gas phase calculations ³¹P shifts calculated for individual conformers of trimethoxyphosphane P(OMe)₃ (**8**) have been collected in Table 2.2 together with the respective relative free energies ΔG_{298} . While the energetically most favorable conformers of **8** have almost the same ³¹P chemical shift at +155.9 and +152.5 ppm, respectively, this is not so for the conformation located 8.5 kJ mol⁻¹ above the global minimum with a ³¹P chemical shift at +128.9 ppm. The Boltzmann weight of this conformer is quite low in the gas-phase and the average shift predicted as +154.4 ppm is thus quite close to the individual values for the best two conformers. However, solvent effects even in apolar organic media can be large enough to change the relative energies of individual conformers and can therefore lead to major changes in ³¹P NMR shifts.

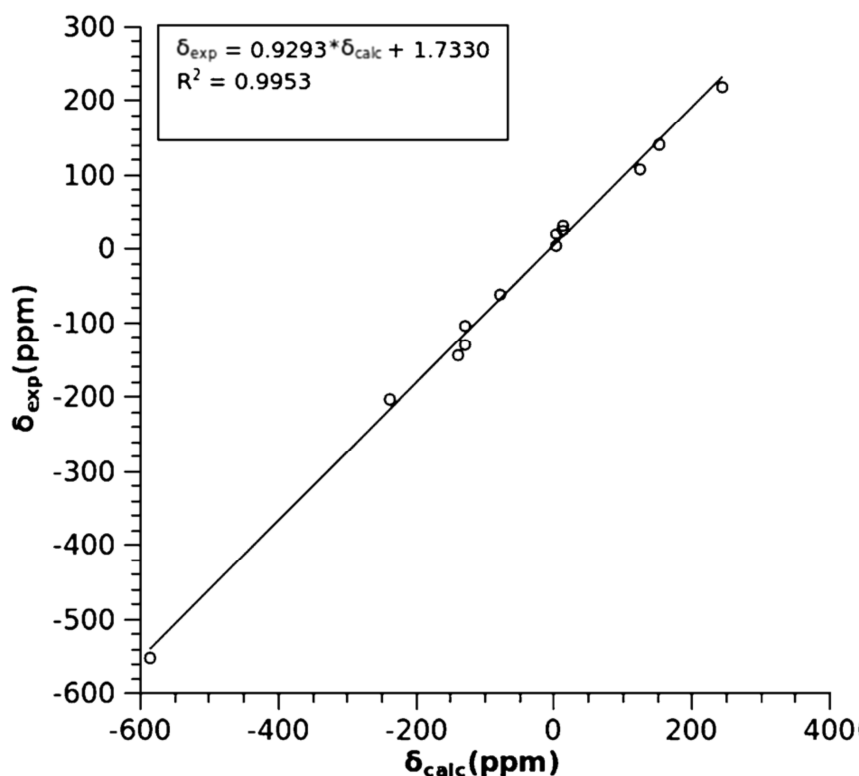


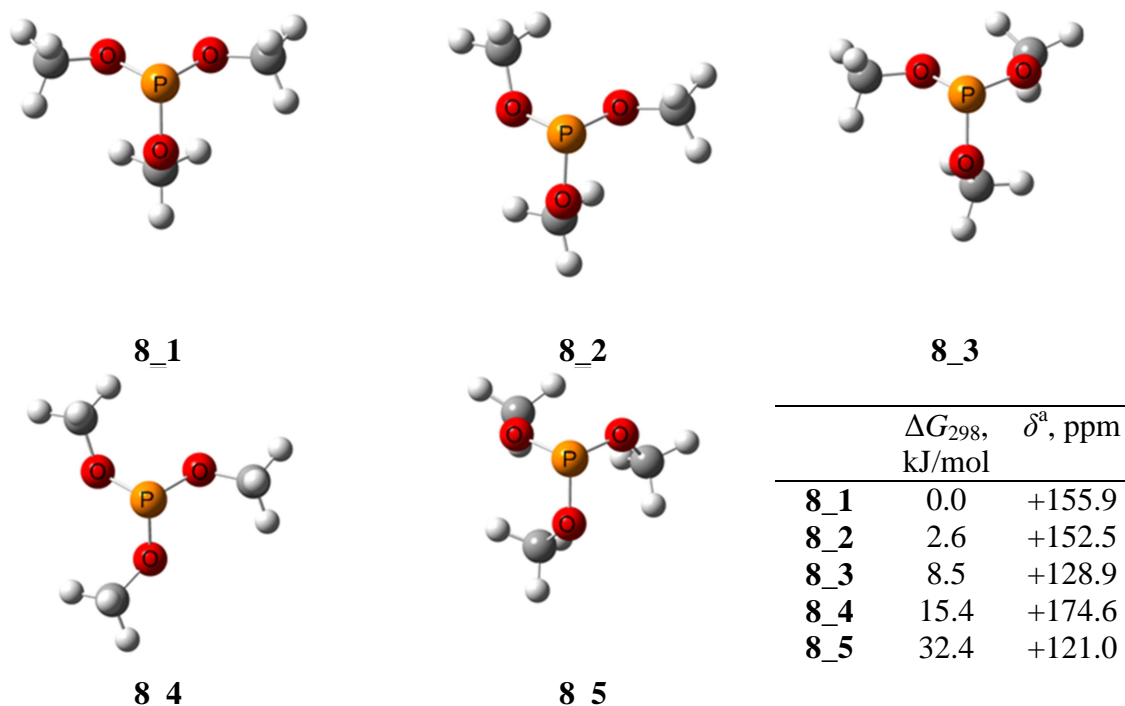
Fig. 2.5 Experimental ³¹P chemical shifts vs. calculated at the GIAO-MPW1K/6-311++G(2d,2p)//MPW1K/6-31G(d) level of theory listed in Table 2.1.

Table 2.1 ^{31}P NMR chemical shifts calculated at selected levels of theory in the gas phase using PH_3 (**3**) as the reference system.

		Method						Exp.	Experimental conditions
		GIAO MPW1K ^a	IGLO BP ^b	IGLO B3LYP ^b	GIAO BP ^b	GIAO B3LYP ^b	GIAO MP2 ^b		
3	PH_3	-266.1	-266.1	-266.1	-266.1	-266.1	-266.1	-266.1	Gas-phase ^[22]
4	PF_3	+126.1	+113.8	+100.8	+132.5	+115.7	+109.7	+106	Gas-phase ^[22]
5	PCl_3	+246.4	+244.3	+236.9	+269.9	+259.6	+224.9	+217	Gas-phase ^[22]
6	$\text{P}(\text{CH}_3)_3$	-77.8	-69.1	-73.9	-53.8	-58.4	-75	-63	Gas-phase ^[22]
7	$\text{P}(\text{C}_3\text{H}_7)_3$	+2.8	+15.5	+11.4	+31.8	+27.3	+10.6	+19.3	Benzene-d ₆ ^[23]
8	$\text{P}(\text{OCH}_3)_3$	+154.4	+115	+109	+137.9	+128.4	+129.3	+140	Toluene-d ₈ ^[24]
9	$\text{OP}(\text{CH}_3)_3$	+13.1	-5.7	-6.7	+19.1	+14	+18.7	+32	Benzene ^[25]
10	$\text{OP}(\text{OCH}_3)_3$	+4.5	-34.4	-37	-9.1	-16.7	-5	+3.7	Benzene ^[26]
11	$\text{Si}(\text{PH}_2)_4$	-236.5	-223.5	-228.9	-219.5	-226	-243.1	-205	Benzene-d ₆ ^[27]
12	$\text{Cr}(\text{CO})_5(\text{PH}_3)$	-127.5	-150.5	-143.3	-128.6	-123	-176.7	-130	Benzene-d ₆ ^[28]
13	PH_4^+	-128.0	-151.4	-156	-122.8	-128.9	-127.6	-105	Methanol ^[29]
14	$\text{P}(\text{CH}_3)_4^+$	+13.2	+2.5	-2.9	+30.4	+22.1	+12.5	+25.1	DMSO ^[30]
15	PF_6^-	-138.7	-119.9	-140.8	-95.1	-120.2	-119.5	-146	Benzene-d ₆ ^[31]
16	P_4	-584.2	-512.9	-524.1	-516.7	-532.5	-549.1	-552	Gas-phase ^[32]
17	PN	+366.4	+307.8	+325.5	+326.1	+342.7	+202.2	+275	Gas-phase ^[33]
R^{2c}		0.9953	0.9805	0.9856	0.9842	0.9890	0.9907		
MAD ^c (ppm)		17.2	24.5	23.4	19.5	16.5	16.5		

^a GIAO-MPW1K/6-311++G(2d,2p)//MPW1K/6-31G(d). ^b Results taken from ref. ^[9n]; basis set for NMR calculations: IGLO-II; geometries optimized at the BP/IGLO-II level. ^c PH_3 (the reference compound) and PN (worst case in the present work as well as in ref. ^[9n]) have been excluded from the error analysis.

Table 2.2 Individual conformations of P(OMe)₃ (**8**) used in Boltzmann-averaged ³¹P chemical shift calculations.

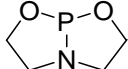
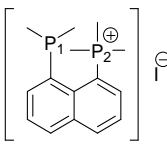
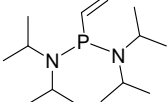


^a Relative to PH₃.

With a protocol in hand for the calculation of gas phase ³¹P chemical shifts of large molecular structures (GIAO-MPW1K/6-311++(2d,2p)//MPW1K/6-31G(d)), we can address the question of how to account for solvent effects in a systematic manner. We compare in the following two different approaches to account for solvent effects: (a) use of the Polarizable Continuum Model (PCM) in combination with NMR shift calculations (solution model 1); and (b) inclusion of one explicit solvent molecule in the geometry optimization of the substrate and subsequent NMR shift calculations on this solvent/solute complex using the PCM continuum solvation model at the stage of NMR shift calculations (solution model 2). These two models have been tested on a set of systems for which there are data measured in solvents of different polarities (chloroform-d₁ and benzene-d₆) and which cover a large range of ³¹P NMR chemical shifts (from -50 to +160 ppm). In order to avoid problems associated with the solution phase properties of PH₃ (**3**) all calculations have been performed using Ph₃P (**1**) as the reference system. As one can see from the data presented in Table 2.3 and in Fig. 2.6 and 2.7 the best results are obtained using solution model 2, where a combination of explicit and continuum solvation is employed. Use of the PCM continuum solvation model alone is particularly unsatisfactory for phosphane oxides **2** and **9**. The large solvent effects observed for this latter class of compounds even for a low polarity solvent such as chloroform are

clearly due to specific hydrogen bonding interactions between the phosphane oxide oxygen atom and the chloroform C–H bond (Fig. 2.8). Our observation is in accordance with the recently demonstrated insufficiency of PCM models for systems with strong directional solvent–solute interactions.^[34]

Table 2.3 Experimentally measured and theoretically calculated ³¹P NMR chemical shifts in the gas phase and in solution using PPh₃ (**1**) as the reference system.

System		³¹ P NMR chemical shift				Solvent
		Gas-phase	Solution model 1	Solution model 2	Exp.	
1	PPh ₃	-4.7	-4.7	-4.7	-4.7	Chloroform-d ₁ ^[12]
		-4.7	-4.7	-4.7	-4.7	Benzene-d ₆ ^[11]
2	OPPh ₃	+24.1	+26.6	+29.6	+29.7	Chloroform-d ₁ ^[12]
		+24.1	+26.6	+25.4	+24.7	Benzene-d ₆ ^[13]
8	P(OCH ₃) ₃	+166.6	+166.9	+167.3	+142	Chloroform ^[35]
9	OP(CH ₃) ₃	+25.3	+29.8	+36.3	+39.3	Chloroform-d ₁ ^[25]
		+25.3	+28.5	+27.3	+32.0	Benzene-d ₆ ^[25]
10	OP(OCH ₃) ₃	+16.7	+16.7	+15.9	+3.0	Chloroform-d ₁ ^[26]
		+16.7	+16.6	+14.6	+3.7	Benzene-d ₆ ^[26]
18	[PPh ₃ Me ⁺] ⁺ I ⁻	+15.5	+17.1	+23.1	+22.2	Chloroform-d ₁ ^[36]
19	PBr ₂ Ph	+175.4	+176.7	+173.8	+150.7	Chloroform-d ₁ ^[37]
20		+160.7	+163.5	+161.8	+139.0	Chloroform-d ₁ ^[38]
21		-56.3	-55.1	-54.1	-50.6(P ₁)	Chloroform-d ₁ ^[39]
		+27.4	+25.1	+24.7	+18.1(P ₂)	Chloroform-d ₁ ^[39]
22		+61.5	+64.7	+62.8	+53.1	Chloroform-d ₁ ^[40]
	R^2 ^a	0.9811	0.9859	0.9912		
	MAD ^a (ppm)	11.9	11.4	9.6		

^a PPh₃ (the reference system) has been excluded from the error analysis.

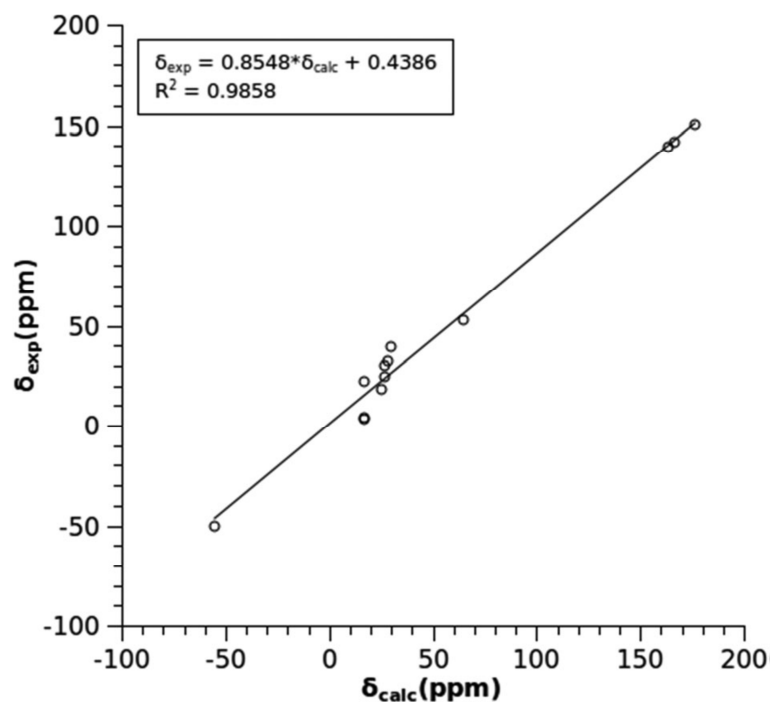


Fig. 2.6 Experimental chemical shifts vs. calculated using solution model 1 for the compounds listed in Table 2.3.

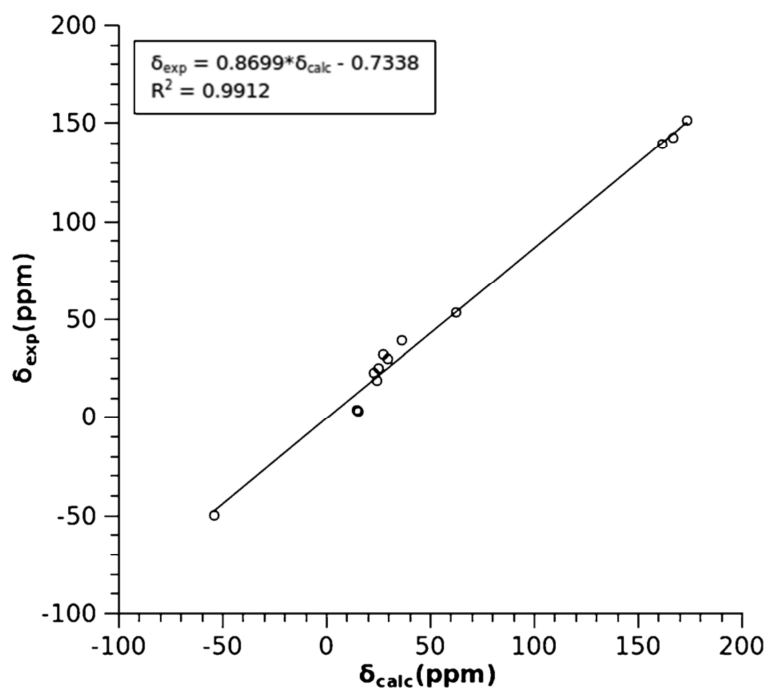


Fig. 2.7 Experimental chemical shifts vs. calculated using solution model 2 for the compounds listed in Table 2.3.

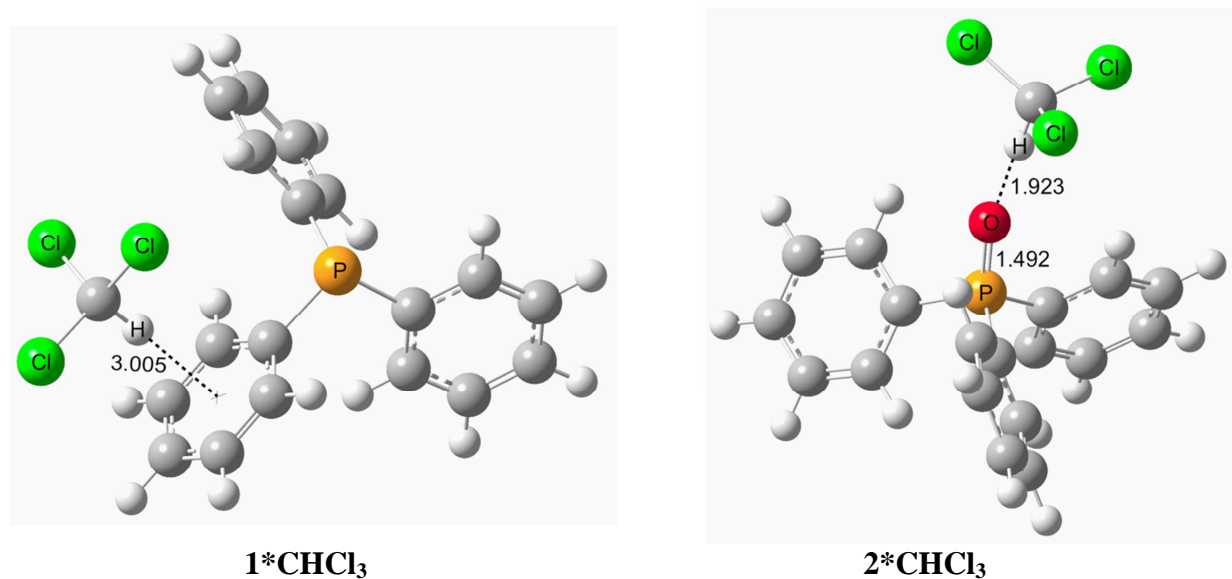


Fig. 2.8 Energetically most favorable complexes of PPh_3 (**1**) and OPPh_3 (**2**) with CHCl_3 as obtained at the MP2(FC)/6-31+G(2d,p)//MPW1K/6-31G(d) level of theory.

It was mentioned before that conformational averaging is an important step in the process of chemical shift calculations inasmuch as the shifts depend dramatically on the conformational state of the molecule. The effects of conformational mobility on the calculated solution phase ^{31}P shifts will here be exemplified by a closer look at system **22**. After gas-phase geometry optimization at the MPW1K/6-31G(d) level 10 individual conformations have been identified as true minima. Chemical shift calculations at the GIAO-MPW1K/6-311++G(2d,2p) level and single point calculations at the MP2(FC)/6-31+G(2d,p)//MPW1K/6-31G(d) level have subsequently been performed for all ten structures in order to calculate ^{31}P NMR shifts and relative free energies ΔG_{298} in the gas-phase and in solution (model 1). The results of this exercise as collected in Table 2.4 show the first three conformers **22_1** to **22_3** (shown graphically in Fig. 2.9) to be energetically accessible at a temperature of 298.15 K. It is quite remarkable to see that the ^{31}P NMR shifts calculated in the gas phase and in the presence of the PCM continuum model (for CHCl_3 as the solvent) hardly differ. The shifts vary largely for individual conformers from +50.7 ppm (conformer **22_2**) to +102.4 ppm (conformer **22_8**). The difference between the Boltzmann-averaged ^{31}P NMR shifts predicted for the gas-phase (+61.5 ppm) and for CHCl_3 solution (+64.7 ppm) is thus solely due to changes in the Boltzmann-weights of individual conformers. In addition to relative energies obtained at the MP2(FC)/6-31+G(2d,p)//MPW1K/6-31G(d) level Table 2.4 shows also values from single-point calculations at the MPW1K/6-311++G(2d,2p)//MPW1K/6-31G(d) level of theory which accompany the chemical shift calculations. Boltzmann-averaged ^{31}P NMR shifts found using DFT energies are also listed in Table 2.4.

Table 2.4 Chemical shifts and energetic characteristics for all conformations of the system **22** calculated for the gas phase and in solution (CHCl₃, solution model 1).

Conformation	Chem. shift ^a , ppm		Free energies, kJ mol ⁻¹			
	Gas-phase ^b	Solution model 1 ^c	MPW1K		MP2	
			ΔG_{298} ^d	$\Delta G_{298, \text{CHCl}_3}$ ^e	ΔG_{298} ^f	$\Delta G_{298, \text{CHCl}_3}$ ^g
22_1	+66.6	+66.3	1.7	0.0	0.0	0.0
22_2	+50.7	+51.2	0.0	1.0	1.1	3.8
22_3	+87.0	+87.2	12.7	11.4	6.9	7.3
22_4	+85.6	+86.4	13.7	12.8	14.1	15.0
22_5	+80.0	+80.8	15.4	14.1	16.5	16.9
22_6	+84.7	+84.3	21.6	18.1	19.7	17.9
22_7	+100.5	+100.3	20.6	17.6	19.9	18.6
22_8	+102.4	+102.6	19.6	19.2	17.4	18.7
22_9	+80.4	+80.8	15.5	18.4	17.8	22.4
22_10	+87.3	+87.5	39.9	35.9	32.0	29.6
$\langle \delta \rangle$ ^h			+56.3	+60.6	+61.5	+64.7

^a Relative to PPh₃. ^b GIAO-MPW1K/6-311++G(2d,2p).

^c GIAO-MPW1K/6-311++G(2d,2p) + PCM/UAHF/MPW1K/6-311++G(2d,2p). ^d MPW1K/6-311++G(2d,2p), free en. corr.: MPW1K/6-31G(d). ^e MPW1K/6-311++G(2d,2p) + PCM/UAHF/MPW1K/6-311++G(2d,2p), free en. corr.: MPW1K/6-31G(d). ^f MP2(FC)/6-31+G(2d,p)//MPW1K/6-31G(d), free en. corr.: MPW1K/6-31G(d). ^g MP2(FC)/6-31+G(2d,p)//MPW1K/6-31G(d)+PCM/UAHF/MPW1K/6-311++G(2d,2p), free en. corr.: MPW1K/6-31G(d). ^h Boltzmann-averaged chemical shift.

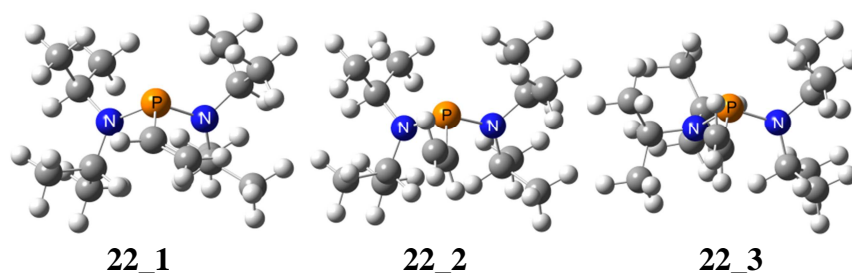


Fig. 2.9 Structures of the three most stable conformations of system **22**.

The ten gas-phase conformers of **22** were subsequently used to calculate ³¹P NMR shifts with solvent model 2, in which explicit chloroform molecules were placed in close vicinity of the phosphorous atom and π -bond, where intermolecular solute/solvent interaction is most likely. The solvent–substrate complexes obtained after geometry optimization illustrate, however, that no close contacts are possible between CHCl₃ solvent molecules and the central phosphorous atom due to severe steric effects. The two energetically most favorable complexes identified in these studies are shown in Fig. 2.10. Relative energies and individual ³¹P NMR shifts for all complexes are collected in Table 2.5. Surveying the chemical shifts calculated for individual conformers in Table 2.5 we note again a large dispersion of shift values. The Boltzmann-averaged chemical shift (based on MP2(FC)/6-31+G(2d,p) free

energies) obtained with solution model 2 for chloroform is +62.8 ppm. Whether to use other relative energies in the Boltzmann-averaging procedure was tested by using free energies derived from MPW1K/6-311++G(2d,2p) single point calculations, but the relative weights of individual conformers are not decisively different with this choice (Table 2.5). How much of this effort is required? Selecting from Table 2.5 only those CHCl_3 complexes derived from the three most stable gas-phase conformations **22_1** through **22_3** the Boltzmann-averaged chemical shift was found to be hardly changed at +62.6 ppm. For this smaller set of structures basis set effects in the MP2(FC) energy calculations were also explored, but the changes in the predicted chemical shift were rather minor (*vide* Table 2.5.1).

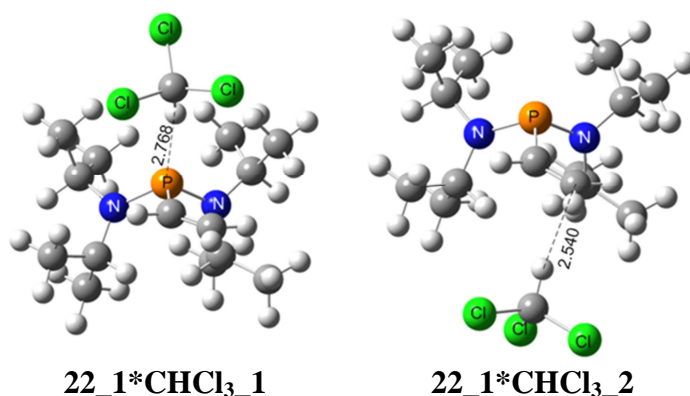


Fig. 2.10 Complexes between the most stable conformation of system **22** and chloroform.

Table 2.5 Chemical shifts and energetic characteristics for solvent–solute complexes of **22** with CHCl₃ as employed for solvent model 2.

Complex	Chem. shift ppm ^a	Free energies, kJ mol ⁻¹			
		MPW1K/ 6-311++G(2d,2p)		MP2(FC)/ 6-31+G(2d,p)	
		ΔG_{298} ^b	$\Delta G_{298, \text{CHCl}_3}$ ^c	ΔG_{298} ^d	$\Delta G_{298, \text{CHCl}_3}$ ^e
22_1*CHCl3_1	+62.4	0.0	0.0	0.0	0.0
22_1*CHCl3_2	+65.9	5.8	4.5	4.9	3.5
22_2*CHCl3_1	+52.1	2.9	5.7	4.0	6.7
22_2*CHCl3_2	+50.8	3.9	1.8	11.8	9.7
22_3*CHCl3_1	+82.7	13.6	14.9	9.8	11.1
22_7*CHCl3_2	+98.7	15.9	13.5	14.9	12.6
22_3*CHCl3_2	+85.1	17.0	13.4	17.7	14.1
22_4*CHCl3_1	+83.4	13.8	15.6	16.2	18.0
22_9*CHCl3_1	+76.6	14.1	15.8	17.8	19.5
22_6*CHCl3_1	+78.2	19.0	19.1	19.5	19.6
22_7*CHCl3_1	+94.5	17.3	17.6	19.9	20.1
22_5*CHCl3_1	+78.1	15.0	17.3	18.5	20.8
22_5*CHCl3_2	+78.9	18.5	13.9	26.0	21.4
22_8*CHCl3_1	+95.3	19.3	21.3	19.5	21.5
22_4*CHCl3_2	+84.1	17.9	13.8	25.8	21.7
22_6*CHCl3_2	+84.3	26.0	22.6	26.9	23.6
22_9*CHCl3_2	+78.7	18.0	14.6	27.2	23.9
22_8*CHCl3_2	+101.0	24.5	21.6	29.3	26.3
22_10*CHCl3_1	+83.0	42.1	40.4	34.2	32.5
22_10*CHCl3_2	+86.3	45.2	41.6	40.7	37.1
$\langle \delta \rangle$ ^f		+59.5	+59.4	+61.6	+62.8

^a Relative to PPh₃, GIAO-MPW1K/6-311++G(2d,2p) + PCM/UAHF/MPW1K/6-311++G(2d,2p).

^b MPW1K/6-311++G(2d,2p), free en. corr.: MPW1K/6-31G(d).

^c MPW1K/6-311++G(2d,2p) + PCM/UAHF/MPW1K/6-311++G(2d,2p), free en. corr.: MPW1K/6-31G(d).^d MP2(FC)/6-31+G(2d,p)//MPW1K/6-31G(d), free en. corr.: MPW1K/6-31G(d).

^e MP2(FC)/6-31+G(2d,p)//MPW1K/6-31G(d) + PCM/UAHF/MPW1K/6-311++G(2d,2p), free en. corr.: MPW1K/6-31G(d).^f Boltzmann-averaged chemical shift.

Table 2.5.1 Chemical shifts and energetic characteristics for solvent-solute complexes of **22** with CHCl₃ as employed for solvent model 2.

Complex	Chem. shift ppm ^a	Free energies, kJ/mol					
		MPW1K/ 6-311++G(2d,2p)		MP2(FC)/ 6-31+G(2d,p)		MP2(FC)/ G3MP2large	
		ΔG_{298}^b	$\Delta G_{298, \text{CHCl}_3}^c$	ΔG_{298}^d	$\Delta G_{298, \text{CHCl}_3}^e$	ΔG_{298}^f	$\Delta G_{298, \text{CHCl}_3}^g$
22_1*CHCl₃_1	+62.4	0.0	0.0	0.0	0.0	0.0	0.0
22_1*CHCl₃_2	+65.9	5.8	4.5	4.9	3.5	5.7	4.4
22_2*CHCl₃_1	+52.1	2.9	5.7	4.0	6.7	4.0	6.7
22_2*CHCl₃_2	+50.8	3.9	1.8	11.8	9.7	12.0	10.0
22_3*CHCl₃_1	+82.7	13.6	14.9	9.8	11.1	11.7	13.0
22_3*CHCl₃_2	+85.1	17.0	13.4	17.7	14.1	19.8	16.2
$\langle \delta \rangle^g$		+59.2	+59.1	+61.5	+62.6	+61.2	+62.3

^a relative to PPh₃, GIAO-MPW1K/6-311++G(2d,2p) + PCM/UAHF/MPW1K/6-311++G(2d,2p); ^b MPW1K/6-311++G(2d,2p), free en. corr.: MPW1K/6-31G(d); ^c MPW1K/6-311++G(2d,2p) + PCM/UAHF/MPW1K/6-311++G(2d,2p), free en. corr.: MPW1K/6-31G(d); ^d MP2(FC)/6-31+G(2d,p)/MPW1K/6-31G(d), free en. corr.: MPW1K/6-31G(d); ^e MP2(FC)/6-31+G(2d,p)/MPW1K/6-31G(d) + PCM/UAHF/MPW1K/6-311++G(2d,2p), free en. corr.: MPW1K/6-31G(d); ^f MP2(FC)/G3MP2large/MPW1K/6-31G(d), free en. corr.: MPW1K/6-31G(d); ^g Boltzmann-averaged chemical shift

One additional technical issue arises for ion pair system **21**, where ³¹P NMR calculations can be performed either for the full ion pair or for the phosphonium portion alone. Gas and solution phase calculations have been performed for both of these choices. The results compiled in Fig. 2.11 clearly illustrate that accurate predictions require the consideration of the full system. The difference for the theoretical and experimental chemical shifts of the phosphane atom P₁ is small, while it is quite large for the phosphonium atom P₂. Similar results have been obtained for system **18**, where application of solution model 2 to the bare phosphonium cation (PPh₃Me⁺) leads to a calculated chemical shift of +27.4 ppm, which is 5.2 ppm larger than the experimental value of +22.2 ppm. Consideration of the full ion pair through inclusion of the iodide counter ion shifts the predicted chemical shift for **18** considerably to +23.1 ppm, just 0.9 ppm away from the experimental value.

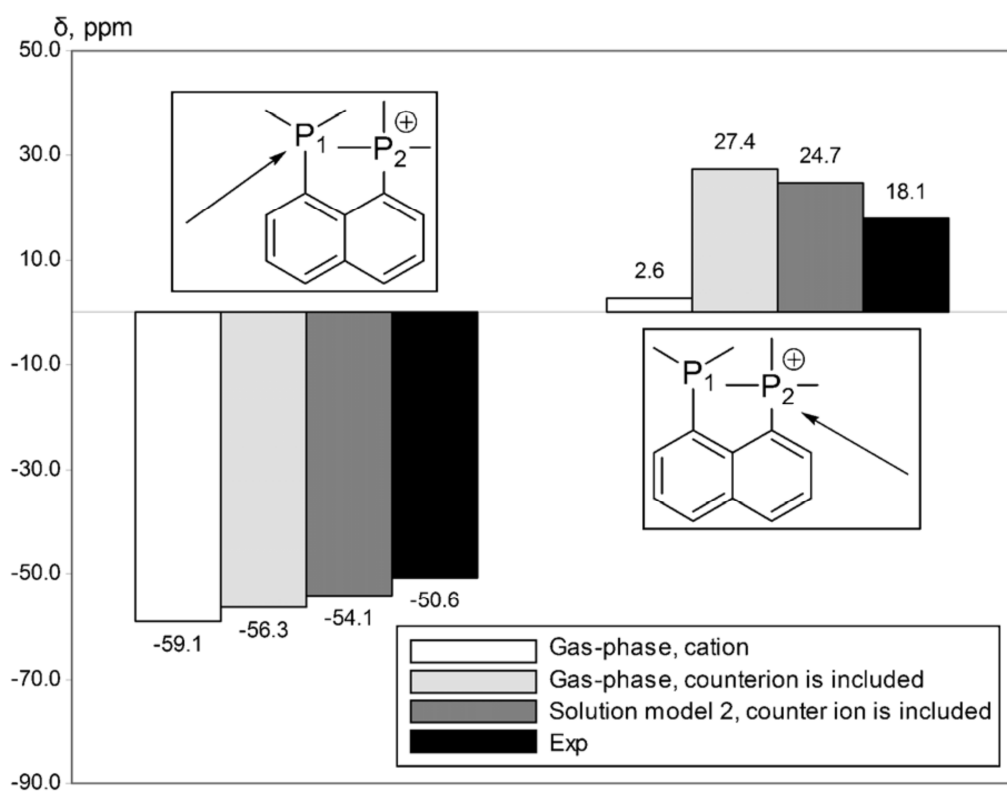


Fig. 2.11 ^{31}P NMR chemical shifts (relative to PPh_3) calculated for ion-pair system **21** in the presence and the absence of the iodide counter ion.

2.1.3. Conclusions

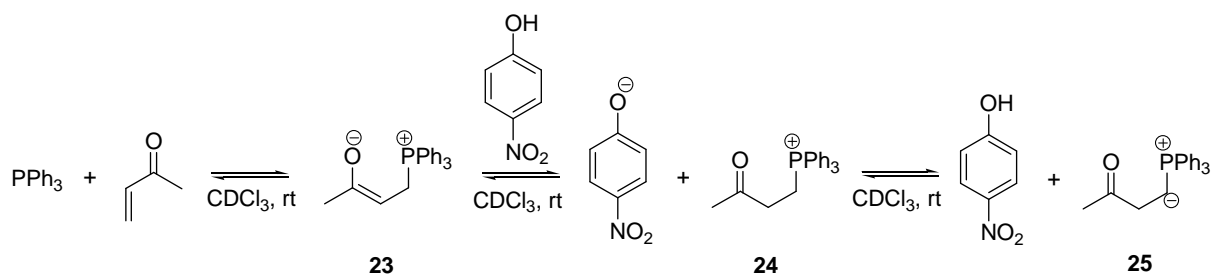
1. The MPW1K functional in combination with the GIAO scheme represents a good basis for gas-phase and condensed-phase calculations of ^{31}P NMR chemical shifts for large molecular systems. Predictions with other hybrid functionals (such as B98 or B3LYP) appear to be less reliable, while predictions at the MP2 level are significantly more expensive.
2. The IGLO-III and 6-311++G(2d,2p) basis sets in combination with GIAO-MPW1K provide ^{31}P NMR chemical shift predictions with good accuracy. Smaller basis sets provide systematically inferior predictions.
3. The ^{31}P NMR shifts calculated for individual conformers vary largely, emphasizing the need for Boltzmann-averaging over the full conformational space of the system.
4. ^{31}P NMR chemical shifts in solution are best predicted by including explicit solvent molecules at the stage of geometry optimization and by performing the GIAO shift calculations in the presence of the PCM/UAHF continuum solvation model.
5. Accurate prediction of ^{31}P NMR chemical shifts of ion pair systems require consideration of the full system.

Finally, in view of the considerably different chemical shifts obtained with different reference compounds it appears that accurate predictions can only be made through relative shift calculations of two structurally and chemically closely related systems. This requirement may reflect the fact that several factors are not accounted for in the current computational approach. This includes the known concentration- and temperature-dependence of experimentally measured ^{31}P spectra as well as the neglect of solvent magnetic polarizability effects in the current form of the PCM continuum solvation model.^[10b, 10c]

2.2. Application of the Proposed Approach to the MBH reaction

2.2.1. Introduction

Having at disposal a reliable approach for ^{31}P NMR chemical shift prediction of large organophosphorus compounds in solution, it has been decided to apply it to the already mentioned Morita-Bayllis-Hillman reaction (MBH). It is one of the most important processes in modern organocatalysis and, in spite of the fact that many experimental and computational studies have been performed in this field (in following chapters this point will arise again), it still poses a number of mechanistically related questions. Obviously, the detection of MBH reaction intermediates would be the best way to clarify the mechanism. And since phosphanes are very popular catalysts for MBH reactions, the ^{31}P NMR spectroscopy could serve as a suitable analytical method and the theoretical support could be helpful in order to assign the measured chemical shifts. Recently a series of ^{31}P NMR experiments to monitor MBH reaction intermediates has been done by Dr. Yinghao Liu.^[41] Three types of signals have been found for the mixture of PPh_3 (catalyst) with methyl vinyl ketone (MVK) dissolved in CDCl_3 : -4.7 ppm (PPh_3), +29.5 ppm (identical to Ph_3PO) and signals group around -60 ppm of unclear nature (Fig. 2.12a). If *p*-nitrophenol (PNP) is added to the mixture of PPh_3 and MVK in CDCl_3 , a new signal appears at +25.72 ppm, in addition to the signal for PPh_3 at -4.7 ppm (Fig. 2.12b). It has been assigned to intermediate **24** (Scheme 2.1) via additional ^1H NMR and 2D NMR experiments.



Scheme 2.1 Protonation/deprotonation equilibria in the mixture of PPh_3 , MVK and PNP in CDCl_3 .

The equilibrium between zwitterionic intermediate **23** (considered to be a key-intermediate in MBH catalytic cycle), cation **24** and ylid **25**, shown in Scheme 2.1, will be discussed in detail in the following chapters. Here the results of the proposed computational scheme of ^{31}P NMR chemical shift for these intermediates are presented. Later a hypothesis about group of signals around -60 ppm will be also suggested.

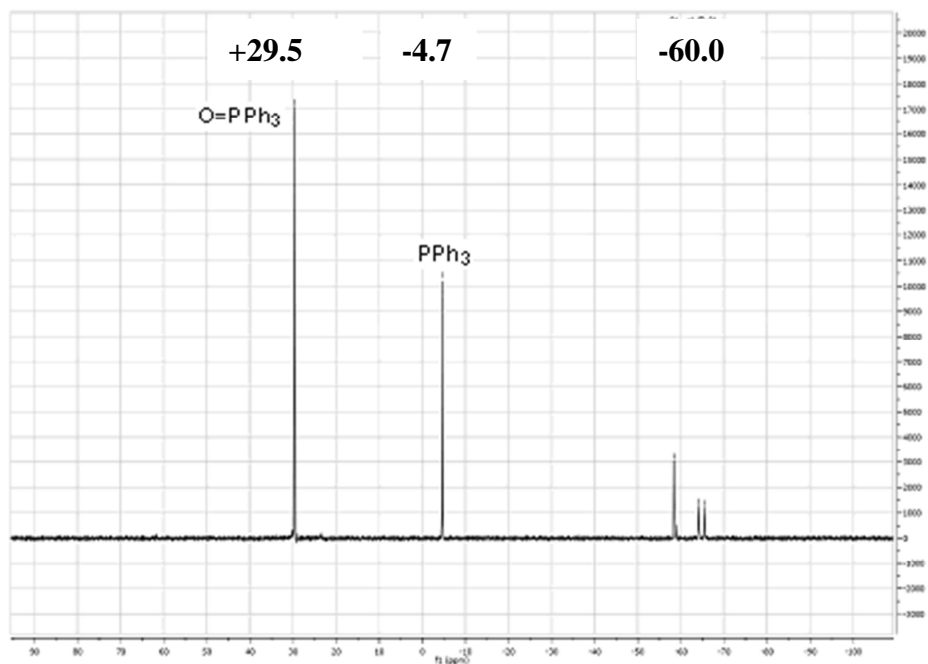


Fig. 2.12a The ^{31}P NMR of PPh₃ (0.32 M) and MVK (3.2 M) in CDCl₃ after 50 mins. Measured by Dr. Yinghao Liu^[41]

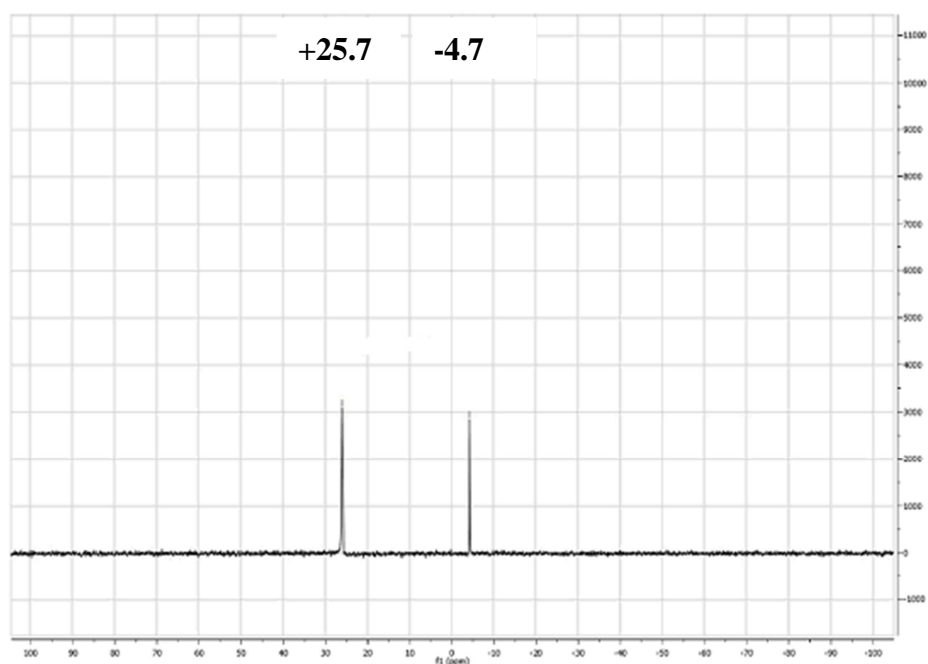
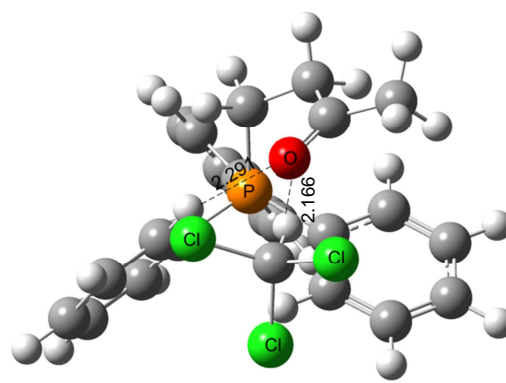


Fig. 2.12b The ^{31}P NMR of PPh₃ (0.32 M), PNP (0.48 M) and MVK (3.2 M) in CDCl₃ after 5 mins. Measured by Dr. Yinghao Liu^[41]

2.2.2. Results and Discussion

In compliance with the suggested computational scheme, we have first optimized the structures of cation **24** at MPW1K/6-31G(d) level of theory and 4 minima have been found. The second step is the explicit consideration of the solvent molecule (here it is chloroform) by forming solute*solvent complexes. In Table 2.6 we show the structure of the most stable conformation of the solute*solvent complex as it has been found at MP2(FC)/6-31+G(2d,p)//MPW1K/6-31G(d) + PCM/UAHF/MPW1K/6-311++G(2d,2p)//MPW1K/6-31G(d) (gas-phase geometries, single point calculation of solvent effect) level together with the relative free energies for all four found minima and their ^{31}P NMR chemicals shifts calculated at GIAO-MPW1K/6-311++G(2d,2p)//MPW1K/6-31G(d) + PCM/UAHF/MPW1K/6-311++G(2d,2p)//MPW1K/6-31G(d) (NMR calculations in combination with the PCM model), where the $\text{PPh}_3\cdot\text{CHCl}_3$ complex was used as the reference system. One can see from the structure shown in Table 2.6, that the best conformation of $\mathbf{24}\cdot\text{CHCl}_3$ is stabilized by formation of two hydrogen bonds – one between the carbonyl oxygen atom and one of the phenyl ring hydrogen atom ($r(\text{O}-\text{H}) = 2.291 \text{ \AA}$), and one between this oxygen atom and the hydrogen atom of the chloroform molecule ($r(\text{O}-\text{H}) = 2.166 \text{ \AA}$).

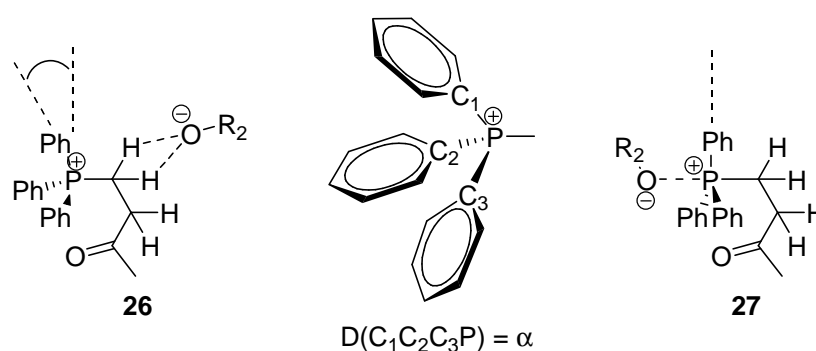
Table 2.6 Calculated relative free energies and chemical shifts for 4 individual conformations of the solute*solvent complexes of cation **24** with CHCl_3 and the structure of the most stable complex.

	$\Delta G_{298,\text{CHCl}_3}^a/\text{kJ mol}^{-1}$	δ^b/ppm
	0.0	28.0
	2.7	32.6
	4.4	28.0
	5.4	29.5

^a MP2(FC)/6-31+G(2d,p)//MPW1K/6-31G(d) + PCM/UAHF/MPW1K/6-311++G(2d,2p)//MPW1K/6-31G(d), free en. corr.: MPW1K/6-31G(d). ^b Relative to $\text{PPh}_3\cdot\text{CHCl}_3$, GIAO-MPW1K/6-311++G(2d,2p)//MPW1K/6-31G(d) + PCM/UAHF/MPW1K/6-311++G(2d,2p)//MPW1K/6-31G(d).

The Boltzmann-averaged chemical shift from these four complexes is +29.0 ppm. If we compare this result with the experimental value of +25.7 ppm, the question immediately arises whether it is possible to improve the calculations. One of the critical points for ^{31}P NMR calculation is that the reference system and the system we are interested in should be

chemically closely related – as was shown before for the $\text{Ph}_3\text{P}/\text{Ph}_3\text{PO}$ pair. Ph_3P **1** and the cation **24** seem to be an adequate pair for the ^{31}P NMR chemical shift calculations too, and we have therefore decided to go forward with the computation, taking into account another aspect – the importance to include the counterion in an ion pair ^{31}P NMR chemical shift calculation. In our case the counterion is *p*-nitrophenolate anion and several ion/anion structural combinations are conceivable for the respective ion pairs. These may include contact pairs such as **26**, in which the phenolate interacts with cation **24** through C-H bond contacts, or actual adducts such as **27**, in which the phenolate is attached to the phosphorus atom through a new bond (*vide* Scheme 2.2)



Scheme 2.2 Different structural variants of ion pair between cation **24** and phenolate.

Molecules of **26** type have ^{31}P NMR chemical shifts in the range of +20 - +40 ppm,^[42] while for the case of **27** the ^{31}P NMR chemical shift is totally different and can amount to -50 – -60 ppm.^[42] Thus, the system can change structure from tetrahedral (**26**-type molecules) to trigonal-bipyramidal (the limit case of **27** if the dihedral angle α (*vide* Scheme 2.2) amounts to zero). Relying on the previously optimized conformations of the cation **24**, a host of probable complexes of both types was constructed, including also one molecule of chloroform, whose position was determined following the electrostatic potential. Fig. 2.13 collects the chemical shifts, relative free energies and magnitudes of distance between phosphorus atom and oxygen atom of phenolate for the ten most stable conformations of the full ion pair and the most important conformations (the largest weight in the Boltzmann averaging) are cross-hatched. One can see that chemical shift values change almost synchronously with the $r(\text{P-O})$ distance and dihedral angle α magnitudes. Fig. 2.14a shows the structures of the four most stable conformations cross-hatched in Fig 2.13. As one can see the global minimum is found to be **26**-type molecule though three other minima are **27**-type.

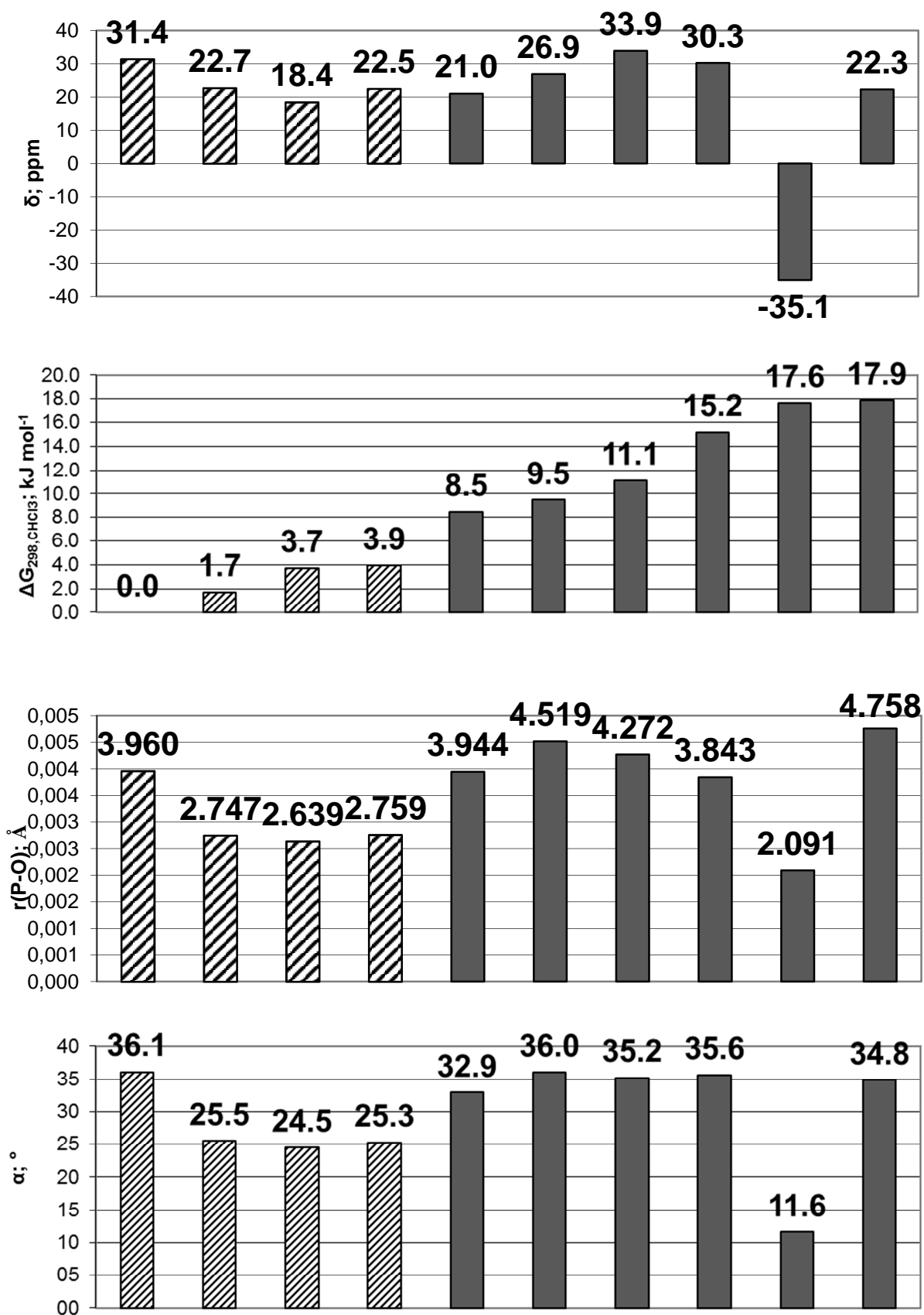


Fig. 2.13 Calculated ³¹P NMR chemical shifts (relative to PPh₃*CHCl₃, GIAO-MPW1K/6-311++G(2d,2p)//MPW1K/6-31G(d) + PCM/UAHF/MPW1K/6-311++G(2d,2p)//MPW1K/6-31G(d) combined with relative free energies (MP2(FC)/6-31+G(2d,p)//MPW1K/6-31G(d) + PCM/UAHF/MPW1K/6-311++G(2d,2p)//MPW1K/6-31G(d), free en. corr.: MPW1K/6-

31G(d); ten most stable conformations), distances between phosphorus atom and oxygen atom of phenolate anion and dihedral angles α (*vide* Scheme 2.2) for different variants of the complex between cation **24**, *p*-nitrophenolate anion and chloroform.

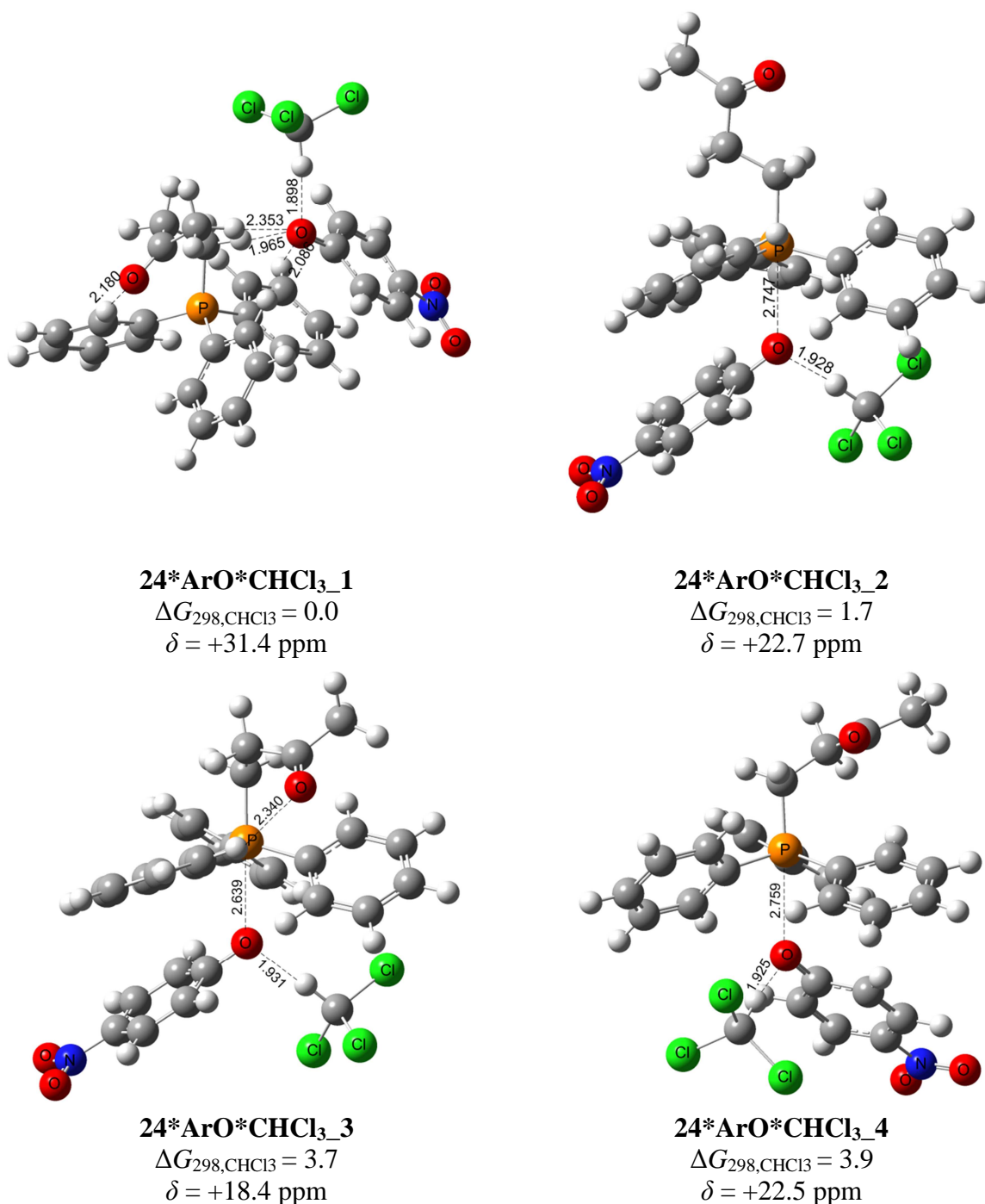


Fig. 2.14a Structures of the four most stable conformations of the complexes between cation **24**, *p*-nitrophenolate anion and chloroform optimized at the MPW1K/6-31G(d), the relative free energies ($\Delta G_{298, \text{CHCl}_3}$) of these four complexes found at the MP2(FC)/6-31+G(2d,p)/MPW1K/6-31G(d) + PCM/UAHF/MPW1K/6-311++G(2d,2p)/MPW1K/6-31G(d) with free en. corr. at the MPW1K/6-31G(d) and ^{31}P NMR chemical shifts (δ) found relative to $\text{PPh}_3^*\text{CHCl}_3$ at the GIAO-MPW1K/6-311++G(2d,2p)/MPW1K/6-31G(d) + PCM/UAHF/MPW1K/6-311++G(2d,2p)/MPW1K/6-31G(d) level.

The tight ion pairs of type **27** ($r(\text{P-O}) \sim 2 \text{ \AA}$), maximally close to the trigonal bipyramid ($\alpha < 12^\circ$) are also found to be minima, but much less stable ($> 17 \text{ kJ mol}^{-1}$ less stable than global minimum). The structures of the most stable such complexes are shown in Fig. 2.14b.

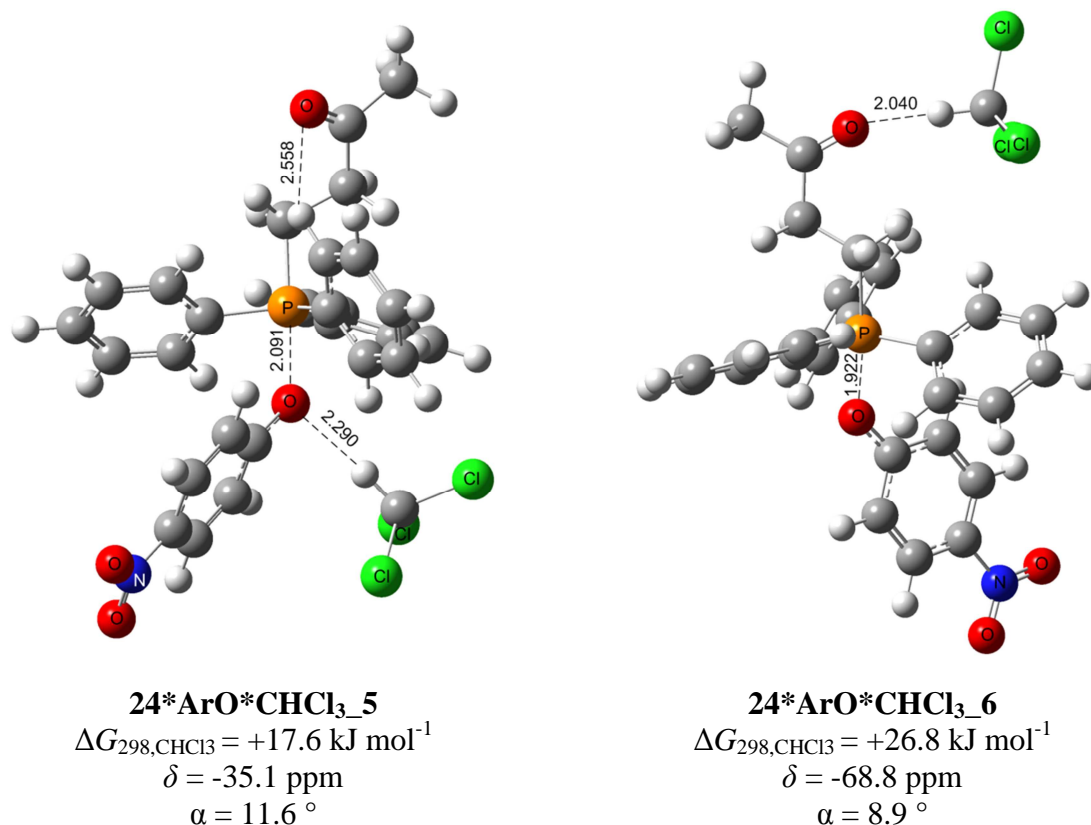


Fig. 2.14b Structure of the most stable **27**-type tight complexes between cation **24**, *p*-nitrophenolate anion and chloroform (MPW1K/6-31G(d)); the relative to global minimum **24*ArO*CHCl₃_1** free energy ($\Delta G_{298, \text{CHCl}_3}$) found at the MP2(FC)/6-31+G(2d,p)//MPW1K/6-31G(d) + PCM/UAHF/MPW1K/6-311++G(2d,2p)//MPW1K/6-31G(d), free en. corr.: MPW1K/6-31G(d) level of theory and ^{31}P NMR chemical shift (δ) found relative to $\text{PPh}_3 \cdot \text{CHCl}_3$ at GIAO-MPW1K/6-311++G(2d,2p) + PCM/UAHF/MPW1K/6-311++G(2d,2p) level.

As compared to **24*ArO*CHCl₃_2** (Fig. 2.14a) there is a dramatic change in chemical shift value. One can also see that the CHCl_3 molecule forms hydrogen bonds differently in these 3 complexes. In **24*ArO*CHCl₃_2** and **24*ArO*CHCl₃_5** CHCl_3 forms a hydrogen bond with the phenolate oxygen of 1.928 Å and 2.290 Å length respectively. In **24*ArO*CHCl₃_6** the CHCl_3 changes its position forming a hydrogen bond with the carbonyl oxygen atom (2.040 Å). Thus, with moving the CHCl_3 molecule away from the phenolate oxygen atom, the P-B distances, the out-of-plane angles α , ^{31}P NMR chemical shifts and relative stability are decreasing sharply. The geometric and energetic data together with ^{31}P NMR chemical shifts for all discussed complexes are collected in the Table 2.7, each of the complexes is assigned

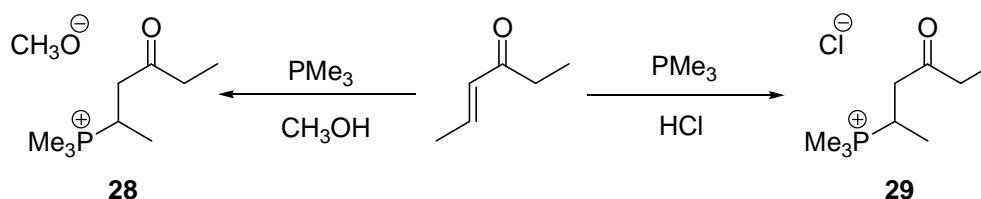
to the **26** or **27** type in accordance with the Scheme 2.2. One can see the “out-of-plane” angle α and P-O distance changes going from the tetrahedral complex to the trigonal bipyramid and the sharp jumps in the ^{31}P NMR chemical shift values.

Table 2.7 Geometric, energetic and ^{31}P NMR chemical shift data for 6 complexes between cation **24**, p-nitrophenolate anion and chloroform.

Name	r(P-O), Å ^a	α , ° ^b	δ , ppm ^c	$\Delta G_{298, \text{CHCl}_3}$, kJ mol ⁻¹ ^d	Type ^e
24*ArO*CHCl3_1	3.960	36.1	+31.4	0.0	26
24*ArO*CHCl3_2	2.747	25.5	+22.7	1.7	27
24*ArO*CHCl3_3	2.639	24.5	+18.4	3.7	27
24*ArO*CHCl3_4	2.759	25.3	+22.5	3.9	27
24*ArO*CHCl3_5	2.091	11.6	-35.1	17.6	27
24*ArO*CHCl3_6	1.922	8.9	-68.8	26.8	27

^a Distance between phosphorus atom and oxygen atom of phenolate anion. ^b dihedral angle in accordance with the Scheme 2.2. ^c calculated relative to $\text{PPh}_3^+\text{CHCl}_3$ at GIAO-MPW1K/6-311++G(2d,2p) + PCM/UAHF/MPW1K/6-311++G(2d,2p) level. ^d MP2(FC)/6-31+G(2d,p)//MPW1K/6-31G(d) + PCM/UAHF/MPW1K/6-311++G(2d,2p)//MPW1K/6-31G(d), free en. corr.: MPW1K/6-31G(d). ^e in accordance with the Scheme 2.2.

The final step of the ^{31}P NMR chemical shift computation is Boltzmann averaging using all found minima in this case yielding a ^{31}P NMR chemical shift value of +26.6 ppm. This result is quite interesting, since it is only 0.9 ppm higher than the experimental result of +25.7 ppm. It should be emphasized, that the Boltzmann averaging is obligatory and involving only the global minimum is not enough, since the global minimum is calculated to have a ^{31}P NMR chemical shift of +31.4 ppm being quite far away from the experimental value. Toste *et al.* have detected for the phosphonium salts **28** and **29** (Scheme 2.3) the ^{31}P NMR chemical shift of +33 ppm.^[3b]

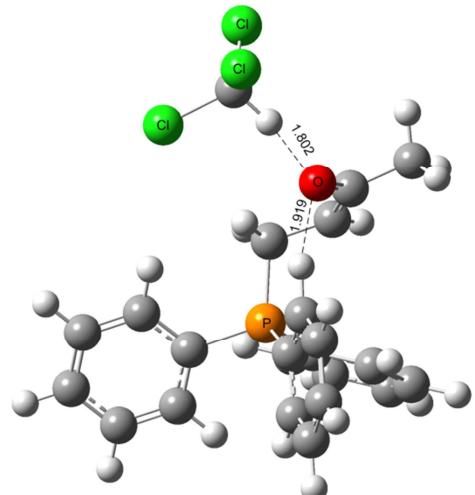
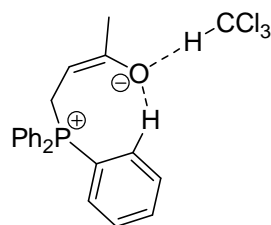


Scheme 2.3 Formation of phosphonium salt studied by Toste *et al.*

The latter coincides with the global minimum found in the present work (**24*ArO*CHCl3_1**, +31.4 ppm) and other less stable minima (*vide* Fig. 2.13). Hypothetically, for the system studied by Toste *et al.*, the complexes with interaction between phosphorus atom and counterion via formation of trigonal-bipyramidal complexes of **27** are less stable and do not play a substantial role in the Boltzmann-averaging.

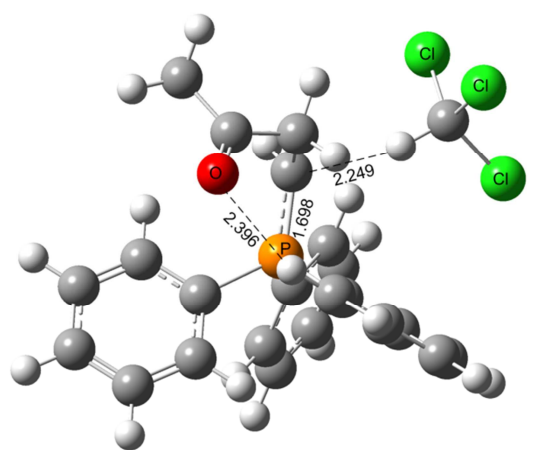
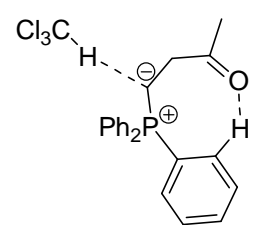
In accordance with Scheme 2.1 the cation **24** is in equilibrium with the zwitterionic intermediate **23** and ylid **25**. Since the ^{31}P NMR chemical shift computational scheme is efficient for **24**, the calculations have been extended to systems **23** and **25**. Results of application of the solution model 2 to **23** and **25** are presented in Tables 2.8 and 2.9 respectively. The Boltzmann-averaged chemical shifts for system **23** amounts to +22.6 ppm and for system **25** to +25.8 ppm.

Table 2.8 Calculated relative free energies and chemical shifts for 4 individual conformations of the solute*solvent complexes of **23** with CHCl_3 and the structure of the most stable complex.

	$\Delta G_{298, \text{CHCl}_3}^a / \text{kJ mol}^{-1}$	δ^b / ppm
	0.0	+23.4
	3.5	+19.3
	18.7	+1.9
	29.7	-7.1
		$\langle \delta \rangle = +22.6$

^a MP2(FC)/6-31+G(2d,p)//MPW1K/6-31G(d) + PCM/UAHF/MPW1K/6-311++G(2d,2p)//MPW1K/6-31G(d), free en. corr.: MPW1K/6-31G(d). ^b Relative to $\text{PPh}_3 \cdot \text{CHCl}_3$, GIAO-MPW1K/6-311++G(2d,2p)//MPW1K/6-31G(d) + PCM/UAHF/MPW1K/6-311++G(2d,2p)//MPW1K/6-31G(d).

Table 2.9 Calculated relative free energies and chemical shifts for 12 individual conformations of the solute*solvent complexes of **25** with CHCl_3 and the structure of the most stable complex.

	$\Delta G_{298, \text{CHCl}_3}^a / \text{kJ mol}^{-1}$	δ^b / ppm
	0.0	+25.0
	1.9	+27.8
	4.9	+27.9
	7.0	+23.1
	8.7	+24.7
	8.7	+25.1
	8.8	+25.0
	10.7	+21.1
	12.2	+23.4
	12.6	+23.7
	22.0	+22.3
	24.7	+20.5
		$\langle \delta \rangle = +25.8$

^a MP2(FC)/6-31+G(2d,p)//MPW1K/6-31G(d) + PCM/UAHF/MPW1K/6-311++G(2d,2p)//MPW1K/6-31G(d), free en. corr.: MPW1K/6-31G(d). ^b Relative to PPh₃*CHCl₃, GIAO-MPW1K/6-311++G(2d,2p)//MPW1K/6-31G(d) + PCM/UAHF/MPW1K/6-311++G(2d,2p)//MPW1K/6-31G(d).

Addition of the phenolate anion into calculation of the ³¹P NMR chemical shift for the system **24** changes the calculated value of the shift substantially. In the experiment the presence of phenol is also necessary to detect the chemical shift of +25.7 ppm.^[41] It has also been found, that geometries and energies of the MBH reaction intermediates are strongly influenced by the intermolecular interactions with the phenol, this will be in detail discussed in the following chapters of this work. In order to take into account the mentioned observations, the systems **23** and **25** have been recalculated considering the phenol molecule in the same way as it has been done for the cation **24**. The structures of the most stable conformations for both systems **23** and **25** are shown in Fig.2.15. The consideration of the phenol molecule leads to very different values of the chemical shifts as compared to the model, where phenol is neglected. The Boltzmann-averaged ³¹P NMR chemical shift for the phenol/chloroform complex with system **23** amounts to -12.0 ppm and for the system **25** to +34.3 ppm. The shift values are very different compared to those obtained by neglecting the phenol molecule, thus the influence of phenol on the geometries and related properties (e.g. ³¹P NMR) is dramatic.

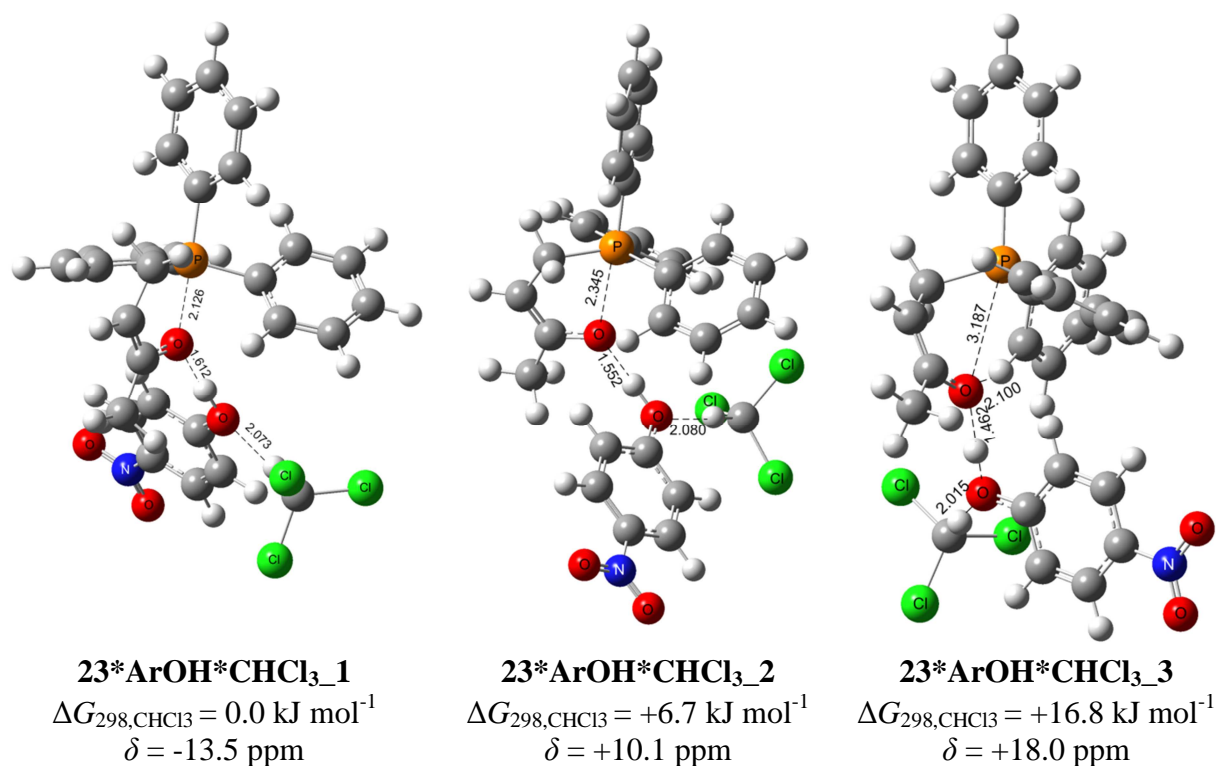


Fig. 2.15a Structures of the three most stable conformations of the complexes between **23**, *p*-nitrophenol and chloroform optimized at the MPW1K/6-31G(d), the relative free energies

($\Delta G_{298, \text{CHCl}_3}$) of these four complexes found at the MP2(FC)/6-31+G(2d,p)//MPW1K/6-31G(d) + PCM/UAHF/MPW1K/6-311++G(2d,2p)//MPW1K/6-31G(d) with free en. corr. at the MPW1K/6-31G(d) and ^{31}P NMR chemical shifts (δ) found relative to $\text{PPh}_3^*\text{CHCl}_3$ at the GIAO-MPW1K/6-311++G(2d,2p)//MPW1K/6-31G(d) + PCM/UAHF/MPW1K/6-311++G(2d,2p)//MPW1K/6-31G(d) level.

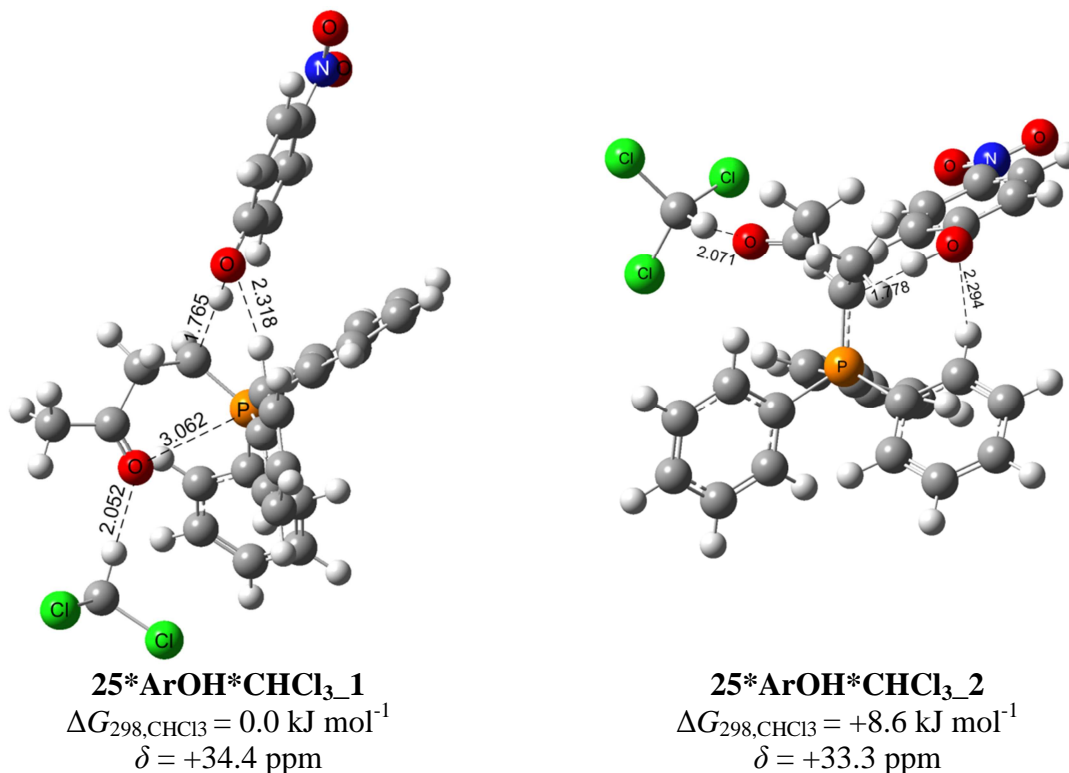


Fig. 2.15b Structures of the two most stable conformations of the complexes between **25**, *p*-nitrophenol and chloroform optimized at the MPW1K/6-31G(d), the relative free energies ($\Delta G_{298, \text{CHCl}_3}$) of these four complexes found at the MP2(FC)/6-31+G(2d,p)//MPW1K/6-31G(d) + PCM/UAHF/MPW1K/6-311++G(2d,2p)//MPW1K/6-31G(d) with free en. corr. at the MPW1K/6-31G(d) and ^{31}P NMR chemical shifts (δ) found relative to $\text{PPh}_3^*\text{CHCl}_3$ at the GIAO-MPW1K/6-311++G(2d,2p)//MPW1K/6-31G(d) + PCM/UAHF/MPW1K/6-311++G(2d,2p)//MPW1K/6-31G(d) level.

Finally there are three values of ^{31}P NMR chemical shifts for the three studied systems: +26.6 ppm for the phosphonium salt **24*ArO*CHCl₃**, -12.0 ppm for the zwitterionic intermediate **23*ArOH*CHCl₃** and +34.3 ppm for the ylid **25*ArOH*CHCl₃**. A comparison of these three values suggests that the experimentally detected +25.7 ppm ^{31}P NMR chemical shift should belong to the phosphonium salt **24*ArO*CHCl₃**. But a question arises: Why is in the experiment only the shift of +26.6 ppm detected and no signals for systems **23** and **25**? In Fig. 2.16 the relative free energies are shown for all three systems (the best conformations are taken).

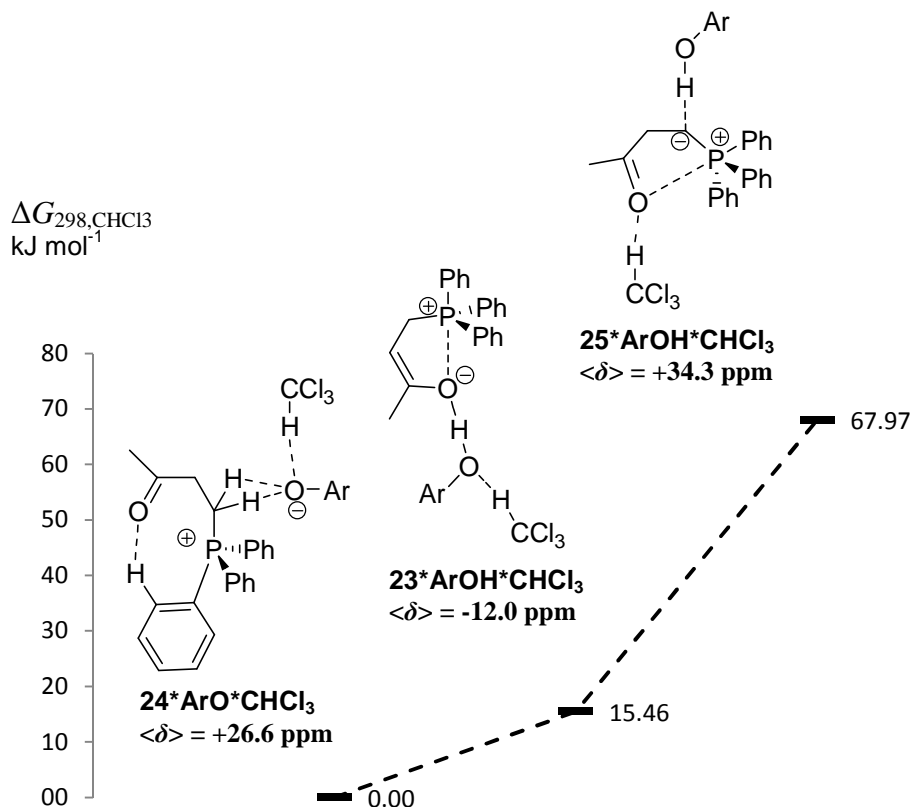
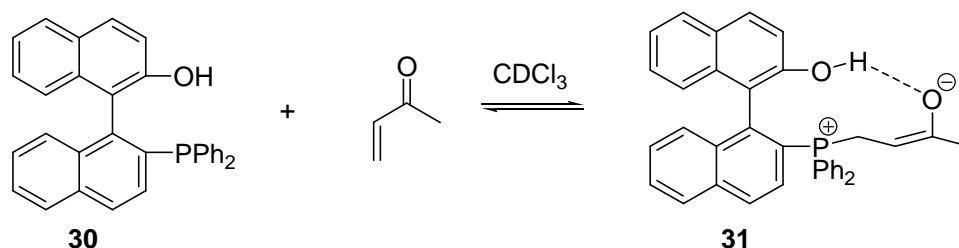


Fig. 2.16. Comparison of the relative free energies $\Delta G_{298, \text{CHCl}_3}$ for the systems **24*ArO*CHCl₃**, **23*ArOH*CHCl₃** and **25*ArOH*CHCl₃**, the relative free energies ($\Delta G_{298, \text{CHCl}_3}$) of these four complexes found at the MP2(FC)/6-31+G(2d,p)//MPW1K/6-31G(d) + PCM/UAHF/MPW1K/6-311++G(2d,2p)//MPW1K/6-31G(d) level with free en. corr. at the MPW1K/6-31G(d).

Easy to see, that ³¹P NMR detection of only system **24** correlates with the stability of this system as compared to the zwitterionic and the ylid intermediates. The protonated intermediate complex is substantially more stable than the zwitterionic intermediate (+15 kJ mol⁻¹) and the ylid (+68 kJ mol⁻¹). Shi *et al.* have studied the reaction between MVK and Lewis base **30** (Scheme 2.4).^[43]

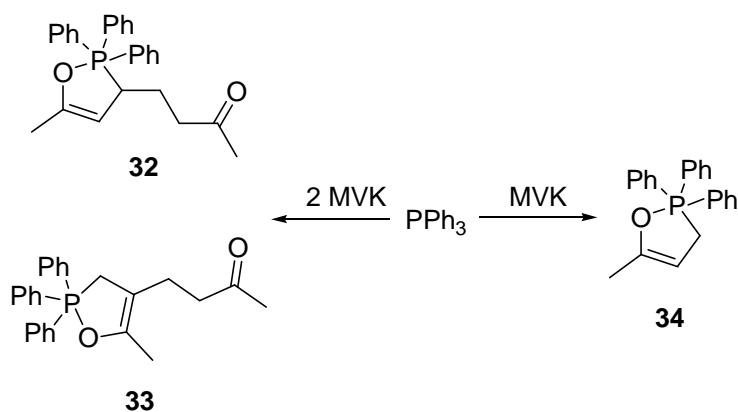


Scheme 2.4 Formation of the zwitterionic intermediate **31** from MVK and Lewis base **30** suggested by Shi *et al.*^[43]

A ³¹P NMR signal at +25.3 ppm has been detected and “believed to correspond to” the zwitterionic intermediate **31**. Noteworthy to say, that we also have found conformations of the

system **23***ArOH*CHCl₃ with ³¹P NMR chemical shifts in the range of 24 – 26 ppm, but these complexes are more than 20 kJ mol⁻¹ less stable as compared to the global minimum **23***ArOH*CHCl₃_1 shown in Fig. 2.15a. Finally, one can state that for the system in the present study the +25.5 ppm (experimental detection by Liu^[41]) and +26.6 ppm (the calculations) correspond to the protonated intermediate and not to the ylid or zwitterionic intermediate.

Additional questions may arise for the group of signals at around -60 ppm, which accompany the signals of Ph₃P and Ph₃PO in the reaction of PPh₃ and MVK in CDCl₃ in the absence of phenol.^[41] ³¹P NMR signals at -60 ppm are known to belong to pentavalent phosphorus compounds and relying on that fact one can suggest a cyclic form of the PPh₃*MVK adduct (or PPh₃*2MVK adduct) as it is shown in Scheme 2.5.



Scheme 2.5. Formation of cyclic adducts between PPh₃ and MVK.

the most simple variant of the PPh₃ adduct with one molecule of MVK **34** will be discussed here. In Fig. 2.17 two possible structures are shown together with relative free energies and ³¹P NMR chemical shifts as calculated with solution model 2. Both structures are trigonal bipyramids. One of the axial positions is occupied by the oxygen atom (as well as in the structures of type **27** discussed before). The latter is the normal situation of the most electronegative elements being axial in the trigonal bipyramids.^[44] The second axial and both equatorial positions are occupied by phenyl rings.

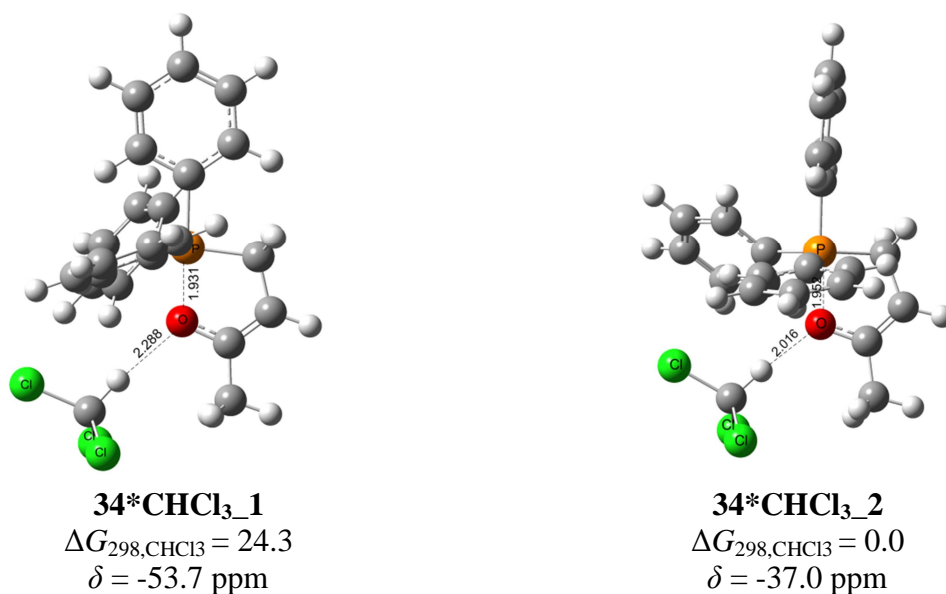


Fig. 2.17 Structures of two possible conformations of the cyclic adduct between one molecule of PPh₃ and one molecule of MVK (MPW1K/6-31G(d)). The relative free energies of these two adducts (MP2(FC)/6-31+G(2d,p)//MPW1K/6-31G(d) + PCM/UAHF/MPW1K/6-311++G(2d,2p)//MPW1K/6-31G(d), free en. corr.: MPW1K/6-31G(d)) and ³¹P NMR chemical shifts (relative to PPh₃*CHCl₃, GIAO-MPW1K/6-311++G(2d,2p)//MPW1K/6-31G(d) + PCM/UAHF/MPW1K/6-311++G(2d,2p)//MPW1K/6-31G(d)).

The first structure has a chemical shift of -53.7 ppm, which is much closer to the experimental result than the shift of the second structure at -37.0 ppm, though this second structure is found to be significantly more stable than the first one. The geometries of the both complexes differ mostly in two factors:

1. the co-orientation of the axial phenyl ring and MVK moiety: for the first complex it locates in one plane with the MVK moiety (which forms here also a planar structure) and for the second complex the plane of the axial phenyl ring is rotated and the MVK moiety is not planar anymore;
2. the length of the hydrogen bond between the chloroform molecule and the oxygen atom of the MVK moiety is longer in adduct **34*CHCl₃_2** at 2.288 Å than in adduct **34*CHCl₃_1** at 2.016 Å. The shorter this bond is, the weaker is the intramolecular interaction between the oxygen and phosphorus atom and the more positive is the ³¹P NMR chemical shift. Thus in the first complex $r(\text{P-O}) = 1.931$ Å and in the second one $r(\text{P-O}) = 1.952$ Å and this lengthening leads to a big change of 16.7 ppm ³¹P NMR chemical shift increase.

The application of the solution model 1 to the both structures (without explicit molecule of the solvent) leads to the ³¹P NMR chemical shifts of -64.4 ppm and -44.8 ppm, which are now closer to the experimental evidence. The presence of more than one signal in the area of -60

ppm can be explained by formation of adducts between PPh_3 and two molecules of MVK (Scheme 2.3). Both systems **32** and **33** are found to have ^{31}P NMR chemical shift values close to the values for system **34**.

2.2.3. Conclusions

1. ^{31}P NMR chemical shift calculations of the MBH reaction intermediates (protonated intermediate, zwitterionic intermediate and ylid) have been performed in accordance with the suggested computational scheme (solution model 2). The protonated intermediate is found to be the most preferable. The ^{31}P NMR chemical shift of this protonated intermediate is in a good accordance with the experimentally measured chemical shift. A model of co-behaviour between catalyst, co-catalyst, Michael acceptor and solvent during the side reaction of the protonated intermediate formation is suggested.
2. A group of signals at around -60 ppm found experimentally for the mixture of PPh_3 , MVK and PNP can be assigned to different cyclic adducts between molecules of MVK and PPh_3 .

2.3. References

- [1] a) D. Basavaiah, A. J. Rao, T. Satyanarayana, *Chem. Rev.* **2003**, *103*, 811-891; b) V. Singh, S. Batra, *Tetrahedron* **2008**, *64*, 4511-4574; c) D. Basavaiah, K. V. Rao, R. Reddy, *J. Chem. Soc. Rev.* **2007**, *36*, 1581; d) P. Langer, *Angew. Chem.* **2000**, *112*, 3177; e) P. Langer, *Angew. Chem. Int. Ed.* **2000**, *39*, 3041-3051; f) Y.-L. Shi, M. Shi, *Eur. J. Org. Chem.* **2007**, 2905.
- [2] a) C. E. Aroyan, A. Dermenci, S. J. Miller, *Tetrahedron* **2009**, *65*, 4069; b) S. A. Frank, D. J. Mergott, W. R. Roush, *J. Am. Chem. Soc.* **2002**, *124*, 2404; c) L.-C.-. Wang, A. L. Luis, K. Agapiou, H.-Y. Jang, M. J. Krische, *J. Am. Chem. Soc.* **2002**, *124*, 2402.
- [3] a) C. Faltin, E. M. Fleming, S. J. Connon, *J. Org. Chem* **2004**, *69*, 6496; b) I. C. Stewart, R. G. Bergman, F. D. Toste, *J. Am. Chem. Soc.* **2003**, *125*, 8696-8697.
- [4] a) E. Vedejs, O. Daugulis, L. A. Harper, M. J. A., D. R. Powell, *J. Org. Chem* **2003**, *68*, 5020; b) E. Vedejs, O. Daugulis, N. Tuttle, *J. Org. Chem* **2004**, *69*, 1389; c) J. A. MacKay, E. Vedejs, *J. Org. Chem* **2004**, *69*; d) J. A. MacKay, E. Vedejs, *J. Org. Chem* **2006**, *71*, 498.
- [5] a) Y. Wei, G. N. Sastry, H. Zipse, *J. Am. Chem. Soc.* **2008**, *130*, 3473; b) Y. Wei, T. Singer, H. Mayr, G. N. Sastry, H. Zipse, *J. Comput. Chem.* **2008**, *29*, 291-297; c) Y. Wei, B. Sateesh, B. Maryasin, G. N. Sastry, H. Zipse, *J. Comput. Chem.* **2009**, 2617 - 2624.
- [6] a) M. Baidya, S. Kobayashi, F. Brotzel, U. Schmidhammer, E. Riedle, H. Mayr, *Angew. Chem. Int. Ed.* **2007**, *46*, 6176; b) T. B. Phan, M. Breugst, H. Mayr, *Angew. Chem. Int. Ed.* **2006**, *45*, 3869; c) B. Kempf, H. Mayr, *Chem. - Eur. J.* **2005**, *11*, 917.
- [7] a) X.-F. Zhu, C. E. Henry, O. Kwon, *J. Am. Chem. Soc.* **2007**, *129*, 6722; b) J.-Y. Wu, Z.-B. Luo, L.-X. Dai, X.-L. Hou, *J. Org. Chem* **2008**, *73*, 9137; c) A. A. Ibrahim, G. D. Harzmann, N. J. Kerrigan, *J. Org. Chem* **2009**, *74*, 1777; d) E. Vedejs, S. T. Diver, *J. Am. Chem. Soc.* **1993**, *115*, 3358.
- [8] J. Gauss, *Ber. Bunsen-Ges. Phys. Chem.* **1995**, *99*, 1001.
- [9] a) T. Ziegler, *Chem. Rev.* **1991**, *91*, 651; b) P. Hohenberg, W. Kohn, *Phys. Rev. B* **1964**, *136*, 864; c) G. Vignale, M. Rasolt, D. J. W. Geldard, *Adv. Quantum Chem.* **1990**, *21*, 235; d) A. M. Lee, N. C. Handy, S. M. Colwell, *J. Chem. Phys.* **1995**, *103*, 10095; e) V. G. Malkin, O. L. Malkina, M. E. Casida, D. R. Salahub, *J. Am. Chem. Soc.* **1994**, *116*, 5898; f) V. G. Malkin, O. L. Malkina, D. R. Salahub, *Chem. Phys. Lett.* **1993**, *204*, 80; g) V. G. Malkin, O. L. Malkina, D. R. Salahub, *Chem. Phys. Lett.*

- 1993, 204, 87; h) W. Kutzelnigg, U. Fleischer, M. Schindler, *Vol. 23*, Springer, Berlin, 1990; i) G. Schreckenbach, T. Ziegler, *Theor. Chem. Acc.* **1998**, 99, 71; j) G. Schreckenbach, T. Ziegler, *J. Phys. Chem.* **1995**, 99, 606; k) G. Rauhut, S. Puyear, K. Wolinski, P. Pulay, *J. Phys. Chem.* **1996**, 100, 6310; l) J. R. Cheeseman, G. W. Trucks, T. A. Keith, M. J. Frisch, *J. Chem. Phys.* **1996**, 104, 5497; m) P. J. Wilson, R. D. Amos, N. C. Handy, *Mol. Phys.* **1999**, 97, 757; n) C. van Wüllen, *Phys. Chem. Chem. Phys.* **2000**, 2, 2137; o) S. T. Epstein, *J. Chem. Phys.* **1973**, 58, 1592; p) M. Schindler, W. Kutzelnigg, *J. Chem. Phys.* **1982**, 76, 1919; q) R. Dietchfield, *J. Chem. Phys.* **1972**, 56, 5688; r) A. E. Hansen, T. D. Bouman, *J. Chem. Phys.* **1985**, 82, 5035; s) T. A. Keith, R. W. F. Bader, *Chem. Phys. Lett.* **1993**, 210, 223; t) T. M. Alam, *Int. J. Mol. Sci.* **2002**, 3, 888; u) K. A. Chernyshev, L. B. Krivdin, *Russ. J. Org. Chem. (Transl. of Zh. Org. Khim.)* **2010**, 46, 785; v) M. Rezaei-Sameti, *THEOCHEM* **2008**, 867, 122; w) J. Přecechtělova, P. Novák, M. L. Munzarová, M. Kaupp, Sklenář, *J. Am. Chem. Soc.* **2010**, 132, 17139; x) S. G. Smith, J. M. Goodman, *J. Am. Chem. Soc.* **2010**, 1132, 12946; y) P. R. Rablen, S. A. Pearlman, J. Finkbiner, *J. Phys. Chem. A* **1999**, 103, 7357.
- [10] a) M. Kaupp, M. Bühl, V. G. Malkin, Wiley, Weinheim, **2004**; b) U. Mayer, V. Gutmann, W. Gerger, *Monatsch. Chem.* **1975**, 106, 1235; c) V. Gutmann, *Electrochim. Acta* **1976**, 21, 661; d) J. L. Cook, C. A. Hunter, C. M. R. Low, A. Perez-Velasco, J. G. Vinter, *Angew. Chem.* **2007**, 119, 3780; e) J. L. Cook, C. A. Hunter, C. M. R. Low, A. Perez-Velasco, J. G. Vinter, *Angew. Chem. Int. Ed.* **2008**, 47, 6275.
- [11] J. Schraml, M. Čapka, V. Blechta, *Magn. Reson. Chem.* **1992**, 30, 544.
- [12] W.-N. Chou, M. Pomerantz, *J. Org. Chem* **1991**, 56, 2762.
- [13] K. L. McKillop, G. R. Gillette, D. R. Powell, R. West, *J. Am. Chem. Soc.* **1992**, 114, 5203.
- [14] B. J. Lynch, P. L. Fast, M. Harris, D. G. Truhlar, *J. Phys. Chem. A* **2000**, 100, 4811.
- [15] D. Roy, R. B. Sunoj, *Org. Lett.* **2007**, 9, 4873-4876.
- [16] K. A. Al-Farhan, *J. Crystallogr. Spectrosc. Res.* **1992**, 22, 687.
- [17] a) V. A. Naumov, T. s. M. A., A. V. Naumov, D. Y. Shorokhov, S. Samdal, *Russ. J. Gen. Chem.* **2001**, 71, 1225; b) B. J. Dunne, A. G. Orpen, *Acta Crystallogr., Sect. C: Cryst. Struct. Commun.* **1991**, 47, 345.
- [18] a) K. W. Wiberg, *J. Comput. Chem* **2004**, 25, 1342; b) A. Y. Li, S. W. Wang, *THEOCHEM* **2007**, 807, 191; c) R. Cuypers, B. Burghof, A. T. Marcelis, E. S. R. Sudhölter, A. B. de Haan, H. Zuilhof, *J. Phys. Chem. A* **2008**, 112, 11714.

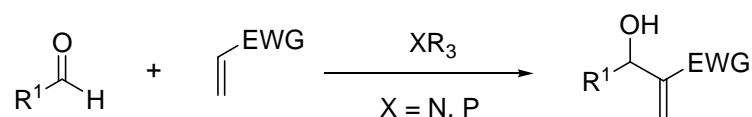
- [19] C. A. Jaska, T. J. Clark, S. B. Clendenning, D. Grozea, A. Turak, Z.-H. Lu, I. Manners, *J. Am. Chem. Soc.* **2005**, *127*, 5116.
- [20] M. Alajarin, P. Molina, A. Vidal, F. Tovar, *Tetrahedron* **1997**, *53*, 13449.
- [21] N. Zumbulyadis, B. P. Dailey, *Mol. Phys.* **1974**, *27*, 633.
- [22] a) C. J. Jameson, A. C. de Dios, A. K. Jameson, *Chem. Phys. Lett.* **1991**, *95*, 9042; b) C. J. Jameson, A. C. de Dios, *Chem. Phys. Lett.* **1990**, *167*, 575.
- [23] C. G. Hrib, F. Ruthe, E. Seppälä, M. Bätcher, C. Druckenbrodt, C. Wismach, P. G. Jones, W.-W. du Mont, V. Lippolis, F. A. Devillanova, M. Bühl, *Eur. J. Inorg. Chem.* **2007**, 4693.
- [24] J. R. Lloyd, N. Lowther, G. Zsabo, D. Hall, *J. Chem. Soc., Perkin Trans. 2* **1985**, 1813.
- [25] a) K. Kirk, P. W. Kuchel, *Biochemistry* **1988**, *27*, 8803; b) T. K. Miyamoto, Y. Suzuki, H. Ichida, *Bull. Chem. Soc. Jpn.* **1992**, *65*, 3386.
- [26] R. Streck, A. J. Barnes, *Spectrochim. Acta, Part A* **1999**, *55*, 1049.
- [27] M. Driess, C. Monsé, R. Boese, D. Bläser, *Angew. Chem.* **1998**, *110*, 2389.
- [28] E. Moser, E. O. Fischer, W. Bathelt, W. Gretner, L. Knauss, E. Louis, *J. Organomet. Chem.* **1969**, *19*, 377.
- [29] R. E. Wasylishen, N. Burford, *Can. J. Chem.* **1987**, *65*, 2707.
- [30] S. O. Grim, W. McFarlane, E. F. Davidoff, T. J. Marks, *J. Phys. Chem.* **1966**, *70*, 581.
- [31] W. K. Seok, L. J. Zhang, *Bull. Korean Chem. Soc.* **2009**, *30*, 2461.
- [32] G. Heckmann, E. Fluck, *Mol. Phys.* **1972**, *23*, 175.
- [33] J. Raymond, W. Klemperer, *J. Chem. Phys.* **1971**, *55*, 232.
- [34] a) T. Mourik, V. I. Danilov, V. V. Dalidonis, N. Kurtia, H. Wakabayashi, T. Tsukamoto, *Theor. Chem. Acc.* **2010**, *125*, 233; b) *The significantly different slope parameters of 0.855 (Fig. 2.6) and 0.870 (Fig. 2.7) as compared to the slope parameter in the gas-phase studies of 0.929 (Fig. 2.5) are due to the smaller range of chemical shifts considered in the solution studies.*
- [35] M. V. Rao, C. B. Reese, Z. Zhengyun, *Tetrahedron Lett.* **1992**, *33*, 4839.
- [36] L. K. Krannich, R. K. Kanjolia, C. L. Watkins, *Magn. Reson. Chem.* **1987**, *25*, 320.
- [37] A. Hinke, W. Kuchen, *Chem. Ber.* **1983**, *116*, 3003.
- [38] D. B. Denney, D. Z. Denney, P. J. Hammond, C. Huang, L.-T. Liu, K.-S. Tseng, *Phosphorus Sulfur* **1983**, *15*, 281.
- [39] T. Costa, H. Schmidbaur, *Chem. Ber.* **1982**, *115*, 1374.
- [40] R. B. King, P. M. Sundaram, *J. Org. Chem.* **1984**, *49*, 1784.

- [41] Y. Liu, PhD thesis, Ludwig-Maximilians-Universität München (München), **2011**.
- [42] J. C. Tebby, *Handbook of Phosphorus-31 Nuclear Magnetic Resonance Data*, CRC-Press, Boca Raton, **1991**.
- [43] M. Shi, L. H. Chen, C.-Q. Li, *J. Am. Chem. Soc.* **2005**, *127*, 3790-3800.
- [44] R. R. Holmes, in *Progress in Inorganic Chemistry*, Vol. 32 (Ed.: J. W. a. Sons), New York, **1984**, pp. 119-235.

3. The Catalytic Cycle of the Morita-Baylis-Hillman Reaction

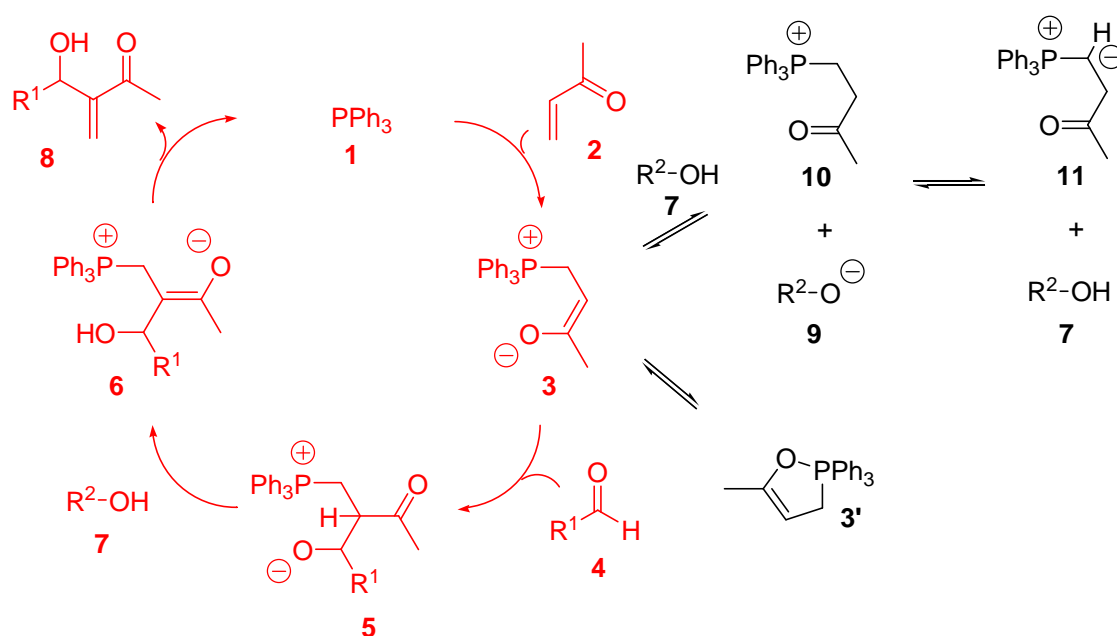
3.1. Introduction

The Morita-Baylis-Hillman (MBH) reaction is a generally useful synthetic method for the construction of densely functionalized products from two simple building blocks, an aldehyde and an acceptor-substituted alkene (Scheme 3.1).^[1]



Scheme 3.1. The MBH reaction.

The mechanism of this reaction has recently been found to be quite variable, depending on the particular nature of the reactants, the catalysts and the solvent used. The reaction is efficiently catalyzed by N- and P-based nucleophiles, and proceeds particularly well in the presence of protic solvents or co-catalysts. Recent spectroscopic, kinetic, and theoretical studies suggest that, under these conditions, the reaction follows the mechanism outlined in Scheme 3.2 shown here using the PPh_3 -catalyzed reaction of methylvinylketone (MVK, **2**) as an example. The regular catalytic cycle is marked in red color, while the side reactions are shown in black

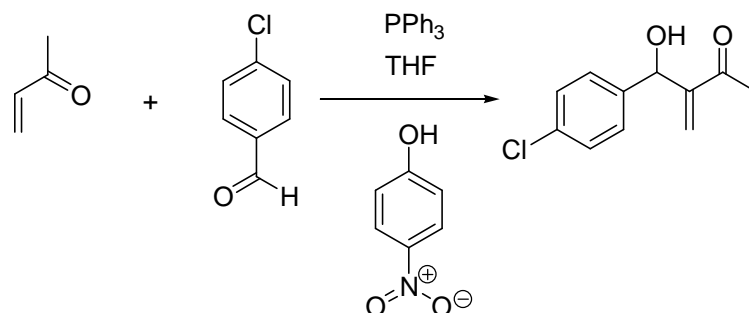


Scheme 3.2. The catalytic cycle and possible side processes of the PPh_3 (**1**) catalyzed MBH reaction with participation of protic co-catalyst **7**.

In this mechanism the phosphine catalyst **1** is expected to add to the Michael acceptor **2** in a rapid and reversible manner, forming zwitterionic adduct **3** as the first transient intermediate. This is followed by nucleophilic addition to aldehyde **4**, yielding a second zwitterionic intermediate **5** as the product. Subsequent hydrogen transfer within intermediate **5** to yield enolate zwitterion **6** is considered to be rate-limiting for many systems and is catalyzed by protic co-catalysts or solvents R^2-OH **7**. The catalytic cycle is completed by elimination of the phosphine catalyst **1** and generation of the MBH product **8**. Excellent computational studies have been published recently on the MBH reaction mechanism.^[2] In spite of the fact that the mechanism shown in Scheme 3.2 is widely accepted for the MBH reaction, there are still open questions. One of these questions is related to the choice of the system to study and the applied theoretical level – while some of the studies operate with small model systems like NMe_3 or PMe_3 (as a catalyst)^[2a, 2c-e, 2h, 2i] using Density Functional Theory (DFT) and only for some minor cases *ab initio* approaches, others consider situations of more frequently applied catalysts in the experimental studies, such as DABCO^[2b, 2g] or N-methylprolinol,^[2f] but using only DFT for the reaction profiles. If one goes to large systems, the problem of a large conformational space for every intermediate or transition state arises, hence a careful search of conformers is necessary for the MBH reaction mechanism, though in combination with expensive theory it makes the calculations especially difficult. In the present work a computational study for a system^[3] composed of PPh_3 as the catalyst, *p*-nitrophenol (PNP) as the co-catalyst, MVK as the Michael acceptor and *p*-chlorobenzaldehyde in THF has been performed. From the side of the level of theory, a combination of single point calculations using second order Møller-Plesset perturbation theory with frozen core approximation (MP2(FC)) and DFT in the variant of MPW1K hybrid functional for geometries and thermal corrections has been applied.

Another noteworthy question considers side reactions which can break the cycle and thus influence the whole processes. Some possible side reactions are shown in Scheme 3.2 in black color. Among these side reactions the protonation of zwitterionic intermediates from the catalytic cycle is especially important, because protonated intermediates can be experimentally detected. In chapter 2 the validity of calculations to explain the ^{31}P NMR chemical shifts of experimentally detected intermediates has been tested. The problem of protonation side reaction will be touched in this chapter 3 again and in detail in the next chapter 4.

3.2. Choice of the Methods



Scheme 3.3 The PPh₃ – catalyzed MBH reaction between MVK and p-chlorobenzaldehyde in THF using PNP as co-catalyst.

The overall process studied here is shown in Scheme 3.3. The geometries of all systems have been optimized at the MPW1K/6-31+G(d) level of theory. The thermal corrections to Gibbs free energies G_{298} and enthalpies H_{298} at 298.15 K have been calculated for all stationary points from unscaled vibrational frequencies obtained at the MPW1K/6-31+G(d) level. The thermal corrections have been combined with single point energies calculated at the MP2(FC)/6-31+G(2d,p)//MPW1K/6-31+G(d) level to yield Gibbs free energies G_{298} and enthalpies H_{298} at 298.15 K. Additional consideration of solvation effects as single point calculations using gas-phase geometries at the PCM/UAHF/RHF/6-31G(d)//MPW1K/6-31+G(d) has been performed.

The choice of the MP2(FC)/6-31+G(2d,p) level for single point calculations is motivated by previously published accurate predictions of thermochemical data of a large set of N- and P-based Lewis bases^[4]. Addition of a solvent model seems to be very important inasmuch as MBH reactions show a huge dependence on the solvent one uses in experiments. The choice of the MPW1K hybrid functional for geometry optimization is synchronized to recent studies,^[2g-i, 4c] which show that this functional works much better than others for treatment of zwitterionic intermediates, which play the most important role in the MBH reaction. The split-valence double zeta polarized basis set including diffuse functions 6-31+G(d) was shown to be the best for zwitterionic intermediates also in our previous study. The authors have found that addition of the diffuse functions can play a significant role, though it raises the computational cost significantly.^[4c]

3.3. Results and Discussion

The resulting energy diagram of the cycle is shown in Fig. 3.1 as relative free energies ($\Delta G_{298, \text{THF}}$) vs. reaction coordinate, all found conformations are shown including diastereomeric pathways (RR is shown in red colour, RS is shown in black). The side process of adduct between MVK and PPh_3 protonation is shown by blue colour. In Fig 3.2a the energy diagram (cycle and protonation side process) is presented as relative free energies ($\Delta G_{298, \text{THF}}$ in black colour) and enthalpies ($\Delta H_{298, \text{THF}}$ in red colour) vs. reaction coordinate in comparison. In Fig 3.2b the gas-phase (solvent effects are excluded) free energies (in black) and enthalpies (in red) are shown. As the reference point (zero point) the reactant complex is taken. Separate molecules of reactants and products are also shown. The relative enthalpies and free energies for the most stable conformations are collected in Table 3.1

As one can see from Fig 3.2ab the enthalpy and free energy potential energy surfaces have similar shape, excepting separate molecules of reactants and products, where the entropic contribution is substantial. The side process of **Int1** protonation yielding **Int_p** (this process will be in detail discussed later) has been found to be exergonic and exothermic if the solvent effects are included (Fig. 3.2a), but slightly endergonic and endothermic for the gas-phase profiles (Fig. 3.2b). Since the protonation product can be experimentally detected without additional efforts to shift the equilibrium to its side, the profiles with inclusion of solvent model seem to be more reliable. Later the free energy profile with inclusion of solvent model ($\Delta G_{298, \text{THF}}$) will be discussed in detail.

Table 3.1 Relative enthalpies and free energies at 298.15 K (in kJ mol^{-1}) for stationary points (best conformations) located on the potential energy surface at MP2(FC)/6-31+g(2d,p)//MPW1K/6-31+G(d) in gas-phase and with additional consideration of solvent effects at PCM/UAHF/RHF/6-31G(d).

	$\Delta H_{298, \text{THF}}$	$\Delta G_{298, \text{THF}}$	ΔH_{298}	ΔG_{298}
Σ reactants	+5.60	-98.03	+103.80	+0.17
Int1	0.00	0.00	0.00	0.00
TS1	+4.47	+34.00	+9.95	+39.88
Int2	-81.13	-40.83	-59.75	-19.45
TS2_RS	-65.10	-5.83	-15.39	+38.76
TS2_RR	-63.18	-8.48	-18.37	+36.33
Int3_RS	-133.34	-80.51	-82.68	-29.84
Int3_RR	-152.77	-89.26	-89.26	-45.88
TS3_RS	-96.48	-34.37	-55.69	+6.42
TS3_RR	-77.83	-17.65	-35.19	+25.49
Int4	-121.23	-71.36	-84.74	-34.87
TS4	-47.67	-1.96	-27.46	+18.25
Int5	-63.36	-35.55	-39.72	-13.07
Σ products	-41.63	-91.32	+46.73	-2.82
Int_p	-88.11	-47.81	-58.36	-18.06
Int_y	-17.49	+12.83	+3.31	+36.11

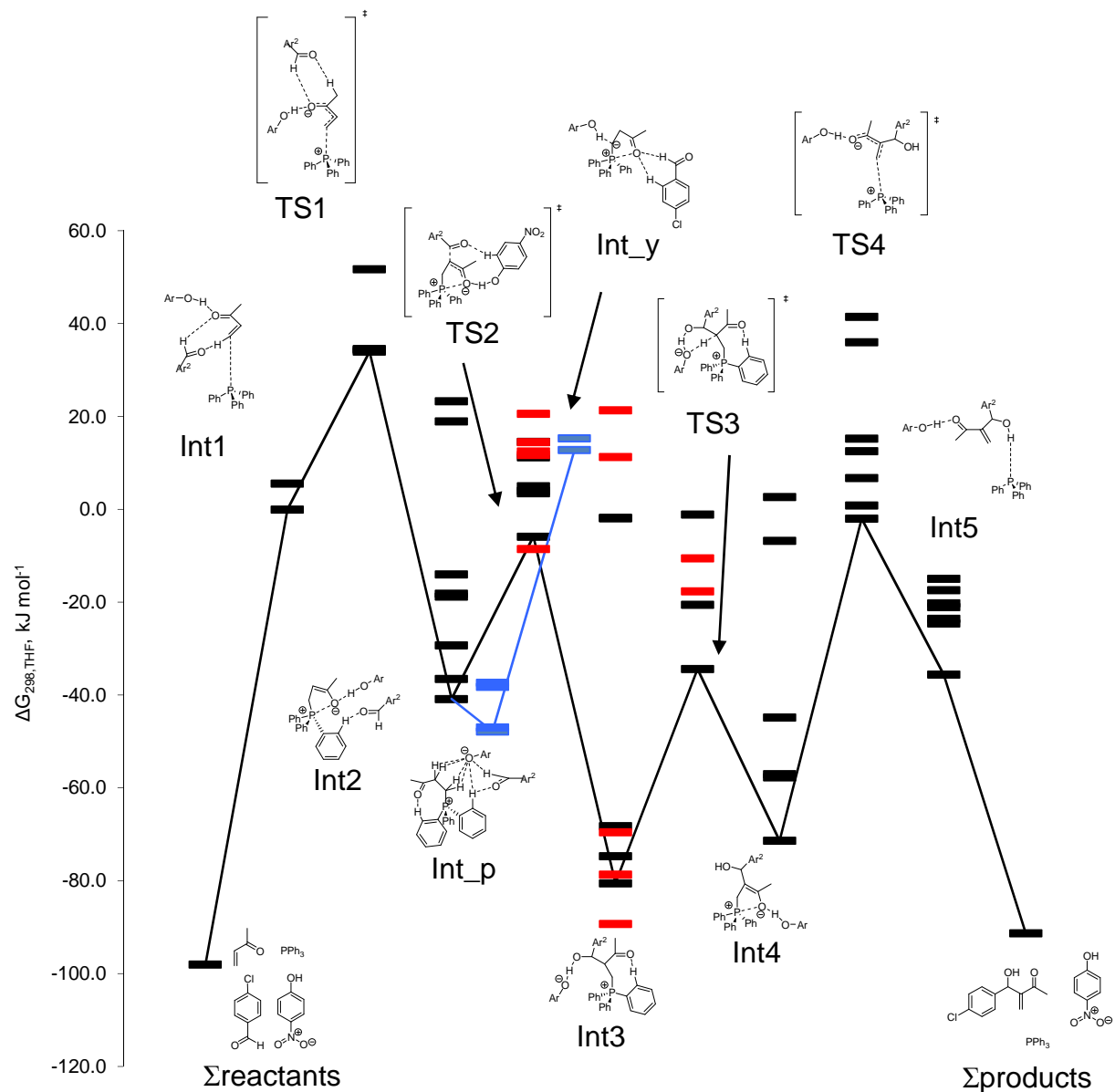


Fig. 3.1 The reaction free energy profile ($\Delta G_{298, \text{THF}}$) calculated at the MP2(FC)/6-31+G(2d,p)//MPW1K/6-31+G(d) level of theory with additional consideration of solvent effects at PCM(THF)/UAHF/RHF/6-31G(d) level. All found conformations are shown.

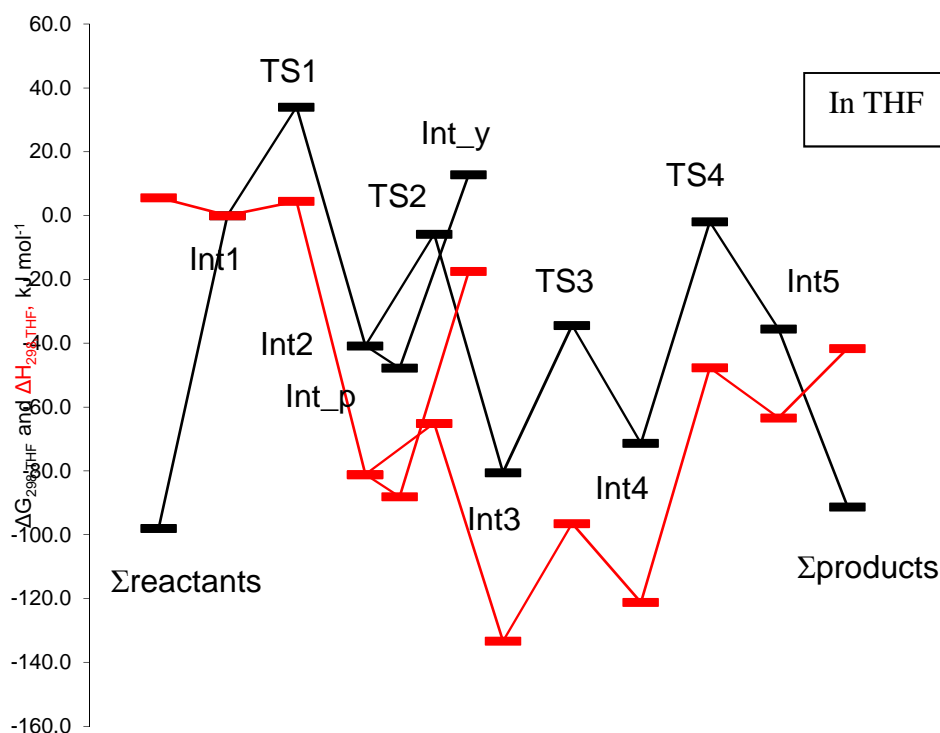


Fig. 3.2a The comparison of reaction free energy ($\Delta G_{298, \text{THF}}$, shown in black colour) and enthalpy ($\Delta H_{298, \text{THF}}$, shown in red colour) profiles calculated at the MP2(FC)/6-31+G(2d,p)//MPW1K/6-31+G(d) level of theory with additional consideration of solvent at PCM(THF)/UAHF/RHF/6-31G(d) level. Only the most stable conformations are shown.

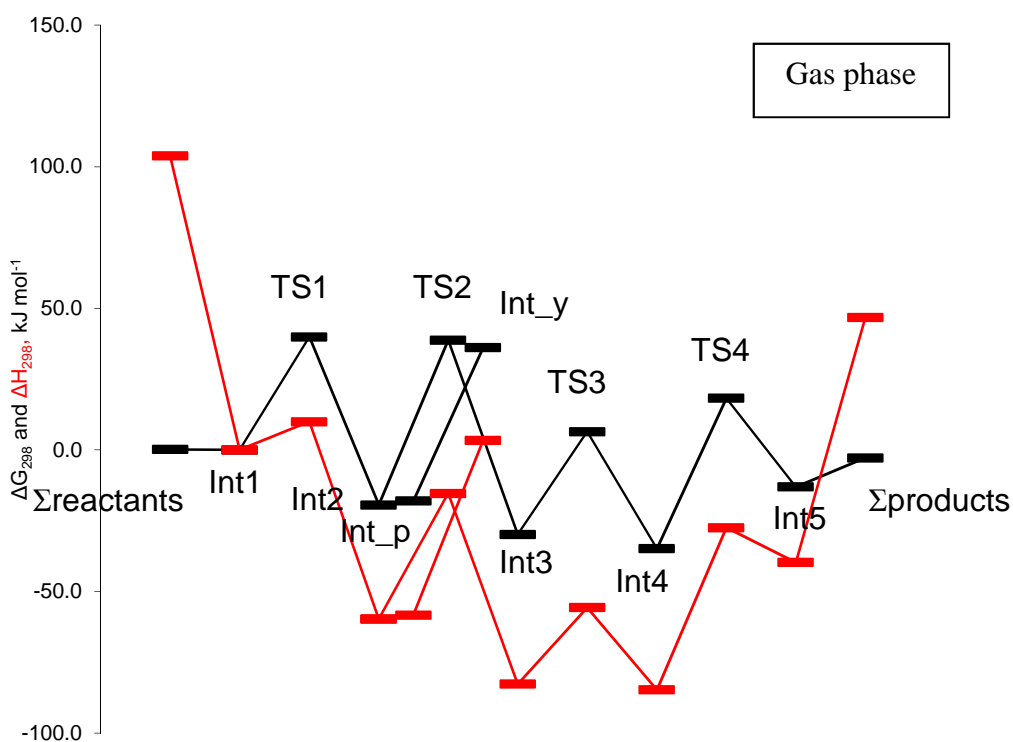


Fig. 3.2b The comparison of reaction free energy (ΔG_{298} , shown in black colour) and enthalpy (ΔH_{298} , shown in red colour) profiles calculated at the MP2(FC)/6-31+G(2d,p)//MPW1K/6-31+G(d) level of theory in the gas-phase. Only the most stable conformations are shown.

The reaction is found to be slightly endergonic ($\Delta G_{298,\text{THF}} = +6.7 \text{ kJ mol}^{-1}$) relative to separate molecules of reactants and products. At the same time the reaction in study is exothermic ($\Delta H_{298,\text{THF}} = -47.23 \text{ kJ mol}^{-1}$). Using eqn. 3.1 the reaction entropy change ($\Delta S_{298,\text{THF}} = -0.181 \text{ kJ mol}^{-1} \text{ K}^{-1}$) and temperature of switch to exergonic reaction ($T = 261 \text{ K}$) can be calculated.

$$\Delta G = \Delta H - T\Delta S = 0 \Rightarrow T = \frac{\Delta H}{\Delta S} \quad (3.1)$$

Thus, carrying out the reaction under reduced temperatures would help to shift the equilibrium to the side of the products. The result is in accordance with the fact that the MBH reaction in general does not go under elevated temperatures^[1g], though an increase in temperature would accelerate the reaction in accordance with Eyring equation (eqn. (3.2)).

$$k = A \frac{k_B T}{h} e^{-\Delta G^\ddagger / RT} \quad (3.2)$$

Noteworthy, in previous computational study by Kappe *et al.* the DABCO-catalyzed MBH reaction between benzaldehyde and methyl acrylate in methanol has been found to be just slightly exergonic $\Delta G_{298,\text{MeOH}} = -6.6 \text{ kJ mol}^{-1}$. Studies by Harvey and Sunoj, unfortunately, do not allow to discuss free energy barriers of the whole MBH reaction, since thermal corrections have not been presented for the overall process.^[2a, 2g-i] Relative to reactant and product complexes **Int1** and **Int5** the reaction is, however, exergonic ($\Delta G_{298,\text{THF}} = -35.6 \text{ kJ mol}^{-1}$). The most stable conformations of reactant complex **Int1** and product complex **Int5** are shown in Fig 3.3. As a typical feature of these two structures one can note a hydrogen bond ($r(\text{O-H}) = 1.743 \text{ \AA}$ in **Int1** and $r(\text{O-H}) = 1.755 \text{ \AA}$ in **Int5**) between the MVK oxygen atom and PNP. This hydrogen bond plays a substantial role in the stabilization of various stationary points on the MBH reaction energy profile.

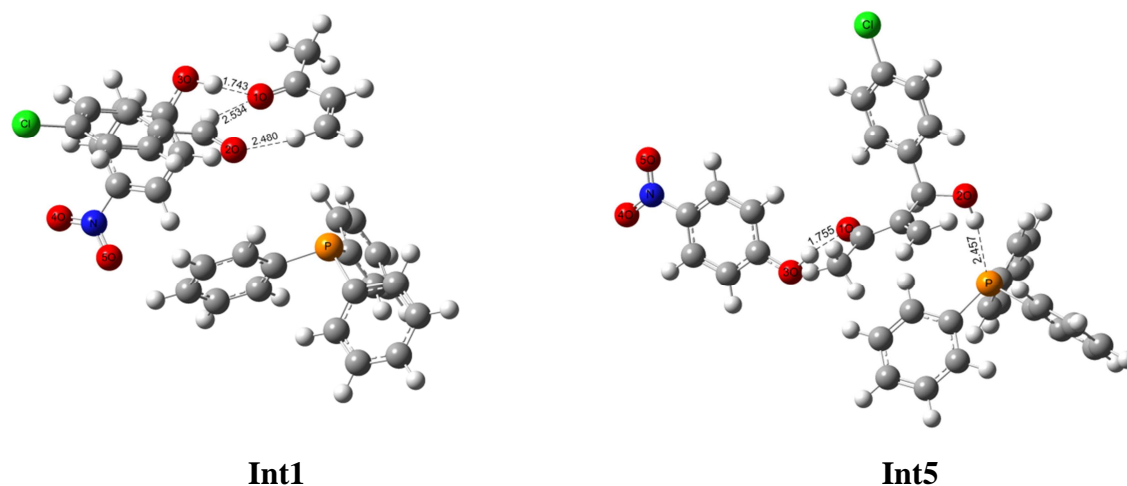
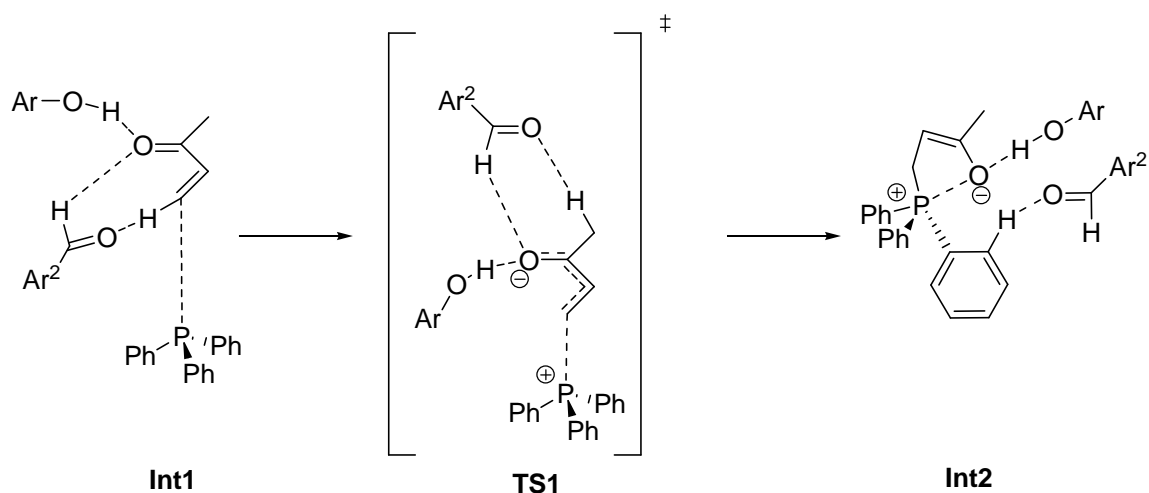


Fig. 3.3 Structures of the most stable conformations of reactant complex **Int1** and product complex **Int5**.

3.3.1. Michael Addition of MVK to PPh₃



Scheme 3.4 Michael addition of MVK to PPh₃.

The first step in the reaction is Michael addition of MVK to PPh₃ (Scheme 3.4) via transition state **TS1** ($\Delta G_{298, \text{THF}}^\ddagger = +34.0 \text{ kJ mol}^{-1}$) yielding zwitterionic intermediate **Int2** has been found to be exergonic $\Delta G_{298, \text{THF}} = -40.8 \text{ kJ mol}^{-1}$. It is important to note here that both **Int2** and **TS1** are stabilized substantially by strong hydrogen bonds between the MVK oxygens and PNP with bond lengths of $r(\text{O-H}) = 1.621 \text{ \AA}$ for **Int2** and $r(\text{O-H}) = 1.641 \text{ \AA}$ for **TS1**. The structures lacking this hydrogen bond are much less stable (more than 55 kJ mol^{-1} for **Int2** and 17 kJ mol^{-1} for **TS1**). The aldehyde molecule forms hydrogen bonds also due to its carbonyl group. In adduct **Int2** the two structurally most relevant characteristics include a C-P bond length of $r(\text{P-C}) = 1.839 \text{ \AA}$ for the newly formed P-C bond and a short distance of $r(\text{P-O}) = 2.247 \text{ \AA}$ between phosphorus and the MVK oxygen atom. Involving of a phenol co-catalyst molecule is important, since the phenol allows the system to be dramatically stabilized not only via hydrogen bonding directly, but also by side effects of this hydrogen bond – the presence of P-O interaction. The structures with such P-O interaction are not found to be minima if the co-catalyst molecule is not involved. Fig. 3.4 collects the structures of the most stable conformations for **TS1** and **Int2**.

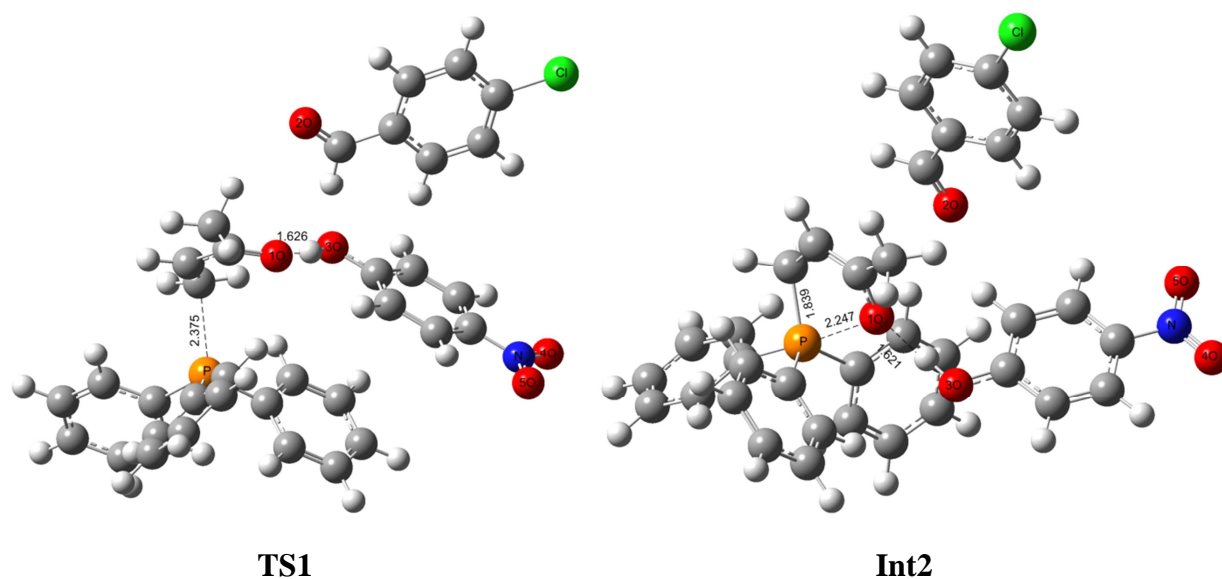
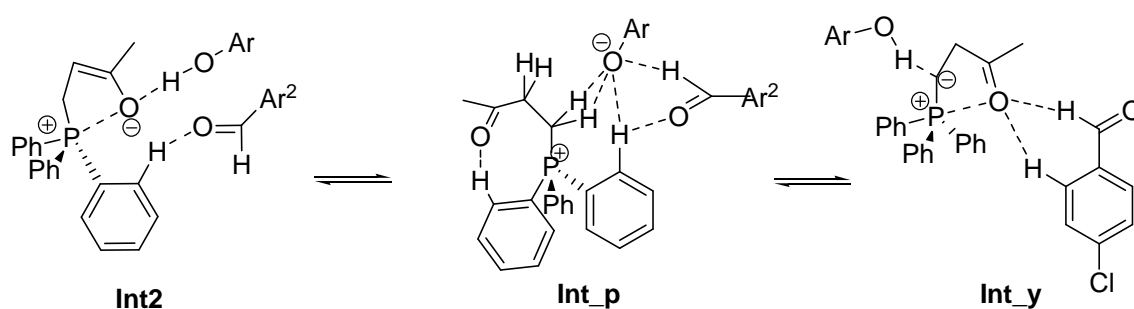


Fig. 3.4 Structures of the most stable conformations of **TS1** and **Int2**.

Int2 can be in equilibrium with protonated intermediate **Int_p** (complex between *p*-chlorobenzaldehyde, *p*-nitrophenolate anion and cation **10** from Scheme 3.2) and with ylid **Int_y** (Scheme 3.5). The ^{31}P NMR chemical shift and acidity of these intermediates are discussed in detail in chapter 2 and chapter 4 of this work. In the current model system **Int_p** is found to be 7 kJ mol^{-1} more stable than **Int2**, while ylid **Int_y** is 53.6 kJ mol^{-1} less favourable. The higher stability of intermediate **Int_p** corresponds to the experimental detection of this protonated intermediate by ^{31}P NMR.^[3] Fig. 3.5 shows the structures of the most stable conformations for **Int_p** and **Int_y**.



Scheme 3.5 Protonation of zwitterionic intermediate **Int2** yielding ion pair **Int_p** and deprotonation to yield ylid **Int_y**.

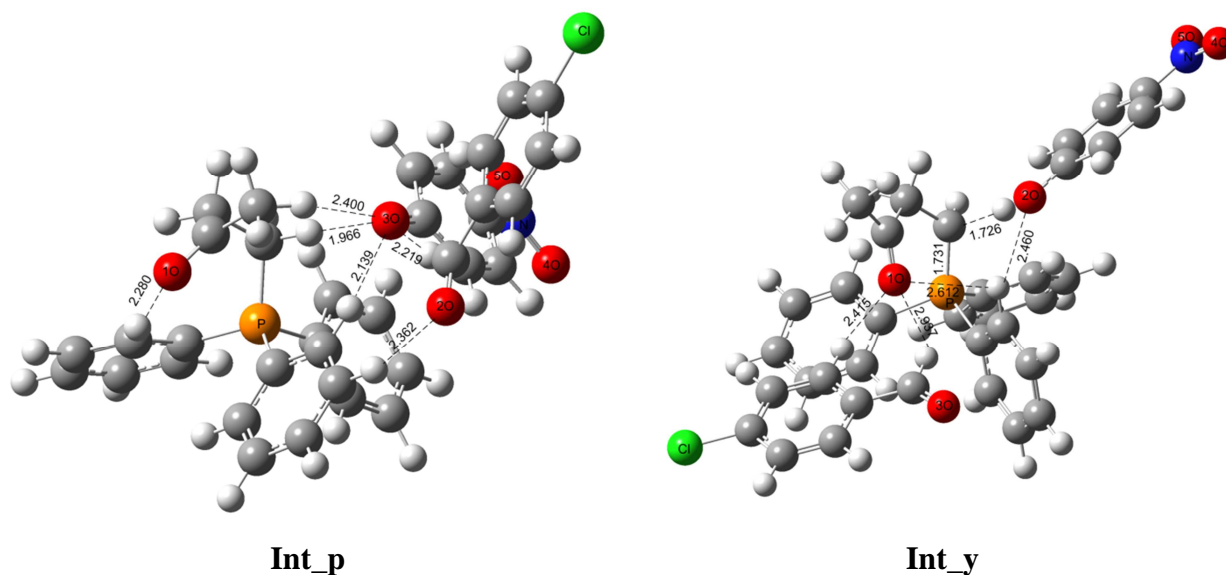
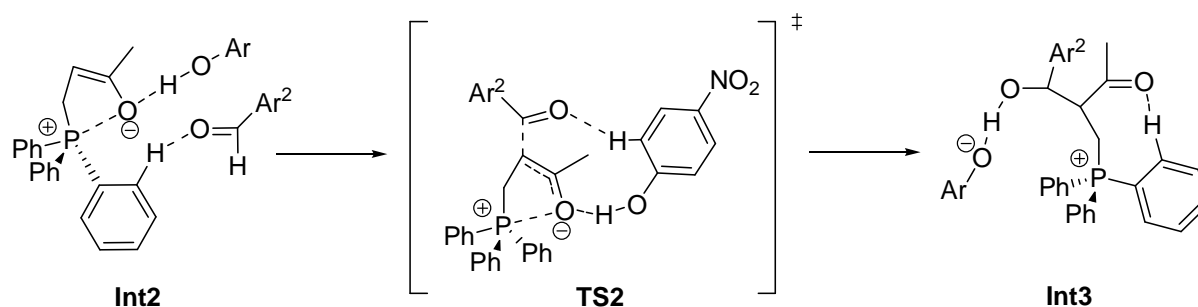


Fig. 3.5 Structures of the most stable conformations of **Int_p** and **Int_y**.

3.3.2. Addition of the Aldehyde: C-C Bond Formation



Scheme 3.6 Addition of the aldehyde: C-C bond formation.

The second step in the MBH reaction is formation of the C-C bond between aldehyde and MVK fragments of **Int2** via **TS2** forming the second zwitterionic intermediate **Int3** with a barrier of $\Delta G_{298, \text{THF}}^{\ddagger} = +35.0 \text{ kJ mol}^{-1}$ and a reaction free energy of $\Delta G_{298, \text{THF}} = -39.7 \text{ kJ mol}^{-1}$. Fig 3.6 shows the structures of the most stable conformations for **TS2** and **Int3**.

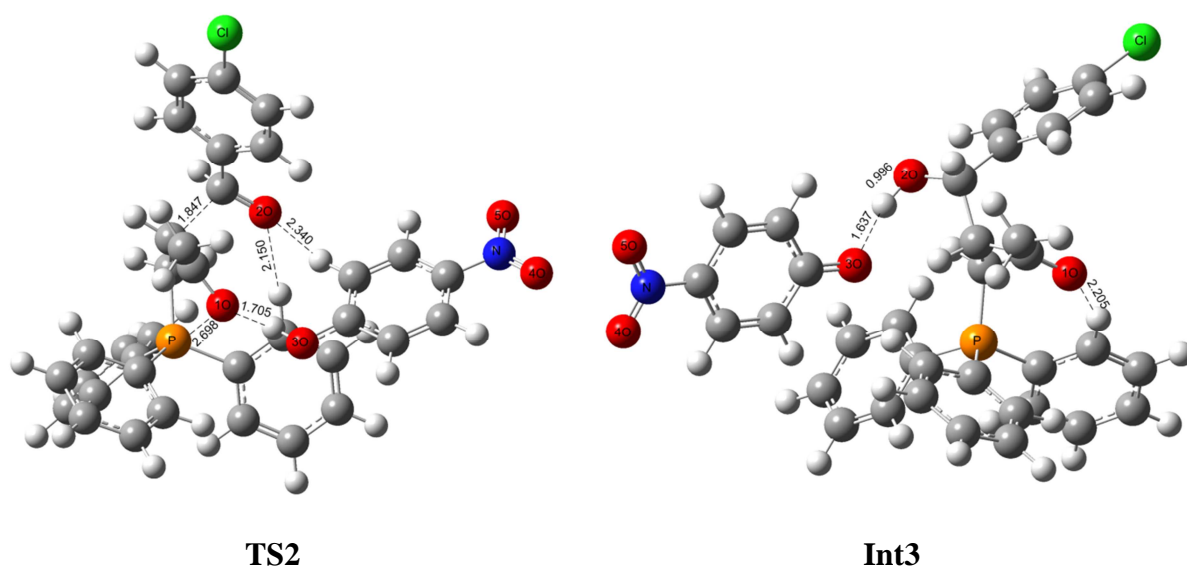
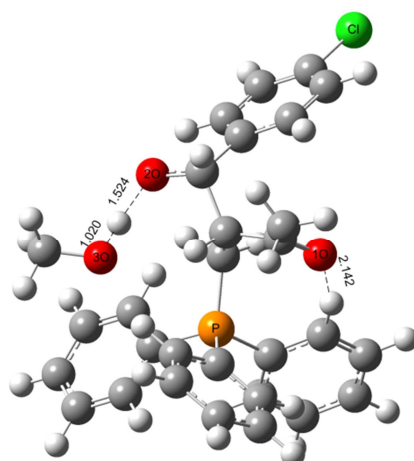


Fig. 3.6 Structures of the most stable conformations of **TS2** and **Int3**.

The structure of **TS2** shows the same (as mentioned before) features, which are responsible for the energetic stabilization: the phenol forms a hydrogen bond with the oxygen atom of the MVK ($r(\text{O}-\text{H}) = 1.705 \text{ \AA}$) and this oxygen comes into interaction ($r(\text{P}-\text{O}) = 2.698 \text{ \AA}$) with the phosphorus atom. The **TS2** structure with phenol making a hydrogen bond with the oxygen atom of aldehyde is 9 kJ mol^{-1} less stable. The situation changes dramatically for intermediate **Int3**. As shown in Scheme 3.2 the carbonyl group of aldehyde turns into an alkoxide while the MVK moiety acquires the carbonyl character. The redistribution of negative charge leads to the redistribution of inter- and intramolecular interactions. Thus the oxygen atom of the aldehyde moiety is now more attractive for phenol to form a hydrogen bond than the oxygen atom of the MVK moiety. Moreover, there is no barrier (neither kinetic nor thermodynamic) for hydrogen transfer between oxygen of the aldehyde moiety and PNP, that is why the hydrogen is shifted in the direction of aldehyde ($r(\text{O}_{\text{aldehyde}}-\text{H}) = 0.996 \text{ \AA}$; $r(\text{O}_{\text{phenol}}-\text{H}) = 1.637 \text{ \AA}$). The protonation of the aldehyde moiety oxygen, however, does not take place if methanol is used as co-catalyst instead of *p*-nitrophenol. In the case of methanol the hydrogen is not shifted to the aldehyde ($r(\text{O}_{\text{aldehyde}}-\text{H}) = 1.524 \text{ \AA}$; $r(\text{O}_{\text{phenol}}-\text{H}) = 1.020 \text{ \AA}$). The structure of **Int3** with methanol instead of phenol (**Int3_MeOH**) is shown in Fig. 3.7.



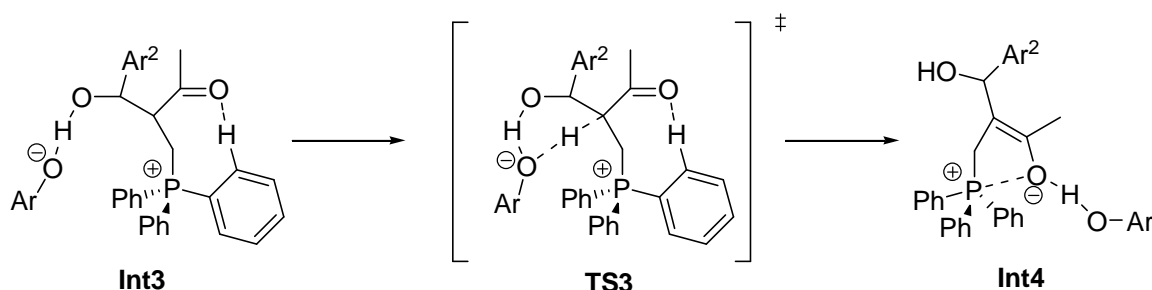
Int3_MeOH

Fig. 3.7 Structure of the **Int3** with methanol instead of phenol.

The fact of this H-transfer for phenol and its absence in the case of methanol is in accordance with acidity properties of these substances (data in DMSO): $pK_a(p\text{-nitrophenol}) = 10.8^{[5]}$ and $pK_a(\text{methanol}) = 29.0.^{[5-6]}$ Thus, the methanol molecule is not appropriate for modelling of the system and the *p*-nitrophenol is to be used, though the methanol molecule is much smaller and easier to calculate. This shows us again that the results of the MBH cycle theoretical investigation depend dramatically on the model. In chapter 4 the important question of acidity of MBH reaction co-catalyst will be raised again.

The mentioned charge redistribution leads also to the disappearance of the intramolecular interaction between phosphorus atom and the oxygen of MVK in **Int3**. The oxygen forms a hydrogen bond with one of the hydrogen atoms of the neighbouring phenyl ring of the PPh_3 moiety ($r(\text{O-H}) = 2.205 \text{ \AA}$).

3.3.3. The Proton Transfer



Scheme 3.7 The proton transfer step.

The third step in the catalytic cycle is the proton transfer step via **TS3** turning **Int3** into **Int4**. In recent computational studies of the MBH reaction mechanism this step has been

found to be rate limiting for many MBH reactions.^[2a, 2b, 2g-i] It seems to be important to consider protonation of **Int3** by co-catalyst, since it is one of the key factors that determine the barrier of this step. The very acidic co-catalysts or a large amount of co-catalyst effectively reduce the reaction rate as was experimentally shown.^[3] This may be due to protonation of zwitterionic intermediates as it has been observed in the present study: the intermediate **Int3** reacts with the co-catalyst, stabilizing the system. The proton transfer step from **Int3** to **Int4** is found to be endergonic ($\Delta G_{298, \text{THF}} = +9.1 \text{ kJ mol}^{-1}$), the free energy barrier of the proton transfer being $\Delta G_{298, \text{THF}}^\ddagger = +46.1 \text{ kJ mol}^{-1}$. Fig. 3.8 shows the structures of the most stable conformations for **TS3** and **Int4**.

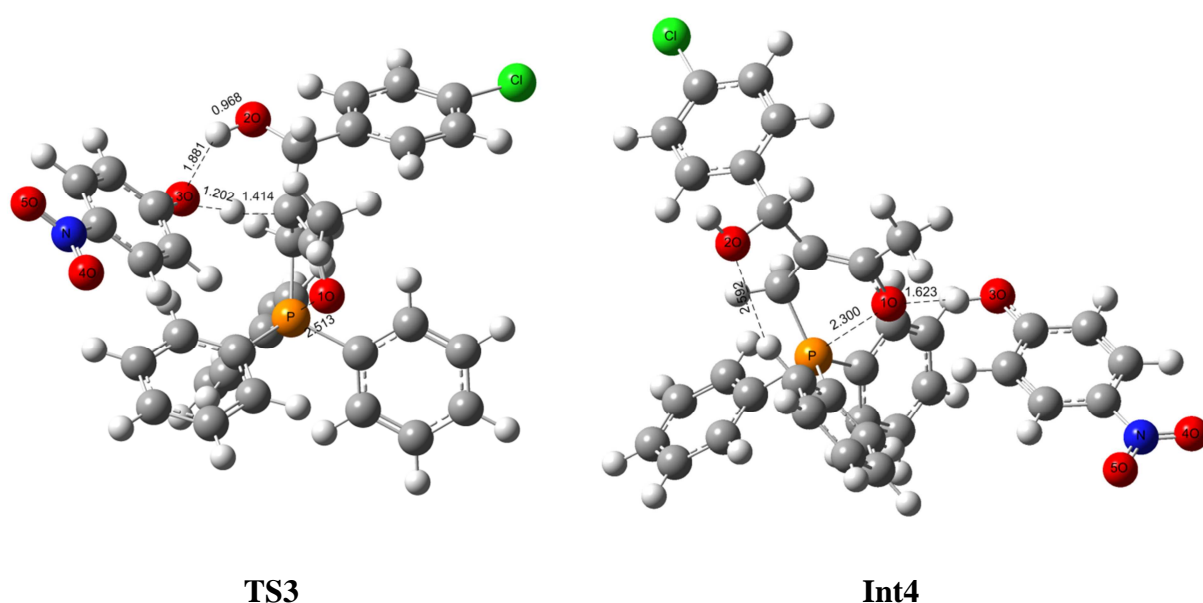
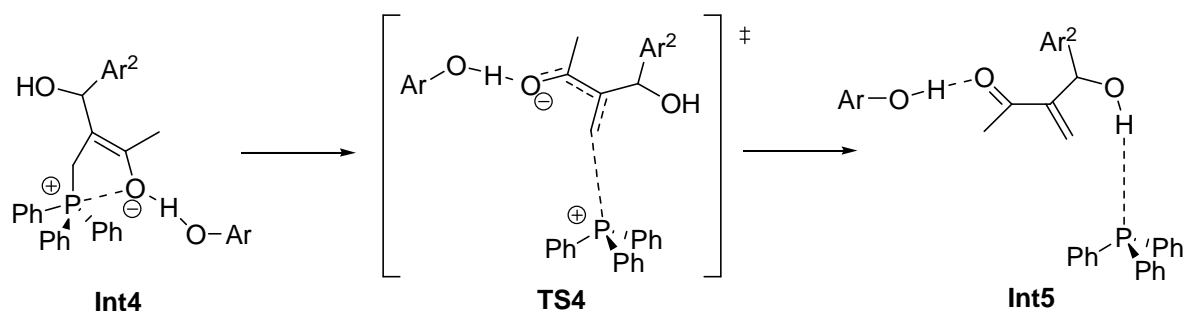


Fig. 3.8 Structures of the most stable conformations of **TS3** and **Int4**.

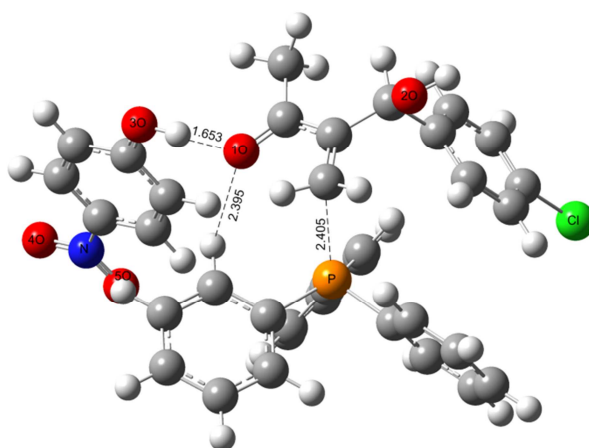
The intramolecular P-O interaction is found for both structures: $r(\text{P-O}) = 2.513 \text{ \AA}$ in **TS3** and $R(\text{P-O}) = 2.300 \text{ \AA}$ in **Int4**. In **TS3** the PNP molecule is involved in a 6-membered ring structure, exchanging the proton between the β -carbon atom of the MVK moiety and the oxygen atom of the aldehyde moiety. In **Int4** the oxygen atom of the aldehyde moiety is protonated, and the phenol molecule now forms a hydrogen bond with the oxygen atom of the MVK moiety.

3.3.4. The Product Elimination Step



Scheme 3.8 The product elimination step.

The last step in the whole MBH process is the product elimination step. It has been found to be strongly endergonic ($\Delta G_{298, \text{THF}} = +35.8 \text{ kJ mol}^{-1}$) and the barrier of this step amounts to $\Delta G_{298, \text{THF}}^\ddagger = +69.4 \text{ kJ mol}^{-1}$. From all steps calculated in the MBH catalytic cycle this is therefore the step with the highest free energy barrier. Fig. 3.9 shows the structure of the most stable conformation for **TS4**. During this last step of the reaction the bond between product and catalyst has to break and this leads also to cleavage of intramolecular interactions, which are responsible for the system stabilization (such as interactions between phosphorus atom and oxygen atoms). Thus in **TS4** the C-P bond between forming MBH-product and catalyst is 2.405 \AA , whereas it remains $\sim 1.8 \text{ \AA}$ on the preceding stages. In analogy to **Int1**, the preferable position for the PNP molecule to form a hydrogen bond with the carbonyl oxygen of the MBH product has been found.



TS4

Fig. 3.9 Structure of the most stable conformation of **TS4**.

3.3.5. The Diastereomeric Pathways

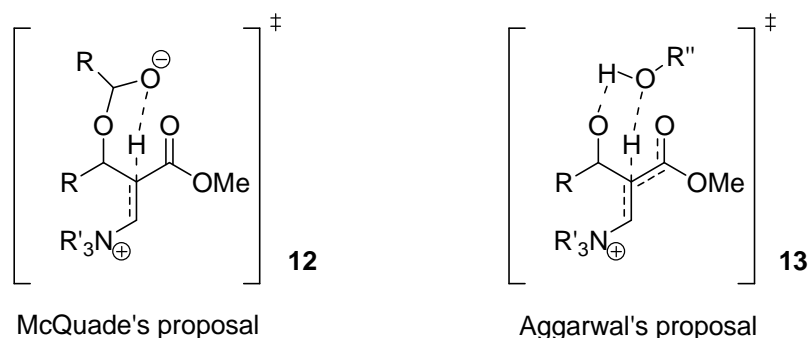
As shown in Fig. 3.1, the system can follow different diastereomeric pathways: RS(SR), shown in black colour or RR(SS), shown in red colour in Fig. 3.1. These diastereomeric pathways are possible starting from the second step of the C-C bond formation via **TS2** and till the hydrogen transfer step via **TS3**. Noteworthy, the RS and SR are isoenergetic as well as RR and SS, thus it is obviously enough to discuss two diastereomeric pathway (e.g. RS and RR) instead of four. Results for the best conformations for both diastereomeric pathways are collected in Table 3.1. Till now the RS(SR) pathway has been discussed. Concerning RR(SS) pathway the **TS2_RR** has been found to be slightly more stable ($\Delta\Delta G_{298,\text{THF}} = 2.7 \text{ kJ mol}^{-1}$), than **TS2_RS**. The **Int3_RR** is also more stable ($\Delta\Delta G_{298,\text{THF}} = 8.8 \text{ kJ mol}^{-1}$), than the RS analogue. The situation is changed in **TS3**, where the **TS3_RS** is substantially more preferable ($\Delta\Delta G_{298,\text{THF}} = 16.7 \text{ kJ mol}^{-1}$). The reason of the energetic discrepancy lies in the overall effect of intramolecular interactions inside of the given transition state or intermediate.

3.3.6. Calculated Results and Literature Kinetic Data in Comparison

Several kinetic studies have been performed in the area of the MBH reaction. For the DABCO-catalyzed MBH reaction of aromatic aldehydes and methyl acrylate (MA) in solvents of different polarity, McQuade^[7] *et al.* have found that the rate law is first order in DABCO and acrylate, and second order in aldehyde (eqn. 3.3). They have suggested the proton transfer step to be the rate-determining step (RDS) proceeding through transition state **12**, where two molecules of aldehyde participate (Scheme 3.10).

$$r = k[\text{DABCO}][\text{MA}][\text{aldehyde}]^2 \quad (3.3)$$

Aggarwal *et al.* have investigated the reaction of ethyl acrylate with benzaldehyde catalyzed by quinuclidine without solvent by means of kinetic isotope effects and also proposed the RDS to be the proton-transfer step, but proceeding via a different transition state **13**^[8] (Scheme 3.10)



Scheme 3.10 Proton transfer step transition states suggested by McQuade and Aggarwal.

It has been shown computationally that both mechanisms (via both suggested transition states) are possible, depending on the reaction conditions and the selected systems. In the system studied here involving an acidic co-catalyst, Aggarwal's proposal is more probable.^[2a, 2b]

Another version of the MBH reaction, so called aza-MBH, where the aldehyde is replaced by an imine, has also been studied kinetically. Thus Leitner *et al.* have studied the aza-MBH reaction of MVK with tosylimine catalyzed by PPh₃ in d₈-THF and found a first-order dependence on MVK and PPh₃, and a broken order of 0.5 on tosylimine^[9] (eqn. 3.4). This means that the RDS could be partially influenced by proton-transfer.

$$r = k[PPh_3][MVK][tosylimine]^{0.5} \quad (3.4)$$

Raheem and Jakobsen have reported for the DABCO-catalyzed aza-MBH reaction of methyl acrylate and aromatic tosylimines in CHCl₃ a first-order dependence on DABCO as well as on methyl acrylate, and rate saturation effects with respect to imine.^[10] The kinetic isotope effect has been observed suggesting the proton transfer to be the RDS. Shibasaki, Berkessel and co-workers investigated the aza-MBH reaction of phosphinoylimine with methyl acrylate catalyzed by DABCO with phenol-type additives.^[11] In contrast to Raheem and Jakobsen's study, they have found no kinetic isotope effect indicating that the proton-transfer step is not the RDS and suggested Michael addition to determine the reaction rate. Recently the protonation/deprotonation process of catalyst and Michael acceptor adduct has been studied for reaction of MVK, PPh₃ in the presence of PNP by Liu.^[3] First order rate law on both MVK and PPh₃ but 0.5 order on PNP has been found (eqn. 3.5)

$$r = k[PPh_3][MVK][PNP]^{0.5} \quad (3.5)$$

Generally for MBH and aza-MBH reactions there is still no single opinion about the RDS as well as about the mechanism on the whole. The present study is based on Aggarwal's proposal. Going from reactant to product complex the reaction is observed as a monomolecular process inside of a cluster formed by *p*-chlorobenzaldehyde, MVK, PPh₃ and PNP. Since processes go inside of such cluster, the reaction molecularity stays constant, one can conclude that RDS is determined by the step with the biggest activation energy barrier. The product elimination step has been found to have the biggest activation energy barrier of $\Delta G_{298,THF}^\ddagger = +69.4 \text{ kJ mol}^{-1}$ and the proton transfer step barrier ranks as the second by its magnitude of $\Delta G_{298,THF}^\ddagger = +46.1 \text{ kJ mol}^{-1}$. The Michael addition step and the C-C bond formation barriers are lower at, respectively, $\Delta G_{298,THF}^\ddagger = +34.0 \text{ kJ mol}^{-1}$ and $\Delta G_{298,THF}^\ddagger = +35.0 \text{ kJ mol}^{-1}$. The equilibrium between cluster **Int1** and separate molecules of the reactants can be described by eqn. 3.6

$$[cluster] = K[aldehyde][MVK][PPh_3][PNP] \quad (3.6)$$

The rate of the first step (Michael addition) can be then written in accordance with eqn. 3.7

$$r = k_1[cluster] = k_1K[aldehyde][MVK][PPh_3][PNP] \quad (3.7)$$

Thus the equilibrium concentration of the cluster on each step can be connected with the separate reactants concentrations. This is important since in the kinetic experiments the rate law is determined relative to free reactants. Noteworthy that relative to separate reactants the first step of Michael addition is found to be energetically very expensive +132 kJ mol⁻¹. Certainly, additional experimental measurements of the MBH reaction kinetic dependences are needed to be compared with the presented computational data.

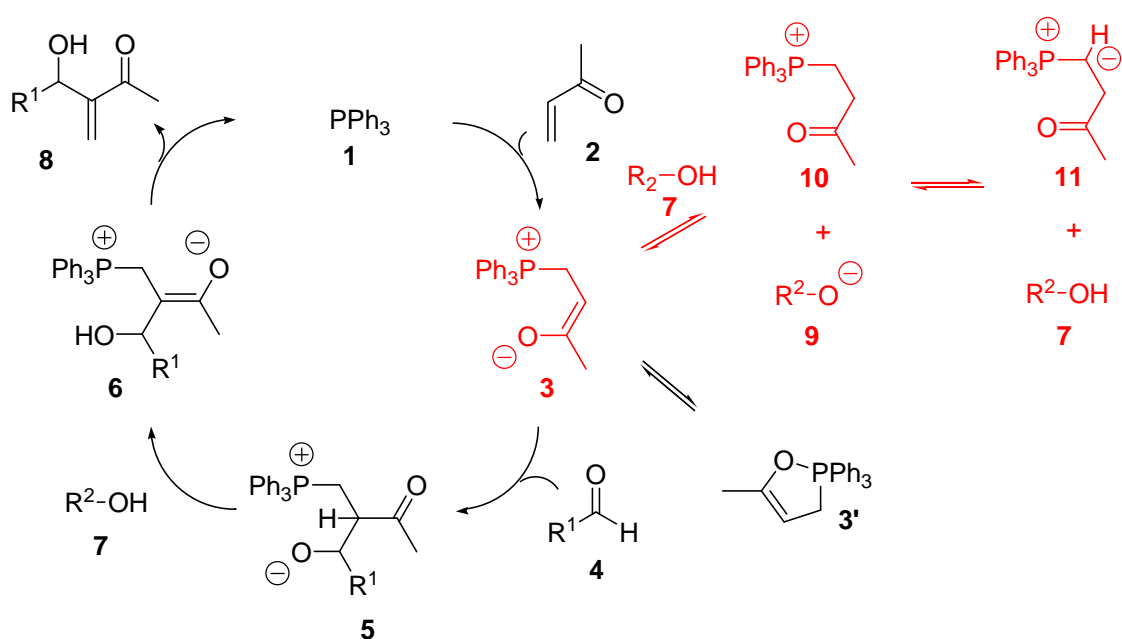
3.4. References

- [1] a) D. Basavaiah, A. J. Rao, T. Satyanarayana, *Chem. Rev.* **2003**, *103*, 811-891; b) V. Singh, S. Batra, *Tetrahedron* **2008**, *64*, 4511-4574; c) D. Basavaiah, K. V. Rao, R. Reddy, *J. Chem. Soc. Rev.* **2007**, *36*, 1581; d) P. Langer, *Angew. Chem.* **2000**, *112*, 3177; e) P. Langer, *Angew. Chem. Int. Ed.* **2000**, *39*, 3041-3051; f) Y.-L. Shi, M. Shi, *Eur. J. Org. Chem.* **2007**, 2905; g) D. Basavaiah, B. S. Reddy, S. S. Badsara, *Chem. Rev.* **2010**, *110*, 5447-5674.
- [2] a) R. Robiette, V. K. Aggarwal, H. J. N., *J. Am. Chem. Soc.* **2007**, *129*, 15513-15525; b) D. Cantillo, C. O. Kappe, *J. Org. Chem* **2010**, *75*, 8615-8626; c) J. Xu, *Journal of Molecular Structure: THEOCHEM* **2006**, *767*, 61-66; d) J. LI, *J. Theor. Comput.* **2010**, *9*, 65-75; e) F. Jian-Fen, Y. Chun-Hong, H. Liang-Jun, *Int. J. Quantum Chem.* **2009**, *109*, 1311-1321; f) L. Dong, S. Qin, Z. Su, H. Yang, C. Hu, *Org. Biomol. Chem.* **2010**, *8*, 3985-3991; g) D. Roy, R. B. Sunoj, *Org. Lett.* **2007**, *9*, 4873-4876; h) D. Roy, R. B. Sunoj, *Chem. - Eur. J.* **2008**, *14*, 10530; i) D. Roy, C. Patel, R. B. Sunoj, *J. Org. Chem* **2009**, *74*, 6936-6943.
- [3] Y. Liu, PhD thesis, Ludwig-Maximilians-Universität München (München), **2011**.
- [4] a) Y. Wei, G. N. Sastry, H. Zipse, *J. Am. Chem. Soc.* **2008**, *130*, 3473; b) Y. Wei, T. Singer, H. Mayr, G. N. Sastry, H. Zipse, *J. Comput. Chem.* **2008**, *29*, 291-297; c) Y. Wei, B. Sateesh, B. Maryasin, G. N. Sastry, H. Zipse, *J. Comput. Chem.* **2009**, 2617 - 2624.
- [5] H. J. Reich, in *Bordwell pKa Table (Acidity in DMSO)*, **2001-2011**.
- [6] W. N. Olmstead, Z. Margolin, F. G. Bordwell, *J. Org. Chem* **1980**, *45*, 3295-3299.
- [7] a) K. E. Price, S. J. Broadwater, M. H. Jung, D. T. McQuade, *Org. Lett.* **2005**, *7*, 147-150; b) K. E. Price, S. J. Broadwater, B. J. Walker, D. T. McQuade, *J. Org. Chem* **2005**, *70*, 3980-3987.
- [8] V. K. Aggarwal, S. Y. Fulford, G. C. Lloyd-Jones, *Angew. Chem. Int. Ed.* **2005**, *44*, 1706-1708.
- [9] P. Buskens, J. Klankermayer, W. Leitner, *J. Am. Chem. Soc.* **2005**, *127*, 16762-16763.
- [10] I. T. Raheem, E. N. Jacobsen, *Adv. Synth. Catal.* **2005**, *347*, 1701-1708.
- [11] T. Yukawa, B. Seelig, Y. Xu, H. Morimoto, S. Matsunaga, A. Berkessel, M. Shibasaki, *J. Am. Chem. Soc.* **2010**, *132*, 11988-11992.

4. Protonation/Deprotonation Equilibria in the Morita-Baylis-Hillman Reaction

4.1. Introduction

In chapter 3 we have discussed the catalytic cycle of the MBH reaction (Scheme 4.1, left part in black colour). We have also mentioned the side reactions of intermediate **3** involving protonation by co-catalyst (Scheme 4.1, the reactions shown in red colour). In this chapter the problems of this side processes will be analyzed in detail.



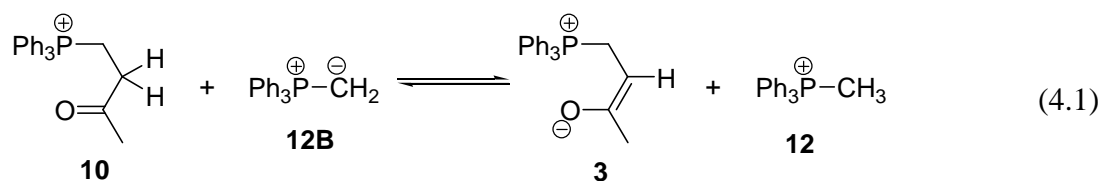
Scheme 4.1. The catalytic cycle of the MBH reaction and possible side processes of the PPh₃ (**1**)-catalyzed MBH reaction with participation of protic co-catalyst **7**

In addition to accelerating the hydrogen-transfer step in intermediate **5**, the protic co-catalysts **7** may also react with enolate zwitterions **3** and **6** in protonation/deprotonation equilibria. This is shown in Scheme 4.1 for zwitterion **3**, whose reaction with alcohol **7** leads to formation of alkoxide **9** and phosphonium cation **10**. Depending on the solvent system used, these may either exist as solvent-separated ions (e.g. in DMSO) or as tight ion pairs (e.g. in THF). Protonation/deprotonation may, of course, also involve the position directly adjacent to phosphorous, yielding ylid **11** as a potential additional intermediate. Ylids such as **11** can subsequently react with a second equivalent of MVK (**2**), forming unwanted side products together with oxidized (and thus deactivated) forms of phosphine catalyst **1**. Even though quantitative data for the basicity of intermediates **3**, **6**, and **11** appear not to be

available in the contemporary literature, indirect evidence suggests that the equilibrium between **3** and **10** is shifted far to the right under most experimental conditions. This is supported by the abundant detection of **10** (as well as protonated forms of **6**) in reaction solutions of MBH reactions by ESI-MS.^[1] β -Ketophosphonium cations such as **10** have also been characterized by NMR spectroscopic techniques in the mechanistically related phosphine-mediated addition of alcohols to Michael acceptors.^[2] In this latter case cations such as **10** are considered to represent the resting state of the phosphine catalysts. The large success of phenolic co-catalysts in a variety of MBH reactions^[3] thus raises the question of the actual basicity of zwitterionic enolates **3** and **6** in different solvent systems, especially comparing to the acidity of the co-catalysts. We try to clarify this point by calculation of the acidity properties for cation **10**.

4.2. The Acidity of Enolate Intermediates

The acidity of the α - and β -positions of phosphonium cation **10** can be estimated with reference to experimentally known systems such as methylphosphonium cation **12**.^[4] The difference in acidities of the β -position of **10** and the methyl group in **12**, for example, can be quantitatively expressed as the reaction free energy in solution for the proton transfer reaction shown in eqn. (4.1). Gas and solution phase reaction energies of isodesmic reactions such as these can be calculated with high accuracy due to the similarity of the species on the reactant and product sides.



A negative free energy for this process $\Delta G(4.1)$ implies that cation **10** is more acidic at its β -position than the methyl group in cation **12**. The reaction free energy is quantitatively related to the $\text{p}K_{\text{a}}$ differences between **10** and **12** as given in eqn. (4.2).

$$\Delta G(4.1) = 2.303RT [\text{p}K_{\text{a}}(\mathbf{10}\beta) - \text{p}K_{\text{a}}(\mathbf{12})] \quad (4.2)$$

The reaction free energy $\Delta G(4.1)$ has been determined using a combination of geometry optimization at MPW1K/6-31+G(d) level, single point calculation at MP2(FC)/G3MP2large level in the gas phase, and additional consideration of solvation free energies in DMSO using

the PCM/UAHF/RHF/6-31G(d) continuum solvation model. Based on these results and assuming $pK_a(\mathbf{12}, \text{DMSO}) = +22.4^{[4a]}$, a value of $pK_a(\mathbf{10}\beta, \text{DMSO}) = +19.3$ has been obtained. A completely analogous approach can be used to assess the acidity in the α -position of **10**, now yielding a value of $pK_a(\mathbf{10}\alpha, \text{DMSO}) = +21.8$. In Table 4.1ab the results of $\Delta G(4.1)$ and pK_a obtained at MP2(FC)/G3MP2large//MPW1K/6-31+G(d) level of theory in solution and in the gas-phase are compared with MPW1K/6-31+G(d) approach. The pK_a values obtained at DFT level differ from MP2 by 2 pK_a units. The inclusion of solvation model effects dramatically. Both DFT and MP2 approaches show that in the gas-phase: $pK_a(\mathbf{10}\alpha) < pK_a(\mathbf{10}\beta)$ and in solution vice-versa: $pK_a(\mathbf{10}\alpha) > pK_a(\mathbf{10}\beta)$. In order to check whether additional effort in solution modeling is necessary, the cluster model calculations (inclusion of one solvent molecule explicitly) have been performed. The results are collected in Table 4.1c. This sophistication, however, does not lead to substantial change as compared to implicit solvation model.

Table 4.1a. Reaction free energies ($\Delta G(4.1)$) and related pK_a values calculated relative to $\text{Ph}_3\text{PCH}_3^+$ ($pK_a(\text{exp.}) = +22.4$) for β -ketophosphonium cation **10** (DMSO, 25 °C) in gas-phase and in solution applying implicit solvation model at the PCM/UAHF/RHF/6-31G(d) level.

	MPW1K/6-31+G(d)				MP2(FC)/G3MP2large// MPW1K/6-31+G(d)			
	ΔG_{298} , kJ mol ⁻¹	pK_a	$\Delta G_{298, \text{DMSO}}$, kJ mol ⁻¹	pK_a	ΔG_{298} , kJ mol ⁻¹	pK_a	$\Delta G_{298, \text{DMSO}}$, kJ mol ⁻¹	pK_a
10β	+1.9	+22.7	-24.2	+18.2	+12.8	+24.6	-17.8	+19.3
10α	-0.8	+22.3	-2.7	+21.9	-2.7	+21.9	-3.6	+21.8

Table 4.1b. Reaction free energies ($\Delta G(4.1)$) and related pK_a values calculated relative to $\text{Ph}_3\text{PCH}_2\text{Ph}^+$ ($pK_a(\text{exp.}) = 17.4$) for β -ketophosphonium cation **10** (DMSO, 25 °C) in gas-phase and in solution applying implicit solvation model at the PCM/UAHF/RHF/6-31G(d) level.

	MPW1K/6-31+G(d)				MP2(FC)/G3MP2large// MPW1K/6-31+G(d)			
	ΔG_{298} , kJ mol ⁻¹	pK_a	$\Delta G_{298, \text{DMSO}}$, kJ mol ⁻¹	pK_a	ΔG_{298} , kJ mol ⁻¹	pK_a	$\Delta G_{298, \text{DMSO}}$, kJ mol ⁻¹	pK_a
10β	+31.3	+22.9	+17.1	+20.4	+33.3	+23.2	+14.8	+20.0
10α	+28.6	+22.4	+38.6	+24.2	+17.8	+20.5	+29.0	+22.5

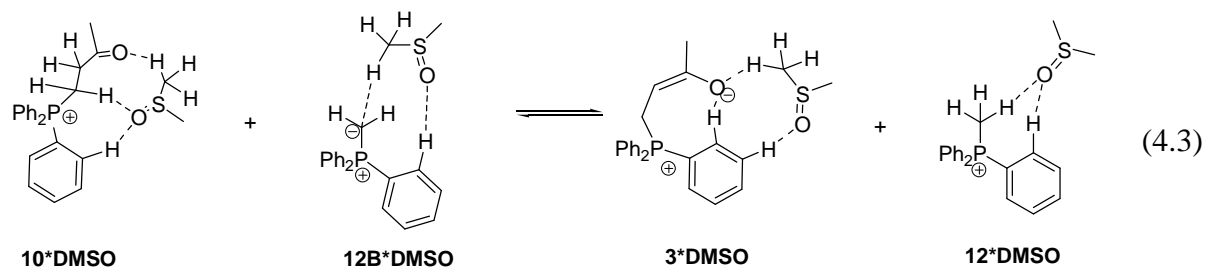
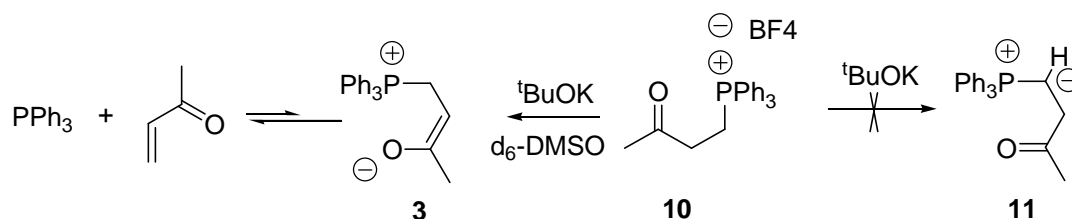


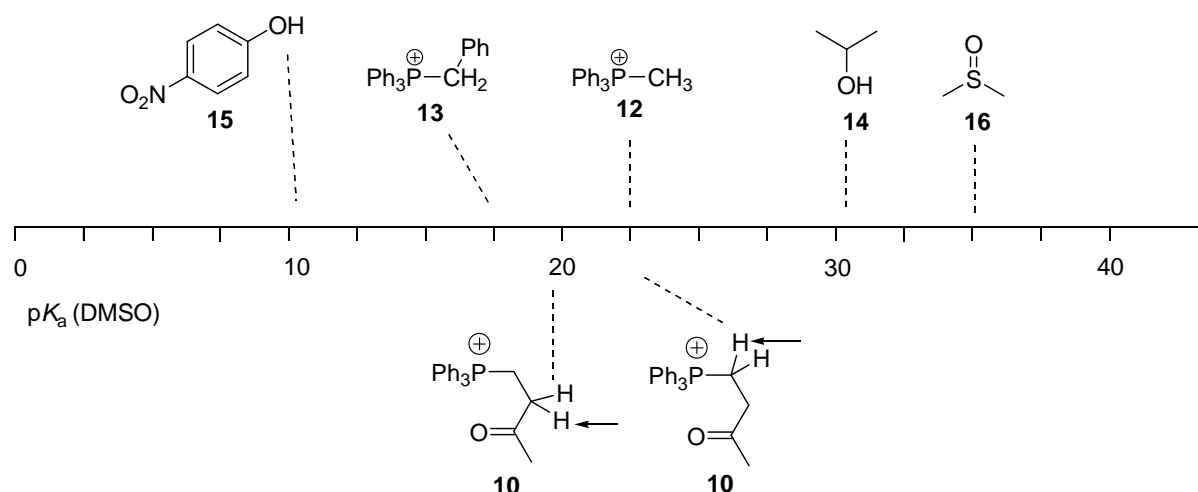
Table 4.1c. Reaction free energies ($\Delta G(4.3)$) and related pK_a values calculated relative to $Ph_3PCH_3^+$ ($pK_a(\text{exp.}) = +22.4$) for β -ketophosphonium cation **10** (DMSO, 25 °C) using explicit solvation model.

MP2(FC)/G3MP2large//MPW1K/6-31+G(d)				
	G_{298} , kJ mol ⁻¹	pK_a	$G_{298,DMSO}$, kJ mol ⁻¹	pK_a
10β	+6.3	+23.5	-11.5	+20.4
10α	+2.7	+22.9	+3.2	+23.0

In order to base the pK_a estimates for **10** on a second reference point, the calculations described in eqn. (4.1) have been repeated using phosphonium cation **13** as the reference. The acidity of **13** is 5.0 pK_a units lower than that of **12** and will thus bracket the acidity of **10** from the lower side.^[4b] In all technical details these calculations are identical to those involving **12** as the reference and values of $pK_a(\mathbf{10}\beta, \text{DMSO}) = 20.0$ and $pK_a(\mathbf{10}\alpha, \text{DMSO}) = 22.5$ have been obtained. Since it is unclear which of the two experimental reference values is more accurate, we will use the arithmetic mean of the calculated values $pK_a(\mathbf{10}\beta, \text{DMSO}) = 19.7$ and $pK_a(\mathbf{10}\alpha, \text{DMSO}) = 22.2$ for further discussion. Recently Dr. Yinghao Liu has experimentally found that $pK_a(\mathbf{10}\beta, \text{DMSO}) < pK_a(\mathbf{10}\alpha, \text{DMSO})$, using the reactions in Scheme 4.2. When the d_6 -DMSO solution of **10** was treated with less than 1.0 equivalent *t*-BuOK, instantly regenerated PPh_3 and MVK, but no ylide **11** was detected by 1H NMR and ^{31}P NMR. This is compatible with rapid deprotonation to **3** and subsequent cleavage of the C-P bond.^[5]



Scheme 4.2. Deprotonation of **10** with *t*BuOK.



Scheme 4.3 The pK_a scale.

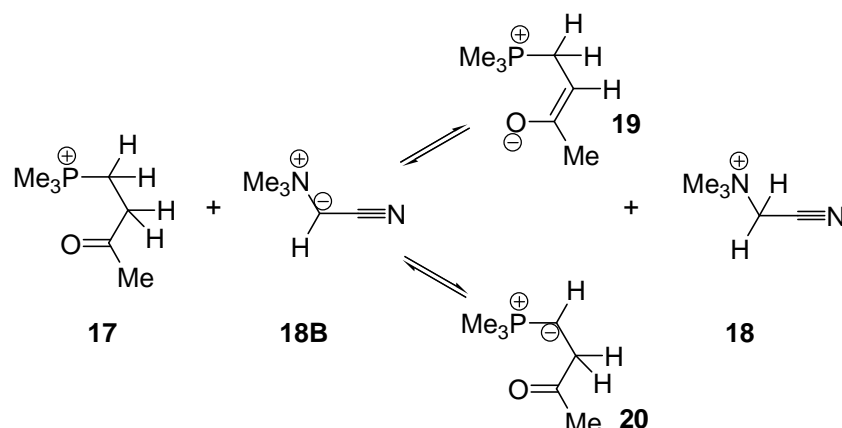
The pK_a values of alkylphosphonium cations described in Table 4.1 are graphically shown in Scheme 4.3 together with those for other constituents of the MBH reaction mixture. Values for MBH reaction products such as **8** appear not to be available in the literature, but we can use the value for isopropanol (**14**) of $pK_a(\mathbf{14}, \text{DMSO}) = 30.2$ as an approximate reference.^[4b] This very high value implies that the MBH reaction products will not be acidic enough to protonate enolate intermediates **3** or **6**. This is also true for aliphatic alcohols used as solvents or co-solvents. Other protic co-catalysts such as *p*-nitrophenol (**15**) are much more acidic with $pK_a(\mathbf{15}, \text{DMSO}) = 10.8$ and will thus be certain to protonate transient intermediates such as **3**, **6**, or **11**. In the presence of such a co-catalyst we can safely assume that the equilibrium between zwitterionic enolate **3** and its protonated analogue **10** is shifted far to the side of the latter, leaving little zwitterionic enolate **3** behind to propagate the catalytic cycle. For reactions run in THF or chloroform, the situation is less clear as experimental reference values for the species shown in Scheme 4.1 appear not to exist. Still, the question of how the enolate intermediates in the catalytic cycle can escape protonation through protic solvents or co-catalysts also remains here.

4.3. Benchmarking Calculations and Extension to Different Nucleophiles and Substrates

The presented results of the pK_a value calculations encouraged us to extend the study on a range of different nucleophiles (catalysts) and substrates tested experimentally in MBH reaction.^[6]

As a first step before extending the range of systems, we have performed benchmarking calculations for the pK_a values in a small model system **19** obtained through addition of Me_3P to MVK. The adduct **19** can be protonated to yield cation **17** (Scheme 4.4)

or isomerized to ylid **20**. As a reference system for these benchmarking calculations we have chosen cyanomethylammonium cation **18** with its pK_a value of 20.6 (DMSO).^[4c, 7]



Scheme 4.4 Protonation/deprotonation equilibrium for MVK/ PMe_3 adduct.

Three computational approaches have been used:

1. MPW1K/6-31+G(d) + PCM(DMSO)/UAHF/RHF/6-31G(d). The most simple approach of those applied for the PPh_3/MVK pK_a value calculations.
2. MP2(FC)/G3MP2large//MPW1K/6-31+G(d) + PCM(DMSO)/UAHF/RHF/6-31G(d). This method has been used for the PPh_3/MVK pK_a value calculations and its quality has to be tested by benchmarking calculations.
3. SCS-MP2(FC)/G3MP2large//MPW1K/6-31+G(d) + PCM(DMSO)/UAHF/RHF/6-31G(d). Close to the method 2 but with spin-component scaled MP2(FC) single point calculations.^[8]
4. G3(MP2)MPW1K(+) + PCM(DMSO)/UAHF/RHF/6-31G(d). The benchmarking calculation.^[9]

It should be emphasized that all of the tested approaches have the same solvation treatment model: the implicit solvation model in the variant of PCM(DMSO)/UAHF/RHF/6-31G(d). The results are shown in Fig 4.1.

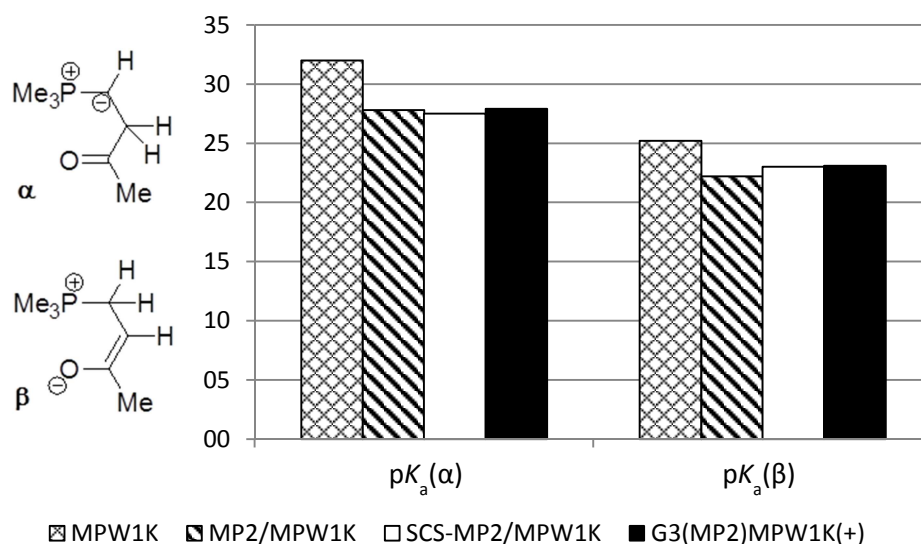


Fig. 4.1 Acidity of cation **17** calculated at different levels of theory.

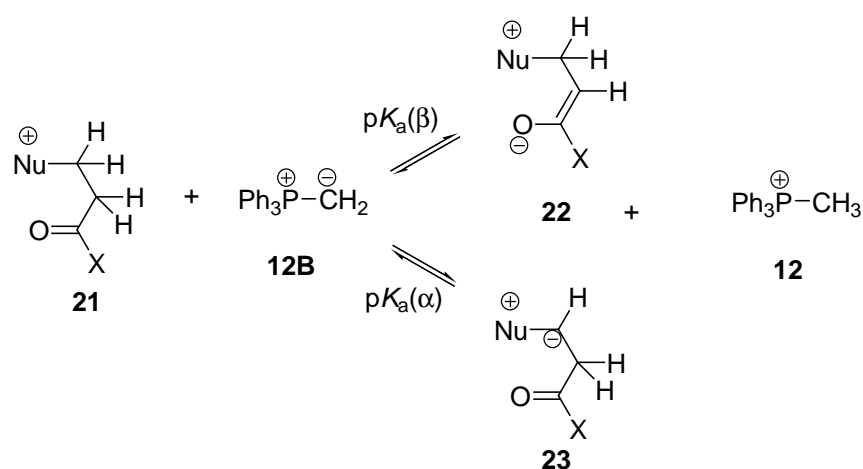
Table 4.2 Acidity of cation **17** calculated at different levels of theory

		α	β
MPW1K/6-31+G(d)	$\Delta G_{298,\text{DMSO}}, \text{kJ mol}^{-1}$	+64.8	+26.1
	pK_a	+32.0	+25.2
MP2(FC)/G3MP2large//MPW1K/6-31+G(d)	$\Delta G_{298,\text{DMSO}}, \text{kJ mol}^{-1}$	+9.1	+40.8
	pK_a	+22.2	+27.8
SCS-MP2(FC)/G3MP2large//MPW1K/6-31+G(d)	$\Delta G_{298,\text{DMSO}}, \text{kJ mol}^{-1}$	+13.6	+39.2
	pK_a	+23.0	+27.5
G3(MP2)MPW1K(+)	$\Delta G_{298,\text{DMSO}}, \text{kJ mol}^{-1}$	+14.5	+41.8
	pK_a	+23.1	+27.9

From the data collected in Fig 4.1 and Table 4.2 it is clear to see that results from method 1 (MPW1K/6-31+G(d)) are inferior as compared to the benchmarking calculations (G3(MP2)MPW1K(+)). The three methods 2-4 are quite close to each other, thus we conclude that application of the easiest from these three approaches (the method 2: MP2(FC)/G3MP2large//MPW1K/6-31+G(d)) is reasonable.

After checking the applicability of our computation scheme we could extend the calculations to other systems of catalysts and substrates. The Scheme 4.5 presents the processes we are interested in. As analogous to our pK_a calculations with the system PPh_3 (or PMe_3)/MVK we have an adduct of the catalyst (“Nu”, nucleophile) with the “X”-ketone – varying the “X” we observe influence of the substrate. The reference system is the same as we have used for PPh_3 /MVK. The results are collected in Table 4.3 and are shown graphically in Fig. 4.2. For all of the studied catalysts we see that $pK_a(\beta)$ values are smaller than $pK_a(\alpha)$ as well as it was shown for PPh_3 . For all of these catalysts the protonated adduct between the catalyst and the Michael acceptor is a pretty weak acid with bigger probability to be

deprotonated from the β position giving the first zwitterionic intermediate of the MBH catalytic cycle. The smallest difference between the ylid and first zwitterionic intermediate (the smallest difference between $pK_a(\beta)$ and $pK_a(\alpha)$ values) corresponds to PPh_3 , and indeed it is often observed experimentally that Ph_3PO is formed as a side product. This oxide can be formed from the ylid, which in accordance to our calculations is more likely to exist as ylids with other catalysts. The popular MBH catalyst DABCO seems to be good concerning the side reaction of ylidization, since for the adduct between DABCO and MVK the probability of the ylid formation is found to be small.



Scheme 4.5 General situation of protonation/deprotonation equilibrium for the adduct between variable catalyst and substrate.

Table 4.3 Acidity values of cation **20** with variable catalyst and substrate.

Nu	X	α		β	
		$\Delta G_{298, DMSO}, kJ mol^{-1}$	pK_a	$\Delta G_{298, DMSO}, kJ mol^{-1}$	pK_a
PMe ₃	Me	+12.9	+24.7	-18.8	+19.1
	OMe	+12.0	+24.5	+2.2	+22.8
	OPh	+0.9	+22.6	-22.2	+18.5
PPh ₃	Me	-3.6	+21.8	-17.8	+19.3
	Ph	+0.3	+22.5	-30.8	+17.0
	OPh	-3.4	+21.8	-17.1	+19.4
	H	-10.3	+20.6	-32.5	+16.7
DMAP	Me	+61.4	+33.2	-1.1	+22.2
	OMe	+56.2	+32.3	+16.7	+25.3
	CN	+16.1	+25.2	-82.2	+8.0
DABCO	Me	+114.7	+42.5	-17.2	+19.4

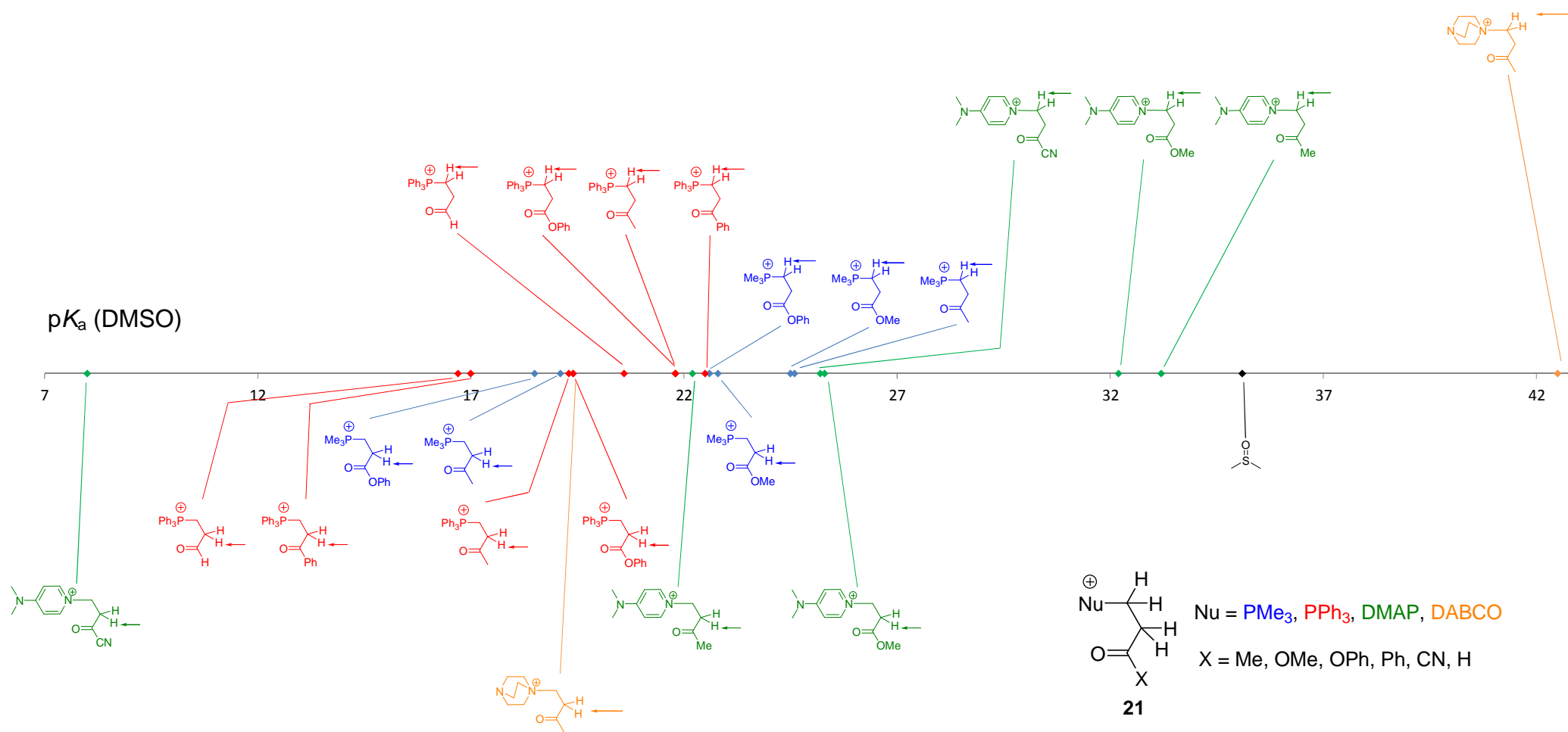


Fig. 4.2 Acidity values of cation **21** with variable catalysts and substrates.

4.4. Conclusions

The protonation/deprotonation equilibrium between the first zwitterionic intermediate of the MBH reaction catalyzed by PPh_3 and with MVK as a Michael acceptor, its protonated form and hypothetical ylid intermediate has been studied computationally at MP2(FC)/G3MP2large//MPW1K/6-31+G(d) + PCM/UAHF/RHF/6-31G(d) level of theory. It has been found that in the presence of phenolic co-catalyst the equilibrium between zwitterionic enolate and its protonated analogue has to be shifted far to the side of the latter, leaving little zwitterionic enolate behind to propagate the catalytic cycle and the ylid formation is the least probable process (25 °C, DMSO). The results are in accordance with the experimental evidence. The computational approach has been verified by benchmarking calculations and extended to some larger series of systems by variation of nucleophile and substrate. Similar to the PPh_3 /MVK case, the order of priority between protonated form, first zwitterionic intermediate and ylid has been found for all tested systems. The probability to form ylids as side products is the smallest for DABCO and the biggest for Ph_3P .

4.5. References

- [1] a) L. S. Santos, C. H. Pavam, W. P. Almeida, F. Coelho, M. N. Eberlin, *Angew. Chem. Int. Ed.* **2004**, *43*, 4330-4333; b) G. W. Amarante, H. M. S. Milagre, B. G. Vaz, B. R. Vilacha Ferreira, M. N. Eberlin, F. Coelho, *J. Org. Chem* **2009**, *74*, 3031-3037.
- [2] I. C. Stewart, R. G. Bergman, F. D. Toste, *J. Am. Chem. Soc.* **2003**, *125*, 8696-8697.
- [3] a) P. Buskens, J. Klankermayer, W. Leitner, *J. Am. Chem. Soc.* **2005**, *127*, 16762-16763; b) Y. Iwabuchi, M. Nakatani, N. Yokoyama, S. Hatakeyama, *J. Am. Chem. Soc.* **1999**, *121*, 10219-10220; c) M. Shi, L. H. Chen, *Chem. Comm.* **2003**, 1310-1311; d) M. Shi, L. H. Chen, C.-Q. Li, *J. Am. Chem. Soc.* **2005**, *127*, 3790-3800; e) M. Shi, Y.-H. Liu, *Org. Biomol. Chem.* **2006**, 1468-1470; f) S. Kawahara, A. Nakano, T. Esumi, Y. Iwabuchi, S. Hatakeyama, *Org. Lett.* **2003**, *5*, 3103-3105; g) R. Krishna, V. Kannan, V. N. Reddy, *Adv. Synth. Catal.* **2004**, *346*, 603-606; h) P. Langer, *Angew. Chem. Int. Ed.* **2000**, *39*, 3041-3051; i) J. E. Imbriglio, M. M. Vasbinder, S. J. Miller, *Org. Lett.* **2003**, *5*, 3741-3743; j) S. Luo, X. Mi, H. Xu, P. G. Wang, J.-P. Cheng, *J. Org. Chem* **2004**, *69*, 8413-8422; k) S. Luo, P. G. Wang, J.-P. Cheng, *J. Org. Chem* **2004**, *69*, 555-558; l) X. Mi, S. Luo, J.-P. Cheng, *J. Org. Chem* **2005**, *70*, 2338-2341; m) K. Matsui, H. Takizawa, H. Sasai, *J. Am. Chem. Soc.* **2005**, *127*, 3680-3681; n) D. Balan, H. Adolfson, *Tetrahedron Lett.* **2003**, *44*, 2521-2524.
- [4] a) X.-M. Zhang, F. G. Bordwell, *J. Am. Chem. Soc.* **1994**, *116*, 968-972; b) F. G. Bordwell, *Acc. Chem. Res.* **1988**, *21*, 456-463; c) H. J. Reich, in *Bordwell pKa Table (Acidity in DMSO)*, **2001-2011**.
- [5] Y. Liu, PhD thesis, Ludwig-Maximilians-Universität München (München), **2011**.
- [6] a) G.-N. Ma, J.-J. Jiang, M. Shi, Y. Wei, *Chem. Comm.* **2009**, 5496; b) X.-Y. Guan, Y. Wei, M. Shi, *J. Org. Chem* **2009**, *74*, 6343-6346; c) G.-N. Ma, F.-J. Wang, J. Gao, M. Shi, *Chem. Comm.* **2008**, 4998-5000; d) X.-G. Liu, M. Shi, *Org. Lett.* **2008**, *10*, 1043-1046; e) M.-J. Qi, M. Shi, *Tetrahedron* **2007**, *63*, 10415-10424; f) Y.-L. Shi, M. Shi, *Eur. J. Org. Chem.* **2007**, 2905.
- [7] F. G. Bordwell, M. Van der Puy, N. R. Vanier, *J. Org. Chem* **1976**, 1885-1886.
- [8] a) S. Grimme, *J. Chem. Phys.* **2003**, *118*, 9095; b) A. Szabados, *J. Chem. Phys.* **2006**, *125*, 214105.
- [9] Y. Wei, PhD thesis, Ludwig-Maximilians-Universität München (München), **2008**.

5. Description of Organocatalytic Reactivity

5.1. Introduction

As it has been shown by previous and the present studies the MBH reaction is a difficult process from a mechanistic point of view – the reaction is multistep and the nature of the rate determining step is not clearly defined, because it depends on the particular system involved. Moreover, the reaction can be driven by different mechanisms depending on the conditions of the reaction^[1] and side reactions play a significant role for the MBH process. Thus, the calculation of the whole catalytic cycle, including side reactions for any new catalyst, is too complicated way. In order to routinely predict and explain experimental data of catalytic activity and selectivity, easy but informative calculations are wanted. Descriptors of catalytic activity (selectivity) are needed. To suggest and to test such descriptors is the goal of the presented in this chapter study.

The affinity of basic compounds towards electrophilic species is clearly one of the criteria of the catalytic activity in organocatalysis and it can be reflected by proton affinity (PA) values or pK_a data. The problem of these easiest approaches is that the most typical organocatalytic step of initial interaction between catalyst and electrophilic carbon is not included. Thus, another approach – the methyl cation affinity (MCA) has been suggested and it has been shown to be much better descriptor of the organocatalytic activity.^[2] The MCA and PA data have been defined in the literature as the reaction enthalpies at 298.15 K for the transformations shown in equations 5.1a and 5.1b^[2]



Recent success of the MCA approach for some organocatalytic processes^[3] has encouraged the authors to apply this approach to the Morita-Bayllis-Hillman reaction. In addition to the application of the MCA scheme, the model is improved by making it more close to the experimental conditions. The use of the molecule of real Michael acceptor instead of the model methyl cation is suggested. If the Michael acceptor is methyl vinyl ketone, then the approach can be named methyl vinyl ketone affinity (MVKA) and the name “X” ketone affinity (XKA) if the ketone is a variable is used. XKA can be determined similarly to MCA as reaction enthalpies at 298 K or, for instance, as free energies at 298 K. The results of

additional consideration of the solvent by implicit solvation model are also discussed in this chapter.

5.2. MCA. Choice of the Systems and Methods

5.2.1. Systems

The MCA calculations are based on eqn. (5.1b), and the MCA values are computed as the reaction enthalpies at 298.15 K and 1 atm pressure. As systems to study we have selected phosphanes – the important MBH, as well as other organocatalytic processes, catalysts.

5.2.2. Methods

Values have been calculated at MP2(FC)/6-31+g(2d,p)//B98/6-31G(d) level. Thermochemical corrections have been calculated at B98/6-31G(d) level and combined with MP2(FC) single point calculations to obtain enthalpies at 298.15 K. The choice of the method is caused by the recent study, where it has been shown that this single point/geometry combination is able to reproduce G3 MCA values within 4 kJ mol⁻¹, being at the same time a much cheaper approach than G3.^[2] The MM3 parameters for the phosphonium cations have been developed and used for pre-optimization calculations within TINKER program^[4].

5.2.3. Development of MM3 Force Field Parameters for Phosphonium Derivatives and a Scheme for Accurate Conformational Search

The MM3 force field fits well to phosphane systems since it is parameterized for phosphane type phosphorus atoms as well as for different hydrocarbons.^[5] Thus it lets to describe with acceptable quality primary geometries (they are taken afterwards for quantum mechanical optimization) of different phosphine catalysts. However, force field parameters for phosphonium phosphorus atoms are not routinely included in popular force field programs. Force field parameters for alkyl phosphonium cations within MM3 paradigm have been parameterized and tested using TINKER software^[4]. This part of the project was done by Sven Österling under supervision of the present work author and Prof. Hendrik Zipse within the scope of research practice.^[6]

To have a basis for the force field phosphonium parameters quantum chemical calculations at MP2(FC)/6-31+G(d) level of theory have been performed. The model phosphonium-type molecule is quantum chemically optimized and then the necessary angles and bonds have been scanned (the results of various scan calculations are collected in

Appendix 9.5). Finally, using the necessary formulae from MM3 theory (vide infra) and the energies obtained from the quantum chemical calculations the set of force field parameters have been determined.^[5a]

The formulae used for the fitting of the parameters relying on the quantum chemically calculated energies are:

1. Van-der-Waals interactions

$$E_{vdw} = \sqrt{k_{v1}k_{v2}} \left[-2.25 \left(\frac{r_{v1} + r_{v2}}{r} \right)^6 + 1.84 \cdot 10^5 e^{\left(\frac{-12}{r_{v1} + r_{v2}} r \right)} \right] \quad (5.2)$$

The parameters to be found are k_v and r_v . k_{v1} and k_{v2} are factors describing relative strengths of interactions. r_{v1} and r_{v2} are the Van-der-Waals radii of the interacting atoms. r is the distance between the interacting atoms. In order to determine the parameters k_v and r_v for the phosphonium phosphorus atom, the distance scan calculation between a phosphonium cation and atom of inert gas have been performed.

2. Bond-stretching

$$E_s = 71.94k_s(l - l_0)^2 \left[1 - 2.55(l - l_0) + 2.55 \frac{7}{12} (l - l_0)^2 \right] \quad (5.3)$$

The parameters to be found are k_s and l_0 . l is the distance between connected atoms, it is varying during the scan calculations.

3. Angle bending

$$E_\theta = 0.021914k_\theta(\theta - \theta_0)^2 \cdot \left[1 - 0.014(\theta - \theta_0) + 5.6 \cdot 10^{-5}(\theta - \theta_0)^2 - 7 \cdot 10^{-7}(\theta - \theta_0)^3 + 9 \cdot 10^{-10}(\theta - \theta_0)^4 \right] \quad (5.4)$$

k_θ and θ_0 are the parameters to be found. θ is the angle varying during the scan calculations. There are three different variants of the parameters depending on the amount of hydrogen atoms connected with the phosphonium phosphorus atom: θ_0 (0 hydrogen atoms), $\theta_0(1H)$ (1 hydrogen atom) and $\theta_0(2H)$ (2 hydrogen atoms).

4. Torsions

$$E_\omega = 0.5[v_1(1 + \cos \omega) + v_2(1 - \cos 2\omega) + v_3(1 + \cos 3\omega)] \quad (5.5)$$

The v_3 -term describes the energy for the sp^3 -centers. The maxima and the minima repeat every 120 °C, it means that maxima are eclipse and minima are staggered conformations. For more complicated situations, when the gauche conformations are necessary to be treated

explicitly (e.g. in butane the *anti*-position is more preferable than *gauche*-) serves the ν_1 -term. The ν_1 -term is by 360 °C rotation a minimum (anti) and maximum (both conformations are eclipsed). For the sp^2 -centers the function of the ν_3 -term belongs to the ν_2 -term.

5. Stretch-bend, bend-bend and torsion-stretch interactions

$$\begin{aligned} E_{s,\theta} &= 2.51118k_{s,\theta}[(l-l_0)+(l'-l'_0)](\theta-\theta_0) \\ E_{\theta\theta'} &= -0.021914k_{\theta\theta'}(\theta-\theta_0)(\theta'-\theta'_0) \\ E_{os} &= 11.995\frac{k_{os}}{2}(l-l_0)(1+\cos(3\omega)) \end{aligned} \quad (5.6)$$

The stretch-bend interaction is used to allow bonds to stretch out when the angle between them is reduced and to shrink when that angle is increased. Bend-bend interaction is included in order to split apart the bending vibration frequencies involving two angles centered on the same atom. Bond lengths have to stretch also upon eclipsing, and to describe it the torsion-stretch interaction is applied.

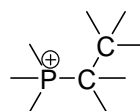
The determined parameters are collected in tables 5.1 – 5.3.

Table 5.1 The determined Van-der-Waals-Parameter for P^+ .

Parameter	Atom ^a	r_v	k_v
Vdw	112	1.850	0.381

^a In accordance with TINKER^[4] MM3 parameter list

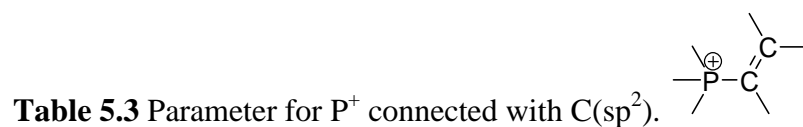
Table 5.2 Parameter for P^+ connected with $C(sp^3)$.



Parameter ^a	Type	Atom ^b	k_s	l_0		
CP	Bond	1 112	4.0595	1.8042		
Parameter ^a	Type	Atom ^b	k_θ	θ_0	$\theta_0(1H)$	$\theta_0(2H)$
CPC	Angle	1 112 1	0.675	109.471		
HCP	Angle	5 1 112	0.659	105.383	106.488	108.529
CCP	Angle	1 1 112	0.882	108.330	110.547	112.255
Parameter ^a	Type	Atom ^b	ν_1	ν_2	ν_3	
HCPC	torsion	5 1 112 1	0.000	0.000	0.226	
CCPC	torsion	1 1 112 1	0.191	0.000	0.352	
HCCP	torsion	5 1 1 112	0.000	0.000	0.217	

CCCP	torsion	1 1 1 112	1.355	0.000	0.681
------	---------	-----------	-------	-------	-------

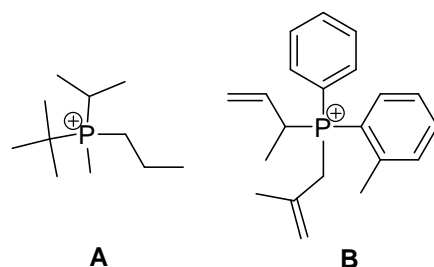
^a C stands for sp³ carbon atom, D – for sp² carbon atom, P- for phosphonium P⁺ atom, H – for hydrogen; ^b In accordance with TINKER^[41] MM3 parameter list.



Parameter ^a	Type	Atom ^b	k_s	l_0		
DP	bond	2 112	3.6318	1.8057		
Parameter ^a	Type	Atom ^b	k_θ	θ_0	$\theta_0(1H)$	$\theta_0(2H)$
DPC	angle	1 112 2	0.613	110.219		
DDP	angle	2 2 112	0.401	123.075		
DPD	angle	2 112 2	0.673	108.842		
DCP	angle	2 1 112	0.595	110.378	109.382	112.966
Parameter ^a	Type	Atom ^b	ν_1	ν_2	ν_3	
DDPC	torsion	2 2 112 1	-0.459	-0.327	1.428	
DDDP	torsion	2 2 2 112	0.000	3.248	0.000	
HDDP	torsion	5 2 2 112	0.000	1.976	0.000	
CDDP	torsion	1 2 2 112	0.000	11.941	0.000	
DDPD	torsion	2 2 112 2	0.000	0.000	1.526	
DPCH	torsion	5 1 112 2	0.000	0.004	0.214	
DPCC	torsion	1 1 112 2	-0.342	0.142	0.541	
DDCP	torsion	2 2 1 112	0.465	-1.667	-0.240	
HDCP	torsion	5 2 1 112	0.000	0.000	0.060	
DCPC	torsion	2 1 112 1	0.000	0.000	0.475	
DCPD	torsion	2 1 112 2	0.000	0.000	1.300	
CDCP	torsion	1 2 1 112	1.622	0.289	0.328	

^a C stands for sp³ carbon atom, D – for sp² carbon atom, P- for phosphonium P⁺ atom, H – for hydrogen; ^b In accordance with TINKER^[41] MM3 parameter list.

To test the quality of the new parameter set, two molecules have been chosen, which contain the moieties as much as possible corresponding to the situations described by the found parameters (e.g different carbon atoms (sp³ and sp²) connected (and not) directly to the phosphonium phosphorus atom). The used molecules are shown in Scheme 5.1.



Scheme 5.1 Molecules used for testing new parameters.

For both molecules potential energy surface scans have been performed. In Fig 5.1 the MM3 energies with use of new parameters are compared with quantum chemical energies (MPW1K/6-31G(d)) for every MM3-structure. It has to be emphasized, that DFT has been chosen due to large amount of necessary calculations, though the new parameters have been parametrized relying on MP2 calculations. Hypothetically, the discrepancy between MM3 calculations including new parameters with MP2 will be smaller as it is with DFT. The energy units in calculations, shown in Fig. 5.1 as well as in other performed scan calculations, are changed from kJ mol^{-1} to kcal mol^{-1} in accordance with the MM3 theory.^[5a]

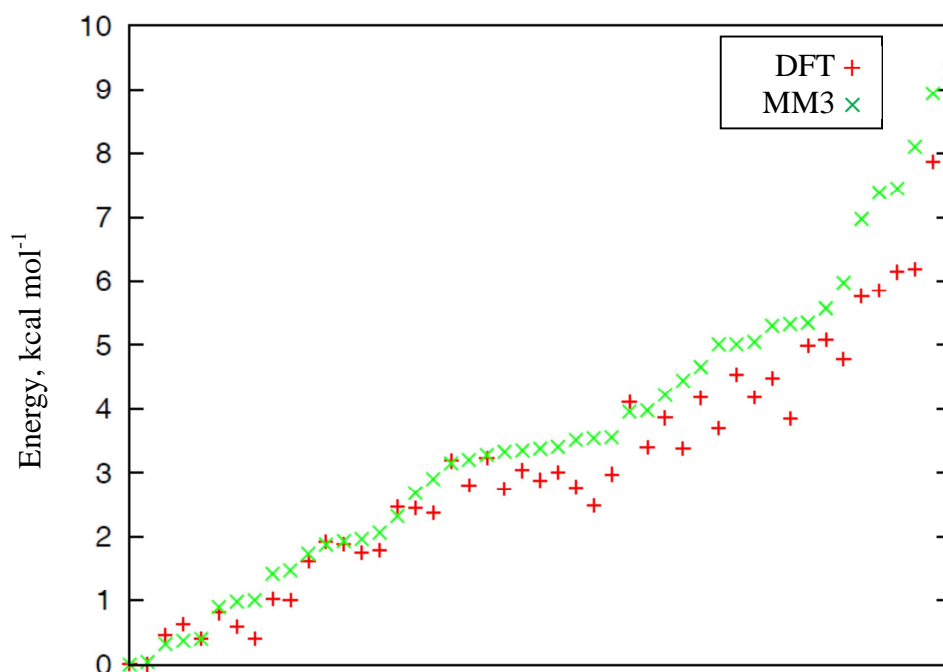


Fig 5.1 MM3-Energies of the potential energy surface scan with new parameters in comparison with DFT-energies for the “ sp^3 -molecule” **A**.

The MM3 and DFT energy trends for the “ sp^3 -molecule” **A** correlate good with each other. The analogous scan for the “ sp^2 -molecule” **B** is presented in Fig. 5.2.

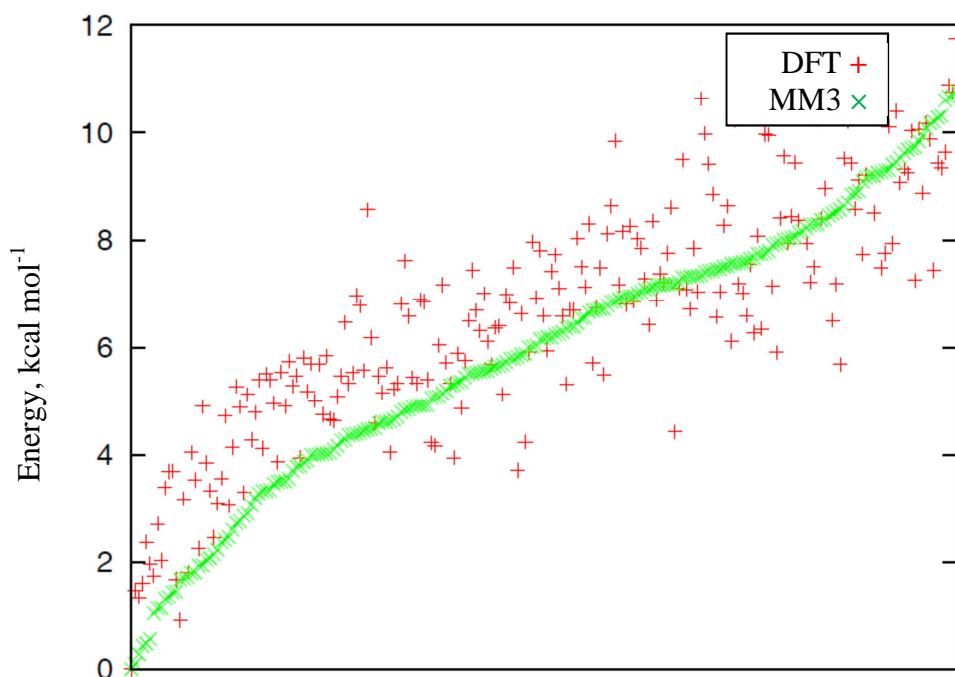


Fig 5.2 MM3-Energies of the potential energy surface scan with new parameters in comparison with DFT-energies for the “ sp^2 -molecule” **B**.

In the latter case the scattering picture has been observed. In order to check whether the reason of the FF/QM discrepancy is only the use of the new parameters, the phosphonium atom was exchanged to another atom (Si has been used), while the substituents have not been changed. The obtained scan is presented in Fig. 5.3

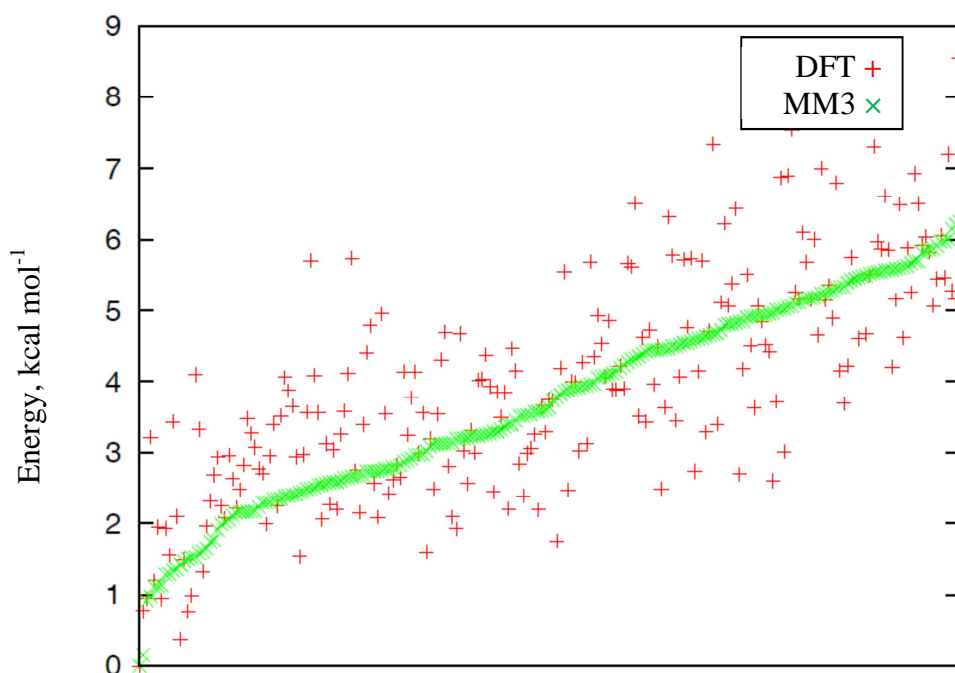


Fig 5.3 MM3-Energies of the potential energy surface scan with new parameters in comparison with DFT-energies for “ sp^2 -molecule” **B** (Si instead of P).

As one can conclude from the Fig. 5.3, the reason of the discrepancy is not only in the new parameters. There is some general problem in MM3 describing molecules containing $C(sp^2)$, thus one can see the structure in Fig. 5.4, where the terminal hydrogen atoms of the allyl group are wrong located.

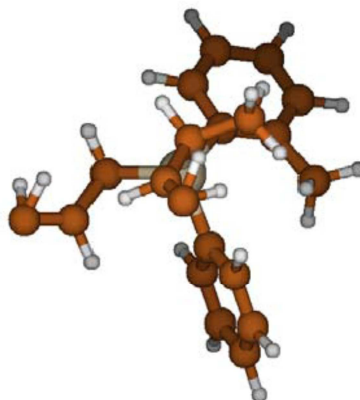


Fig 5.4 A random structure (local minimum) of the sp^2 -Si-molecule. Noteworthy the allyl-H atom positions are wrong.

Thus, additional work in the force field parametrization is required to describe the phosphonium cations containing sp^2 carbon atoms. However, it is important to note, that the global minimum has also been correctly found by the force field approach for the “ sp^2 molecule” **B**.

In the following MCA and XKA calculations the TINKER program in combination with the MM3 force field, including the new phosphonium parameters, and for some selected systems the MM3* force field as implemented in MACROMODEL 9.7 have been used.^[4, 7]

The accurate search of the conformational space for flexible systems (large amount of structures generated by force field calculations) takes a lot of CPU time. In order to make the calculations cheaper without considerable loss of accuracy, the following scheme was used (in graphical manner shown in Fig. 5.5):

1. The force field conformational search. (“FF structures” in Fig. 5.5).
2. Single point calculations for all FF-derived structures at DFT level in the variant of B98/6-31(d) level for MCA calculations, MPW1K/6-31G(d) for MVKA calculations or MPW1K/6-31+G(d) for XKA calculations.
3. Comparison of the obtained relative energy values and discarding unstable conformations (everything that is $\sim 30 \text{ kJ mol}^{-1}$ less stable than the global minimum can be neglected).
4. Quantum chemical (DFT) optimization of selected stable conformations and comparison of the optimized structures energies (“DFT structures” in Fig. 5.1). DFT is

used in the variant of B98/6-31(d) for MCA calculations, MPW1K/6-31G(d) for MVKA calculations or MPW1K/6-31+G(d) for XKA calculations.

- MP2(FC)/6-31+G(2d,p) single point calculations for the most stable conformations after DFT optimization (again everything that is ~ 30 kJ mol⁻¹ less stable than global minimum can be neglected).
- The conformations that have MP2(FC)/6-31+G(2d,p) relative energies in a range of ~ 15 kJ mol⁻¹ (“result” in Fig. 5.5) should be taken for the Boltzmann averaging procedure.

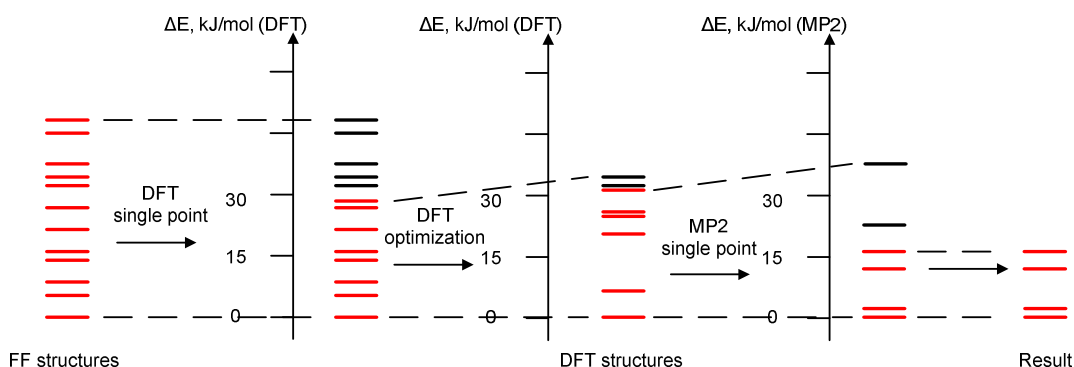


Fig. 5.5 Scheme of an accurate conformational search (black – neglected conformers, red – important conformers).

5.3. MCA Values for Phosphanes

5.3.1. Phosphanes With Unbranched and Branched Acyclic Alkyl Substituents and Cyclic Substituents

MCA calculations for a sample of phosphanes with unbranched and branched acyclic and cyclic substituents have been performed. The results are collected in Table 5.4 and graphically shown in Fig. 5.9.

Cristoph Lindner (PhD student of Prof. Hendrik Zipse) has carefully analysed the calculated data (from Boris Maryasin and Christoph Lindner) and some general regularities have been found.^[8]

- The effects of the substituents are largely additive - for phosphanes with the general formula PR_n with $n = 0-3$, there is an “impressively good”^[8] correlation between MCA values and the value of n (Fig. 5.6). The MCA value of trisubstituted phosphanes PR_3 can be estimated from the MCA values of PMe_2R and PMe_3 using eqn (5.2).

$$\text{MCA}(\text{PMe}_{3-n}\text{R}_n) = \text{MCA}(\text{PMe}_3) + n \times (\text{MCA}(\text{PMe}_2\text{R}) - \text{MCA}(\text{PMe}_3)) \quad (5.7)$$

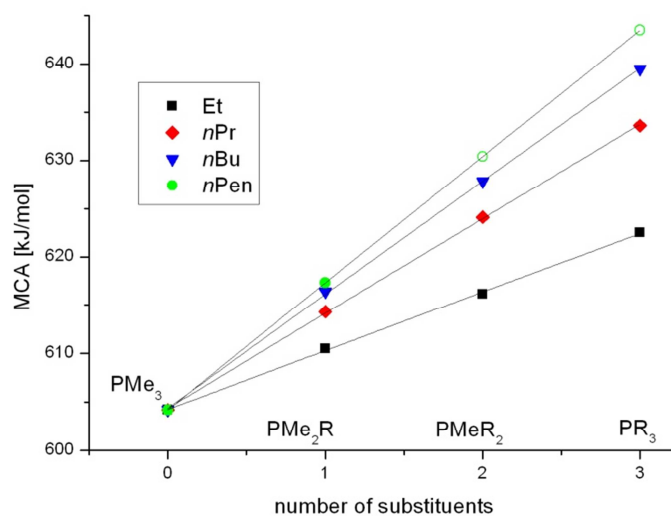


Fig. 5.6 MCA values of trialkylphosphanes with linear alkyl substituents.

- The slope of the linear correlation MCA vs. n depends on the length of the alkyl substituent. Eqn. (5.3) expresses the exponential character of this dependence for unbranched acyclic substituents (Fig. 5.7), eqn. (5.4) – analogously for cyclic substituents.

$$\text{MCA}(\text{Me}_2\text{P}(\text{CH}_2)_n\text{H}, \text{kJ mol}^{-1}) = 618.8 - 26.1 \times 0.56^n \quad (5.8)$$

$$\text{MCA}(\text{Me}_2\text{P}(\text{CH})(\text{CH}_2)_{n+1}), \text{kJ mol}^{-1}) = 625.3 - 35.5 \times 0.51^n \quad (5.9)$$

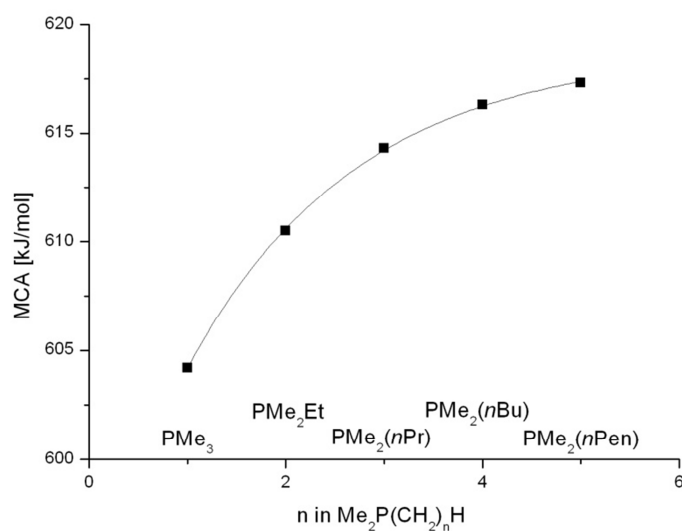


Fig. 5.7 MCA values of monosubstituted phosphanes of general formula $\text{Me}_2\text{P}(\text{CH}_2)_n\text{H}$ ($n = 1 - 5$, in kJ/mol).

- A general eqn. (5.10) can be built for all the systems. This equation connects the MCA values with the size parameters of the alkyl groups attached to the phosphorus atom.

$$\text{MCA}[\text{kJ mol}^{-1}] = 604.2 + 6.1b + 3.7c + 2.0d + 1.0e + x \quad (5.10)$$

In the eqn. (5.10) the parameters a, b, c, d and e are the numbers of methyl and methylene groups in β -, γ -, δ - and ϵ -positions and x represents a varying correction factor depending on the class of compound. Representation of the correlation of MCA values obtained at MP2(FC)/6-31+G(2d,p)//B98/6-31G(d) level with those found using eqn. 5.10 are shown in Fig. 5.8.

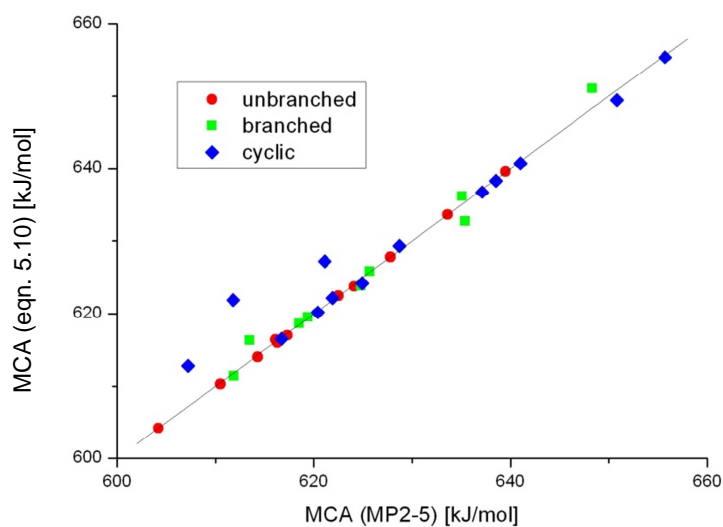


Fig. 5.8 Correlation of MCA values calculated with eqn. (5.10) with those obtained by MP2(FC)/6-31+G(2d,p)//B98/6-31G(d) method.

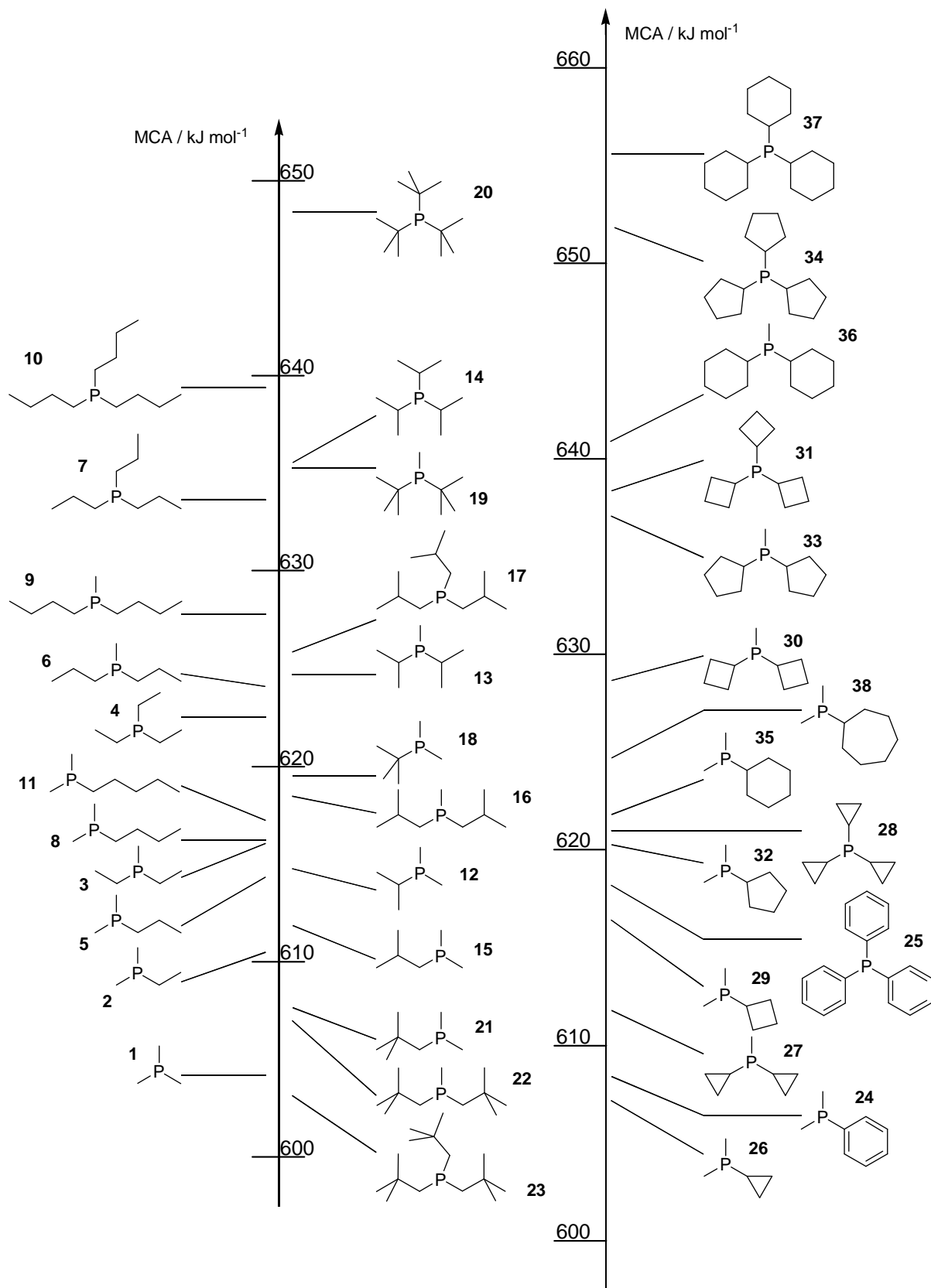


Fig. 5.9 Structures of trisubstituted phosphanes with acyclic and cyclic alkyl substituents, ordered by their respective MCA values (in kJ mol^{-1}).

Table 5.4. Methyl Cation Affinity (MCA) values for a variety of phosphanes calculated according to eqn. (5.1b) at MP2(FC)/6-31+G(2d,p)//B98/6-31G(d) level (in kJ mol⁻¹).^a

System	MCA [kJ mol ⁻¹]	System	MCA [kJ mol ⁻¹]
P(CH ₂ <i>t</i> Bu) ₃ (23) ^b	+603.3	PMe ₃ (1)	+604.2
PMe(CH ₂ <i>t</i> Bu) ₂ (22) ^b	+606.9	Pme ₂ (<i>c</i> Pr) (26)	+607.2
PMe ₂ (CH ₂ <i>t</i> Bu) (21) ^b	+607.9	PMe ₂ Ph (24) ^c	+608.5
PMe ₂ Et (2)	+610.5	PMe(<i>c</i> Pr) ₂ (27) ^b	+611.8
PMe ₂ (<i>i</i> Bu) (15) ^b	+611.9	PMe ₂ (<i>i</i> Pr) (12)	+613.5
PMe ₂ (<i>n</i> Pr) (5)	+614.3	PMeEt ₂ (3) ^b	+616.1
PMe ₂ (<i>n</i> Bu) (8)	+616.	PMe ₂ (<i>c</i> Bu) (29)	+616.7
PMe ₂ (<i>n</i> Pen) (11) ^b	+617.3	PPh ₃ (25) ^b	+618.4
PMe(<i>i</i> Bu) ₂ (16) ^b	+618.5	PMe ₂ (<i>t</i> Bu) (18) ^b	+619.4
PMe ₂ (<i>c</i> Pen) (32)	+620.4	P(<i>c</i> Pr) ₃ (28) ^b	+621.8
PMe ₂ (<i>c</i> Hex) (35)	+621.9	PEt ₃ (4) ^b	+622.5
PMe(<i>n</i> Pr) ₂ (6) ^b	+624.1	PMe(<i>i</i> Pr) ₂ (13)	+624.8
PMe ₂ (<i>c</i> Hep) (38) ^b	+624.9	P(<i>i</i> Bu) ₃ (17) ^b	+625.7
PMe(<i>n</i> Bu) ₂ (9) ^b	+627.8	PMe(<i>c</i> Bu) ₂ (30) ^b	+628.7
P(<i>n</i> Pr) ₃ (7)	+633.6	PMe(<i>t</i> Bu) ₂ (19) ^b	+633.9
PMe(<i>t</i> Bu) ₂ (19) ^b	+635.1	P(<i>i</i> Pr) ₃ (14)	+635.4
PMe(<i>c</i> Pen) ₂ (33)	+637.1	P(<i>c</i> Bu) ₃ (31) ^b	+638.5
P(<i>n</i> Bu) ₃ (10) ^b	+639.5	PMe(<i>c</i> Hex) ₂ (36) ^b	+641.0
P(<i>t</i> Bu) ₃ (20) ^b	+648.3	P(<i>c</i> Pen) ₃ (34)	+650.8
P(<i>c</i> Hex) ₃ (37) ^b	+655.7		

^aAbbreviations: Pen stands for pentyl, Hex for hexyl, Hep for heptyl. ^bCalculated by Cristoph Lindner

5.3.2. Cyclophane-substituted and Cyclic Phosphanes

Organocatalysts with a cyclophane motif are potentially interesting due to their intrinsic planar chirality. However, examples of such organocatalysts are relatively rare.^[9] MCA values have therefore been calculated for substituted phosphanes in order to have preliminary information about potential efficiency of that type molecules for organocatalytic processes. Another class of phosphanes that has been checked via the MCA approach concerns cyclic phosphanes. The results of MCA calculations of cyclophane-substituted systems are shown graphically in Fig. 5.10.

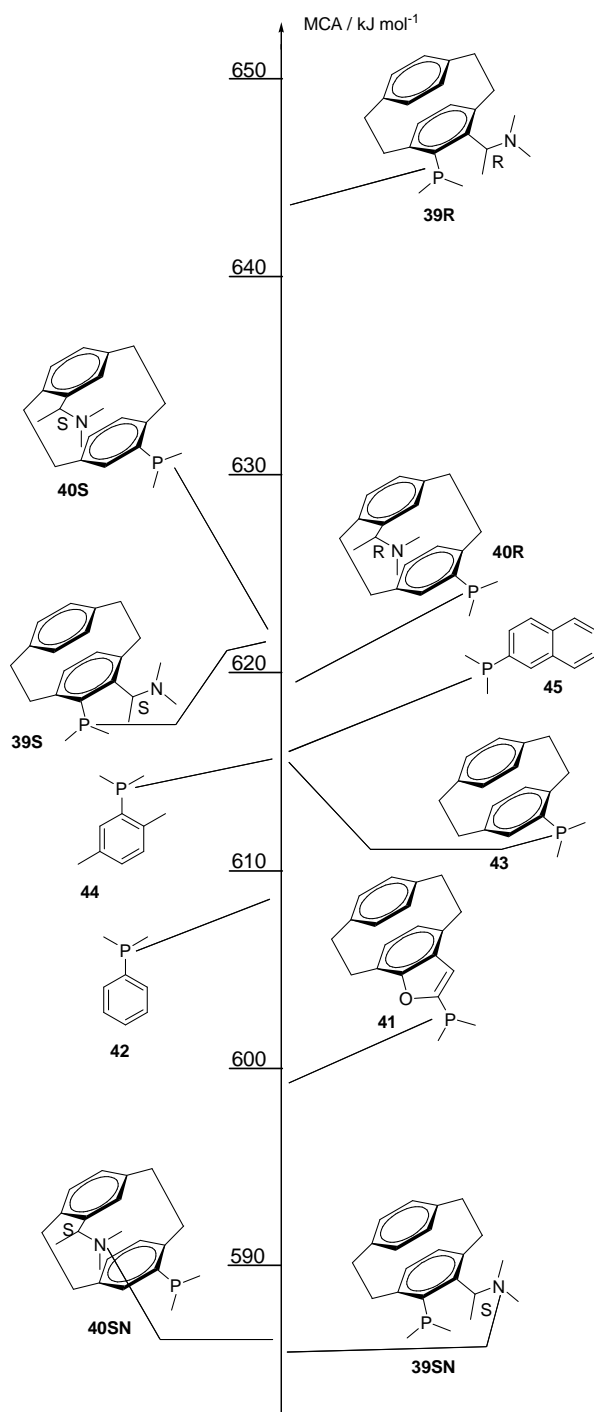


Fig. 5.10 Structures of cyclophane-substituted phosphanes ordered by their MCA values.

Table 5.5. Methyl Cation Affinity (MCA) values for a variety of cyclophane-substituted phosphanes calculated according to eqn. (5.1b) at MP2(FC)/6-31+G(2d,p)//B98/6-31G(d) level (in kJ mol⁻¹).

System	MCA [kJ mol ⁻¹]	System	MCA [kJ mol ⁻¹]
39SN	586.0	40SN	586.6
41	591.3	42	608.5
43	614.0	44	614.3
45	616.4	40R	619.7
39S	620.8	40S	621.3
39R	642.0		

The MCA values are relatively low (+591.3 – +616.4 kJ mol⁻¹) for systems **41** – **45** as compared to the MCA values of the series phosphanes with cyclic and acyclic alkyl substituents analyzed in the previous chapter (+603.3 – 650.8 kJ mol⁻¹). It should be emphasized that, the bigger the MCA value is, the bigger the efficiency of the catalyst expected is. Interestingly, the MCA of the systems **45**, **44** and **43** are almost equal (616.4, 614.3 and 614.0 kJ mol⁻¹ respectively), showing that the influence of the 2-naphtyl, *p*-xylyl and cyclophane groups are relatively equivalent. In both systems **39** and **40** one of the cyclophane phenyl rings has a 1-(dimethylamino)ethyl substituent. The distinction is that this group and the phosphorus atom are connected to the same aromatic ring in catalyst **39**, while in the catalyst **40** the substituents are separated by one per aromatic ring. The 1-(dimethylamino)ethyl group contains a chiral C atom and since the cyclophane group induces planar chirality, there are two possible diastereomers for each of the catalyst **39** and **40**. As one can easily see from the Fig. 5.4 and Table 5.5 the catalyst **39**, where the substituents are in the same ring, has quite large MCA value of 642 kJ mol⁻¹ but only if the chiral C atom of the 1-(dimethylamino)ethyl group is R-configured (**39R**) and this is the biggest MCA from all studied cyclophane family members. If the chiral atom is S-configured (**39S**), then the MCA value is much smaller (620.8 kJ mol⁻¹) and similar to values calculated for catalyst **40** in R or S configuration: 619.7 kJ mol⁻¹ (**40R**) and 623.1 kJ mol⁻¹ (**40S**). The big difference between two diastereomers of the catalyst **39** can mean that significant diastereoselectivity could be expected. The predicted value of 642 kJ mol⁻¹ for MCA means also, that this catalyst can be effective. It has to be stated here, that the MCA values (from Lindner and Maryasin) have been compared by Liu^[10] with the kinetic data for several phosphane catalysts in aza-

MBH reaction. It has been shown, that for the most effective catalysts the MCA values amount to $\sim 620 \text{ kJ mol}^{-1}$.

The reason for the big (and so different to its analogous) MCA value for catalyst **39R** is the strong stabilization in the phosphonium adduct between catalyst **39R** and methyl cation (Fig. 5.11).

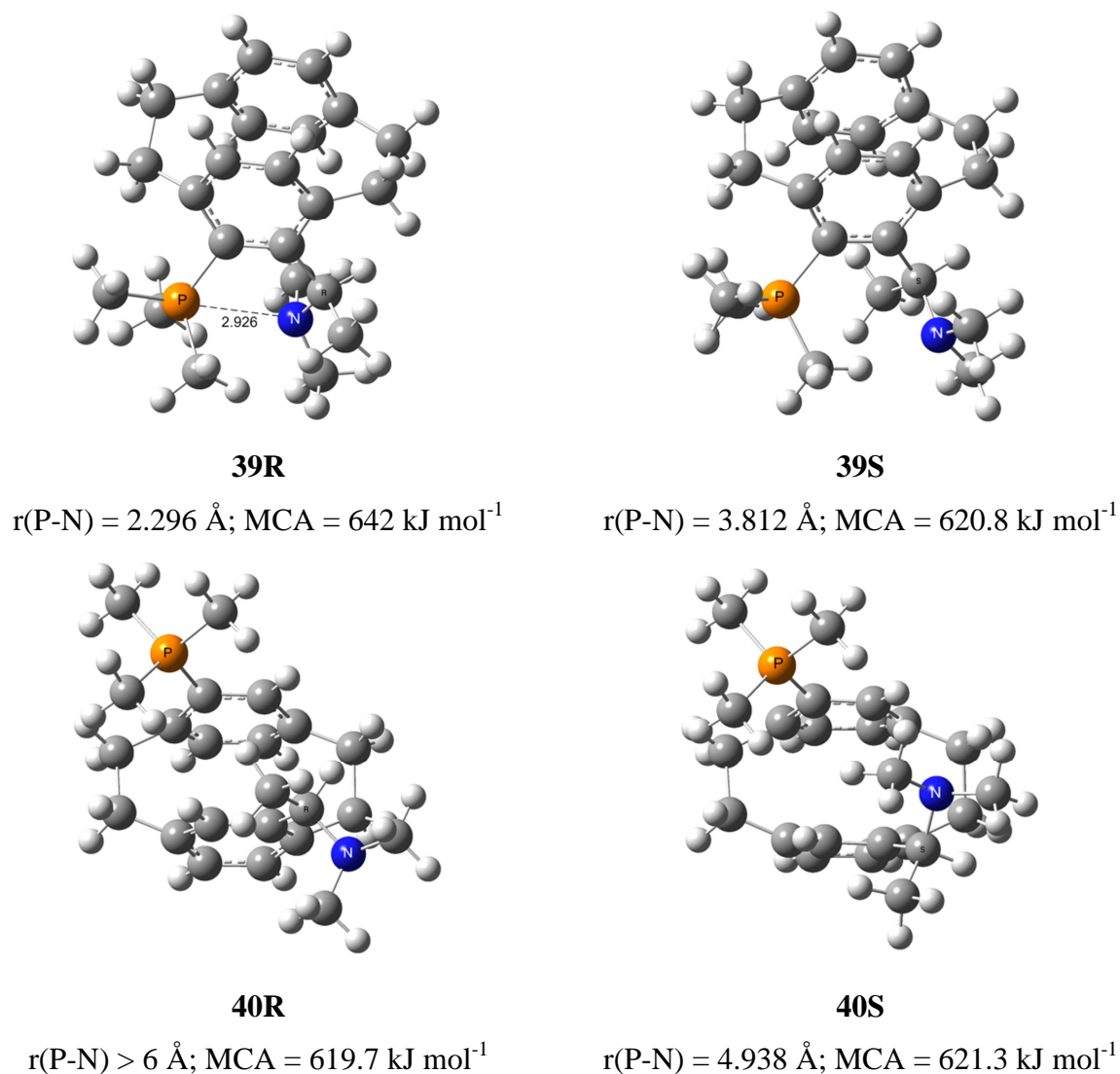


Fig. 5.11 Structures of the most stable conformations for adducts between catalysts **39** and **40** (both diastereomers) and methyl cation. Distances between phosphorus and nitrogen atoms and MCA values in comparison.

The two factors – the neighbourhood of the substituents, containing phosphorus and nitrogen atoms and the R configuration of the chiral C atom – appear to be necessary and sufficient to form the intramolecular interaction between the P and N atoms ($r(\text{R-N}) = 2.926 \text{ \AA}$). Neither the S-configured variant of catalyst **39** adduct nor both diastereomers of system **40** have such a stabilization feature and thus have much smaller MCA. This is one additional example

of the importance of inter- and intramolecular interactions for organocatalytic processes. For systems **39** and **40** methyl cation addition is also possible to the nitrogen atom. The ability of a competition between the ammonium and the phosphonium cation formation has been checked. Much smaller MCA value of $586.0 \text{ kJ mol}^{-1}$ for the ammonium vs. $620.8 \text{ kJ mol}^{-1}$ for the phosphonium cation, formed from the catalyst **39** with *S* configuration of chiral C atom, and 586.6 vs. $621.3 \text{ kJ mol}^{-1}$ – from catalyst **40** have been obtained.

In Fig. 5.12 and in Table 5.6 MCA values for cyclic phosphanes are shown.

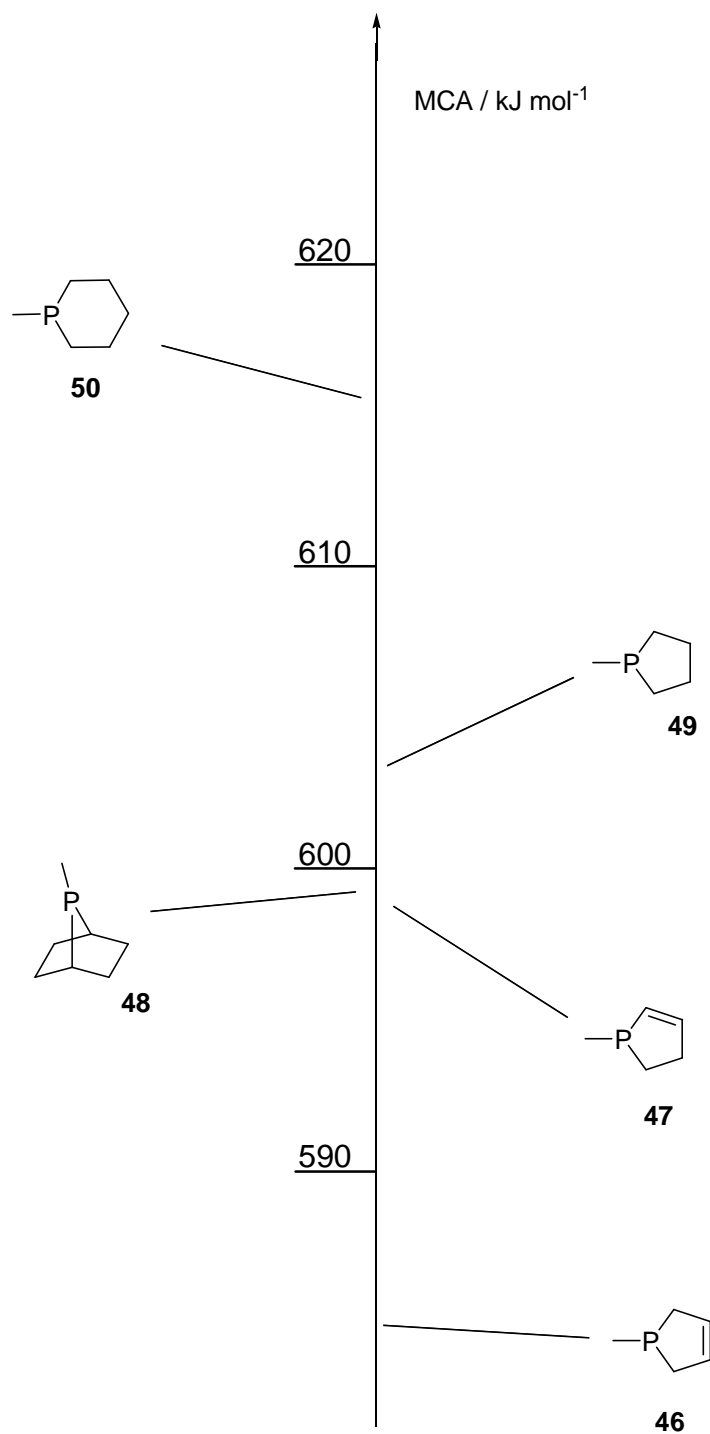


Fig 5.12 Structures of cyclic phosphanes, ordered by their respective MCA values.

Table 5.6 Methyl Cation Affinity (MCA) values for cyclic phosphanes, calculated according to eqn. (5.1b) at MP2(FC)/6-31+G(2d,p)//B98/6-31G(d) level (in kJ mol^{-1}).

System	MCA [kJ mol^{-1}]	System	MCA [kJ mol^{-1}]
46	584.0	47	597.0
48	598.5	49	602.0
50	616.8		

These systems show quite moderate MCA values, the largest is $616.8 \text{ kJ mol}^{-1}$ for system **50**. In Fig. 5.13 the MCA values of the cyclic phosphanes are compared to similar acyclic systems.

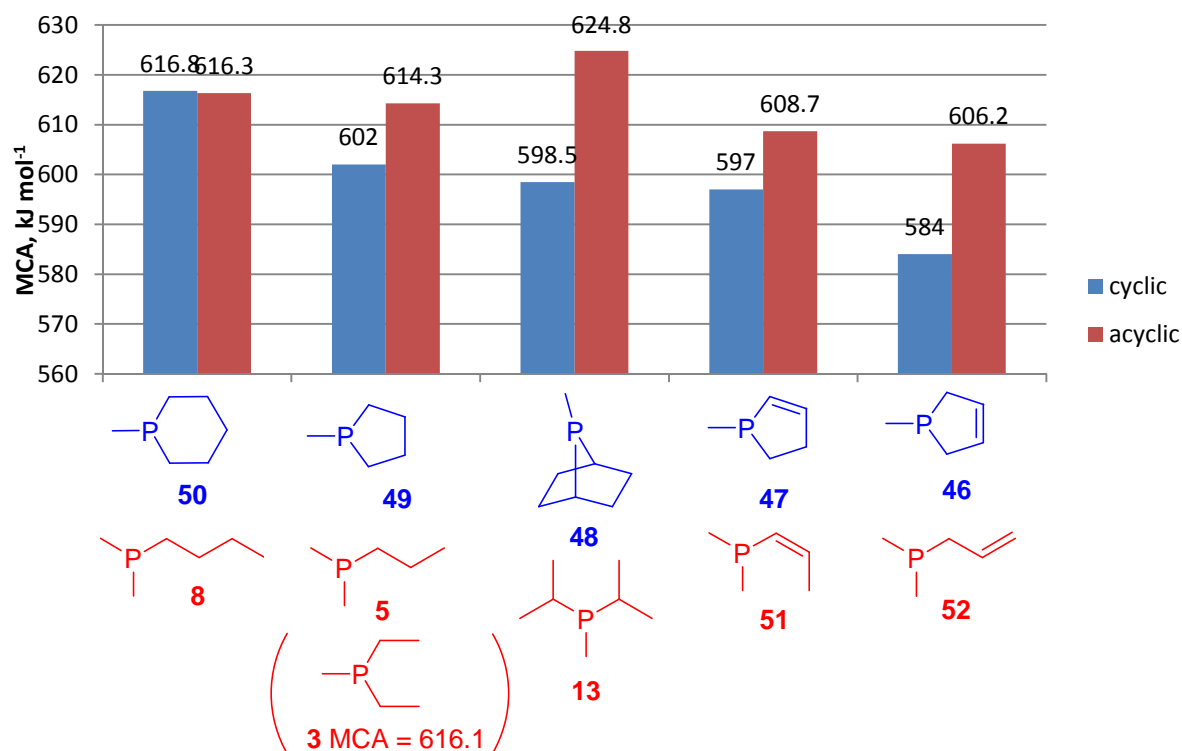
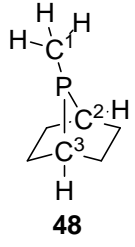


Fig. 5.13 The MCA values of cyclic phosphanes as compared to acyclic analogues.

The acyclic systems have larger values of MCA excepting the case of system **50**, which has almost the same value of the MCA as its acyclic analogue. As it should be expected the cyclic phosphanes have strain due to the cycle structure. Latter makes the discrepancy between these phosphanes and the acyclic analogues. For the phosphanes **48** and **13** the MCA values difference is the largest and amounts to 26.3 kJ mol^{-1} . In order to clarify this difference, the geometries of the corresponding systems (both phosphanes and both adducts

with methyl cation) can be compared. In the Table 5.7 the out-of-plane displacements (in terms of dihedral angles α in accordance with the Table 5.7) are collected.

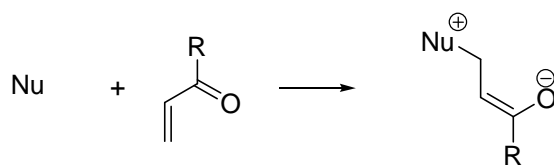
Table 5.7 Pyramidalization in the systems **48/48Me⁺** and **13/13Me⁺**

	System	α	$\alpha(\text{PR}_3) - \alpha(\text{PR}_3\text{Me}^+)$
48	48	39.9	8.7
	48Me⁺	31.2	
	13	45.7	10.9
	13Me⁺	34.8	

One can see that pyramidalization is bigger in the acyclic system **13/13Me⁺**. The difference in the dihedral angles α shows, that in the case of system **48/48Me⁺** the geometrical change (on the example of α) is a bit smaller, than in the system **13/13Me⁺**. The acyclic system **13/13Me⁺** has no strain and therefore it is more flexible. Thus, smaller energetic difference between phosphane **48** and adduct **48Me⁺** (it is represented by the MCA value) as compared to the system **13/13Me⁺** correlates with the geometries of the phosphanes and the methyl cation adducts. The system **50** is the most unstrained among all cyclic systems due to the cycle size, thus there is no big difference between its MCA (616.8 kJ mol⁻¹) and MCA of the acyclic system (616.3 kJ mol⁻¹).

5.4. MVKA and XKA

The XKA is defined as the reaction energy for the transformation shown in Scheme 5.2

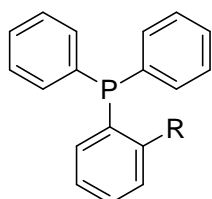


Scheme 5.2 Michael addition step of the MBH reaction.

The “X” means that the ketone is varying. If the ketone is MVK, then the descriptor of catalytic activity is called MVKA.

5.4.1. MVKA of Recently Synthesized Bifunctional Phosphane Catalysts

A new family of bifunctional phosphane catalysts (BPC) with general formula shown in Scheme 5.3, have been recently synthesized and their efficiency in the MBH reaction (reaction between *p*-chlorbenzaldehyde and MVK) has been tested.^[10]



BPC1: R = NHC(O)C(CH₃)₃;

BPC2: R = NHC(O)Me;

BPC3: R = NHC(O)Ph;

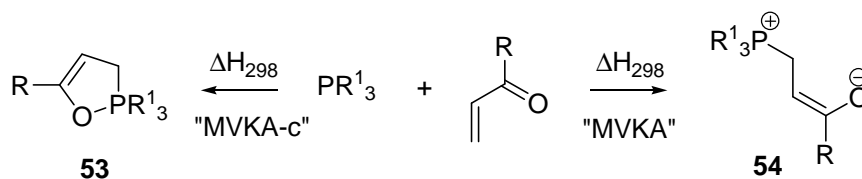
BPC4: R = NHC(O)C₆H₄(*p*-MeO);

BPC5: R = NHC(O)C₆H₄(*p*-CN);

BPC6: R = OH;

Scheme 5.3 Bifunctional phosphane catalysts.

The conversion [%], corresponding reaction time [h] and (for some cases) the half-life time [h] have been presented^[10] for this family of catalysts, that allows to rank the catalysts by its activity. In this chapter the comparison of the experimental kinetic data (qualitative data (conversion and reaction time) and (if available) quantitative (half-life time)) with the values of MVKA will be shown. Reaction between phosphorus-containing Lewis base and MVK can lead to the acyclic zwitterionic intermediate **54** (*vide* Scheme 5.4) or cyclic adduct **53**. The enthalpies at 298 K of the formation of acyclic zwitterionic adduct **54** will in the following be termed “MVKA” and in the case of cyclic complex **53** “MVKA-c”.

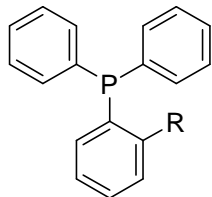
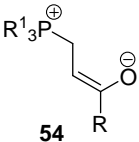
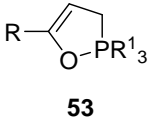


Scheme 5.4 Formation of acyclic and cyclic adducts between phosphane catalyst and Michael acceptor.

Geometry optimization has been performed at MPW1K/6-31G(d) level of theory. The thermal corrections to the enthalpies H_{298} at 298.15 K have been calculated for all stationary points from unscaled vibrational frequencies obtained at the MPW1K/6-31G(d) level. In previous chapters the importance to use MPW1K/6-31+G(d) for zwitterionic intermediates has been noted. The calculations of “MVKA” and “MVKA-c” presented here are based, however, on the MPW1K/6-31G(d) geometries. The reason of this inconsistency is that the “MVKA”/“MVKA-c” calculations have been performed before the observation made by Wei,

Sateesh, Maryasin, Sastry and Zipse about better efficiency of the MPW1K/6-31+G(d) level.^[3c] Nevertheless, the adequacy of MPW1K/6-31G(d) application for the MVKA calculations of **BPC** family has been checked. For instance, such basis set improvement changes the MVKA value of the **BPC0** only by 0.8 kJ mol⁻¹. This small energy difference can be neglected. The thermal corrections have been combined with single point energies calculated at the MP2(FC)/6-31+G(2d,p)//MPW1K/6-31G(d) level to yield enthalpies H₂₉₈ at 298.15 K. Table 5.8 collects the result of the MVKA and MVKA-c calculations.

Table 5.8 Experimental results of the BPC family as compared with the MVKA and MVKA-c values of these catalysts.

Catalyst	Experimental data: time and conversion; experimental rank ^a	Half-life time/min ^b	MVKA ^c	MVKA-c ^c
				
BPC0 (PPh ₃), R = H	15h, 19%, +	1020	+23.1	-41.5
BPC1 , R = NHC(O)C(CH ₃) ₃	22h, 64%, +++	320	-31.1	-57.1
BPC2 , R = NHC(O)Me	20h, 62%, +++	400	-28.9	-59.8
BPC3 , R = NHC(O)Ph	20h, 47%, ++	630	-26.7	-60.7
BPC4 , R = NHC(O)C ₆ H ₄ (<i>p</i> -MeO)	20h, 53%, ++	-	-26.0	-60.5
BPC5 , R = NHC(O)C ₆ H ₄ (<i>p</i> -CN)	19h, 12%, +	-	-31.4	-62.3
BPC6 , R = OH	~0%, -	-	-67.0	-49.4

^aThe experimental data are taken from Liu.^[10] Since the kinetic data are rather qualitative (not for all systems the half-life time is available), qualitative “experimental rank” – the degree of catalyst efficiency is involved: the more “+” a catalysts has, the more efficient it is.

^bUnpublished results of Yinghao Liu, available only for four systems

^cGas-phase; MP2(FC)/6-31+G(2d,p)//MPW1K/6-31G(d); thermochemical corrections: MPW1K/6-31G(d).

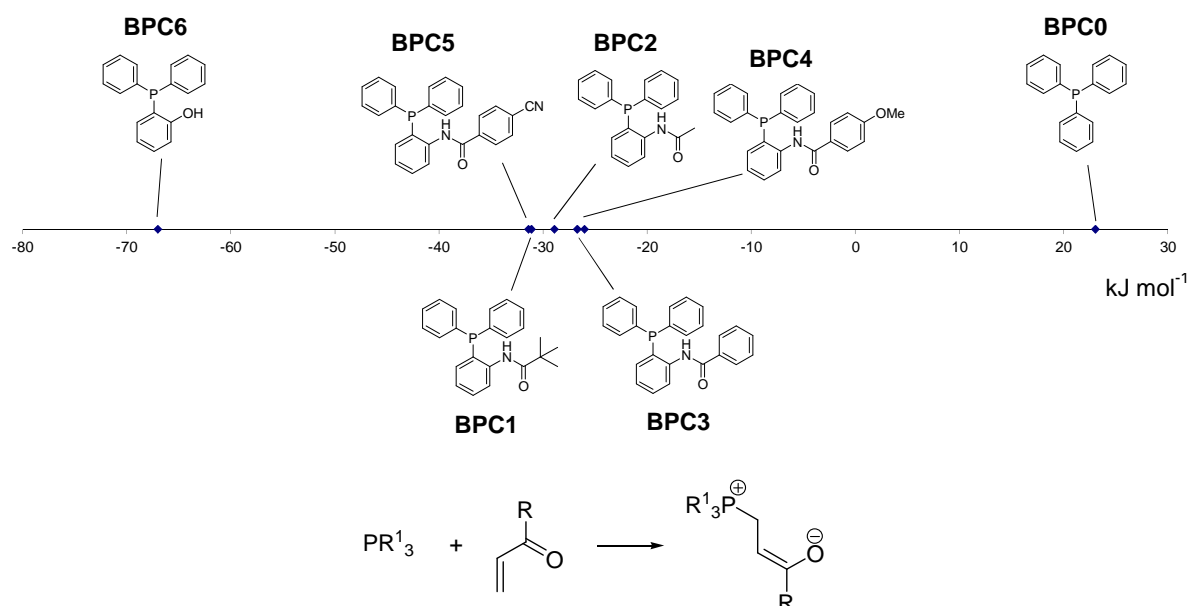


Fig. 5.14 The MVKA scale of the BPC family.

The results of MVKA calculations are shown in graphical form in Fig. 5.14. From Fig. 5.14 and Table 5.7 it is clear to see two very different MVKA values: of PPh_3 ($+23.1 \text{ kJ mol}^{-1}$) and **BPC6** ($-67.0 \text{ kJ mol}^{-1}$), though 5 other catalysts have MVKA values around -30 kJ mol^{-1} . These two catalysts PPh_3 and **BPC6** are also very special in view of the experimental results. For PPh_3 (without co-catalyst) the conversion is very small (15h, 19%) and for **BPC6** no conversion is observed. Relying on the MVKA calculations, a hypothesis can be proposed, that the reason of inefficiency of the **BPC6** is the dramatic stabilization of the adduct with MVK via protonation, that proceeds without barrier ($r(\text{O}_{\text{MVK}}\text{-H}_{\text{OH}}) = 0.996 \text{ \AA}$ – the distance between oxygen atom of the MVK moiety of the adduct and hydrogen atom from the OH group). As a result the system is away from the catalytic cycle and stays in the protonated state. In the case of PPh_3 the zwitterionic adduct is stabilized through hydrogen bonding between a hydrogen atom of the phenyl ring and the MVK oxygen atom with $r(\text{O-H}) = 1.896 \text{ \AA}$. The situation is changed significantly if one of the BPC catalysts with MVKA around -30 kJ mol^{-1} (Fig. 5.14) is observed. As an example in **BPC1** (one of the most efficient among the BPC family (*vide* Table 6.7), a strong stabilizing hydrogen bond ($r(\text{O}_{\text{MVK}}\text{-H}_{\text{NH}}) = 1.541 \text{ \AA}$) is formed between the MVK moiety and the hydrogen of the -NH- fragment. The intermediate is not completely protonated and still involved in the catalytic cycle, but stabilized and thus likely to be formed. The structures of the acyclic adducts for **BPC6**, PPh_3 and **BPC1** are shown in Fig. 5.15.

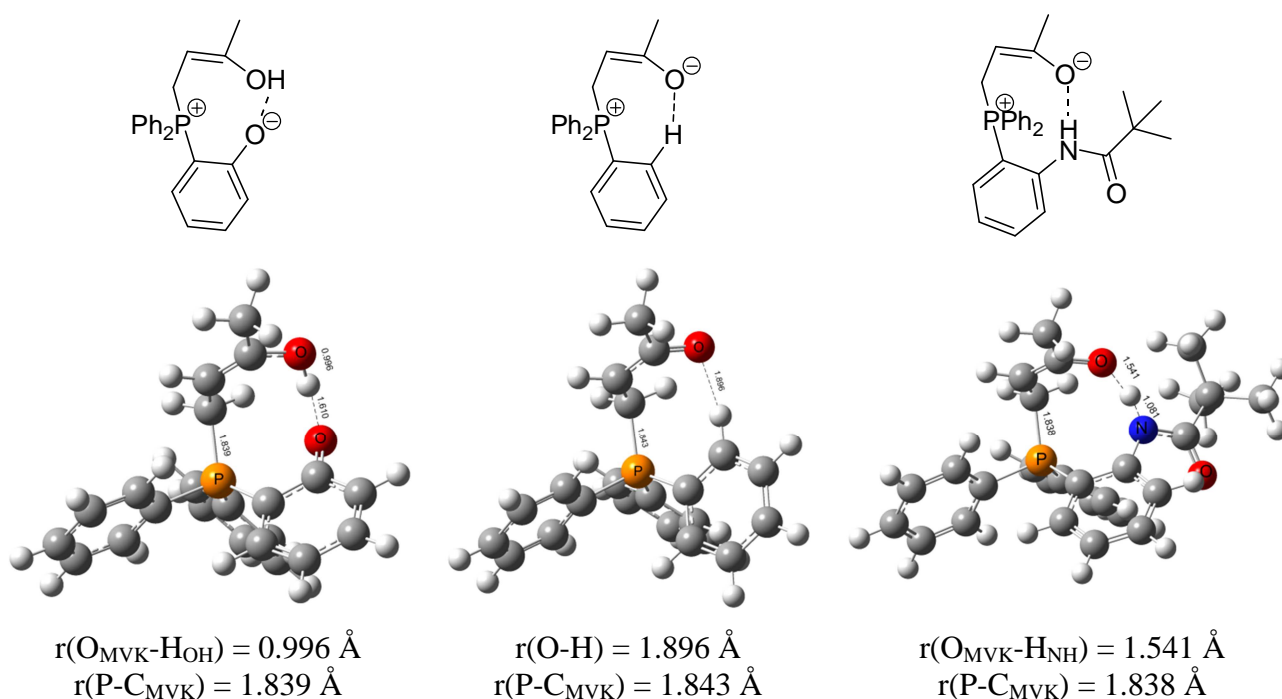


Fig. 5.15 Structures of the acyclic adducts between **BPC6**, PPh_3 and **BPC1**.

Several conclusions can be drawn from the calculated MVKA values:

- PPh_3 can be inefficient as a catalyst (if the co-catalyst is not involved) due to the endothermic nature of the Michael addition step ($\text{MVKA} > 0$). It is important to note here that the situation is very different if the co-catalyst is involved (*vide* chapter 3) – then the zwitterionic intermediate is stabilized via the intermolecular interaction with the co-catalyst. Indeed, from the experiment one can see, that without co-catalyst the catalyst PPh_3 does not work properly (Table 5.4) and with *p*-nitrophenol as a co-catalyst the reaction reaches the 60% conversion after 20h^[10]
- In the case of **BPC6** the MVKA is too negative, thus the reaction may be trapped in a “super” stabilized system. The acyclic adduct between **BPC6** and MVK is stabilized via hydrogen transfer from the OH group to the oxygen of the MVK moiety. This correlates with the experimental result, that **BPC6** is ineffective catalyst.^[10]
- Five other catalysts (**BPC1-5**) take the middle position. The zwitterionic intermediates are significantly stabilized via hydrogen bonding between the MVK moiety and the -NH- group of the catalyst, but they are still not completely protonated and can continue in the catalytic cycle. The smallest (the best) values are obtained from **BPC1** and **BPC5**. The result of **BPC1** is in accordance with the experimental evidence, since the **BPC1** has been found to be the most effective from the family. The **BPC5** gave only modest conversion in experiment, though its MVKA value is almost equal to the MVKA of the **BPC1**. Thus, the MVKA alone is not enough to explain the poor performance of **BPC5**.

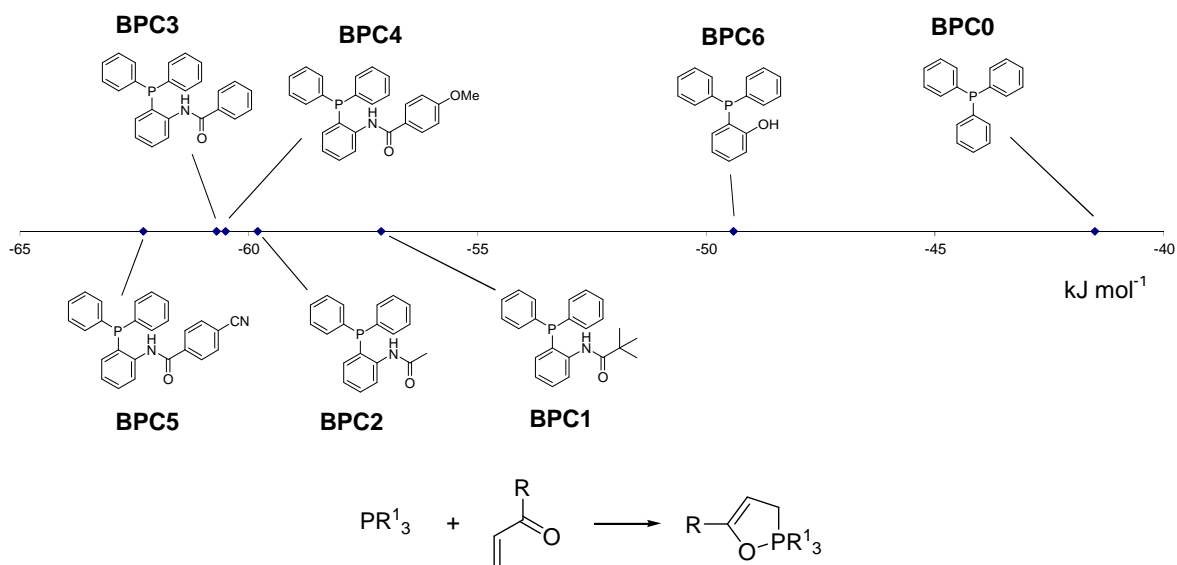


Fig. 5.16 The MVKA-c scale of the BPC family.

In Fig. 5.16 the MVKA-c results are collected. Inasmuch as the formation of the cyclic adduct is a side reaction, which leads the system away from the catalytic cycle, the understanding of the MVKA-c values are opposite to MVKA – the more exothermic the reaction (*vide* Fig. 5.16) is, the worse the catalyst is. Fig. 5.16 shows that MVKA-c is the most negative for the **BPC5**, hence this catalyst is the worst catalyst from the point of view of the cyclic side product formation. This fact can explain the experimentally found poor efficiency of this catalyst. On the other hand the MVKA-c of the best catalyst **BPC1** is 5.2 kJ mol⁻¹ less exothermic. This fact supports the best efficiency of this catalyst among the BPC family. The fact of the best efficiency of **BPC1** has been found experimentally (*vide* Table 5.7) and predicted by MVKA calculation (*vide* Fig. 5.14). The reason for the strong stabilization of the cyclic adducts is related to hydrogen bond formation. Thus, the intramolecular stabilizing interactions can play a dual role in the MBH process – supporting the catalytic cycle and supporting the side processes on the other hand. The structure of the cyclic adduct between MVK and **BPC5** is shown in Fig. 5.17. The structure corresponds to the trigonal bipyramid, with the oxygen atom of MVK moiety in the apical position.

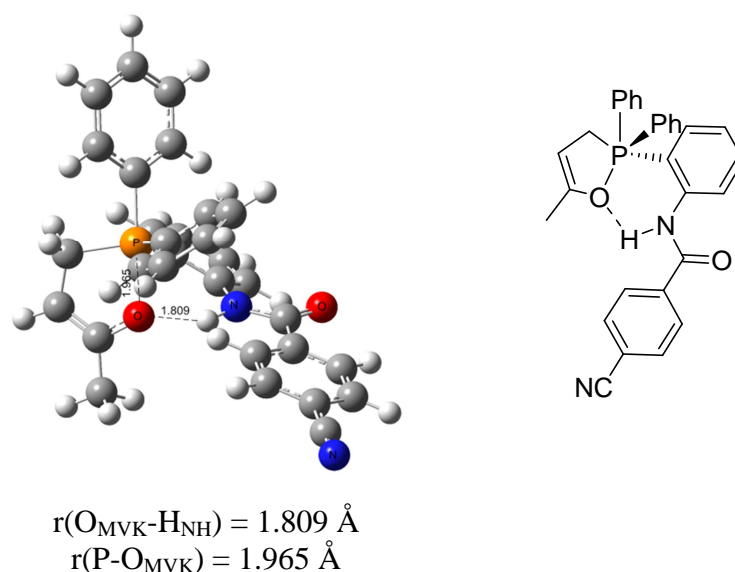
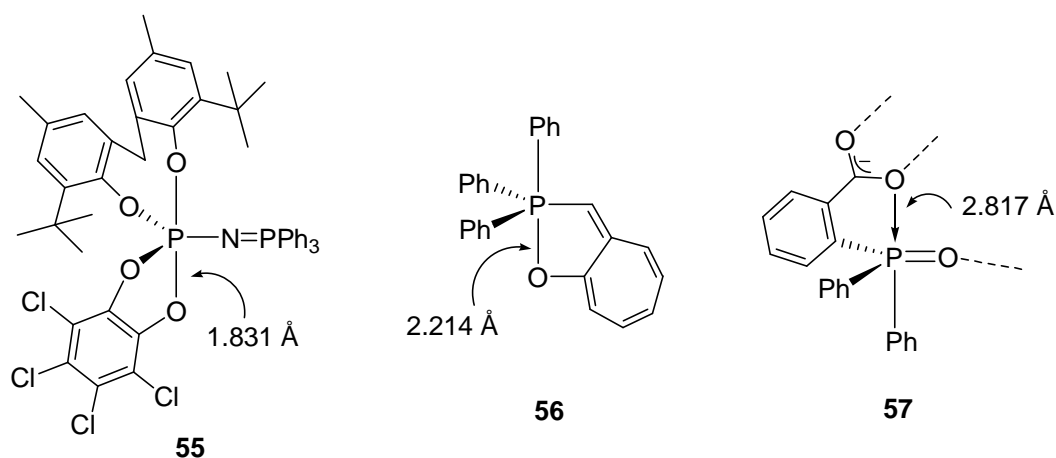


Fig. 5.17 The structure of the cyclic adduct between MVK and **BPC5**.

The length of P-O distance in this structure amounts to 1.965 Å. This bond is quite long, since in known structures of pentaoxyphosphoranes the P-O distance generally fall in the range 1.57 – 1.77 Å.^[11] However, pentacovalent phosphoranes with longer apical P-O distances have been detected (e.g. **55** and **56**^[12] Scheme 5.5). The complex **57** shows, that this distance

can be even longer, depending on the extent of contribution from coordinate covalent character.^[11, 13]



Scheme 5.5 Known pentacoordinated phosphorus compounds with apical P-O distance in the range 1.8 – 2.9 Å.

Noteworthy, this is larger than single P-O bond in tri- or tetracoordinated phosphorus compounds. For comparison, in the optimized at MPW1K/6-31G(d) level structure of P(OMe)₃ the $r(\text{P-O})$ amounts to 1.628 Å and in the Me₃PO the distance $r(\text{P-O}) = 1.468$ Å. Latter reflects double P-O bond.

5.4.2. Correlation of MVKA and Experimentally Measured Kinetic Data for BPC Catalysts

It has been shown qualitatively that the results of MVKA calculations reflect and explain the experimental results in many cases. Of course it would be an additional advantage if the calculations correlate with the experimental data in a more quantitative manner. Unfortunately, half-life times are not available for all of the systems, but only for four of them (Table 5.7). In the left side of Fig. 5.18 the correlation between the kinetic data ($\log_{10}(1/t_{1/2})$) and MVKA values is plotted for all four systems, and in the right side of Fig. 5.18 the PPh₃ point (which seems to be completely out of the regression line) is excluded. The correlation coefficient for all available data amount $R^2 = 0.76$. Exclusion of the PPh₃ yields a better correlation: $R^2 = 0.96$. In general the MVKA approach can successfully give a rough estimate of the catalyst/substrate pair for MBH.

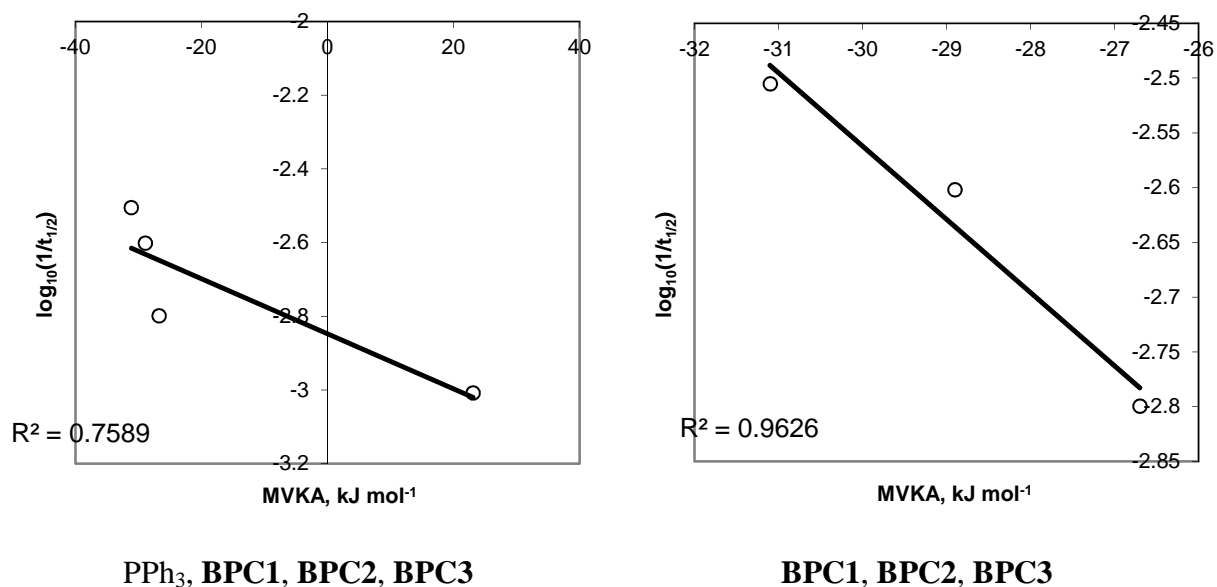
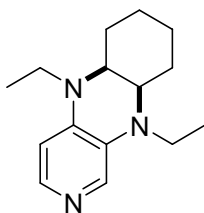


Fig. 5.18 Experimental kinetic data vs. MVKA for BPC catalysts.

5.4.3. XKA of Triphenylphosphane and Pyridine-derived Lewis Base Catalysts Using Three Different Michael Acceptors. Experiment and Theory in Comparison

The efficiency of the MVKA approach to characterize BPC catalysts has been discussed. Another family of organocatalysts has recently been studied experimentally in its applicability to aza-MBH and MBH reactions – 4-substituted pyridine-derived Lewis bases (PDLB). The best results have been achieved with so called **PDLB2** (Scheme 5.5), which has also been found to be the most effective in acylation reactions.^[10, 14]



Scheme 5.5. The **PDLB2** catalyst – one of the most active pyridine catalysts for acylation reactions.

Interesting results have been obtained by Liu comparing **PDLB2** with PPh₃ for the aza-MBH reaction between N-tosylimine and three different Michael acceptors: MVK (**MA1**), ethyl acrylate (**MA2**) and 2-cyclohexenone (**MA3**).^[10] The kinetic data (reaction time, conversion and (if available) half-life time) are collected in Table 5.9

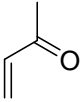
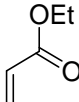
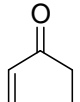
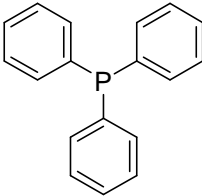
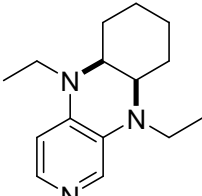
Table 5.9 Kinetic data (reaction time, conversion and (if available) half-life time) for aza-MBH reaction involving PPh₃ and PDLB2 as catalysts and three different Michael acceptors (MA1-3).

Catalyst	MA1	MA2	MA3
	++ 4h;99% conv ^a ; t _{1/2} = 38 min	+ 5d;93% conv ^a	- 30h;<3% conv ^a
	+++ 4h;99% conv ^a ; t _{1/2} = 26 min	+ 5d;75% conv ^a	++ 40h;99% conv ^a

^a Experimental study from Yinghao Liu.^[10]

Using PPh₃ as the catalyst, the following substrate-reactivity order is observed: **MA1** > **MA2** >> **MA3**. The trend is then changed when **PDLB2** is used: **MA1** > **MA3** > **MA2**. For both catalysts the best Michael acceptor is **MA1**. **MA2** and **MA3** change the positions with catalyst variation. Noteworthy, for the case of **PDLB2**, **MA1** is more reactive than for PPh₃. In Table 5.8 with symbol “+” or “-” a rough grade for a substrate is given, the more “+” signs a substrate has, the more reactive the substrate to respective catalyst is. Trying to explain these observations the XKA approach has been applied. The XKA calculations have been performed in much the same way as MVKA, but the model has been slightly strengthened by improving the basis set used for geometrical and thermochemical calculations from 6-31G(d) to 6-31+G(d) and by implicit inclusion of the solvent effect via PCM approach (in chloroform). The results are collected in the Table 5.9, where the affinities are named XKA1-4, respectively presented as the reaction enthalpies at 298K, zero point corrected energies, free energies in the gas phase and free energies in solution at 298K. In Table 5.9 the calculated results are compared with the experimental data.

Table 5.10. Affinities (XKA) of Ph₃P and PDLB2 to different Michael acceptors.

Catalyst	XKA			
		MA1	MA2	MA3
	XKA1 ^a ; H ₂₉₈ , kJ mol ⁻¹	+23.9	+50.3 ^b	+82.7
	XKA2; E ₀ , kJ mol ⁻¹	+25.7	+51.2	+83.0
	XKA3; G ₂₉₈ , kJ mol ⁻¹	+81.9	+106.8	+139.9
	XKA4 ^c ; G _{298, CHCl₃} , kJ mol ⁻¹	+69.8	+94.1	+121.7
	Experiment ^d	++ 4h;99% conv; t _{1/2} = 38 min	+ 5d;93% conv	- 30h;<3% conv
	XKA1 ^a ; H ₂₉₈ , kJ mol ⁻¹	+12.8	+40.5	+61.1; +60.3 ^e
	XKA2; E ₀ , kJ mol ⁻¹	+14.5	+41.2	+61.2; +60.3
	XKA3; G ₂₉₈ , kJ mol ⁻¹	+70.3	+95.2	+114.7; +113.1
	XKA4 ^c ; G _{298, CHCl₃} , kJ mol ⁻¹	+64.6	+86.7	+100.9; +99.6
	Experiment ^d	+++ 4h;99% conv; t _{1/2} = 26 min	+ 5d;75% conv	++ 40h;99% conv

^a In general for XKA: MP2(FC)/6-31+G(2d,p)/MPW1K/6-31+G(d); thermochemical corrections: MPW1K/6-31+G(d)

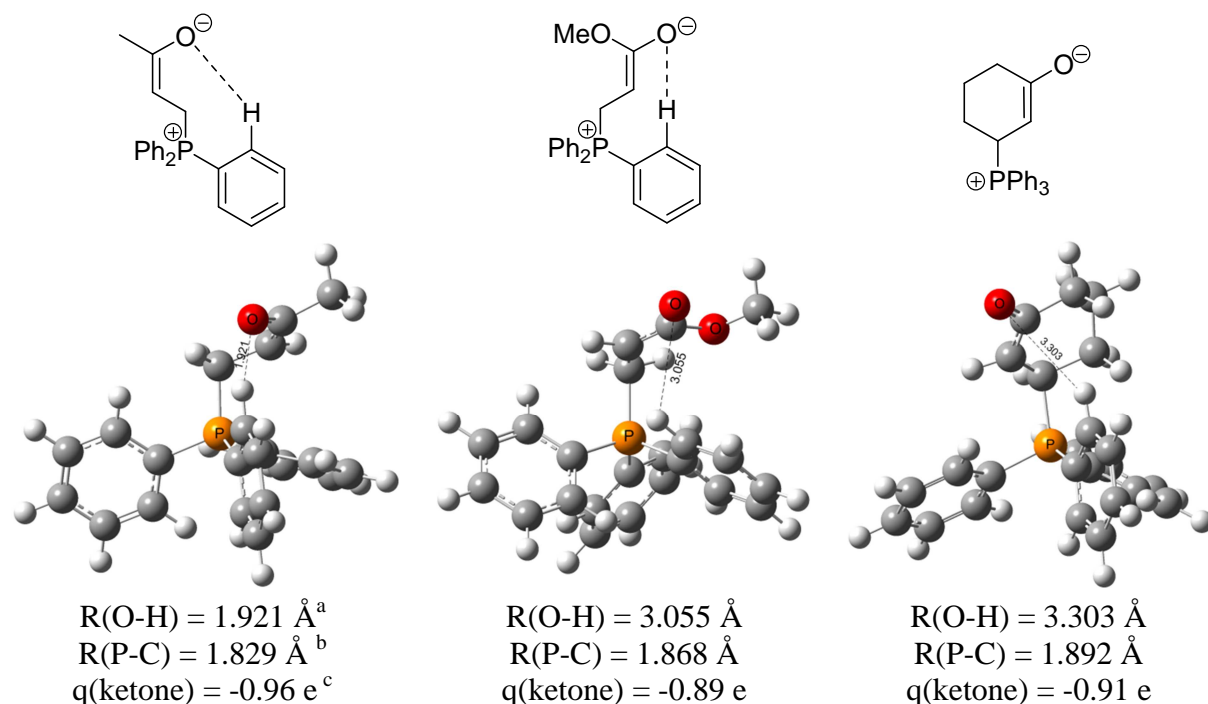
^b For XKA calculations OMe group instead of OEt has been used

^c PCM calculation: RHF/6-31G(d) using UAHF radii and CHCl₃ as the solvent to model

^d Experimental study from Yinghao Liu. Conditions: RT, CHCl₃, 10 mol% Lewis base; with symbol "+" or "-" a rough grade for a substrate is given, the more "+" signs a substrate has, the more reactive the substrate to respective catalyst is. The grade is giving relying on the experimental kinetic data.

^e Complex of PDLB2 and cyclohexenone can exist in two diastereomeric variants.

In the case of the PPh₃, the calculated affinity values are in accordance with experimental data, putting into the first place MVK (MA1), to the intermediate place – methyl acrylate (MA2), to the worst, third place – cyclohexenone (MA3). The structures of the optimized adducts are shown in Fig. 5.19.



^a Distance between oxygen atom of alkoxide function and the nearest hydrogen of one of the phenyl rings.
^b Distance between “accepting” carbon atom of ketone and “donating” P atom of catalyst.
^c The overall charge of the “ketone” moieties in the shown adducts at the NPA/MPW1K/6-31+G(d) level.

Fig 5.19. Structures of the most stable (in terms of $\Delta G_{298, \text{CHCl}_3}$) conformations of adducts between ketones **MA1-3** and PPh_3 .

One can see dramatic differences between the adducts for these three ketones. In the case of cyclohexenone the important stabilizing hydrogen-bond between one of the phenyl rings and the ketone oxygen is absent due to structural properties of cyclohexenone. The structure of the cyclohexenone/ PPh_3 adduct has been found to be similar to one of the unstable conformations (Z isomer) for complexes of MVKA with PPh_3 , though in the case of MVKA formation of the hydrogen-bond in this conformation is still possible. As one can see from the Fig 5.19 the most stable conformation of methyl acrylate/ PPh_3 in terms of G_{298, CHCl_3} is also the Z-isomer (with OMe cis to CH_2PR_3^+) as well as for cyclohexanone. There is only weak electrostatic interaction with the nearest hydrogen of a phenyl ring. This conformation is found to be 1.3 and 1.5 kJ mol^{-1} more stable than the E-isomers (in the gas phase the E-isomers are more stable) with hydrogen bonds structurally similar to the MVKA/ PPh_3 adduct. As one can see from Fig. 5.19, the overall charges (NPA/MPW1K/6-31+G(d)) of the “ketone” moieties for adducts with PPh_3 are quite significant: from -0.891 e (ethyl acrylate, **MA2**) to -0.960 e (MVK, **MA1**), this illustrates a substantial charge transfer from PPh_3 to the ketones.

The experimental data show that in the case of **PDLB2** the reaction runs in general faster (excepting substrate ethyl acrylate (**MA2**), which gives almost the same results for both catalysts), compared to PPh_3 . This fact is in accordance with calculated affinity values (Table

5.9). In contrast to Ph_3P , experiment puts the substrate **MA3** on the second and substrate **MA2** on the third position in the reactivity row. This doesn't appear so clear from the calculations of ketone affinities. The main reason for the position change of the substrates **MA2** and **MA3** for **PDLB2** can be hidden not in the Michael addition, which is only reflected by these calculations, but in other steps of the aza-MBH process. Structurally the adducts between catalyst and substrate for **PDLB2** (the structures are shown in Fig. 5.20) are quite similar to the PPh_3 case, though for **PDLB2** the systems are much more conformationally flexible, than for PPh_3 due to the unsymmetrical geometry of **PDLB2**.

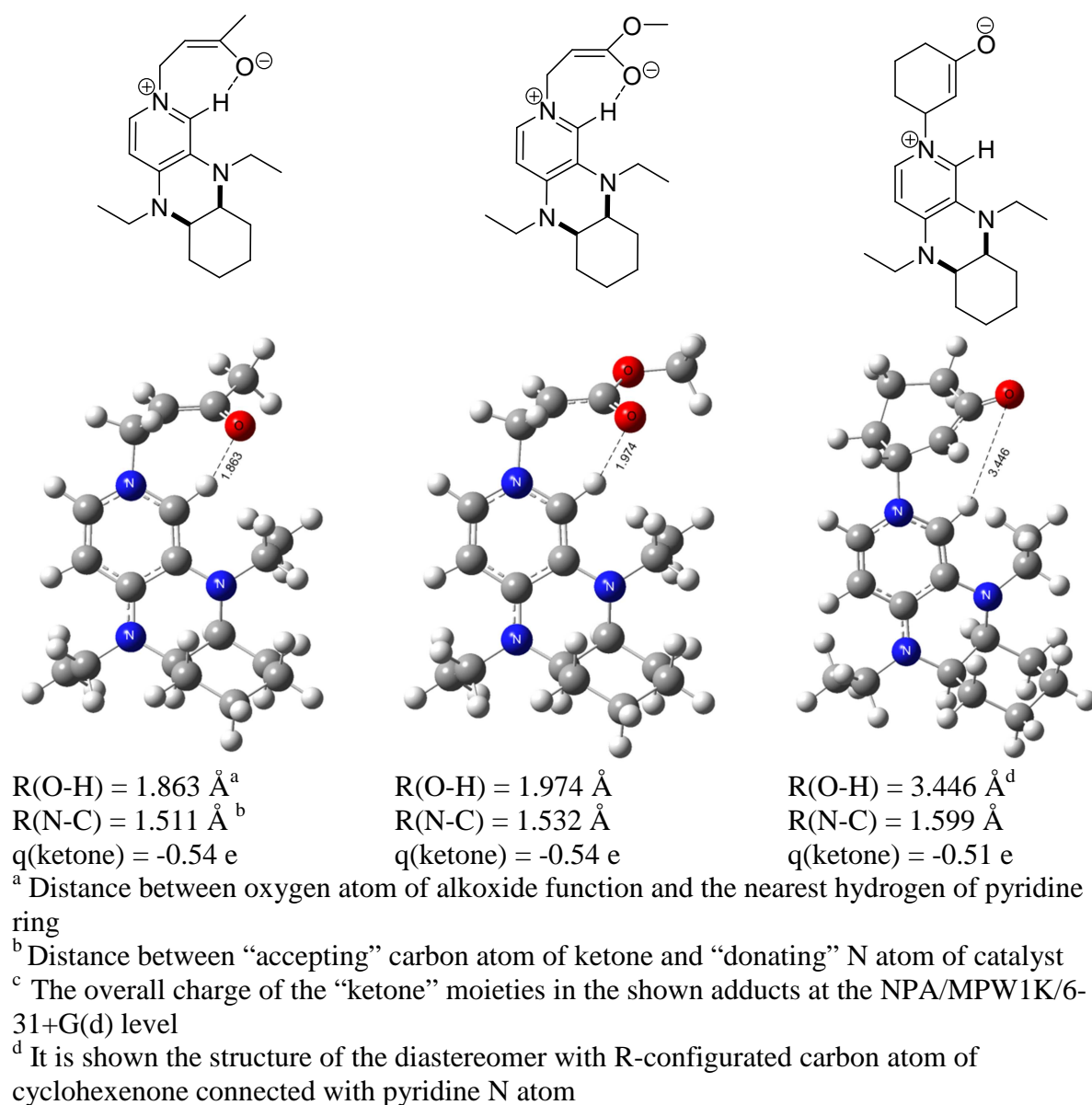


Fig 5.20. Structures of the most stable (in terms of $\Delta G_{298, \text{CHCl}_3}$) conformations of adducts between ketones **MA1-3** and **PDLB2**.

The interactions between the nearest hydrogen atom (for **PDLB2** this hydrogen is one of the pyridine ring hydrogens) and ketone are similarly to PPh₃ very important. For **PDLB2** these interactions can be stronger as compared to PPh₃ because the distance between ketone and catalyst (distance between “accepting” carbon atom of ketone and “donating” phosphorus (PPh₃) or nitrogen (**PDLB2**) atom of catalyst) is getting substantially smaller for the **PDLB2** as it is shown in Fig. 5.19 and Fig. 5.20. Thus in general, for **PDLB2** the magnitude of the interaction between ketone and catalyst is expected to be bigger than for PPh₃, and it correlates with the bigger affinity of **PDLB2** to all studied substrates as compared to PPh₃ which is in accordance with experimental evidence of bigger efficiency of **PDLB2**. As it is shown in Fig. 5.20, the overall charges (NPA/MPW1K/6-31+G(d)) of the “ketone” moieties for adducts with **PDLB2** are moderate: from -0.509 e (2-cyclohexenone **MA3**) to -0.544 e (MVK (**MA1**)). These values are significantly smaller as compared to the adduct with PPh₃, showing that charge-transfer from catalyst to ketone in the case of **PDLB2** is less significant than it is found for PPh₃. This difference between nitrogen and phosphorus based zwitterionic species is in accordance with a recent study where PMe₃ and NMe₃ complexes with methylvinylketone have been analyzed.^[3c]

Fig. 5.21 shows the dependence of XKA4 (G_{298,CHCl3}, kJ/mol) on the studied substrate. The line of PPh₃ is in accordance with the experiment showing that MVK is the best substrate, the second one is ethyl acrylate and the worst one is the 2-cyclohexenone. The line of **PDLB2** shows a higher activity (XKA4 value is smaller) towards MVK and significantly much higher activity towards 2-cyclohexenone as compared to PPh₃. These results of the calculations are also in complete accordance with experimental evidence. One can see from the Fig. 5.21 that for **PDLB2** the difference between substrates **MA2** and **MA3** is smaller:

$$\Delta XKA4(\mathbf{PDLB2}, \mathbf{MA3-MA2}) = XKA4(\mathbf{PDLB2}, \mathbf{MA3}) - XKA4(\mathbf{PDLB2}, \mathbf{MA2}) = 100.9 - 85.2 = 15.7 \text{ (kJ mol}^{-1}\text{)}$$

as compared to the difference between substrate **MA1** and **MA2**:

$$\Delta XKA4(\mathbf{PDLB2}, \mathbf{MA2-MA1}) = XKA4(\mathbf{PDLB2}, \mathbf{MA2}) - XKA4(\mathbf{PDLB2}, \mathbf{MA1}) = 85.2 - 64.6 = 20.6 \text{ (kJ mol}^{-1}\text{)},$$

while for PPh₃ the trend is inversed: $\Delta XKA4(\text{PPh}_3, \mathbf{MA3-MA2}) = 27.6 \text{ kJ mol}^{-1}$ and $\Delta XKA4(\text{PPh}_3, \mathbf{MA2-MA1}) = 24.3 \text{ kJ mol}^{-1}$. This is illustrated on the Fig. 5.11 by the concave

character of the function for **PDLB2** and convex – for PPh_3 . The change of the character of “XKA(substrate)” dependence seems to correlate with the fact of the total loss of activity for substrate **3** in reaction with Ph_3P and its validity for **PDLB2**.

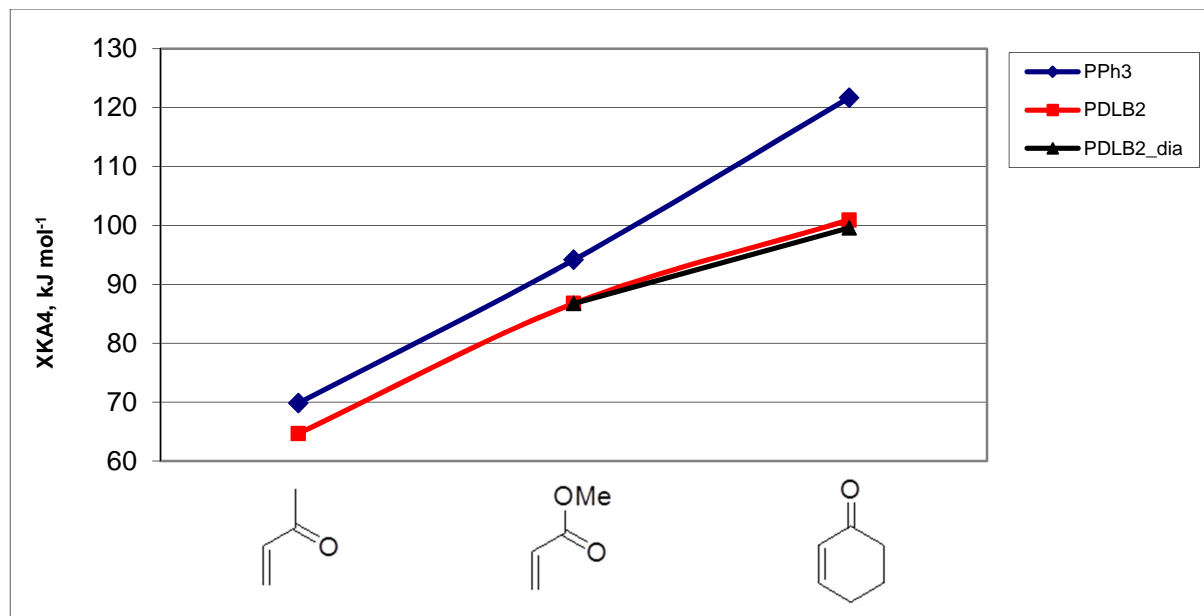


Fig 5.21. XKA4 (G_{298, CHCl_3} , kJ mol^{-1}) vs. Michael acceptor.

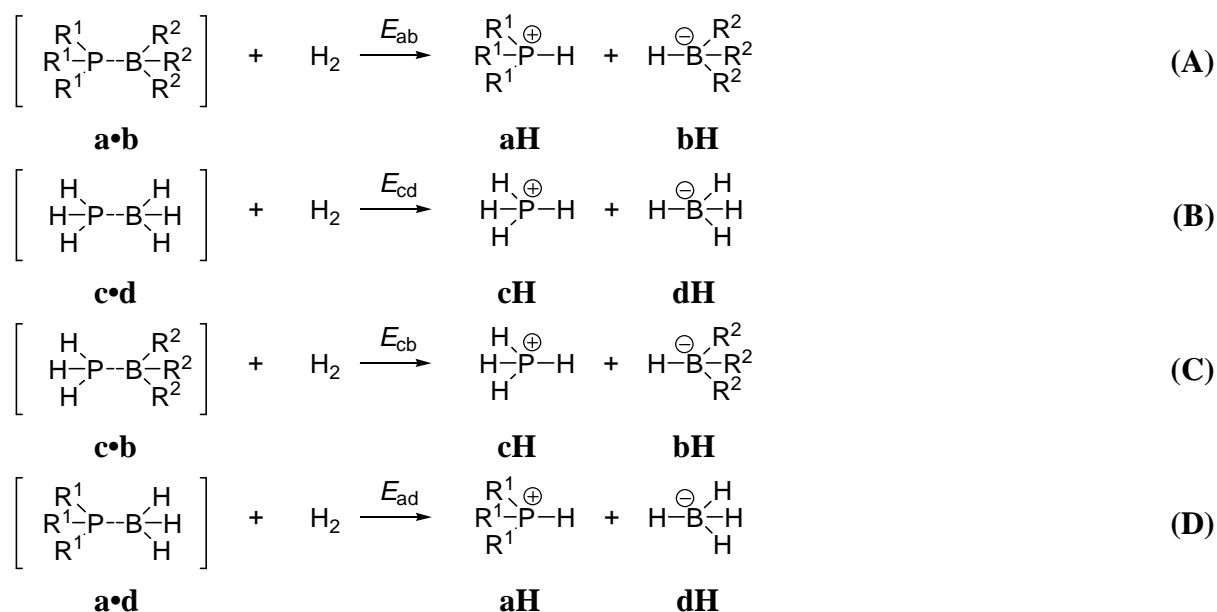
5.5. Conclusions

- The MCA calculations have been performed for a series of phosphanes, including subfamilies such as cyclophane substituted phosphanes. The obtained MCA values can be used as a guideline for optimization of phosphane-catalyzed organocatalytic transformations, e.g. MBH reaction.
- A new descriptor of catalytic activity is suggested for the MBH reaction: XKA (“X”-ketone affinity) – affinity of catalyst to MBH-substrate (“X”-ketone). The XKA and its particular case MVKA (Methyl Vinyl Ketone Affinity) work well for a rough estimate of the efficiency for selected combinations of catalyst/substrate.

5.6. References

- [1] D. Cantillo, C. O. Kappe, *J. Org. Chem* **2010**, *75*, 8615-8626.
- [2] Y. Wei, PhD thesis, Ludwig-Maximilians-Universität München (München), **2008**.
- [3] a) Y. Wei, G. N. Sastry, H. Zipse, *J. Am. Chem. Soc.* **2008**, *130*, 3473; b) Y. Wei, T. Singer, H. Mayr, G. N. Sastry, H. Zipse, *J. Comput. Chem.* **2008**, *29*, 291-297; c) Y. Wei, B. Sateesh, B. Maryasin, G. N. Sastry, H. Zipse, *J. Comput. Chem.* **2009**, 2617 - 2624.
- [4] J. W. Ponder, TINKER 4.2 ed., **2004**.
- [5] a) N. L. Allinger, Y. H. Yuh, J.-H. Lii, *J. Am. Chem. Soc.* **1989**, *111*, 8551-8556; b) J.-H. Lii, N. L. Allinger, *J. Am. Chem. Soc.* **1989**, *111*, 8566-8575; c) J.-H. Lii, N. L. Allinger, *J. Am. Chem. Soc.* **1989**, *111*, 8576-8582; d) N. L. Allinger, H. J. Geise, W. Pyckhout, L. A. Paquette, J. C. Gallucci, *J. Am. Chem. Soc.* **1989**, *111*, 1106-1114; e) N. L. Allinger, F. Li, L. Yan, *J. Comput. Chem.* **1990**, *11*, 848-867; f) N. L. Allinger, F. Li, L. Yan, J. C. Tai, *J. Comput. Chem* **1990**, *11*, 868-895; g) J.-H. Lii, N. L. Allinger, *J. Phys. Org. Chem* **1994**, *7*, 591-609; h) J.-H. Lii, N. L. Allinger, *J. Comput. Chem* **1998**, *19*, 1001-1016.
- [6] S. Oesterling, Forschungspraktikum thesis, Ludwig-Maximilians-Universität München (München), **2009**.
- [7] MacroModel 9.7 ed., Schrödinger, LLC, New York, **2009**.
- [8] C. Lindner, B. Maryasin, F. Richter, H. Zipse, *J. Phys. Org. Chem* **2010**, *23*, 1036-1042.
- [9] J. F. Schneider, F. C. Falk, R. Fröhlich, J. Paradies, *Eur. J. Org. Chem.* **2010**, 2265-2269.
- [10] Y. Liu, PhD thesis, Ludwig-Maximilians-Universität München (München), **2011**.
- [11] K. C. Kumara Swamy, N. Satish Kumar, *Acc. Chem. Res.* **2005**, *39*, 324-333.
- [12] a) S. Kumaraswamy, C. Muthiah, K. C. Kumara Swamy, *J. Am. Chem. Soc.* **2000**, *122*, 964-965; b) S. Naya, M. Nitta, *J. Chem. Soc., Perkin Trans. 2* **2002**, 1017-1023.
- [13] A. Chandrasekaran, N. V. Timosheva, R. O. Day, R. R. Holmes, *Inorg. Chem.* **2003**, *42*, 3285-3292.
- [14] a) I. Held, S. Xu, H. Zipse, *Synthesis* **2007**, 1185-1196; b) I. Held, E. Larionov, C. Bozler, W. F., H. Zipse, *Synthesis* **2009**, 2267-2277.

between reaction energy E_{ad} for model reaction (D) with that of the unbiased reference reaction (B).

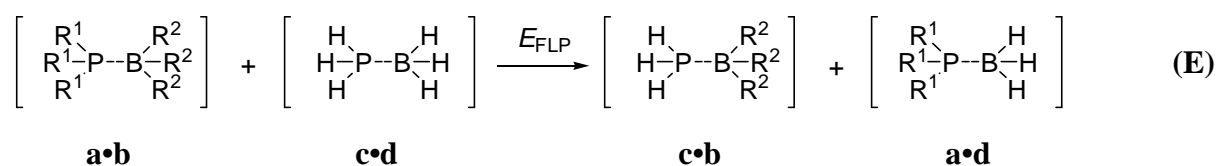


Scheme 6.2. Reference reactions for the quantitative definition of "frustration energy" E_{FLP} .

With these definitions the frustration energy E_{FLP} can quantitatively be expressed as given in eqn. (6.2).

$$E_{FLP} = E_{cd} + (E_{cb} - E_{cd}) + (E_{ad} - E_{cd}) - E_{ab} = E_{cb} + E_{ad} - E_{cd} - E_{ab} \quad (6.2)$$

Closer inspection of the systems involved in the calculation of the reaction energies in eqn. (6.2) reveals that several energy terms will cancel in the evaluation of E_{FLP} (that of $E(H_2)$, E_{aH} , E_{bH} , E_{cH} , and E_{dH}). Further analysis shows that the definition of E_{FLP} given in eqn. (6.2) is exactly identical to the reaction energy for the exchange reaction between two Lewis pairs **a•b** and **c•d** as shown in Scheme 6.3.



Scheme 6.3. Exchange reaction between Lewis pairs **a•b** and **c•d**.

In contrast to the reference reactions (A) - (D) shown in Scheme 6.2 involving heterolytic splitting of H₂, exchange reaction (E) makes no reference to a specific substrate activation reaction and is thus a much more general definition of the frustration energy E_{F_{LP}} in Lewis pair **a•b**.

6.2. Results and Discussion

Initial studies have been performed for selected small systems, for which experimental or high-level theoretical data are available (Scheme 6.4).



Scheme 6.4 Small Lewis base – Lewis acid pairs.

6.2.1. Geometry Optimization

In order to identify a reliable approach for geometry optimization we have compared seven methods (Table 6.1). Five of them are within DFT and two – *ab initio* in the variant of MP2 with and without FC approximation. First objective is the determination of a relatively cheap approach, which could be applicable farther for real-life FLP systems. Therefore we have consciously limited us to use as possible small basis sets. Thus we have checked 6-31G(d) and 6-31+G(d) with different DFT functionals and aug-cc-pVDZ with MP2. Fig. 6.1 presents a cumulative picture of the geometry optimization results, showing mean absolute deviation relative to experimental values ($\text{MAD} = 1/n \sum |r_{\text{exp}} - r_{\text{calc}}|$) in bond length (*r*) for several sets of P-B bonds. Table 6.1 collects all found values together with complexation enthalpies found at the respective level of theory.

Table 6.1. Enthalpies (ΔH_{298} , kJ mol⁻¹) of formation reactions of Lewis pairs from phosphines and boranes and P-B Bond length (Å) at different levels of theory.

Method	PH ₃ BH ₃		PMe ₃ BH ₃		PH ₃ BMe ₃		PMe ₃ BMe ₃		PH ₃ BF ₃ ^a				PMe ₃ BF ₃	
	ΔH	$r(\text{B-P})$	ΔH	$r(\text{B-P})$	ΔH	$r(\text{B-P})$	ΔH	$r(\text{B-P})$	ΔH	$r(\text{B-P})$	ΔH	$r(\text{B-P})$	ΔH	$r(\text{B-P})$
1)B3LYP/6-31G(d)	-75.9	1.960	-122.6	1.934	19.3	2.134	-14.3	2.024	NM	~2.0	-5.0	3.166	-44.8	2.097
2)B98/6-31G(d)	-85.3	1.966	-142.8	1.940	7.1	2.114	-39.5	2.027	NM	~2.0	-8.1	3.137	-49.2	2.109
3)MPW1K/6-31G(d)	-97.2	1.936	-159.9	1.913	-2.4	2.047	-53.7	1.986	NM	~2.0	-7.7	3.040	-61.9	2.060
4)MPW1K/6-31+G(d)	-97.9	1.937	-159.9	1.914	-4.0	2.043	-53.3	1.988	-8.1	2.292	-7.8	2.883	-70.5	2.055
5)MP2(FC)/aug-cc-pVDZ	-85.6	1.964	-152.7	1.934	-22.6	2.054	-94.6	1.984	-8.8	2.262	-12.1	3.041	-80.5	2.041
6)MP2(FULL)/aug-cc-pVDZ	-89.6	1.958	-157.7	1.929	-27.6	2.043	-101.6	1.977	-11.5	2.237	-13.9	3.000	-84.9	2.034
7)B97-D/6-31G(d)	-78.5	1.967	-141.3	1.938	5.2	2.106	-57.1	1.993	NM	~2.0	NM ^b	~3.0 ^b	-51.7	2.099
8)G3MPW1K(+)									+2.4	2.292	-9.9	2.883		
Expt.	-	1.937 ^[3]	-334.0 ^[4]	1.901 ^[3]	-	-	-171.4 ^[4]	-	-	1.921 ^[5]	-	-	-190.2 ^[4]	-
													-79.0 ^[6]	
Calc.	-84.0 ^{[7]c}	1.945 ^[7]	-166.2 ^[8]	1.924 ^[8]	-4.5 ^[8]	2.070 ^[8]	-50.0 ^[8]	2.014 ^[8]	-41.4 ^[9]	2.185 ^[9]	-1.8 ^[11]	3.075 ^[11]	-169.4 ^[11]	2.055 ^[11]
	-110.1 ^{[8]d}	1.939 ^[8]	-159.3 ^{[10]c}	1.917 ^[10]							-8.0 ^[12]	3.495 ^[12]	-69.0 ^{[10]c}	2.046 ^[10]
		2.041 ^[9]									-12.7 ^[12]	3.220 ^[12]		
											-12.4 ^{[7]c}	3.089 ^{[7]c}		

^a For this system at MP2(FC)/aug-cc-pVDZ, MP2(FC)/aug-cc-pVDZ and MPW1K/6-31+G(d) levels two minima are located (at around 2 Å and the second one at around 3 Å), all the methods have been tried to locate both minima, if the methods fails, then it stays in the table NM (no minimum) in the ΔH cell and in the adjacent $r(\text{B-P})$ cell the minimum type (~2.0 Å or ~3.0 Å) is pointed.

^b at B97-D/6-31+G(d) level the minimum $r(\text{B-P}) = 3.237$ is found.

^c ZPE corrected.

^d The calculated data are lacking the information about thermal corrections.

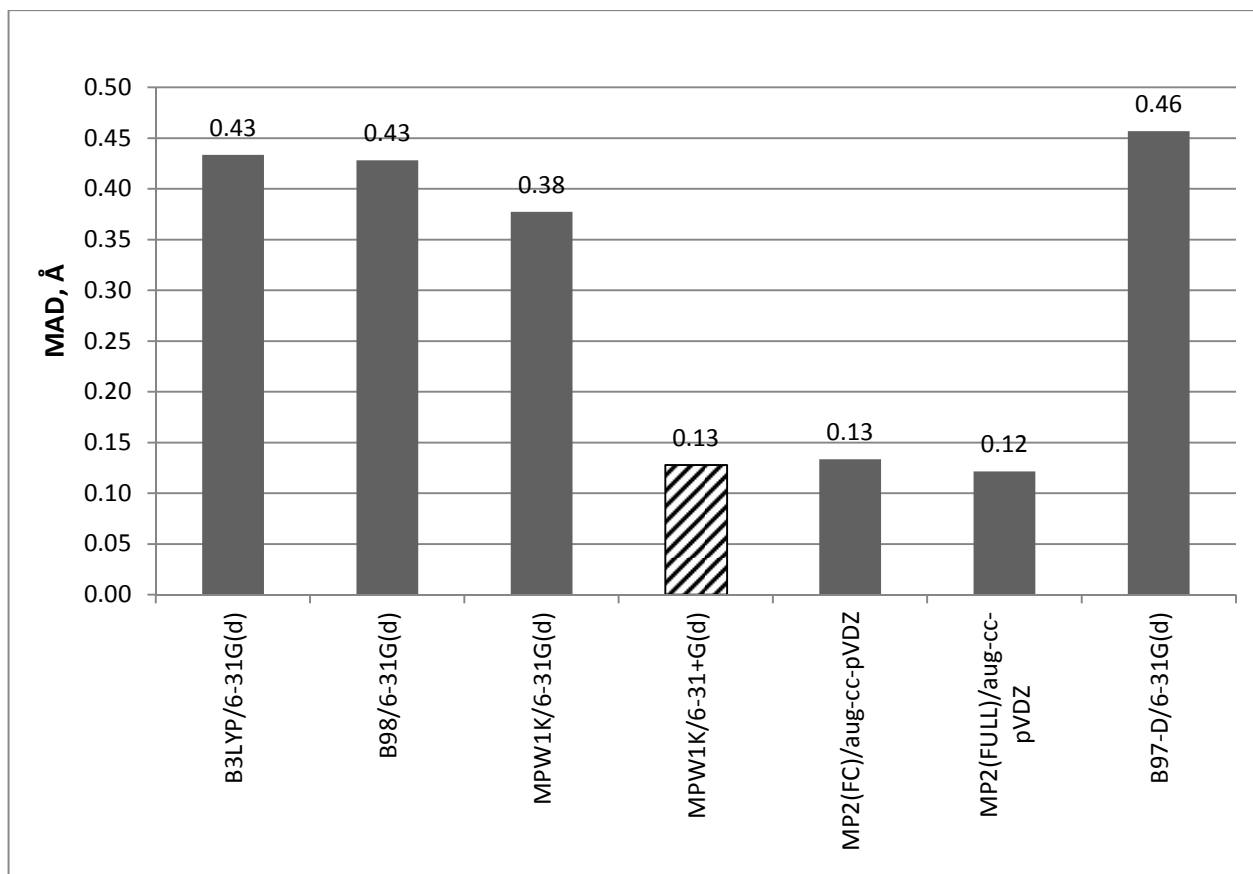


Fig. 6.1 Mean absolute deviation relative to experimental values (Å) of the calculated P-B bond length (for systems: PH_3BH_3 , PMe_3BH_3 and PH_3BF_3).

All systems in Scheme 6.4 are found to be C_{3v} symmetric by all methods selected here, with the only exception of PMe_3BMe_3 showing C_3 symmetry after optimization with MP2(FC)/aug-cc-pVDZ and MP2(FULL)/aug-cc-pVDZ due to the increasing of dihedral angle $d(\text{C}'\text{PBC}'')$ (Fig. 6.2) value from 60.0 (C_{3v}) to 68.0 (C_3). Frenking *et al.* have studied the geometries and bond dissociation energies of the main group complexes $\text{X}_3\text{B-PX}_3$ ($\text{X} = \text{H}, \text{Me}, \text{Cl}$) using gradient-corrected functional theory at the BP86/TZ2P level^[8]. The calculations of Frenking *et al.* are in accordance with our DFT results and suggest C_{3v} for PMe_3BMe_3 .

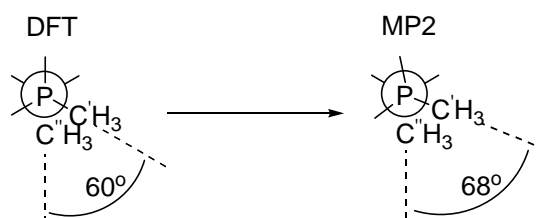


Fig. 6.2. The PMe_3BMe_3 conformations presented by Newman projections.

For the geometry of PMe_3BMe_3 we have performed additional calculations at MP2(FC) level of theory using different basis sets: 6-31G(d), 6-31G(d,p) and 6-311++G(3df,2p) and with one of the DFT functionals using aug-cc-pVDZ basis set (B98/aug-cc-pVDZ). All these calculations yield a minimum with C_{3v} geometry, which we subsequently assume to be the correct structure.

It is clear to see from Fig. 6.1 that the best (smallest MAD) results are obtained at MPW1K/6-31+G(d) and both MP2 levels of theory. The other DFT approaches (B3LYP/6-31G(d), B98/6-31G(d), MPW1K/6-31G(d) and B97-D/6-31G(d)) are clearly inferior. From the DFT functionals using the 6-31G(d) basis set, the best one is MPW1K. The big improvement in the quality of the geometry optimization results corresponds to addition of the diffuse function to the basis set. The geometry, which is changed the most dramatically with the switch to 6-31+G(d) basis set, corresponds to the PH_3BF_3 Lewis pair. It is obvious after comparison with the experimental result, that the 6-31G(d) basis set underestimates the P-B interaction in the PH_3BF_3 molecule. To evaluate the effect of the further basis set complication on the length of P-B length in the PH_3BF_3 complex, we performed geometry optimization at MPW1K/6-311++G(d,p) level, that led to P-B length equal 2.267 Å (*vide* Table 6.2). Change to the much more complicated basis set 6-311++G(d,p) does not improve the result significantly, though the cost of the calculation is strongly increased.

Table 6.2. The influence of basis set on the P-B bond length (Å) in PH_3BF_3 .

Method	$r_{\text{calc}}(\text{P-B}) - r_{\text{exp}}(\text{P-B}), \text{Å}$
MPW1K/6-31G(d)	1.119
MPW1K/6-31+G(d)	0.371
MPW1K/6-311++G(d,p)	0.346

In order to rationalize the large changes observed for the B-P distance in Lewis pair PH_3BF_3 as a function of basis set, a relaxed potential energy scan was performed for this system at MPW1K/6-31+G(d) level from $r(\text{P-B}) = 2.0 \text{ Å}$ to 3.5 Å (Fig 6.3). From Fig. 6.3 one can clearly see two minima which are energetically almost equal: $r(\text{P-B}) = 2.29 \text{ Å}$ – the global minimum and $r(\text{P-B}) = 2.88 \text{ Å}$ – the second one, which is only 0.16 kJ mol^{-1} less stable. The transition state between the minima corresponds to $r(\text{P-B}) = 2.56 \text{ Å}$ and locates 0.51 kJ mol^{-1} higher than the global minimum.

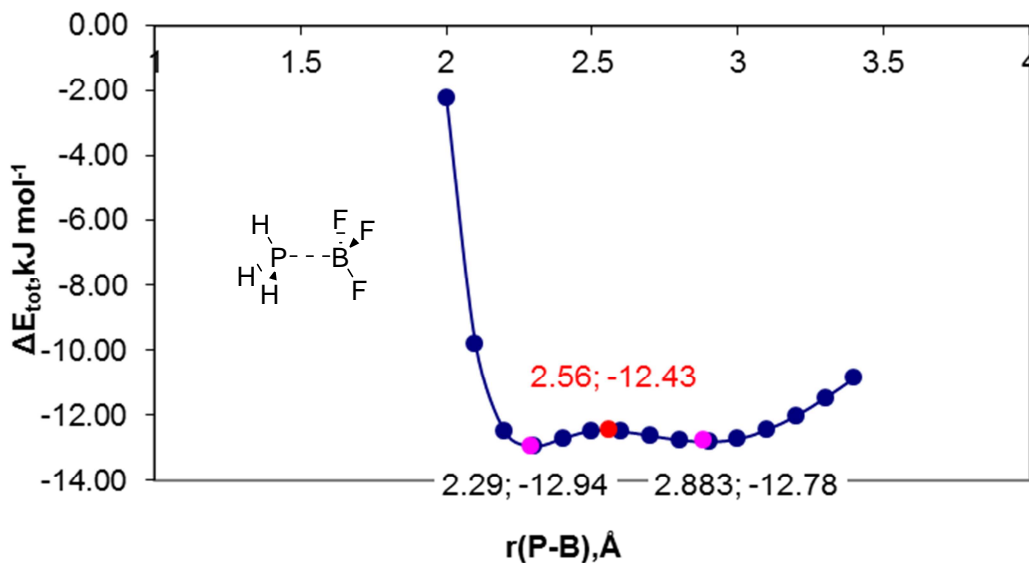


Fig. 6.3 Potential energy curve for the interaction of PH₃ with BF₃ computed at MPW1K/6-31+G(d) level.

Literature analysis has shown that either one or the other minimum was constantly ignored by computational studies.^[7, 9, 11-12] In 1988 Hirota, Miyata and Shibata have studied PH₃BF₃ complex by *ab initio* SCF MO theory, applying the 3-21G basis set.^[9] Only the first minimum has been located at $r(\text{P-B}) = 2.185 \text{ \AA}$ with $-41.4 \text{ kJ mol}^{-1}$ formation energy (thermal corrections are not discussed). In 1991 Ahlrichs, Bär, Häser and Sattler have reinvestigated the PH₃BF₃ by SCF and MP2 involving TZP basis set^[12] and, on the contrary, have found only a weak complex with a P-B distance of 3.495 \AA (SCF) and 3.220 \AA (MP2). The corresponding formation energies (no thermal corrections) have been -8.0 and $-12.7 \text{ kJ mol}^{-1}$. In 1998 Anane, Boutalib, Nebot-Gil and F. Tomás have applied G2(MP2) scheme to the PH₃BF₃ system.^[7] Thus for the geometries the MP2(FULL)/6-31G(d) level has been used. And again only a weak complex at $r(\text{P-B}) = 3.089 \text{ \AA}$ has been found. The ZPE corrected formation energy at G2(MP2) level amounts to $-12.4 \text{ kJ mol}^{-1}$. Finally, in 2008 Ford has analyzed the PH₃BF₃ system by MP2(FC)/6-311++G(d,p) calculations.^[11] The author has located only the complex at $r(\text{P-B}) = 3.075 \text{ \AA}$ with -1.8 kJ mol^{-1} enthalpy of formation. However, the experimental data published in 1975 by Odom, Kalasinsky and Durig point vice versa only to the first complex with $r(\text{P-B}) = 1.921 \text{ \AA}$ ^[5] (found via observed moments of inertia). And in all mentioned computational studies, the authors compare their observations with this experimental value, and the discrepancy was unclear. This discrepancy has encouraged us to go forward with additional energy vs. geometry scan-calculations and to apply *ab initio* theory in the variant of MP2(FC)/6-311++G(d,p). This method has been used in the most novel published computational study of the PH₃BF₃ molecule made by Ford.^[11] The resulting plot is shown in Fig. 6.4

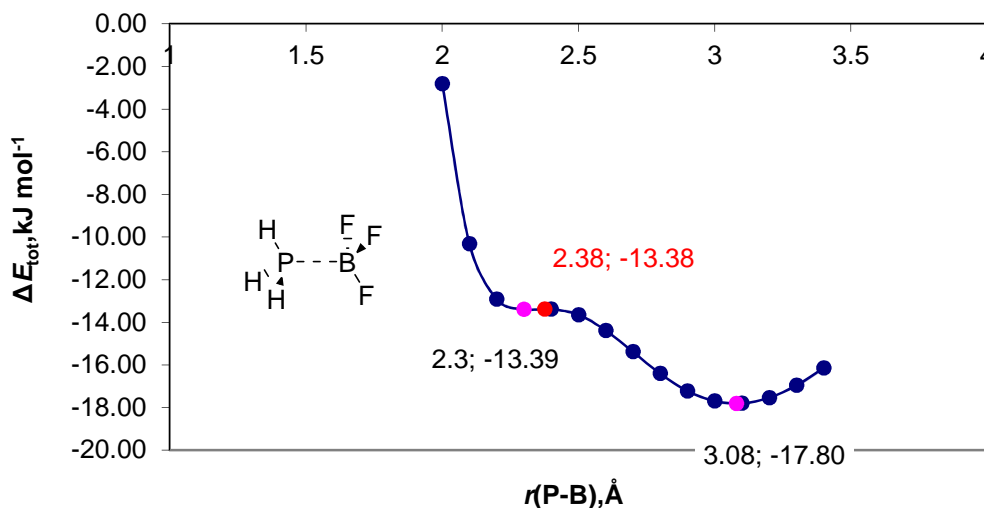


Fig. 6.4 Potential energy curves for the interaction of PH_3 with BF_3 computed at MP2(FC)/6-311++G(d,p) level.

Both minima have again been found at this level, and though structurally the minima are close to the DFT optimized geometries (2.3 Å and 3.08 Å), they are significantly different energetically and, on the contrary to the DFT calculations, the second minimum is 4.41 kJ mol^{-1} more stable than the first one. The $r(\text{B-P})$ distance (3.08 Å) of the global minimum is in accordance with the result of Ford.^[11] The transition state is very close to the first minimum with $r(\text{B-P}) = 2.38$ Å. In order to clarify the electronic structure of the both minima we have performed NBO analysis at MPW1K/6-31+G(d) level. Table 6.2 collects the important molecular orbitals and natural orbitals together with geometrical parameters. In the first minimum a sigma P-B bond is formed by the $\text{sp}^{2.19}$ orbital of phosphorus and $\text{sp}^{6.09}$ of boron atom. Corresponding natural orbital constitutes the HOMO (MO 25 with energy of -0.370939 a.u.). The respective antibonding orbital contributes in unoccupied MO 29 (+0.041331 a.u.). The formation of the sigma bond corresponds to significant change of the geometries for both phosphane and trifluoroborane moieties turning into the adduct from isolated molecules – the planar molecule of trifluoroborane is pyramidalized by 35.22° (*vide* Table 6.2). The second complex is formed by 64.1 kJ mol^{-1} strong donor-acceptor interaction between donating lone pair orbital localized on phosphorus ($\text{sp}^{0.99}$), which constitutes the HOMO (MO 25 with energy of -0.343258 a.u.), with accepting antibonding (p) orbital localized on boron. No covalent P-B bond present for this minimum. Existence of almost pure p orbital on the boron atom is in accordance with a nearly planar of trifluoroborane moiety.

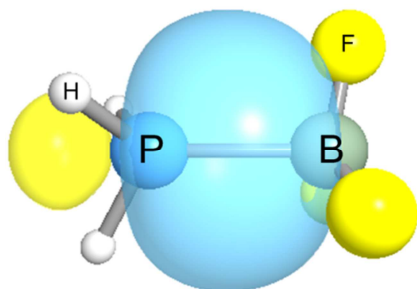
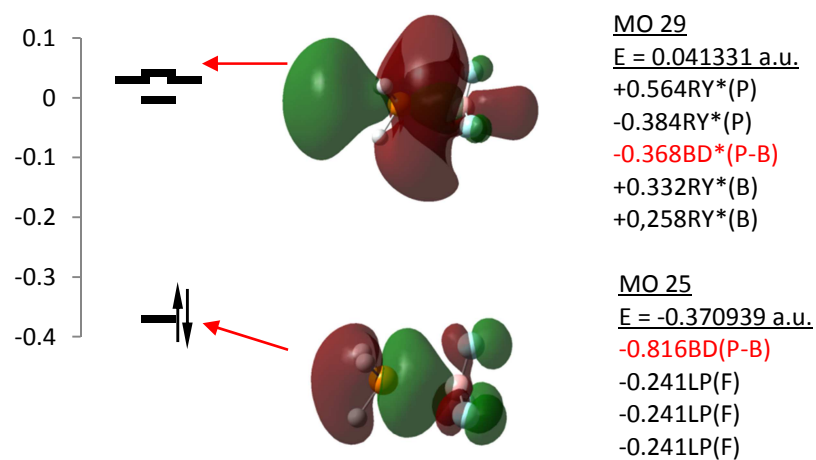
Table 6.2 Formation of chemical bonding between PH₃ and BF₃ in both possible minima.

$$r(\text{P-B}) = 2.292 \text{ \AA}$$

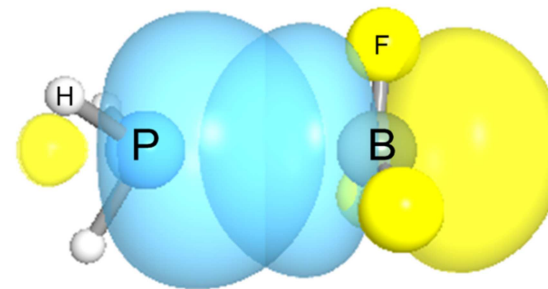
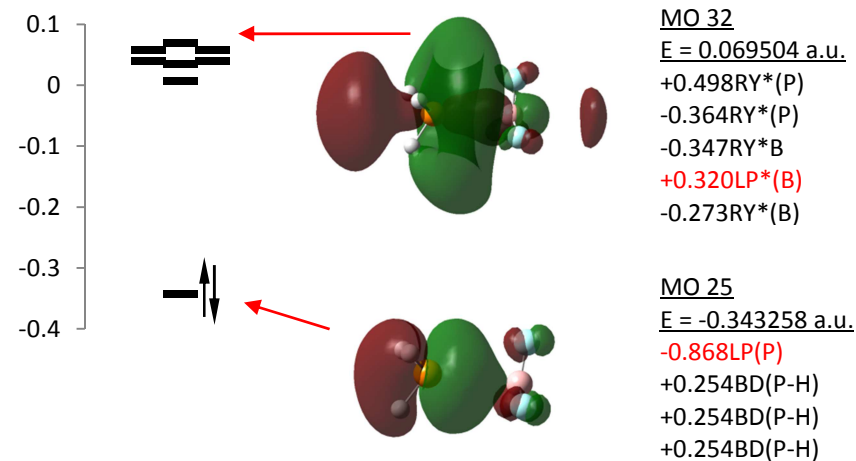
$$\text{OOP(P)}^a = 78.7^\circ; \text{OOP(B)} = 35.22^\circ$$

$$r(\text{P-B}) = 2.883 \text{ \AA}$$

$$\text{OOP(P)} = 83.6^\circ; \text{OOP(B)} = 12.4^\circ$$



$$\text{Sigma (P-B) bond: } 0.9092\text{P}(\text{sp}^{2.19}) + 0.4165\text{B}(\text{sp}^{6.09})$$



$$\text{Donor/Acceptor complex: } \text{P}(\text{sp}^{0.99}) + \text{B}(\text{p}) \rightarrow 64.1 \text{ kJ mol}^{-1}$$

^a Out-of-plane angle for P (phosphorus) or B (boron) moieties

The system has been enlarged by changing the H-P bonds into C-P and check whether both minima still can be found, and the $\text{PMe}_3\text{B}(\text{CF}_3)_3$ complex has been examined by analogous scan-calculation. For that system only one, strongly bound complex has been determined – the result of the scanning is shown in Fig.6.5

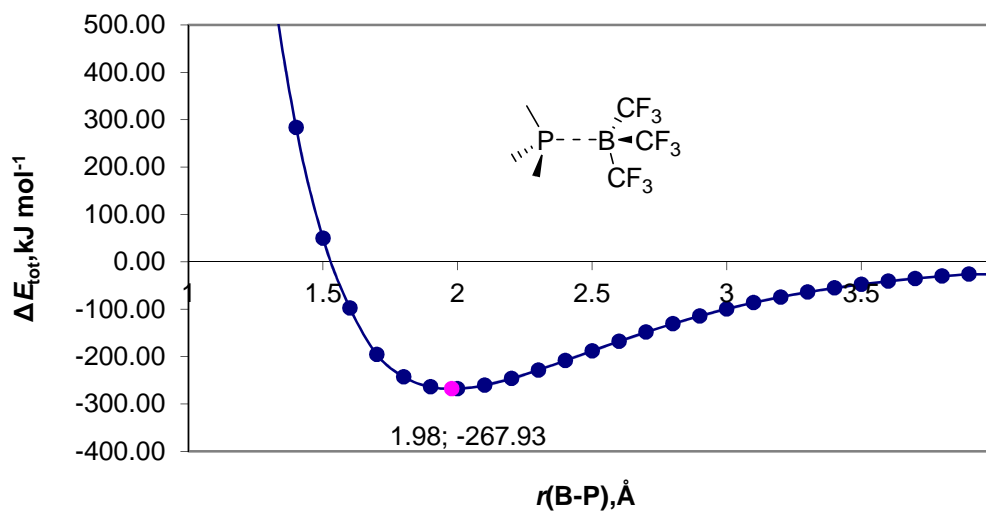


Fig. 6.5 Potential energy curve for the interaction of PMe_3 with $\text{B}(\text{CF}_3)_3$ computed at MPW1K/6-31+G(d) level.

Obviously this interesting property to exhibit more than one minimum on the potential energy surface depends on the system and does not appear as a general character of the Lewis pairs. Though for phosphorus/boron Lewis pairs the literature data seem to be scarce, a similar situation with two minima has been recently published for nitrogen/boron frustrated Lewis pairs, where M05-2X/6-311++G(d,p)//M05-2X/6-31G(d) theory has been applied^[13] and for small nitrogen/boron Lewis pair $\text{CH}_3\text{CN-BF}_3$ using MP2, B3LYP and BWP91 methods with basis sets ranging from STO-3G to aug-cc-pVQZ.^[14] These studies in combination with the present work show clearly the necessity to have a reliable approach of the geometry optimization for Lewis pair and FLP computations. The approach must be able to treat also complicated cases of multiple minima on the potential energy surfaces. This is a challenge taking into account the importance to have not only reliable but also cheap method suitable for large systems.

The MPW1K/6-31+G(d) geometry optimization approach suggested here seems to be satisfactory for phosphorus/boron Lewis pairs. It has shown low MAD from experimental data almost equal to MP2. Moreover, it can equally to MP2 locate both possible minima in the H_3PBF_3 system.

6.2.2. Energies

Unfortunately literature data about experimentally measured formation energies of the complexes in study are scarce (as well as only few examples of experimental geometries). The known energies and geometries are collected together with calculations in Table 6.1. From the calculations we present in Table 6.1 the MP2(FULL)/aug-cc-pVDZ is the highest hierarchy approach, thus it seems to be reasonable to discuss it in more detail. In Fig. 6.6 the MP2(FULL)/aug-cc-pVDZ formation enthalpies vs. P-B distances for 6 studied systems are presented.

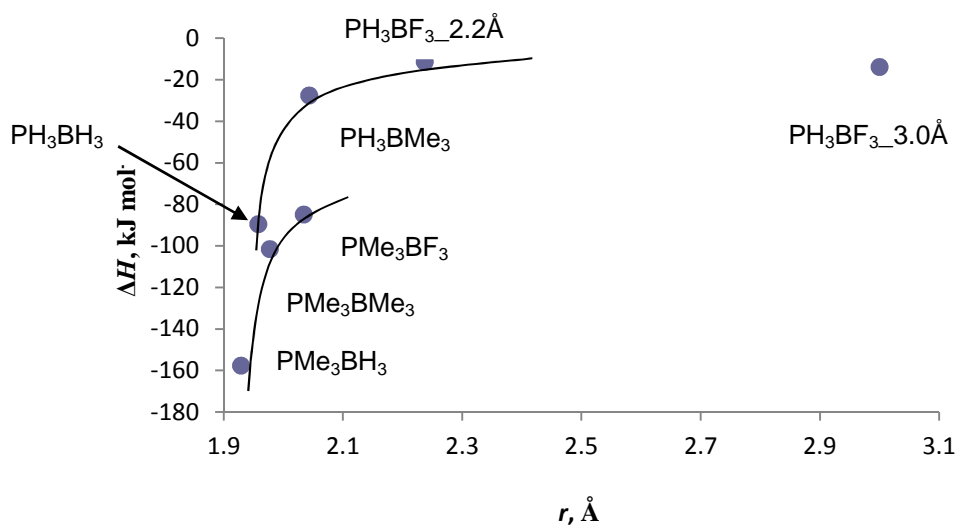
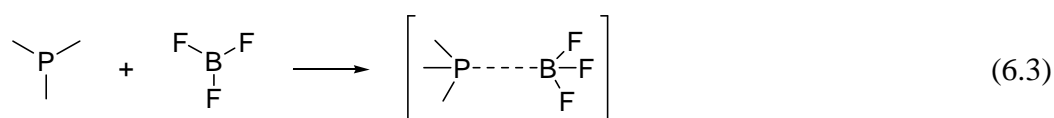


Fig. 6.6 Enthalpies of formation reactions vs. P-B length for all systems in Table 6.1 obtained at MP2(FULL)/aug-cc-pVDZ.

One can see that the formation energies and lengths of P-B bonds coincide and the absolute enthalpy values are increasing, while the distances become shorter. On the whole, complexes of PMe_3 are stronger bonded as compared to PH_3 . The latter seems to correlate with the fact of electron donation effect of the methyl groups. Two curves in Fig. 6.6 show two families of the Lewis pairs. One of them is formed by PMe_3 and another - by PH_3 . In each of the family formation energies and the distances are in good accordance. However, the question about energies as compared to distances for the borane complexes is difficult and not always understandable, thus Frenking *et al.* have studied borane-phosphane complexes of $\text{X}_3\text{B-PY}_3$ ($\text{X} = \text{H, F, Cl}$; $\text{Y} = \text{F, Cl, Me, CN}$) by *ab initio* calculations at MP2/6-311+G(2d)//MP2/6-31G(d) and DFT at BP86/TZP and it has been found, that for comparison of these systems “there is no correlation between bond length and bond strength”. It has been suggested (hypothetically), that the reason is hybridization of the donor lone-pair orbital. “A higher %s character makes a sp^n hybridized donor-orbital more compact which leads to shorter bonds, but at the same time the orbital becomes lower in energy.”^[10] It is

necessary to emphasize, that all results shown in this chapter are lack of BSSE corrections. The calculations of Lewis pairs and FLP taking into account BSSE effect are on-going.

Grimme *et al.*^[1c] have performed quite extensive benchmarking calculations for PMe_3BF_3 system to find out an example of well described reaction energy of Lewis pair formation. Results of this study are compared with our methods screening and collected together in Fig. 6.6 and Table 6.3 (1-4 methods). The reaction energies (for our calculations we show both – relative enthalpies and relative total energies) are calculated for reaction (6.3) shown in Scheme 6.4.



Scheme 6.4. Reaction of formation Lewis pair from trimethyl phosphine and trifluoroborane.

In addition to our results and results of Grimme *et al.* we have also added to the Fig. 6.6 and Table 6.3 experimental complexation enthalpy of reaction (6.3). In the literature one can find two different values of experimentally measured (gas phase calorimetry) complexation enthalpy of the reaction (6.3) – one of them, that we use, is -79 kJ mol^{-1} from Brown^[6], and another one equal to $-190.2 \text{ kJ mol}^{-1}$ comes from Mente and Mills.^[4] The latter is totally out of the computational results area and in previous study by Frenking *et al.* has been already mentioned to be probably mistaken.^[10]

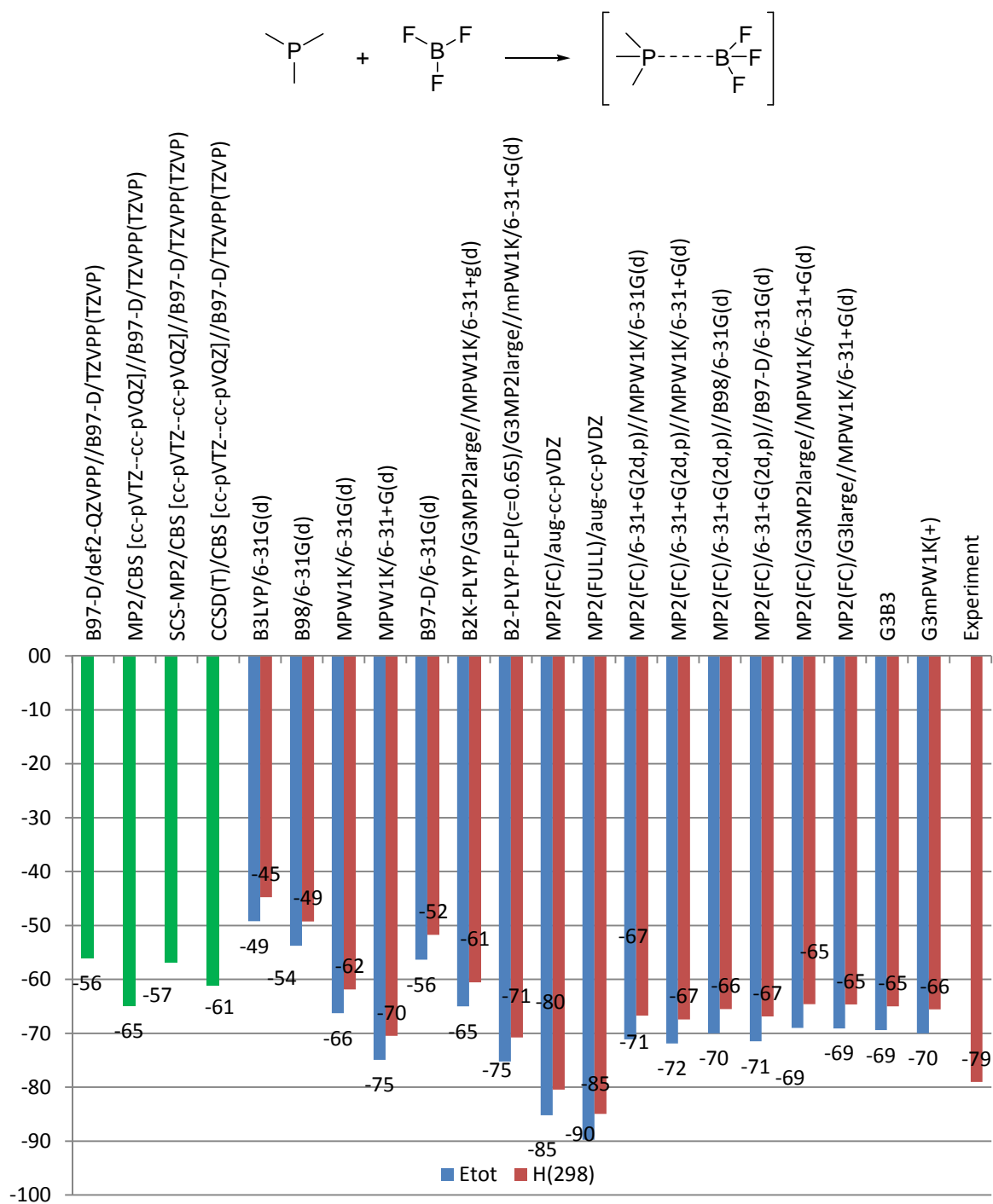


Fig. 6.6. Reaction (6.3) energies obtained at different levels of theory (presented using total energies and enthalpies at 298K).

Table 6.3 Reaction (6.3) energies obtained at different levels of theory (presented using total energies and enthalpies at 298K).

Method	ΔE_{tot} , kJ mol ⁻¹	ΔH_{298} , kJ mol ⁻¹
1 B97-D/def2-QZVPP//B97-D/TZVPP(TZVP) ^[1c]	-56.1	0.0
2 MP2/CBS [for CBS: cc-pVTZ--cc-pVQZ]//B97-D/TZVPP(TZVP) ^[1c]	-64.9	0.0
3 SCS-MP2/CBS [for CBS: cc-pVTZ--cc-pVQZ]//B97-D/TZVPP(TZVP) ^[1c]	-56.9	0.0
4 CCSD(T)/CBS [for CBS: cc-pVTZ--cc-pVQZ]//B97-D/TZVPP(TZVP) ^[1c]	-61.1	0.0
5 B3LYP/6-31G(d)	-49.2	-44.8
6 B98/6-31G(d)	-53.8	-49.2
7 MPW1K/6-31G(d)	-66.3	-61.9
8 MPW1K/6-31+G(d)	-74.9	-70.5
9 B97-D/6-31G(d)	-56.4	-51.7
10 B2K-PLYP/G3MP2large//MPW1K/6-31+g(d) ^[15]	-65.0	-60.6
11 B2-PLYP-FLP(c=0.65)/G3MP2large//MPW1K/6-31+G(d) ^a	-75.2	-70.8
12 MP2(FC)/aug-cc-pVDZ	-85.2	-80.5
13 MP2(FULL)/aug-cc-pVDZ	-89.8	-84.9
14 MP2(FC)/6-31+G(2d,p)//MPW1K/6-31G(d)	-71.1	-66.7
15 MP2(FC)/6-31+G(2d,p)//MPW1K/6-31+G(d)	-71.9	-67.4
16 MP2(FC)/6-31+G(2d,p)//B98/6-31G(d)	-70.0	-65.5
17 MP2(FC)/6-31+G(2d,p)//B97-D/6-31G(d)	-71.5	-66.9
18 MP2(FC)/G3MP2large//MPW1K/6-31+G(d)	-69.0	-64.6
19 MP2(FC)/G3large//MPW1K/6-31+G(d)	-69.1	-64.6
20 G3B3	-69.4	-65.0
21 G3MPW1K(+) ^[16]	-70.0	-65.6
22 Experiment ^[6]		-79.0

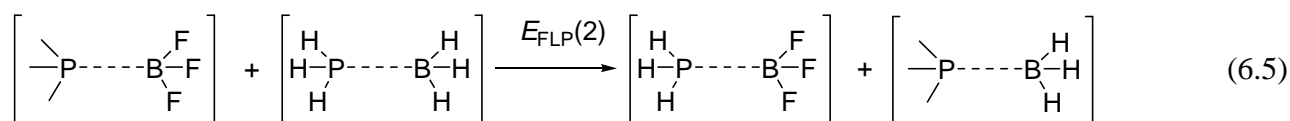
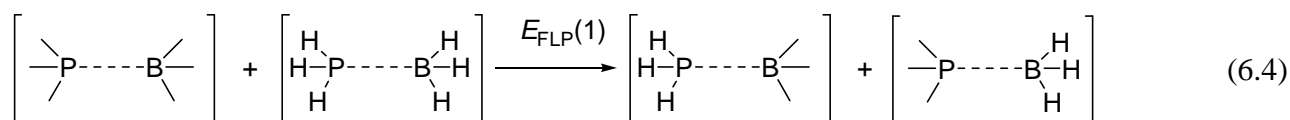
^a B2K-PLYP with bigger contribution of correlation energy from second-order perturbation energy calculation (c = 0.65 instead of original c = 0.42).

Both benchmarking approaches G3B3 and G3MPW1K(+) give values closer to the experimental data^[6], than methods applied by Grimme *et al.*^[1c] Results of MP2/aug-cc-pVDZ (with and without

FC approximation) are inferior. Probably the reason is hidden in already mentioned (on the example of PMe_3BMe_3) mistakes of these approaches for geometry optimization. From DFT approaches the MPW1K/6-31+G(d) gives a surprisingly good result as compared to experiment, all other tested DFT variants fail. Latter coincides with their abilities in geometry optimization of studied small Lewis pairs. Results close to benchmarking approaches are obtained with B2K-PLYP^[15] and B2K-PLYP-FLP (B2K-PLYP with enlarged contribution of correlation energy derived from second-order perturbation energy calculation $c = 0.65$) schemes using geometries from MPW1K/6-31+G(d). Very similar values to benchmarking calculations are shown by MP2(FC)/G3MP2large//MPW1K/6-31+G(d) or MP2(FC)/G3large//MPW1K/6-31+G(d). These two approaches we consider to be the best for several reasons:

1. The geometry optimization approach is shown to be the best.
2. The energy value obtained for model transformation is in good (and the best among all tested approaches) agreement with benchmarking G3-like schemes as well as with experimental data.
3. Producing results close to values from benchmarking approaches for the model transformation, these methods are substantially cheaper.

As the next step the frustration energies for reactions (6.4) and (6.5) (Scheme 6.5) have been calculated using the set of the methods we used before, excepting energies obtained from DFT approaches of geometry optimization.



Scheme 6.5. Exchange reaction between Lewis pairs **a•b** (where $\text{R}_1 = \text{Me}$ and $\text{R}_2 = \text{Me}$ or $\text{R}_2 = \text{F}$) and **c•d**.

Fig.6.4 and Table 6.4 collect the results of frustration energy calculations. It is clear to see, that two methods MP2(FC)/G3MP2large//MPW1K/6-31+G(d) and MP2(FC)/G3MP2large//MPW1K/6-31+G(d) are again in the closest agreement with benchmarking approach G3MPW1K(+). Noteworthy there is a discrepancy between G3B3 and G3MPW1K in estimation of $E_{\text{FLP}}(2)$. This energy corresponds to the reaction (6.5), where the PH_3BF_3 system is involved, which has been in detail discussed due to its particular property to have two minima on the potential energy surface.

We knowingly took for this $E_{\text{FLP}}(2)$ calculation the first minimum (~ 2.3 Å) since it better correlates with the experiment. Since in G3B3 the B3LYP/6-31G(d) geometries are used, and this level of theory is not able to describe the first minimum, the discrepancy presents. The fact of this discrepancy shows us again how it is important – to take reasonable geometries for calculations of Lewis pairs frustration energies. The methods based on MPW1K/6-31+G(d) geometries are always able to locate both minima. For the G3MPW1K(+) level the $E_{\text{FLP}}(2)$ is also calculated for the second minima (~ 2.9 Å) and it is also shown in the Fig. 6.8. The $E_{\text{FLP}}(2)$ related to the second minimum is indeed close to the G3B3 value, pointing the reason of discrepancy between G3B3 and G3MPW1K(+).

At the benchmarking approach of G3MPW1K(+) the $E_{\text{FLP}}(1)$ and $E_{\text{FLP}}(2)$ (first minimum) amount to -2.0 and -2.9 kJ mol⁻¹ respectively. These small magnitudes show quantitatively that there is no substantial frustratedness in the both studied systems, as it was expected.

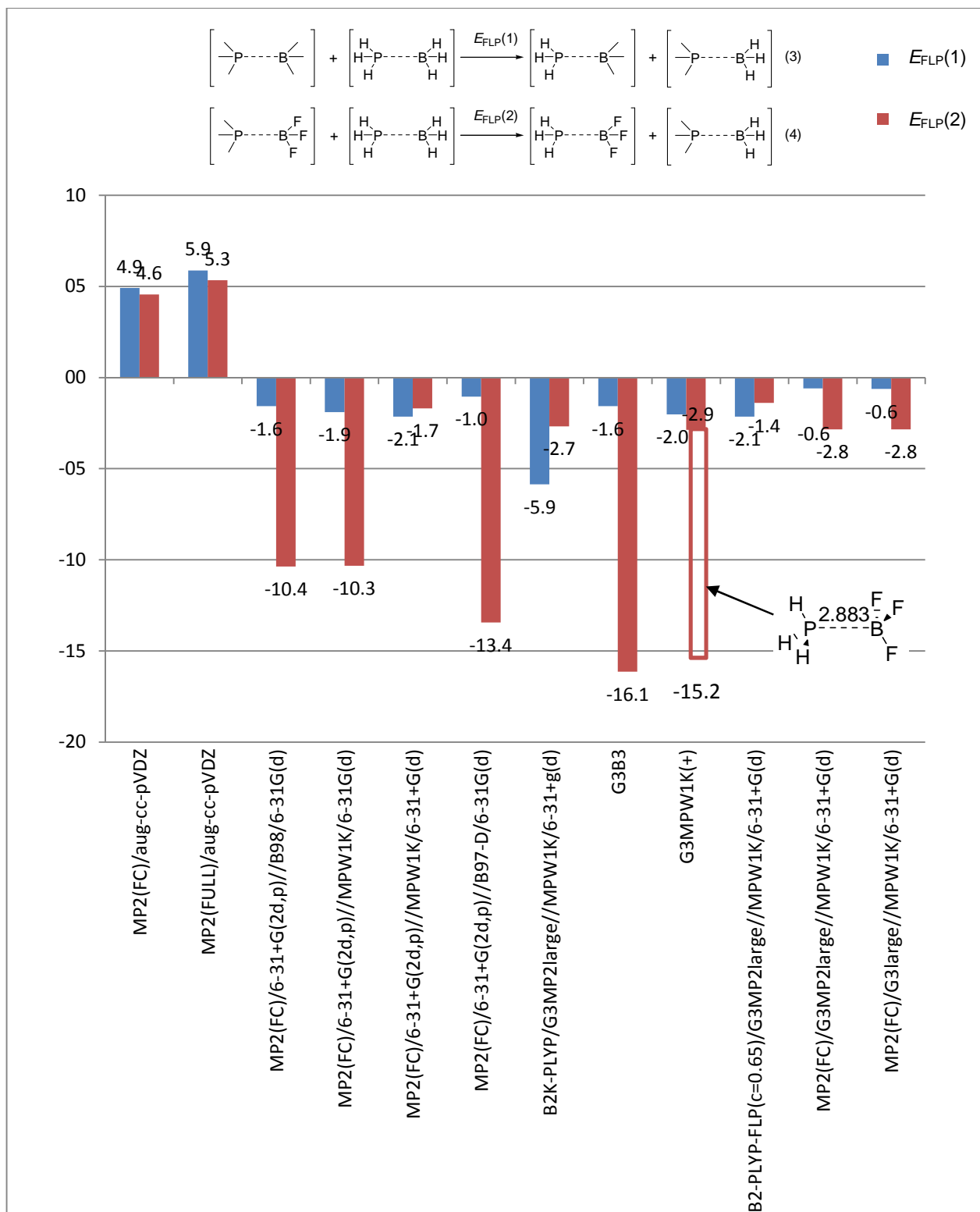


Fig. 6.8. Frustration energies $E_{\text{FLP}}(1)$ and $E_{\text{FLP}}(2)$ for reactions (6.4) and (6.5) respectively (presented as enthalpies at 298K) obtained at different levels of theory.

Table 6.4. Frustration energies $E_{\text{FLP}}(1)$ and $E_{\text{FLP}}(2)$ for reactions (6.4) and (6.5) respectively (presented as enthalpies at 298K) obtained at different levels of theory.

	Method	$E_{\text{FLP}}(1)$	$E_{\text{FLP}}(2)$
1	MP2(FC)/aug-cc-pVDZ	4.9	4.6
2	MP2(FULL)/aug-cc-pVDZ	5.9	5.3
3	MP2(FC)/6-31+G(2d,p)//B98/6-31G(d)	-1.6	-10.4
4	MP2(FC)/6-31+G(2d,p)//MPW1K/6-31G(d)	-1.9	-10.3
5	MP2(FC)/6-31+G(2d,p)//MPW1K/6-31+G(d)	-2.1	-1.7
6	MP2(FC)/6-31+G(2d,p)//B97-D/6-31G(d)	-1.0	-13.4
7	B2K-PLYP/G3MP2large//MPW1K/6-31+g(d)	-5.9	-2.7
8	G3B3	-1.6	-16.1
9	G3MPW1K(+)	-2.0	-2.9
10	B2-PLYP-FLP(c=0.65)//MPW1K/6-31+G(d)	-2.1	-1.4
11	MP2(FC)/G3MP2large//MPW1K/6-31+G(d)	-0.6	-2.8
12	MP2(FC)/G3large//MPW1K/6-31+G(d)	-0.6	-2.8

6.3. Conclusions

A computational approach for the treatment of Lewis pair systems is suggested. The approach is selected with the goal to use it in further studies for large frustrated Lewis pair systems, with consideration of delicate geometrical properties of Lewis pairs, the necessity to give high quality thermochemical predictions and limitation to be computationally affordable cheap. The MP2(FC)/G3MP2large//MPW1K/6-31+G(d) level of theory seems to satisfy all requirements. The studies of FLP systems can now be extended to large systems. For a theoretical description of FLP systems we suggest calculation of the “frustration energy” as energy of the exchange reaction between the FLP $\text{P}(\text{R}^1)_3\text{B}(\text{R}^2)_3$ and unbiased reference system PH_3BH_3 relying on the proposed level of theory.

6.4. References

- [1] a) D. W. Stephan, *Org. Biomol. Chem.* **2008**, *6*, 1535-1539; b) D. W. Stephan, G. Erker, *Angewandte Chemie International Edition* **2009**, *49*, 46-76; c) S. Grimme, H. Kruse, L. Goerigk, G. Erker, *Angew. Chem. Int. Ed.* **2010**, *49*, 1402-1405; d) C. Jiang, O. Blacque, H. Berke, *Organometallics* **2009**, *28*, 5233 - 5239.
- [2] G. C. Welch, D. W. Stephan, *J. Am. Chem. Soc.* **2007**, *129*, 1880-1881.
- [3] J. R. Durig, Y. S. Li, L. A. Carreira, J. D. Odom, *J. Am. Chem. Soc.* **1973**, 2491-2496.
- [4] D. C. Mente, J. L. Mills, *Inorg. Chem.* **1975**, *8*, 1862.
- [5] J. D. Odom, V. F. Kalasinsky, J. R. Durig, *Inorg. Chem.* **1975**, *14*, 2837.
- [6] H. C. Brown, *J. Chem. Soc.* **1956**, 1248.
- [7] H. Anane, A. Boutalib, I. Nebot-Gil, F. Tomás, *J. Phys. Chem. A* **1998**, *102*, 35.
- [8] F. Bessac, G. Frenking, *Inorg. Chem.* **2006**, *45*, 6956-6964.
- [9] F. Hirota, K. Miyata, S. Shibata, *J. Mol. Struct.: THEOCHEM* **1989**, *201*, 99.
- [10] C. Loschen, K. Voigt, J. Frunzke, A. Diefenbach, M. Diefenbach, G. Frenking, *Z. Anorg. Allg. Chem.* **2002**, *628*, 1294.
- [11] T. A. Ford, *J. Phys. Chem. A* **2008**, *112*, 7296-7302.
- [12] R. Ahlrichs, M. R. Bär, M. Häser, E. Sattler, *Chem. Phys. Lett.* **1991**, *184*, 353.
- [13] G. Erős, H. Mehdi, I. Pápai, T. A. Rokob, P. Király, G. Tárkányi, T. Soós, *Angew. Chem. Int. Ed.* **2010**, *49*, 6559-6563.
- [14] D. J. Giesen, J. A. Phillips, *J. Phys. Chem. A* **2003**, *107*, 4009 - 4017.
- [15] A. Tarnopolsky, A. Karton, R. Sertchook, D. Vuzman, R. L. Martin, *J. Phys. Chem. A* **2008**, *112*, 3-8.
- [16] Y. Wei, B. Sateesh, B. Maryasin, G. N. Sastry, H. Zipse, *J. Comput. Chem.* **2009**, 2617 - 2624.

7. Theoretical Studies of the Acylation Reaction Catalyzed by DMAP With Participation of Aryl Derivatives

7.1. Introduction.

A fundamental mechanistic study of the DMAP-catalyzed acylation reaction of alcohols has been published by the Zipse group^[1]. The reaction to study has been chosen the acetylation of *tert*-butanol by acetic anhydride in the presence of DMAP. Two hypothetically competing mechanisms have been compared: nucleophilic and the general base catalysis pathways. Both pathways are shown in Fig. 7.1

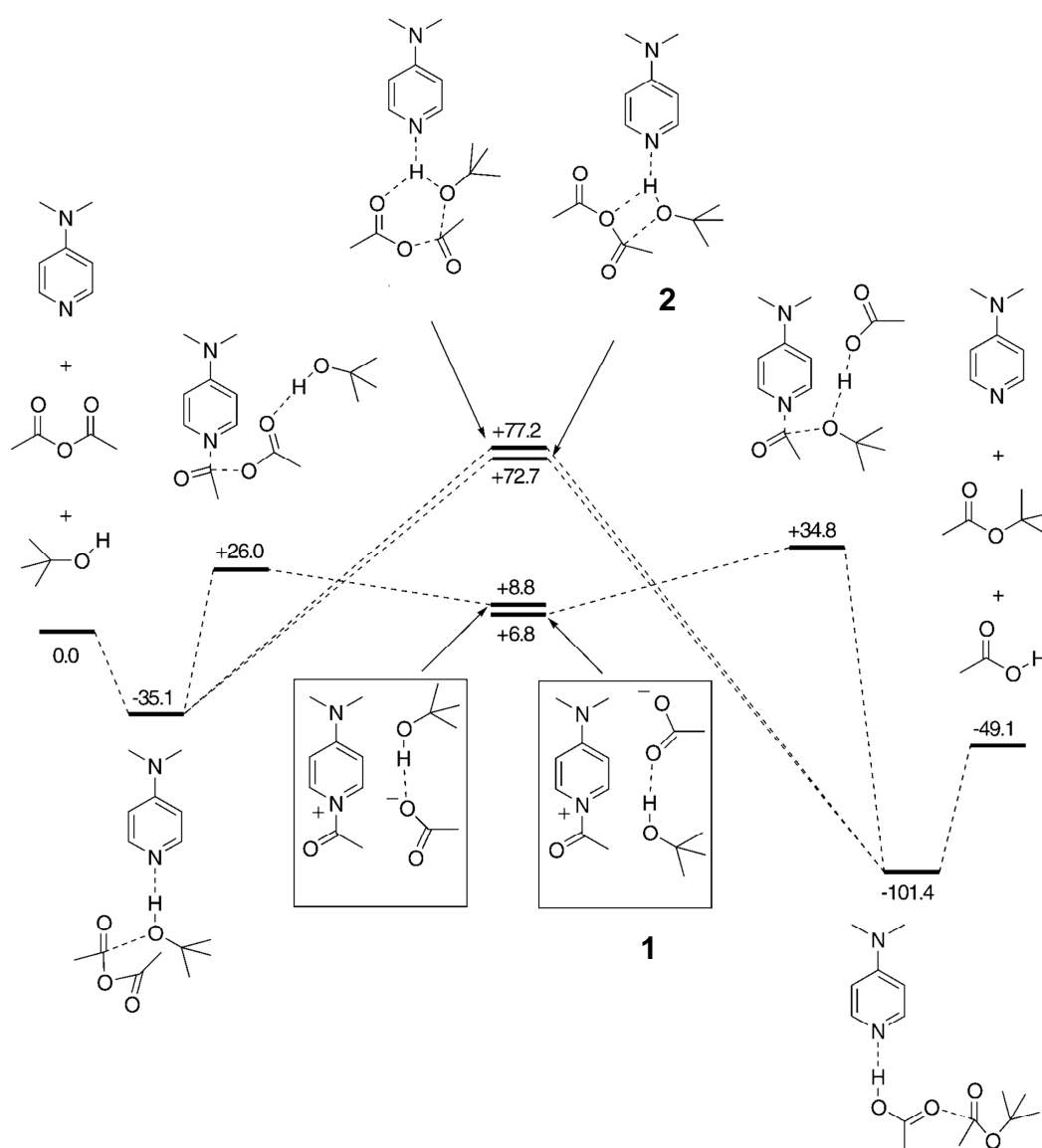


Fig.7.1 Gas-phase enthalpy profile (ΔH_{298}) for the competing nucleophilic and base catalysis mechanisms in the DMAP-catalyzed reaction of acetic anhydride with *tert*-butanol as calculated at the B3LYP/6-311+G(d,p)//B3LYP/6-31G(d) level of theory.

The nucleophilic catalytic cycle includes formation of an acetylpyridinium cation of DMAP and then its reaction with the alcohol (the rate-determining step). The general base catalysis goes via transition state **2**. For the studied case of *tert*-butanol and acetic anhydride the latter mechanism has been found to be much less favourable than the nucleophilic catalytic cycle. Another system has been also applied for analogous calculations – it is reaction between racemic 1-(1-naphthyl)ethanol with isobutyric anhydride catalyzed by chiral derivative of DMAP.^[2] The aims of this study were an investigation of enantioselectivities of chiral DMAP-catalysts and checking whether previously suggested mechanism stay relevant with changing of the system. The conclusions about mechanism were similar to the preceding study. However, the first step of the acetylpyridinium cation formation in the nucleophilic catalytic cycle has been found to have slightly larger activation energy as compared to the second step. The nucleophilic pathway still has been found preferable. It has been recently found for desymmetrization of cyclic *meso*-anhydrides by chiral amino alcohols that the base-catalyzed pathway, on the contrary, becomes preferable as compared to nucleophilic.^[3] Other examples of comparison nucleophilic *vs.* base-catalysis, where the last one can be a favourable, have been also shown.^[4] Thus, depending on the system, one or the other pathway is preferable, and within the nucleophilic pathway the transition states can exchange the rate-determining nature.

In this chapter of the present work we show results of a computational study for benzyl alcohol and benzoic acid anhydride in the presence of DMAP. To the best of our knowledge the aryl derivatives from the side of an acylation agent have not yet been applied in mechanistic studies. We have compared both catalytic pathways with background reaction (no catalyst is involved) and studied the influence of donor and acceptor substituents in the aromatic ring of the reacting alcohol. In order to be consistent with the previous studies^[1] we have chosen to use the same level of theory: B3LYP/6-311+G(d,p)//B3LYP/6-31G(d)//OPLS-AA.

7.2. The Background Reaction

In contrast to the previous studies in the field of the catalyzed acylation reactions mechanism,^[1-2] the background (uncatalyzed) reaction is also shown in the present work. Surprisingly, there are only few theoretical studies for the uncatalyzed esterification reaction.^[5] Kruger has studied acylation of methanol by acetic anhydride at the MP2/6-31+G(d,p) level.^[5a] It has been suggested that the reaction proceeds through a six-membered ring transition state. Aminolysis of succinic anhydride has been studied theoretically (MP2/6-

311++G(d,p)//B3LYP/6-311++G(d,p) and CCSD(T)/6-31G(d)//B3LYP/6-311++G(d,p)) by Leszczynski *et al.*^[5b] The authors have compared a concerted mechanism with stepwise pathways. The concerted pathway has been found to be preferable. In the present work the concerted pathway is involved in the calculation, having in mind that the stepwise is possible but less preferable.

The background reaction pathway is plotted in Fig. 7.2 by using the relative enthalpies at 298K (the enthalpies are collected in Table 7.1). We have chosen enthalpies and not free energies in order to be consistent with the previous studies in this area.^[1-2]

Table 7.1 Relative enthalpies (kJ mol⁻¹) for stationary points (best conformations, X = H) located on the potential energy surface at B3LYP/6-311+G(d,p)//B3LYP/6-31G(d) level.

ΔH_{298} (gas phase)	
Background reaction (uncatalyzed)	
3 + 4	0.0
5	-16.5
6	+67.9
7	-78.4
8 + 9	-65.7

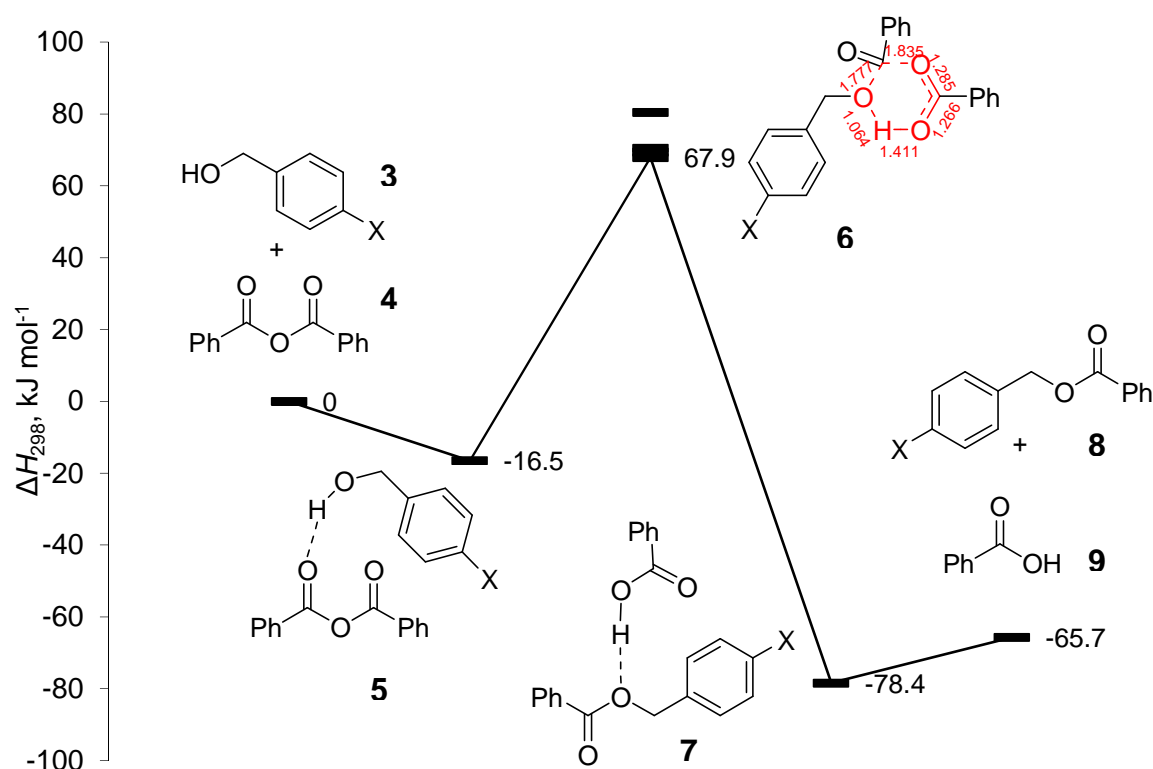


Fig. 7.2 Gas-phase enthalpy profile (ΔH_{298}) for the uncatalyzed acylation of benzyl alcohol with benzoic anhydride as calculated at the B3LYP/6-311+G(d,p)//B3LYP/6-31G(d) level of theory.

The system forms a reactant complex and then, via a six-membered-ring transition state, goes finally to the product complex. The barrier relative to the reactant complex is found to be 84.4 kJ mol⁻¹.

7.3. Nucleophilic Catalysis vs. Base Catalysis

In order to check whether in the case of our system the reaction mechanism is similar to that in the previously studied systems, calculations include both modes of catalysis. The results are shown in Fig. 7.3 using relative enthalpies at 298 K (the enthalpies are collected in Table 7.2).

Table 7.2 Relative enthalpies (kJ mol⁻¹) for stationary points (best conformations) located on the potential energy surface at B3LYP/6-311+G(d,p)//B3LYP/6-31G(d) level.

	ΔH_{298} (gas phase)
Nucleophilic catalysis	
3 + 4 + 10	0.0
11	-42.2
12	+33.7
13	+7.5
14	+20.1
15	-114.0
8 + 9 + 10	-65.7
Base catalysis (concerted)	
3 + 4 + 10	0.0
11	-42.2
16	+38.7
15	-114.0
8 + 9 + 10	-65.7

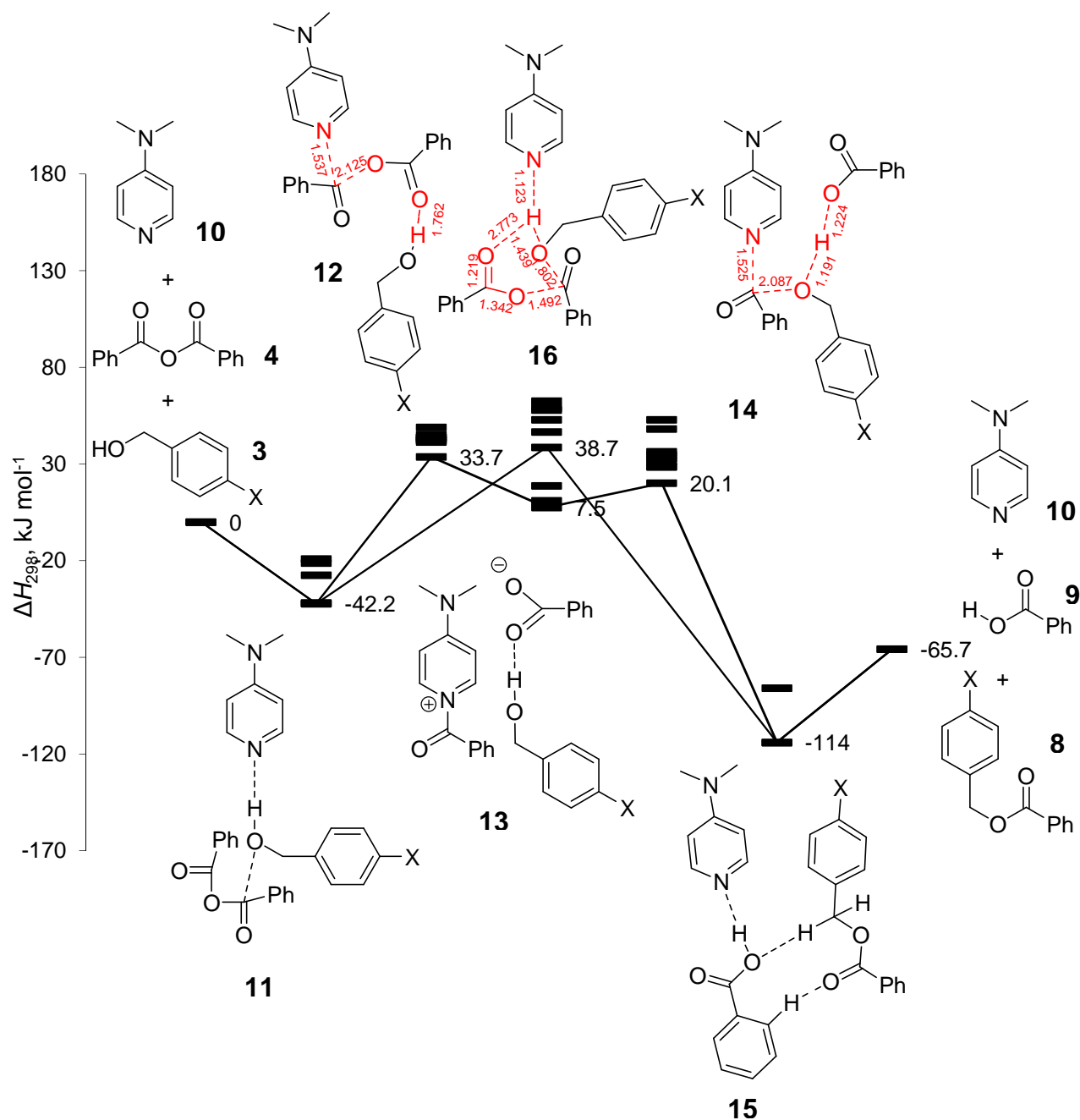


Fig. 7.3 Gas phase enthalpy profile (ΔH_{298}) for the competing nucleophilic and base catalysis mechanisms in the DMAP-catalyzed reaction of benzoic anhydride with benzyl alcohol as calculated at the B3LYP/6-311+G(d,p)//B3LYP/6-31G(d) level of theory. Enthalpies represent the case of X = H.

The nucleophilic pathway starts from reactant complex **11** and via TS **12** yields the intermediate **13**, a loose complex between acetylpyridinium cation of DMAP and a complex of benzoate and benzyl alcohol. This loose complex then continues through TS **14** to form the stable product complex **15**. If the base catalysis pathway is chosen, then the reactant complex **11** goes through TS **16** and finally falls into the same product complex **15**. As before the most important conclusions can be immediately drawn from the results shown in Fig. 7.3:

- The difference between nucleophilic and base catalysis pathways is not significant - the nucleophilic catalysis is found to be only 5 kJ mol⁻¹ more preferable.
- The first step of the nucleophilic catalysis pathway is the rate-determining step instead of the last step. This is in contrast to the reaction of *tert*-butanol with acetic anhydride,^[1] but similar to the reaction of 1-(1-naphthyl)ethanol with isobutyric anhydride.^[2]

7.4. The Influence of Donor and Acceptor Substituents in the Aromatic Ring of the Alcohol

We have studied the influence of the substitution in *p*-position of the alcohol aromatic ring. In order to avoid expensive transition state optimizations and assuming unsubstantial changes of the geometries varying the substituent, we suggest the following “cheap” computational scheme:

1. Substitution of -H to -R (here -NO₂ or -CH₃) in the agreed position of important stationary points (the best conformations of TSs, reactants and products). We have used two of the best conformations. If the stability order was changed in the B3LYP/6-311+G(d,p)//B3LYP/6-31G(d) single-point calculations as compared with the B3LYP/6-31G(d) geometry optimization, then we have used two of the best conformations after single-point as well as two of the best after the geometry optimization.
2. Optimization with constrains (we freeze the distances in the reacting part of the transition states. The frozen bonds are shown by red colour in Fig 7.2 and 7.3).
3. Single point calculations at the B3LYP/6-311+G(d,p)//B3LYP/6-31G(d) level.

In Fig. 7.4 we show the changes in the total energy barriers for the background reaction, the first and second transition states of the nucleophilic pathway, and for the base-catalyzed pathway, respectively. The relative total energies are also collected in Table 7.3.

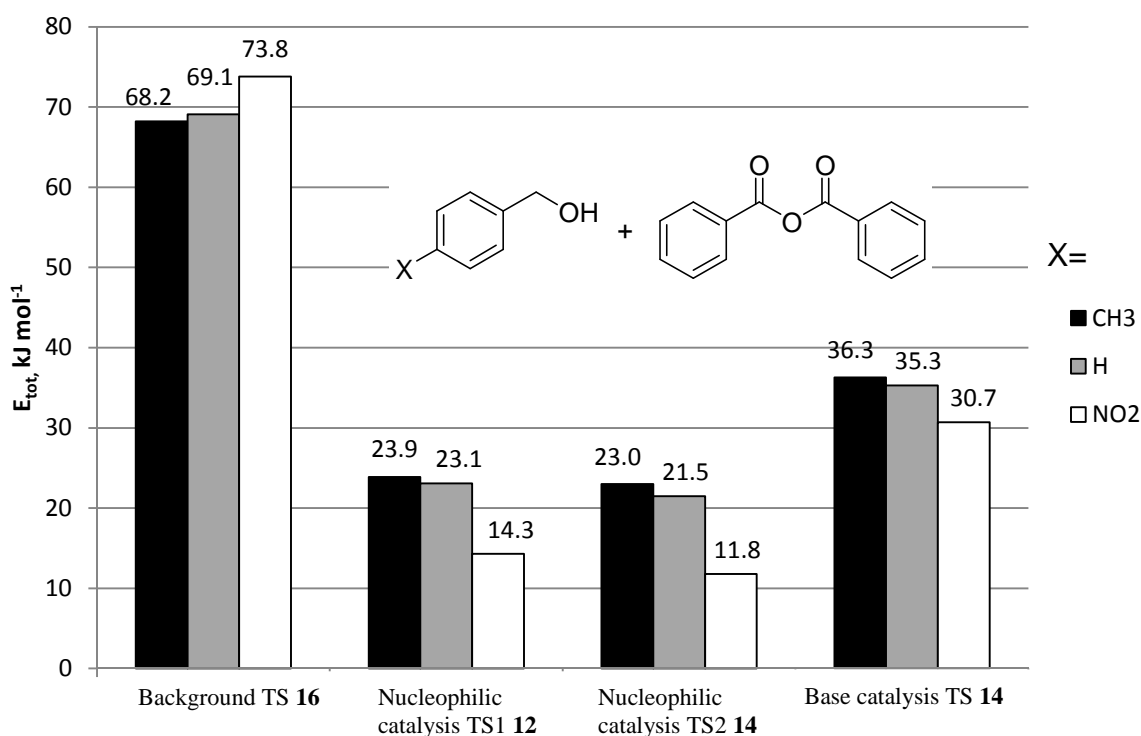


Fig. 7.4 Reaction barriers for uncatalyzed and DMAP-catalyzed acylation of *p*-substituted benzyl alcohol by benzoic anhydride.

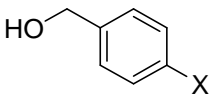
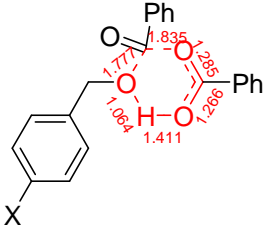
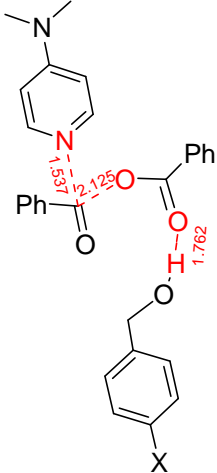
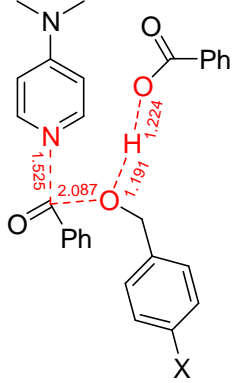
Table 7.3 Relative total energies (kJ mol⁻¹) for stationary points (best conformations) located on the potential energy surface at B3LYP/6-311+G(d,p)//B3LYP/6-31G(d) level with X = H. For X = CH₃ and NO₂ energies of products, reactants and transition states are shown.

X = H	ΔE_{tot} (gas phase)	X = CH ₃	ΔE_{tot} (gas phase)	X = NO ₂	ΔE_{tot} (gas phase)
Background reaction (uncatalyzed)					
3 + 4	0.0	3c + 4	0.0	3n + 4	0.0
5	-22.7				
6	+69.1	6c	+68.2	6n	+73.8
7	-88.6				
8 + 9	-68.3	8c + 9	-69.3	8n + 9	-62.6
Nucleophilic catalysis					
3 + 4 + 10	0.0	3c + 4 + 10	0.0	3n + 4 + 10	0.0
11	-54.8				
12	+23.1	12c	+23.9	12n	+14.3
13	-6.5				
14	+21.5	14c	+23.0	14n	+11.8
15	-128.2				
8 + 9 + 10	-68.3	8c + 9 + 10	-69.3	8n + 9 + 10	-62.6
Base catalysis (concerted)					
3 + 4 + 10	0.0	3c + 4 + 10	0.0	3n + 4 + 10	0.0
11	-54.8				
16	+35.3	16c	+36.3	16n	+30.7
15	-128.2				
8 + 9 + 10	-68.3	8c + 9 + 10	-69.3	8n + 9 + 10	-62.6

Moving from donor substituent to acceptor substituents in the benzyl alcohol reactant, the background reaction barrier is increasing, while reaction barriers for all catalyzed pathways

systematically decrease. For all three alcohols the nucleophilic catalysis mechanism is slightly more preferable than the base-catalyzed and within the nucleophilic pathway the first step is the rate-determining. Trying to explain the effect of the substituent plotted in Fig. 7.4 we have calculated the overall charges (NPA/B3LYP/6-311+G(d,p)) on the alcohol moiety in the transition state of the background reaction and in the rate-determining transition state of the nucleophilic catalysis reaction.

Table 7.4. The overall charge (e) on the alcohol moiety in the transition states of the background and catalyzed reactions calculated at NPA/B3LYP/6-311+G(d,p)//B3LYP/6-31G(d) level of theory.

Alcohol	Background reaction TS 16	Nucleophilic catalysis TS1 12	Nucleophilic catalysis TS2 14
			
X =			
CH ₃	+0.204	-0.010	-0.025
H	+0.201	-0.024	-0.022
NO ₂	+0.188	-0.019	-0.048

In the case of the background reaction change of the overall charge on the alcohol moiety coincides with the change of the reaction. The barrier is getting smaller, while the overall charge is increasing. For the case of first transition state in the nucleophilic pathway **12** the magnitude of the overall charge on alcohol stays close to zero (~20 times smaller than for the background reaction case), and there is no strong interdependence between the charge and the barrier. In the transition state of the background reaction, the alcohol is in close contact with the anhydride. It donates concerting the hydrogen and accepts the benzoic group, though in the **12** the alcohol role leads to the hydrogen bond formation, due to this its overall charge is close to zero. In the second transition state of the nucleophilic pathway **14** the alcohol overall charge is bigger, than in the **12** but substantially smaller as compared to background reaction TS **16**, though the role of the alcohol moiety is similar to both **14** and background reaction TS **16**. On the whole, the charge transfer within the alcohol is substantially bigger for background

TS comparing to the catalyzed pathway. The higher overall charge of the alcohol moiety is (the larger charge transfer inside of the transition state is), the smaller the barrier is.

In Fig. 7.5 we show the differences between background reaction and catalyzed reaction barriers for three studied systems. It can be seen from Fig, 7.5 that the difference is increasing with increasing of electron accepting effect. This can also be interpreted in the way that catalyst works most effectively for the aromatic alcohol with an acceptor substituent in the aromatic ring and least effectively if the substituent has donor character.

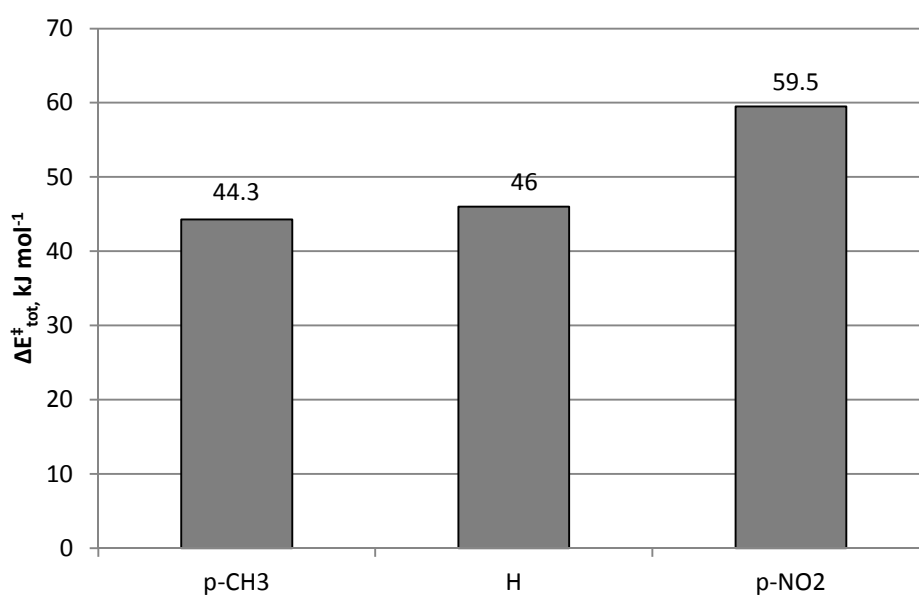


Fig. 7.5 Differences between barriers of uncatalyzed and catalyzed reactions for three studied systems.

7.5. Conclusions

As a whole our study continues the series of the works in the topic of the mechanism of DMAP derivatives catalyzed acylation reactions. Particularly we have found:

- Similar to the previously studied acylation reactions where *tert*-butanol and racemic 1-(1-naphthyl)ethanol have been acylated by aliphatic anhydrides in the presence of DMAP derivatives, the nucleophilic mechanism is more favourable than the general base mechanism for the presently studied DMAP catalyzed reaction of aromatic alcohols with benzoic acid anhydride. But in this latter case the difference between nucleophilic and base catalysis becomes much smaller.
- There is a substantial influence of the substituent in the *para*-position of the alcohol aromatic ring. For an acceptor substituent the difference between background and catalyzed reaction (the “performance of catalyst”) is bigger than in the unsubstituted benzyl alcohol and for donor substituent this difference is the smallest.

7.6. References

- [1] S. Xu, I. Held, B. Kempf, H. Mayr, W. Steglich, H. Zipse, *Chem. Eur. J.* **2005**, *11*, 4751-4757.
- [2] Y. Wei, PhD thesis, Ludwig-Maximilians-Universität München (München), **2008**.
- [3] B. Dedeoglu, S. Catak, K. N. Houk, V. Aviyente, *ChemCatChem* **2010**, *2*, 1122-1129.
- [4] a) C. Bonduelle, B. Martín-Vaca, F. P. Cossío, D. Bourissou, *Chem. Eur. J.* **2008**, *14*, 5304-5312; b) M. Kieseewetter, M. D. Scholten, N. Kirn, R. L. Weber, J. L. Hedrick, R. M. Waymouth, *J. Org. Chem* **2009**, *74*, 9490-9496.
- [5] a) H. Kruger, *J. Mol. Struct.: THEOCHEM* **2002**, *577*; b) T. Petrova, S. Okovytyy, L. Gorb, J. Leszczynski, *J. Phys. Chem. A* **2008**, *112*, 5224-5235.

General Conclusions

(1) A reliable scheme for the prediction of ^{31}P NMR chemical shifts of large phosphorus containing molecular systems in solution has been developed. The suggested strategy involved NMR shift calculations at the GIAO-MPW1K/6-311++G(2d,2p)//MPW1K/6-31G(d) level in combination with a dual solvation model including the explicit consideration of single solvent molecules (*vide* Fig. 8.1) and a continuum (PCM) solvation model. We have found that Boltzmann averaging over all accessible conformations in solution is essential for ^{31}P NMR shift predictions. We have explored that for ion pairs, such as those involving phosphonium salts, the consideration of the full system (inclusion of counterion) is necessary.

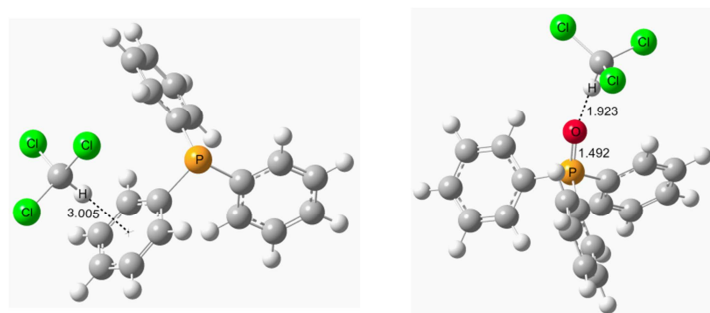


Fig. 8.1 Energetically most favorable complexes of PPh_3 and OPPh_3 with CHCl_3 as obtained - at the MP2(FC)/6-31+G(2d,p)//MPW1K/6-31G(d) level of theory.

The validity of the suggested scheme has been tested in the MBH reaction. For the experimentally detected phosphonium salt, formed via a side reaction of MBH, the ^{31}P NMR chemical shift is predicted with experimental accuracy of less than 1 ppm error. The ^{31}P NMR chemical shifts of the key zwitterionic intermediate of MBH as well as its isomeric ylid are predicted. A model of co-behaviour between catalyst, co-catalyst, Michael acceptor and solvent during the possible side reaction of the phosphonium intermediate formation is suggested.

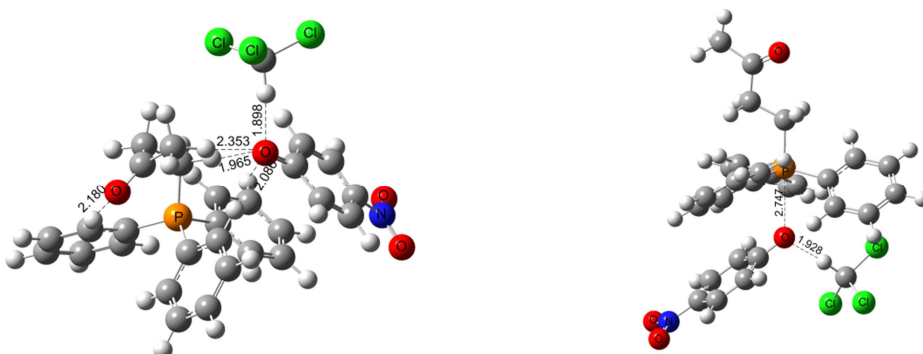


Fig. 8.2 Structures of the most stable complexes between phosphonium salt (side product of MBH reaction) and chloroform.

(2) The catalytic cycle of the MBH reaction is studied in detail for the triphenylphosphane-catalyzed coupling of methyl vinyl ketone with *p*-chlorobenzaldehyde in the presence of *p*-nitrophenol as a co-catalyst in tetrahydrofuran. The catalytic cycle has been compared with possible side reactions. It has been shown that there is a probability for reaction to be trapped in very stable intermediates due to protonation by co-catalyst. Such dual role of co-catalyst (assistance and disturbance) explains the experimental evidence of strong interdependence between MBH reaction rate and concentration of co-catalyst. The resulting energy diagram of the cycle is shown in Fig. 8.3 as relative free energies ($\Delta G_{298,\text{THF}}$) vs. reaction coordinate

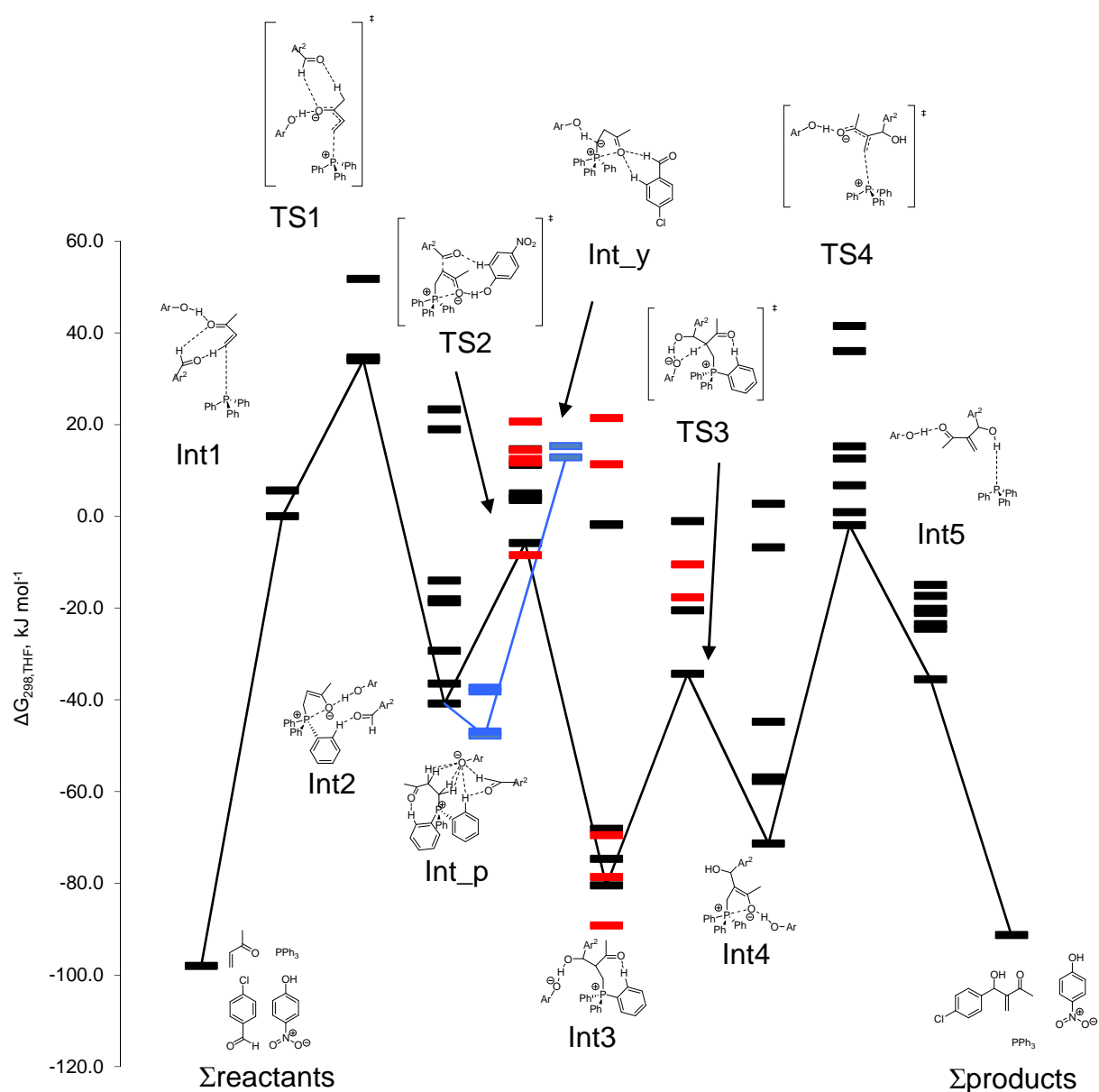
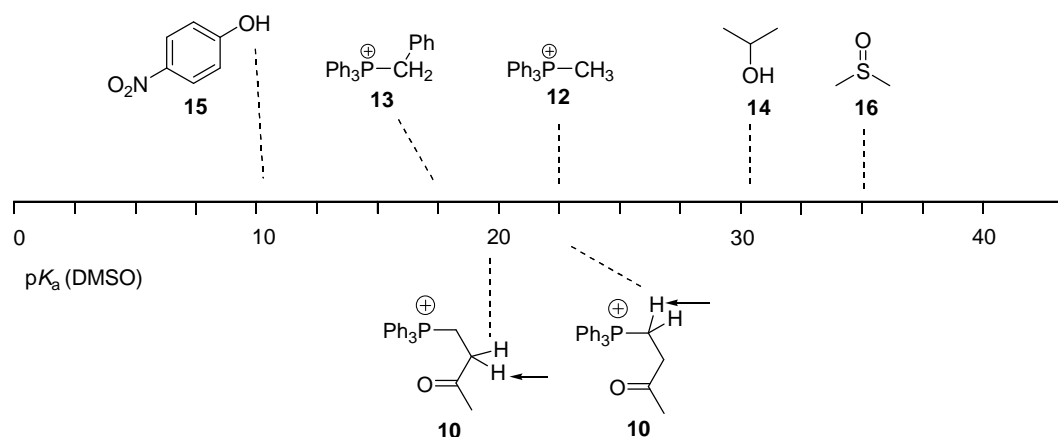


Fig. 8.3 The reaction free energy profile ($\Delta G_{298,\text{THF}}$) calculated at the MP2(FC)/6-31+G(2d,p)//MPW1K/6-31+G(d) level of theory with additional consideration of solvent at PCM(THF)/UAHF/RHF/6-31G(d) level. All found conformations are shown. The

diastereomeric pathways are shown in black colour (RS) and in red colour (RR). In blue colour the side reactions of protonation and ylidization are shown.

(3) The protonation/deprotonation equilibrium between the first key intermediate of the MBH catalytic cycle, the phosphonium species formed from this intermediate and an ylid formed from the phosphonium intermediate has been studied in detail. On the pK_a scale shown in Scheme 8.1 the phosphonium intermediate of the MBH reaction is compared with *p*-nitrophenol (popular MBH reaction co-catalyst), isopropanol (system similar to the MBH reaction product), reference systems for the pK_a calculations and DMSO (solvent used for the pK_a calculations). The results explain experimental observations of side products, whose formation interferes with the MBH processes. The calculations of acidity properties have been extended to a series of catalysts and substrates showing potential of the catalyst/substrate combination to be “good”, giving more catalytic cycle intermediate and less side products, or “bad” if the situation is reversed.



Scheme 8.1 The pK_a scale.

(4) We have applied the methyl cation affinity approach (MCA) as a descriptor of catalytic activity for a series of phosphanes, including cyclophane-substituted phosphanes and cyclophosphanes. The obtained MCA values can be used as a guideline for the optimization of phosphane-catalyzed organocatalytic transformations, e.g. the MBH reaction. A new descriptor of catalytic activity is suggested for MBH reactions: XKA (“X”-Ketone Affinity) is the affinity of a catalyst to the MBH-substrate (“X”-Ketone). The XKA and its particular case MVKA (Methyl Vinyl Ketone Affinity) work well for a rough estimate of the efficiency for chosen catalyst/substrate combinations. The Fig. 8.4 collects in the graphical manner the MVKA values for one of the studied family of catalysts (so called bifunctional phosphane catalysts BPC).

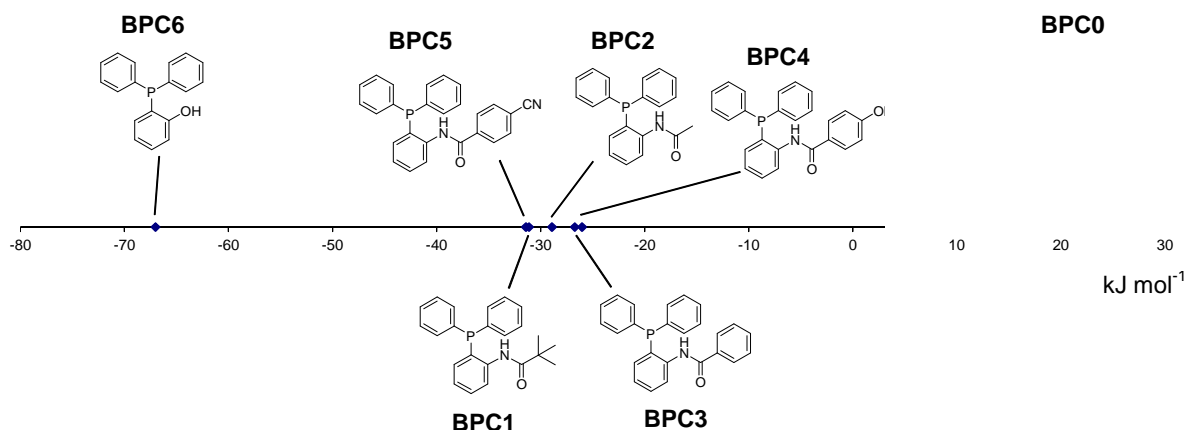


Fig. 8.4 The MVKA scale of the BPC family.

(5) A computational approach for the treatment of Lewis pair systems is suggested. The proposed MP2(FC)/G3MP2large//MPW1K/6-31+G(d) approach accurately reflects geometries and energies of the Lewis pairs even for complicated cases with multiple minima on the potential energy surfaces (for the PH_3BF_3 system two minima have been located, as it is shown in Fig. 8.5). At the same time this method is computationally economical enough to be applicable even to large real-life systems of frustrated Lewis pairs. For a theoretical description of FLP systems we suggest the calculation of “frustration energy” as the energy of the exchange reaction between the FLP $\text{P}(\text{R}^1)_3\text{B}(\text{R}^2)_3$ and unbiased reference system PH_3BH_3 relying on proposed level of theory.

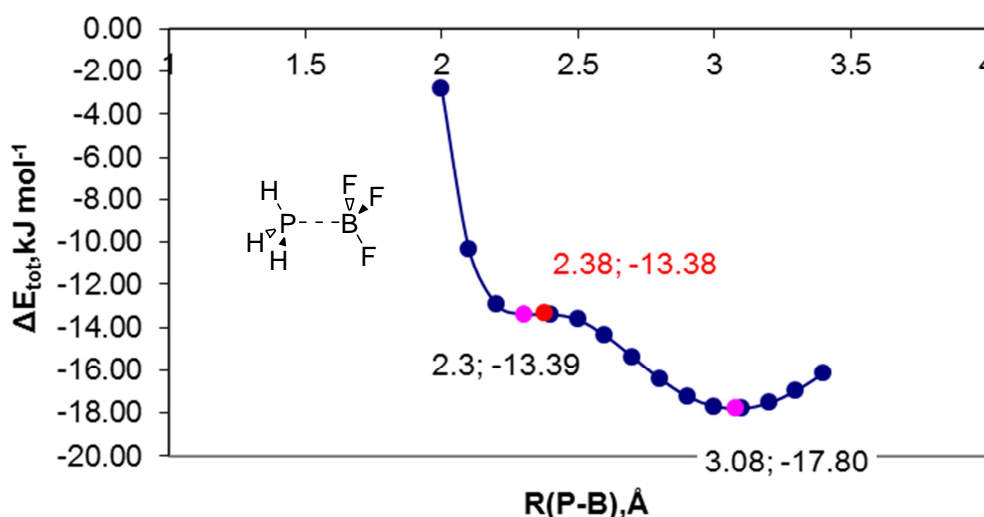


Fig. 8.5 Potential energy curves for the interaction of PH_3 with BF_3 computed at MP2(FC)/6-311++G(d,p) level.

(6) In continuation of the series theoretical studies in catalyzed esterification processes performed by the Zipse group, we have studied the DMAP-catalyzed acylation of aromatic alcohols by benzoic anhydride. In contrast to previous studies we apply an aromatic acylation agent and compare not only the catalyzed pathways with each other, but also with uncatalyzed background reaction. The situation of competing nucleophilic and base-catalyzed pathways has been discussed. The effect of the substitution in *para*-position of aromatic alcohol has been studied. The catalyzed reaction profile for the case of unsubstituted alcohol is shown in Fig. 8.6.

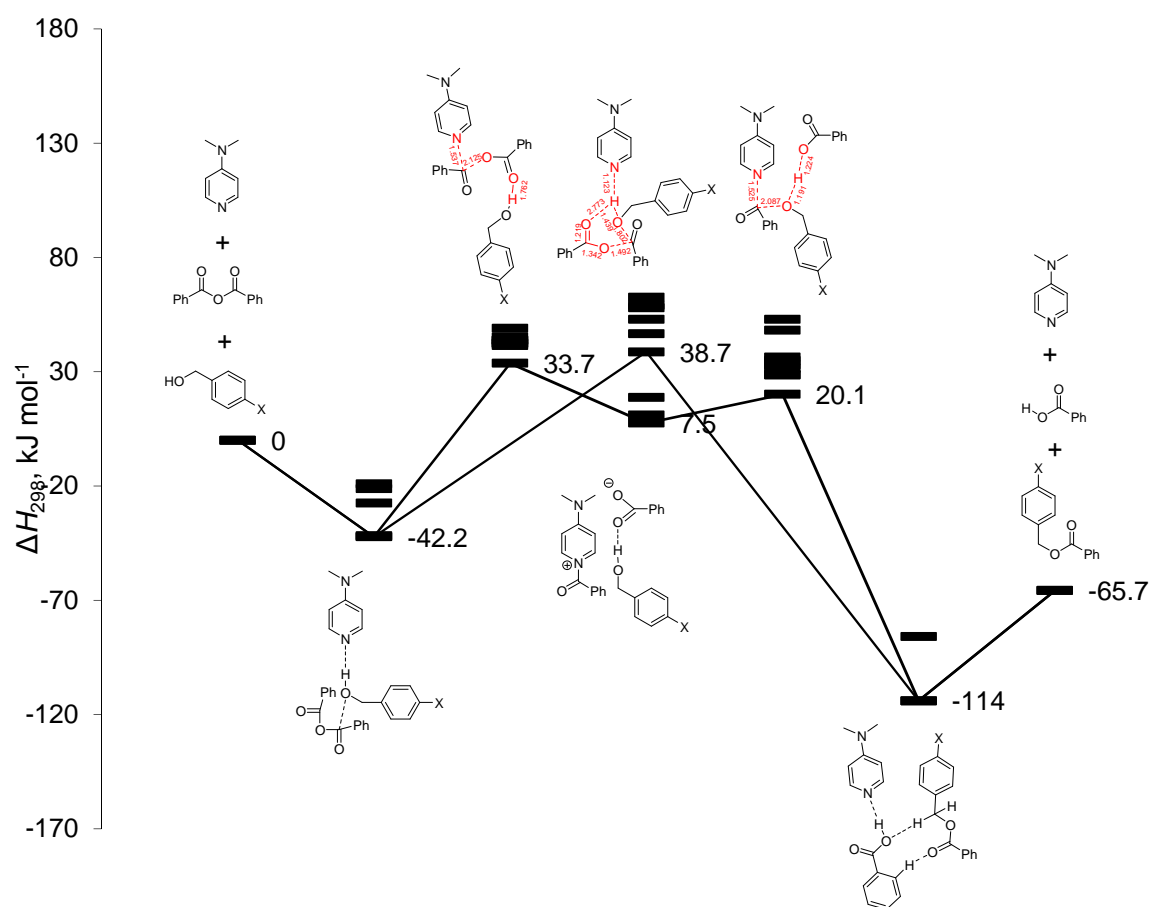


Fig. 8.6 Gas phase enthalpy profile (ΔH_{298}) for the competing nucleophilic and base catalysis mechanisms in the DMAP-catalyzed reaction of benzoic anhydride with benzyl alcohol as calculated at the B3LYP/6-311+G(d,p)//B3LYP/6-31G(d) level of theory. Enthalpies represent case of X = H.

9. Appendix

9.1. General Details

All calculated data (shielding values, total energies, free energies, enthalpies etc) are collected here. The quantum chemical calculations have been performed with Gaussian03.^[3] The force field calculations have been performed with TINKER^[1] and MACROMODEL.^[2]

- 1 J. W. Ponder, *TINKER*; 4.2 ed., 2004.
- 2 Schrödinger, LLC., *MacroModel* 9.7, 2009.
- 3 Gaussian 03, Revision D.01, M. J. Frisch, G. W. Trucks, H. B. Schlegel, G. E. Scuseria, M. A. Robb, J. R. Cheeseman, J. A. Montgomery, Jr., T. Vreven, K. N. Kudin, J. C. Burant, J. M. Millam, S. S. Iyengar, J. Tomasi, V. Barone, B. Mennucci, M. Cossi, G. Scalmani, N. Rega, G. A. Petersson, H. Nakatsuji, M. Hada, M. Ehara, K. Toyota, R. Fukuda, J. Hasegawa, M. Ishida, T. Nakajima, Y. Honda, O. Kitao, H. Nakai, M. Klene, X. Li, J. E. Knox, H. P. Hratchian, J. B. Cross, V. Bakken, C. Adamo, J. Jaramillo, R. Gomperts, R. E. Stratmann, O. Yazyev, A. J. Austin, R. Cammi, C. Pomelli, J. W. Ochterski, P. Y. Ayala, K. Morokuma, G. A. Voth, P. Salvador, J. J. Dannenberg, V. G. Zakrzewski, S. Dapprich, A. D. Daniels, M. C. Strain, O. Farkas, D. K. Malick, A. D. Rabuck, K. Raghavachari, J. B. Foresman, J. V. Ortiz, Q. Cui, A. G. Baboul, S. Clifford, J. Cioslowski, B. B. Stefanov, G. Liu, A. Liashenko, P. Piskorz, I. Komaromi, R. L. Martin, D. J. Fox, T. Keith, M. A. Al-Laham, C. Y. Peng, A. Nanayakkara, M. Challacombe, P. M. W. Gill, B. Johnson, W. Chen, M. W. Wong, C. Gonzalez, and J. A. Pople, Gaussian, Inc., Wallingford CT, 2004.

9.2. Calculated Data for Chapter 2: Shielding Values, Total Energies, Free Energies

1 C₃

Level of theory	Shielding, ppm
MPW1K/6-311+G(d,p)	346.9819
B98/6-311+G(d,p)	323.3616
B3LYP/6-311+G(d,p)	305.7122
HF/6-311+G(d,p)	379.9194
MP2/6-311+G(d,p)	362.4713
MPW1K/6-311++G(2d,2p)	337.0432
MPW1K/IGLOIII	342.6872
MPW1K/3-21G	504.5147
MPW1K/6-31G(d)	403.1655
MPW1K/6-311++G(2d,2p) + PCM(CHCl ₃ ,UAHF)	337.3980
MPW1K/6-311++G(2d,2p) + PCM(CHCl ₃ ,UAKS)	337.4117
MPW1K/6-311++G(2d,2p) + PCM(C ₆ H ₆ ,UAHF)	337.3727
MPW1K/6-311++G(2d,2p) + PCM(C ₆ H ₆ ,UAKS)	337.3857
MPW1K/IGLOIII + PCM(CHCl ₃ ,UAHF)	343.0746
MPW1K/IGLOIII + PCM(CHCl ₃ ,UAKS)	343.0750
MPW1K/IGLOIII + PCM(C ₆ H ₆ ,UAHF)	343.0124
MPW1K/IGLOIII + PCM(C ₆ H ₆ ,UAKS)	343.0147

1*CHCl₃_1

Level of theory	Shielding, ppm
MPW1K/6-311++G(2d,2p)	336.8437
MPW1K/IGLOIII	342.6131
MPW1K/6-311++G(2d,2p) + PCM(CHCl ₃ ,UAHF)	336.7176
MPW1K/6-311++G(2d,2p) + PCM(CHCl ₃ ,UAKS)	336.6920
MPW1K/IGLOIII + PCM(CHCl ₃ ,UAHF)	342.6838
MPW1K/IGLOIII + PCM(CHCl ₃ ,UAKS)	342.6780

1*CHCl₃_2

Level of theory	Shielding, ppm			
MPW1K/6-311++G(2d,2p)	334.7652			
MPW1K/IGLOIII	334.6193			
MPW1K/6-311++G(2d,2p) + PCM(CHCl ₃ ,UAHF)	334.6221			
MPW1K/6-311++G(2d,2p) + PCM(CHCl ₃ ,UAKS)	334.6221			
MPW1K/IGLOIII + PCM(CHCl ₃ ,UAHF)	334.6221			
MPW1K/IGLOIII + PCM(CHCl ₃ ,UAKS)	334.6221			
	MPW1K/6-311++G(2d,2p)	MP2(FC)/6-31+G(2d,p)/MPW1K/6-31G(d)	+	
	+	PCM/UAHF/MPW1K/6-311++G(2d,2p)		
	PCM/UAHF/MPW1K/6-311++G(2d,2p)			
Shielding, ppm	E _{tot}	„G“ _{298, gas}	„G“ _{298, CHCl₃}	
1*CHCl₃_1	336.7176	-2451.298781	-2451.055107	-2451.043044
1*CHCl₃_2	334.6193	-2451.295285	-2451.052558	-2451.040463

 $\langle\sigma\rangle = 336.5897$ ppm**1*C₆H₆_1**

Level of theory	Shielding, ppm			
MPW1K/6-311++G(2d,2p)	335.7529			
MPW1K/IGLOIII	341.6665			
MPW1K/6-311++G(2d,2p) + PCM(C ₆ H ₆ ,UAHF)	335.7325			
MPW1K/6-311++G(2d,2p) + PCM(C ₆ H ₆ ,UAKS)	335.7386			
MPW1K/IGLOIII + PCM(C ₆ H ₆ ,UAHF)	341.7266			
MPW1K/IGLOIII + PCM(C ₆ H ₆ ,UAKS)	341.7323			

1*C₆H₆_2

Level of theory	Shielding, ppm			
MPW1K/6-311++G(2d,2p)	333.6551			
MPW1K/IGLOIII	333.7080			
MPW1K/6-311++G(2d,2p) + PCM(C ₆ H ₆ ,UAHF)	333.7080			
MPW1K/6-311++G(2d,2p) + PCM(C ₆ H ₆ ,UAKS)	333.7080			
MPW1K/IGLOIII + PCM(C ₆ H ₆ ,UAHF)	333.7080			
MPW1K/IGLOIII + PCM(C ₆ H ₆ ,UAKS)	333.7080			
	MPW1K/6-311++G(2d,2p)	MP2(FC)/6-31+G(2d,p)/MPW1K/6-31G(d)	+	
	+	PCM/UAHF/MPW1K/6-311++G(2d,2p)		
	PCM/UAHF/MPW1K/6-311++G(2d,2p)			
Shielding, ppm	E _{tot}	„G“ _{298, gas}	„G“ _{298, CHCl₃}	
1*C₆H₆_1	335.7325	-1265.382840	-1265.055205	-1265.046041
1*C₆H₆_2	333.7080	-1265.383835	-1265.056668	-1265.045672

 $\langle\sigma\rangle = 334.9158$ ppm**2_1 C₁**

Level of theory	Shielding, ppm			
MPW1K/6-311+G(d,p)	319.7633			
B98/6-311+G(d,p)	307.4676			
B3LYP/6-311+G(d,p)	292.8302			
HF/6-311+G(d,p)	351.0237			
MP2(FC)/6-311+G(d,p)	336.2062			
MPW1K/6-311+G(2d,p)	308.0225			
MPW1K/6-311+G(2df,2pd)	307.1925			
MPW1K/3-21G	481.4436			
MPW1K/6-31G(d)	371.5699			
MPW1K/6-311++G(2d,2p)	308.0144			
MPW1K/6-311++G(2d,2p) + PCM(CHCl ₃ ,UAHF)	306.4356			
MPW1K/6-311++G(2d,2p) + PCM(CHCl ₃ ,UAKS)	306.2551			
MPW1K/6-311++G(2d,2p) + PCM(C ₆ H ₆ ,UAHF)	307.0724			
MPW1K/6-311++G(2d,2p) + PCM(C ₆ H ₆ ,UAKS)	306.9890			

MPW1K/IGLOIII	312.4864
MPW1K/IGLOIII + PCM(CHCl ₃ ,UAHF)	308.9998
MPW1K/IGLOIII + PCM(CHCl ₃ ,UAKS)	310.7379
MPW1K/IGLOIII + PCM(C ₆ H ₆ ,UAHF)	311.5517
MPW1K/IGLOIII + PCM(C ₆ H ₆ ,UAKS)	311.4672

2_2 C₃

Level of theory	Shielding, ppm
MPW1K/6-311+G(d,p)	320.9482
B98/6-311+G(d,p)	308.9801
B3LYP/6-311+G(d,p)	294.3596
HF/6-311+G(d,p)	352.6781
MP2(FC)/6-311+G(d,p)	337.2729
MPW1K/6-311++G(2d,2p)	308.4744
MPW1K/IGLOIII	312.9412
MPW1K/3-21G	484.0238
MPW1K/6-31G(d)	372.7677
MPW1K/6-311++G(2d,2p)	308.4744
MPW1K/6-311++G(2d,2p) + PCM(CHCl ₃ ,UAHF)	305.3405
MPW1K/6-311++G(2d,2p) + PCM(CHCl ₃ ,UAKS)	306.9241
MPW1K/6-311++G(2d,2p) + PCM(C ₆ H ₆ ,UAHF)	307.6548
MPW1K/6-311++G(2d,2p) + PCM(C ₆ H ₆ ,UAKS)	307.5553
MPW1K/IGLOIII	312.9412
MPW1K/IGLOIII + PCM(CHCl ₃ ,UAHF)	311.5801
MPW1K/IGLOIII + PCM(CHCl ₃ ,UAKS)	311.4219
MPW1K/IGLOIII + PCM(C ₆ H ₆ ,UAHF)	312.1449
MPW1K/IGLOIII + PCM(C ₆ H ₆ ,UAKS)	312.0409

MPW1K/6-311++G(2d,2p)//MPW1K/6-31G(d)	MP2(FC)/6-31+G(2d,p)/MPW1K/6-31G(d)
Chemical shift, ppm (relative to PPh ₃)	E _{tot} „G ^{cc} _{298, gas}
2_1	24.3 -1108.914974 -1108.673297
2_2	23.9 -1108.915735 -1108.673065

<δ> = 24.1 ppm

MPW1K/6-311++G(2d,2p) + PCM(UAHF)/MPW1K/6-311++G(2d,2p)	MP2(FC)/6-31+G(2d,p)/MPW1K/6-31G(d) + PCM(UAHF)/MPW1K/6-311++G(2d,2p)
Chemical shift, ppm (relative to PPh ₃)	E _{tot} „G ^{cc} _{298, gas} „G ^{cc} _{298, CHCl₃}
2_1	26.3 -1108.914974 -1108.673297 -1108.672978
2_2	27.4 -1108.915735 -1108.673065 -1108.672204

<δ> = 26.6 ppm

MPW1K/6-311++G(2d,2p) + PCM(UAHF)/MPW1K/6-311++G(2d,2p)	MP2(FC)/6-31+G(2d,p)/MPW1K/6-31G(d) + PCM(UAHF)/MPW1K/6-311++G(2d,2p)
Chemical shift, ppm (relative to PPh ₃)	E _{tot} „G ^{cc} _{298, gas} „G ^{cc} _{298, C₆H₆}
2_1	26.2 -1108.914974 -1108.673297 -1108.671161
2_2	27.3 -1108.915735 -1108.673065 -1108.670563

<δ> = 26.6 ppm

2*CHCl₃

Level of theory	Shielding, ppm
MPW1K/6-311++G(2d,2p)	302.9821
MPW1K/IGLOIII	306.9763
MPW1K/6-311++G(2d,2p) + PCM(CHCl ₃ ,UAHF)	302.2425
MPW1K/6-311++G(2d,2p) + PCM(CHCl ₃ ,UAKS)	302.2417
MPW1K/IGLOIII + PCM(CHCl ₃ ,UAHF)	306.2497
MPW1K/IGLOIII + PCM(CHCl ₃ ,UAKS)	306.2487

2*C₆H₆

Level of theory	Shielding, ppm
MPW1K/6-311++G(2d,2p)	305.4242
MPW1K/IGLOIII	309.7354
MPW1K/6-311++G(2d,2p) + PCM(C ₆ H ₆ ,UAHF)	304.8235
MPW1K/IGLOIII + PCM(C ₆ H ₆ ,UAHF)	309.1385

3

Level of theory	Shielding, ppm
MPW1K/6-311+G(d,p)	588.6318
MPW1K/6-311++G(2d,2p)	586.2645
MPW1K/IGLO-III	592.0708
HF/6-311++G(2d,2p)	595.2526
B98/6-311++G(2d,2p)	577.3875
B3LYP/6-311++G(2d,2p)	568.2426
MP2/6-311++G(2d,2p)	611.7305

4

Level of theory	Shielding, ppm
MPW1K/6-311++G(2d,2p)	194.0557
MPW1K/IGLO-III	207.9761

5

Level of theory	Shielding, ppm
MPW1K/6-311++G(2d,2p)	73.7237
MPW1K/IGLO-III	80.7244

6

Level of theory	Shielding, ppm
MPW1K/6-311++G(2d,2p)	397.9419
MPW1K/6-311+G(d,p)	409.5647
MPW1K/IGLO-III	401.9422
HF/6-311++G(2d,2p)	435.2273
B98/6-311++G(2d,2p)	384.0079
B3LYP/6-311++G(2d,2p)	366.9421
MP2/6-311++G(2d,2p)	427.8159

7_1

Level of theory	Shielding, ppm
MPW1K/6-311++G(2d,2p)	317.6473

7_2

Level of theory	Shielding, ppm
MPW1K/6-311++G(2d,2p)	316.7730

7_3

Level of theory	Shielding, ppm
MPW1K/6-311++G(2d,2p)	315.6641

7_4

Level of theory	Shielding, ppm
MPW1K/6-311++G(2d,2p)	318.1632

7_5

Level of theory	Shielding, ppm
MPW1K/6-311++G(2d,2p)	315.8336

7_6

Level of theory	Shielding, ppm
MPW1K/6-311++G(2d,2p)	322.2977

7_7

Level of theory	Shielding, ppm
MPW1K/6-311++G(2d,2p)	311.6041

	MPW1K/6-311++G(2d,2p)//MPW1K/6-31G(d)	MP2(FC)/6-31+G(2d,p)//MPW1K/6-31G(d)		
	Chemical shift, ppm (relative to PH ₃)	Chemical shift, ppm (relative to PPh ₃)	E _{tot}	„G“ _{298, gas}
7_1	2.5172	14.7	-695.337277	-695.082770
7_3	3.3915	15.6	-695.336113	-695.080627
7_5	4.5004	16.7	-695.334107	-695.080404
7_2	2.0013	14.2	-695.335158	-695.080115
7_4	4.3309	16.5	-695.334409	-695.080070
7_7	-2.1332	10.0	-695.332921	-695.076711
7_6	8.5604	20.7	-695.331065	-695.076146

<δ> = 14.9 ppm (relative to PPh₃)

<δ> = 2.8 ppm (relative to PH₃)

8_1

Level of theory	Shielding, ppm
MPW1K/6-311++G(2d,2p)	164.2884

8_2

Level of theory	Shielding, ppm
MPW1K/6-311++G(2d,2p)	167.6754

8_3

Level of theory	Shielding, ppm
MPW1K/6-311++G(2d,2p)	191.2445

8_4

Level of theory	Shielding, ppm
MPW1K/6-311++G(2d,2p)	145.5871

8_5

Level of theory	Shielding, ppm
MPW1K/6-311++G(2d,2p)	199.1895

	MPW1K/6-311++G(2d,2p)//MPW1K/6-31G(d)	MP2(FC)/6-31+G(2d,p)//MPW1K/6-31G(d)		
	Chemical shift, ppm (relative to PPh ₃)	E _{tot}	„G“ _{298, gas}	
8_1		168.1	-685.411875	-685.316081
8_2		164.7	-685.413133	-685.315107
8_3		141.1	-685.410670	-685.312847
8_4		186.8	-685.408176	-685.310219
8_5		133.2	-685.404419	-685.303744

<δ> = 166.6 ppm (relative to PPh₃)

8_1*CHCl₃_1

Level of theory	Shielding, ppm
MPW1K/6-311++G(2d,2p) + PCM(CHCl ₃ ,UAHF)	165.5506

8_2*CHCl₃_1

Level of theory	Shielding, ppm
MPW1K/6-311++G(2d,2p) + PCM(CHCl ₃ ,UAHF)	166.3742

8_4*CHCl₃_1

Level of theory	Shielding, ppm
MPW1K/6-311++G(2d,2p) + PCM(CHCl ₃ ,UAHF)	146.8236

8_1*CHCl₃_2	
Level of theory	Shielding, ppm
MPW1K/6-311++G(2d,2p) + PCM(CHCl ₃ ,UAHF)	169.6337

8_3*CHCl₃_1	
Level of theory	Shielding, ppm
MPW1K/6-311++G(2d,2p) + PCM(CHCl ₃ ,UAHF)	190.3348

8_3*CHCl₃_2	
Level of theory	Shielding, ppm
MPW1K/6-311++G(2d,2p) + PCM(CHCl ₃ ,UAHF)	193.5683

8_4*CHCl₃_2	
Level of theory	Shielding, ppm
MPW1K/6-311++G(2d,2p) + PCM(CHCl ₃ ,UAHF)	152.2356

8_5*CHCl₃_2	
Level of theory	Shielding, ppm
MPW1K/6-311++G(2d,2p) + PCM(CHCl ₃ ,UAHF)	201.0740

	MPW1K/6-311++G(2d,2p) + PCM(UAHF/MPW1K/6-311++G(2d,2p))	MP2(FC)/6-31+G(2d,p)//MPW1K/6-31G(d) + PCM(UAHF/MPW1K/6-311++G(2d,2p))			
	Chemical shift, ppm	E _{tot}	„G“ _{298, gas}	„G“ _{298, CHCl₃}	
	(relative to PPh ₃)				
8_1*CHCl ₃ _1	166.3391	-2102.905420	-2102.802752	-2102.795629	
8_2*CHCl ₃ _1	165.5155	-2102.905303	-2102.800769	-2102.793199	
8_4*CHCl ₃ _1	185.0661	-2102.902432	-2102.800623	-2102.793149	
8_1*CHCl ₃ _2	162.256	-2102.898157	-2102.797380	-2102.791404	
8_3*CHCl ₃ _1	141.5549	-2102.899183	-2102.796847	-2102.790839	
8_3*CHCl ₃ _2	138.3214	-2102.896857	-2102.793321	-2102.787855	
8_4*CHCl ₃ _2	179.6541	-2102.894943	-2102.791641	-2102.785203	
8_5*CHCl ₃ _2	130.8157	-2102.890032	-2102.785269	-2102.781364	

<δ> = 167.3 ppm

9

Level of theory	Shielding, ppm
MPW1K/6-311++G(2d,2p)	307.0808
MPW1K/6-311++G(2d,2p) + PCM(CHCl ₃ ,UAHF)	302.8686
MPW1K/6-311++G(2d,2p) + PCM(CHCl ₃ ,UAKS)	302.4897
MPW1K/6-311++G(2d,2p) + PCM(C ₆ H ₆ ,UAHF)	304.5230
MPW1K/6-311++G(2d,2p) + PCM(C ₆ H ₆ ,UAKS)	304.3111
MPW1K/IGLOIII	309.7277
MPW1K/IGLOIII + PCM(CHCl ₃ ,UAHF)	305.6400
MPW1K/IGLOIII + PCM(CHCl ₃ ,UAKS)	305.3037
MPW1K/IGLOIII + PCM(C ₆ H ₆ ,UAHF)	307.2554
MPW1K/IGLOIII + PCM(C ₆ H ₆ ,UAKS)	307.0572

9*C₆H₆

Level of theory	Shielding, ppm
MPW1K/6-311++G(2d,2p)	304.6040
MPW1K/IGLOIII	307.3231
MPW1K/6-311++G(2d,2p) + PCM(C ₆ H ₆ ,UAHF)	302.9428
MPW1K/6-311++G(2d,2p) + PCM(C ₆ H ₆ ,UAKS)	302.8898
MPW1K/IGLOIII + PCM(C ₆ H ₆ ,UAHF)	305.7132
MPW1K/IGLOIII + PCM(C ₆ H ₆ ,UAKS)	305.6632

9*CHCl₃

Level of theory	Shielding, ppm
MPW1K/6-311++G(2d,2p)	298.4922
MPW1K/IGLOIII	301.2428
MPW1K/6-311++G(2d,2p) + PCM(CHCl ₃ ,UAHF)	295.6368
MPW1K/IGLOIII + PCM(CHCl ₃ ,UAHF)	298.4888

10_1 C₃

Level of theory	Shielding, ppm
MPW1K/6-311++G(2d,2p)	313.1888
MPW1K/6-311++G(2d,2p) + PCM(CHCl ₃ ,UAHF)	312.8775
MPW1K/6-311++G(2d,2p) + PCM(CHCl ₃ ,UAKS)	312.8453
MPW1K/6-311++G(2d,2p) + PCM(C ₆ H ₆ ,UAHF)	312.9986
MPW1K/6-311++G(2d,2p) + PCM(C ₆ H ₆ ,UAKS)	312.9823
MPW1K/IGLOIII	322.5535
MPW1K/IGLOIII + PCM(CHCl ₃ ,UAHF)	322.2479
MPW1K/IGLOIII + PCM(CHCl ₃ ,UAKS)	322.2172
MPW1K/IGLOIII + PCM(C ₆ H ₆ ,UAHF)	322.3696
MPW1K/IGLOIII + PCM(C ₆ H ₆ ,UAKS)	322.3541

10_2 C₁

Level of theory	Shielding, ppm
MPW1K/6-311++G(2d,2p)	319.4004
MPW1K/6-311++G(2d,2p) + PCM(CHCl ₃ ,UAHF)	318.3833
MPW1K/6-311++G(2d,2p) + PCM(CHCl ₃ ,UAKS)	318.3086
MPW1K/6-311++G(2d,2p) + PCM(C ₆ H ₆ ,UAHF)	318.7836
MPW1K/6-311++G(2d,2p) + PCM(C ₆ H ₆ ,UAKS)	318.7424
MPW1K/IGLOIII	328.7141
MPW1K/IGLOIII + PCM(CHCl ₃ ,UAHF)	327.7280
MPW1K/IGLOIII + PCM(CHCl ₃ ,UAKS)	327.6565
MPW1K/IGLOIII + PCM(C ₆ H ₆ ,UAHF)	328.1158
MPW1K/IGLOIII + PCM(C ₆ H ₆ ,UAKS)	328.0757

10_3 C_s

Level of theory	Shielding, ppm
MPW1K/6-311++G(2d,2p)	316.8600
MPW1K/6-311++G(2d,2p) + PCM(CHCl ₃ ,UAHF)	315.3937
MPW1K/6-311++G(2d,2p) + PCM(CHCl ₃ ,UAKS)	315.9187
MPW1K/6-311++G(2d,2p) + PCM(C ₆ H ₆ ,UAHF)	316.3318
MPW1K/6-311++G(2d,2p) + PCM(C ₆ H ₆ ,UAKS)	316.2902
MPW1K/IGLOIII	326.5091
MPW1K/IGLOIII + PCM(CHCl ₃ ,UAHF)	325.6488
MPW1K/IGLOIII + PCM(CHCl ₃ ,UAKS)	325.5763
MPW1K/IGLOIII + PCM(C ₆ H ₆ ,UAHF)	325.9871
MPW1K/IGLOIII + PCM(C ₆ H ₆ ,UAKS)	325.9485

	MPW1K/6-311++G(2d,2p)//MPW1K/6-31G(d)	MP2(FC)/6-31+G(2d,p)/MPW1K/6-31G(d)
	Chemical shift, ppm (relative to PH ₃)	Chemical shift, ppm (relative to PPh ₃)
10_1	6.9757	19.1544
10_2	0.7641	12.9428
10_3	3.3045	15.4832

<δ> = 16.7 ppm (relative to PPh₃)

<δ> = 4.5 ppm (relative to PH₃)

10_3*C₆H₆

Level of theory	Shielding, ppm
MPW1K/6-311++G(2d,2p)	317.3162
MPW1K/IGLOIII	326.7555
MPW1K/6-311++G(2d,2p) + PCM(C ₆ H ₆ ,UAHF)	316.9913
MPW1K/6-311++G(2d,2p) + PCM(C ₆ H ₆ ,UAKS)	316.9829

MPW1K/IGLOIII + PCM(C ₆ H ₆ ,UAHF)	326.4295
MPW1K/IGLOIII + PCM(C ₆ H ₆ ,UAKS)	326.4222

10_1*C₆H₆

Level of theory	Shielding, ppm
MPW1K/6-311++G(2d,2p)	313.2352
MPW1K/IGLOIII	322.4000
MPW1K/6-311++G(2d,2p) + PCM(C ₆ H ₆ ,UAHF)	313.1300
MPW1K/6-311++G(2d,2p) + PCM(C ₆ H ₆ ,UAKS)	313.1220
MPW1K/IGLOIII + PCM(C ₆ H ₆ ,UAKS)	322.2874

10_2*C₆H₆

Level of theory	Shielding, ppm
MPW1K/6-311++G(2d,2p)	319.3150
MPW1K/IGLOIII	328.4058
MPW1K/6-311++G(2d,2p) + PCM(C ₆ H ₆ ,UAHF)	318.8362
MPW1K/6-311++G(2d,2p) + PCM(C ₆ H ₆ ,UAKS)	318.8070
MPW1K/IGLOIII + PCM(C ₆ H ₆ ,UAHF)	327.9443
MPW1K/IGLOIII + PCM(C ₆ H ₆ ,UAKS)	327.9139

MPW1K/6-311++G(2d,2p) + PCM(UAHF/MPW1K/6-311++G(2d,2p))	MP2(FC)/6-31+G(2d,p)//MPW1K/6-31G(d) + PCM(UAHF/MPW1K/6-311++G(2d,2p))	Chemical shift, ppm (relative to PPh ₃)	E _{tot}	„G“ _{298, gas}	„G“ _{298, C₆H₆}
10_3*C ₆ H ₆	13.2	-992.116994	-991.928039	-991.925569	
10_1*C ₆ H ₆	17.1	-992.1211642	-991.929749	-991.925478	
10_2*C ₆ H ₆	11.4	-992.1200939	-991.927889	-991.924367	

<δ> = 14.6 ppm (relative to PPh₃)

10_1*CHCl₃

Level of theory	Shielding, ppm
MPW1K/6-311++G(2d,2p)	315.0754
MPW1K/IGLOIII	324.3176
MPW1K/6-311++G(2d,2p) + PCM(CHCl ₃ ,UAHF)	314.8869
MPW1K/6-311++G(2d,2p) + PCM(CHCl ₃ ,UAKS)	314.8881
MPW1K/IGLOIII + PCM(CHCl ₃ ,UAHF)	324.1264
MPW1K/IGLOIII + PCM(CHCl ₃ ,UAKS)	324.1285

10_2*CHCl₃

Level of theory	Shielding, ppm
MPW1K/6-311++G(2d,2p)	320.3781
MPW1K/IGLOIII	329.6535
MPW1K/6-311++G(2d,2p) + PCM(CHCl ₃ ,UAHF)	319.7309
MPW1K/6-311++G(2d,2p) + PCM(CHCl ₃ ,UAKS)	319.7176
MPW1K/IGLOIII + PCM(CHCl ₃ ,UAHF)	329.0210
MPW1K/IGLOIII + PCM(CHCl ₃ ,UAKS)	329.0062

10_3*CHCl₃

Level of theory	Shielding, ppm
MPW1K/6-311++G(2d,2p)	316.8740
MPW1K/IGLOIII	326.4599
MPW1K/6-311++G(2d,2p) + PCM(CHCl ₃ ,UAHF)	316.3608
MPW1K/6-311++G(2d,2p) + PCM(CHCl ₃ ,UAKS)	316.3450
MPW1K/IGLOIII + PCM(CHCl ₃ ,UAHF)	325.9458
MPW1K/IGLOIII + PCM(CHCl ₃ ,UAKS)	325.9300

MPW1K/6-311++G(2d,2p) + PCM(UAHF/MPW1K/6-311++G(2d,2p))	MP2(FC)/6-31+G(2d,p)//MPW1K/6-31G(d) + PCM(UAHF/MPW1K/6-311++G(2d,2p))	Chemical shift, ppm (relative to PPh ₃)	E _{tot}	„G“ _{298, gas}	„G“ _{298, C₆H₆}
10_1*CHCl ₃	17.0	-2178.038722	-2177.932073	-2177.925826	
10_2*CHCl ₃	12.2	-2178.037242	-2177.929764	-2177.924680	
10_3*CHCl ₃	15.5	-2178.035824	-2177.928884	-2177.923609	

<δ> = 15.9 ppm (relative to PPh₃)

11	
Level of theory	Shielding, ppm
MPW1K/6-311++G(2d,2p)	556.6147
12	
Level of theory	Shielding, ppm
MPW1K/6-311++G(2d,2p)	447.6852
13	
Level of theory	Shielding, ppm
MPW1K/6-311++G(2d,2p)	448.1596
14	
Level of theory	Shielding, ppm
MPW1K/6-311++G(2d,2p)	306.9167
MPW1K/IGLOIII	307.9990
15	
Level of theory	Shielding, ppm
MPW1K/6-311++G(2d,2p)	458.8171
16	
Level of theory	Shielding, ppm
MPW1K/6-311++G(2d,2p)	904.4006
17	
Level of theory	Shielding, ppm
MPW1K/6-311++G(2d,2p)	-46.2557
18_cation	
Level of theory	Shielding, ppm
MPW1K/6-311++G(2d,2p)	304.9854
MPW1K/IGLOIII	308.2132
MPW1K/6-311++G(2d,2p) + PCM(CHCl ₃ ,UAHF)	304.5109
MPW1K/IGLOIII + PCM(CHCl ₃ ,UAHF)	307.8174
18_cation*CHCl₃	
Level of theory	Shielding, ppm
MPW1K/6-311++G(2d,2p)	304.7771
MPW1K/IGLOIII	308.0217
MPW1K/6-311++G(2d,2p) + PCM(CHCl ₃ ,UAHF)	304.5229
MPW1K/IGLOIII + PCM(CHCl ₃ ,UAHF)	307.7840
18_ionic_associate_1	
Level of theory	Shielding, ppm
MPW1K/6-311++G(2d,2p); for I atom: MPW1K/6-311G(d,p)	313.0141
MPW1K/6-311++G(2d,2p) + PCM(CHCl ₃ ,UAHF); for I atom: MPW1K/6-311G(d,p)	313.0282
18_ionic_associate_2	
Level of theory	Shielding, ppm
MPW1K/6-311++G(2d,2p); for I atom: MPW1K/6-311G(d,p)	319.9455
MPW1K/6-311++G(2d,2p) + PCM(CHCl ₃ ,UAHF); for I atom: MPW1K/6-311G(d,p)	319.8243
MPW1K/6-311++G(2d,2p) [+ PCM(UAHF/MPW1K/6-311++G(2d,2p)] ^a	[+ MP2(FC)/6-31+G(2d,p)/MPW1K/6-31G(d) + PCM(UAHF/MPW1K/6-311++G(2d,2p)
Chemical shift, ppm (relative to PPh ₃)	E _{tot} „G“ _{298, gas} „G“ _{298, CHCl₃}

	Gas-phase	Solution model 1			
18_ionic_associate_1	19.3	19.7	-7990.575319	-7990.302402	-7990.311295
18_ionic_associate_2	12.4	12.9	-7990.574105	-7990.302606	-7990.310829
*the theory shown in square brackets relates to solution model 1 and not to gas-phase calculations					
$\langle\delta\rangle = 15.5 \text{ ppm (gas-phase)}$					
$\langle\delta\rangle = 17.1 \text{ ppm (solution model 1)}$					
18_ionic_associate_1*CHCl₃_1					
Level of theory					Shielding, ppm
MPW1K/6-311++G(2d,2p) + PCM(CHCl ₃ ,UAHF); for I atom: MPW1K/6-311G(d,p)					305.4268
18_ionic_associate_2*CHCl₃_1					
Level of theory					Shielding, ppm
MPW1K/6-311++G(2d,2p) + PCM(CHCl ₃ ,UAHF)					315.5837
18_ionic_associate_1*CHCl₃_2					
Level of theory					Shielding, ppm
MPW1K/6-311++G(2d,2p) + PCM(CHCl ₃ ,UAHF); for I atom: MPW1K/6-311G(d,p)					307.6611
18_ionic_associate_1*CHCl₃_3					
Level of theory					Shielding, ppm
MPW1K/6-311++G(2d,2p) + PCM(CHCl ₃ ,UAHF); for I atom: MPW1K/6-311G(d,p)					312.1285
18_ionic_associate_2*CHCl₃_3					
Level of theory					Shielding, ppm
MPW1K/6-311++G(2d,2p) + PCM(CHCl ₃ ,UAHF); for I atom: MPW1K/6-311G(d,p)					316.3598
18_ionic_associate_1*CHCl₃_4					
Level of theory					Shielding, ppm
MPW1K/6-311++G(2d,2p) + PCM(CHCl ₃ ,UAHF); for I atom: MPW1K/6-311G(d,p)					305.9459
18_ionic_associate_2*CHCl₃_2					
Level of theory					Shielding, ppm
MPW1K/6-311++G(2d,2p) + PCM(CHCl ₃ ,UAHF); for I atom: MPW1K/6-311G(d,p)					318.0986
		MPW1K/6-311++G(2d,2p)	+	MP2(FC)/6-31+G(2d,p)/MPW1K/6-31G(d) + PCM(UAHF)/MPW1K/6-311++G(2d,2p)	
		PCM(UAHF)/MPW1K/6-311++G(2d,2p)			
		Chemical shift, (relative to PPh ₃)	ppm	E _{tot}	„G“ _{298, gas} „G“ _{298, CHCl₃}
18_ionic_associate_1*CHCl ₃ _1	26.5			-9408.065275	-9407.786178 -9407.783676
18_ionic_associate_2*CHCl ₃ _1	16.3			-9408.063140	-9407.786532 -9407.782994
18_ionic_associate_1*CHCl ₃ _2	24.2			-9408.062679	-9407.782659 -9407.780252
18_ionic_associate_1*CHCl ₃ _3	19.8			-9408.061179	-9407.780773 -9407.778876
18_ionic_associate_2*CHCl ₃ _3	15.5			-9408.059436	-9407.780425 -9407.777876
18_ionic_associate_1*CHCl ₃ _4	25.9			-9408.057140	-9407.778408 -9407.777404
18_ionic_associate_2*CHCl ₃ _2	13.8			-9408.051094	-9407.774153 -9407.774424
$\langle\delta\rangle = 23.1 \text{ ppm}$					
19					
Level of theory					Shielding, ppm
MPW1K/6-311++G(2d,2p)					156.9698
19*CHCl₃_1					
Level of theory					Shielding, ppm
MPW1K/6-311++G(2d,2p) + PCM(CHCl ₃ ,UAHF)					158.1013
19*CHCl₃_2					
Level of theory					Shielding, ppm

MPW1K/6-311++G(2d,2p) + PCM(CHCl ₃ ,UAHF)	159.4190				
19*CHCl₃_3					
Level of theory	Shielding, ppm				
MPW1K/6-311++G(2d,2p) + PCM(CHCl ₃ ,UAHF)	154.7541				
19*CHCl₃_4					
Level of theory	Shielding, ppm				
MPW1K/6-311++G(2d,2p) + PCM(CHCl ₃ ,UAHF)	159.5320				
MPW1K/6-311++G(2d,2p) PCM/UAHF/MPW1K/6- 311++G(2d,2p)	+ MP2(FC)/6-31+G(2d,p)/MPW1K/6-31G(d) PCM/UAHF/MPW1K/6-311++G(2d,2p) +				
Chemical shift, ppm (relative to PPh ₃)	E _{tot}	„G“ _{298, gas}	„G“ _{298, CHCl₃}		
19*CHCl ₃ _1	173.8	-7129.755150	-7129.689742	-7129.682571	
19*CHCl ₃ _2	172.5	-7129.754516	-7129.688209	-7129.681245	
19*CHCl ₃ _3	177.1	-7129.754901	-7129.689460	-7129.680807	
19*CHCl ₃ _4	172.4	-7129.752551	-7129.688714	-7129.680395	
<δ> = 173.8 ppm					
20_1					
Level of theory	Shielding, ppm				
MPW1K/6-311++G(2d,2p)	171.9077				
MPW1K/6-311++G(2d,2p) + PCM(CHCl ₃ ,UAHF)	169.3983				
20_2					
Level of theory	Shielding, ppm				
MPW1K/6-311++G(2d,2p)	152.5953				
MPW1K/6-311++G(2d,2p) + PCM(CHCl ₃ ,UAHF)	150.5037				
MPW1K/6-311++G(2d,2p) PCM/UAHF/MPW1K/6-311++G(2d,2p)] ^a	[+ MP2(FC)/6-31+G(2d,p)/MPW1K/6-31G(d) PCM/UAHF/MPW1K/6-311++G(2d,2p) +				
Chemical shift, ppm (relative to PPh ₃)	E _{tot}	„G“ _{298, gas}	„G“ _{298, CHCl₃}		
Gas-phase	Solution model 1				
20_1	160.4	163.3	-702.374270	-702.271149	-702.279882
20_2	179.7	182.2	-702.369998	-702.267031	-702.275763
^a the theory shown in square brackets relates to solution model 1 and not to gas-phase calculations					
<δ> = 160.7 ppm (gas-phase)					
<δ> = 163.5 ppm (solution model 1)					
20_1*CHCl₃					
Level of theory	Shielding, ppm				
MPW1K/6-311++G(2d,2p) + PCM(CHCl ₃ ,UAHF)	170.1380				
21_cation					
Level of theory	Shielding, ppm				
MPW1K/6-311++G(2d,2p)	391.4385				
	329.7804				
21_ionic_associate					
Level of theory	Shielding, ppm				
MPW1K/6-311++G(2d,2p); for I atom: MPW1K/6-311G(d,p)	388.6395 304.9301				
21_ionic_associate*CHCl₃_1					
Level of theory	Shielding, ppm				
MPW1K/6-311++G(2d,2p) + PCM(CHCl ₃ ,UAHF); for I atom: MPW1K/6-311G(d,p)	385.9969 307.2375				

21_ionic_associate*CHCl₃_2

Level of theory	Shielding, ppm
MPW1K/6-311++G(2d,2p) + PCM(CHCl ₃ ,UAHF); for I atom: MPW1K/6-311G(d,p)	387.0484
	305.5388

MPW1K/6-311++G(2d,2p) + PCM(UAHF/MPW1K/6-311++G(2d,2p))	MP2(FC)/6-31+G(2d,p)/MPW1K/6-31G(d) + PCM(UAHF/MPW1K/6-311++G(2d,2p))			
Chemical shift, ppm (relative to PPh ₃)	E _{tot}	„G“ _{298, gas}	„G“ _{298, CHCl₃}	
21_ia*CHCl₃_1	-54.1	-9598.694016	-9598.407812	-9598.407541
	24.7			
21_ia*CHCl₃_2	-55.2	-9598.687798	-9598.403959	-9598.404373
	26.4			

 $\langle\delta_1\rangle = -54.1$ ppm $\langle\delta_2\rangle = 24.7$ ppm**22_1**

Level of theory	Shielding, ppm
MPW1K/6-311++G(2d,2p)	265.7888
MPW1K/6-311++G(2d,2p) + PCM(CHCl ₃ ,UAHF)	266.4206

22_2

Level of theory	Shielding, ppm
MPW1K/6-311++G(2d,2p)	281.5945
MPW1K/6-311++G(2d,2p) + PCM(CHCl ₃ ,UAHF)	281.4732

22_3

Level of theory	Shielding, ppm
MPW1K/6-311++G(2d,2p)	245.3870
MPW1K/6-311++G(2d,2p) + PCM(CHCl ₃ ,UAHF)	245.5205

22_4

Level of theory	Shielding, ppm
MPW1K/6-311++G(2d,2p)	246.6964
MPW1K/6-311++G(2d,2p) + PCM(CHCl ₃ ,UAHF)	246.3052

22_5

Level of theory	Shielding, ppm
MPW1K/6-311++G(2d,2p)	252.3767
MPW1K/6-311++G(2d,2p) + PCM(CHCl ₃ ,UAHF)	251.9034

22_6

Level of theory	Shielding, ppm
MPW1K/6-311++G(2d,2p)	247.6572
MPW1K/6-311++G(2d,2p) + PCM(CHCl ₃ ,UAHF)	248.4291

22_7

Level of theory	Shielding, ppm
MPW1K/6-311++G(2d,2p)	231.8476
MPW1K/6-311++G(2d,2p) + PCM(CHCl ₃ ,UAHF)	232.4019

22_8

Level of theory	Shielding, ppm
MPW1K/6-311++G(2d,2p)	229.9567
MPW1K/6-311++G(2d,2p) + PCM(CHCl ₃ ,UAHF)	230.1054

22_9

Level of theory	Shielding, ppm
MPW1K/6-311++G(2d,2p)	251.9917
MPW1K/6-311++G(2d,2p) + PCM(CHCl ₃ ,UAHF)	251.8790

22_10

Level of theory	Shielding, ppm
MPW1K/6-311++G(2d,2p)	245.0854
MPW1K/6-311++G(2d,2p) + PCM(CHCl ₃ ,UAHF)	245.2238

MPW1K/6-311++G(2d,2p) PCM(UAHF/MPW1K/6- 311++G(2d,2p)] ^a		[+ MP2(FC)/6-31+G(2d,p)/MPW1K/6-31G(d) PCM(UAHF/MPW1K/6-311++G(2d,2p)	+ +		
Chemical shift, ppm (relative to PPh ₃)		E _{tot}	„G“ _{298, gas}	„G“ _{298, CHCl₃}	
Gas-phase	Solution model 1				
22_1	66.6	66.3	-1000.520008	-1000.118416	-1000.110927
22_2	50.7	51.2	-1000.517667	-1000.117992	-1000.109468
22_3	87.0	87.2	-1000.516425	-1000.115793	-1000.108145
22_4	85.6	86.4	-1000.513206	-1000.113047	-1000.105224
22_5	80.0	80.8	-1000.512755	-1000.112136	-1000.104503
22_6	84.7	84.3	-1000.512573	-1000.110910	-1000.104106
22_7	100.5	100.3	-1000.512714	-1000.110846	-1000.103851
22_8	102.4	102.6	-1000.512417	-1000.111790	-1000.103823
22_9	80.4	80.8	-1000.511937	-1000.111630	-1000.102404
22_10	87.3	87.5	-1000.508684	-1000.106245	-1000.099648

^athe theory shown in square brackets relates to solution model 1 and not to gas-phase calculations

<δ> = 61.5 ppm (gas-phase)

<δ> = 64.7 ppm (solution model 1)

22_1*CHCl₃_1

Level of theory	Shielding, ppm
MPW1K/6-311++G(2d,2p) + PCM(CHCl ₃ ,UAHF)	269.5152

22_1*CHCl₃_2

Level of theory	Shielding, ppm
MPW1K/6-311++G(2d,2p) + PCM(CHCl ₃ ,UAHF)	265.9469

22_2*CHCl₃_1

Level of theory	Shielding, ppm
MPW1K/6-311++G(2d,2p) + PCM(CHCl ₃ ,UAHF)	279.7620

22_2*CHCl₃_2

Level of theory	Shielding, ppm
MPW1K/6-311++G(2d,2p) + PCM(CHCl ₃ ,UAHF)	281.0781

22_3*CHCl₃_1

Level of theory	Shielding, ppm
MPW1K/6-311++G(2d,2p) + PCM(CHCl ₃ ,UAHF)	249.2158

22_7*CHCl₃_2

Level of theory	Shielding, ppm
MPW1K/6-311++G(2d,2p) + PCM(CHCl ₃ ,UAHF)	233.1692

22_3*CHCl₃_2

Level of theory	Shielding, ppm
MPW1K/6-311++G(2d,2p) + PCM(CHCl ₃ ,UAHF)	246.7699

22_4*CHCl₃_1					
Level of theory			Shielding, ppm		
MPW1K/6-311++G(2d,2p) + PCM(CHCl ₃ ,UAHF)			248.4409		
22_9*CHCl₃_1					
Level of theory			Shielding, ppm		
MPW1K/6-311++G(2d,2p) + PCM(CHCl ₃ ,UAHF)			255.3035		
22_6*CHCl₃_1					
Level of theory			Shielding, ppm		
MPW1K/6-311++G(2d,2p) + PCM(CHCl ₃ ,UAHF)			253.6456		
22_7*CHCl₃_1					
Level of theory			Shielding, ppm		
MPW1K/6-311++G(2d,2p) + PCM(CHCl ₃ ,UAHF)			237.4259		
22_5*CHCl₃_1					
Level of theory			Shielding, ppm		
MPW1K/6-311++G(2d,2p) + PCM(CHCl ₃ ,UAHF)			253.7436		
22_5*CHCl₃_2					
Level of theory			Shielding, ppm		
MPW1K/6-311++G(2d,2p) + PCM(CHCl ₃ ,UAHF)			252.9543		
22_8*CHCl₃_1					
Level of theory			Shielding, ppm		
MPW1K/6-311++G(2d,2p) + PCM(CHCl ₃ ,UAHF)			236.5452		
22_4*CHCl₃_2					
Level of theory			Shielding, ppm		
MPW1K/6-311++G(2d,2p) + PCM(CHCl ₃ ,UAHF)			247.8256		
22_6*CHCl₃_2					
Level of theory			Shielding, ppm		
MPW1K/6-311++G(2d,2p) + PCM(CHCl ₃ ,UAHF)			247.5471		
22_9*CHCl₃_2					
Level of theory			Shielding, ppm		
MPW1K/6-311++G(2d,2p) + PCM(CHCl ₃ ,UAHF)			253.1536		
22_8*CHCl₃_2					
Level of theory			Shielding, ppm		
MPW1K/6-311++G(2d,2p) + PCM(CHCl ₃ ,UAHF)			230.8414		
22_10*CHCl₃_1					
Level of theory			Shielding, ppm		
MPW1K/6-311++G(2d,2p) + PCM(CHCl ₃ ,UAHF)			248.8534		
22_10*CHCl₃_2					
MPW1K/6-311++G(2d,2p) + PCM(CHCl ₃ ,UAHF)			245.5574		
	MPW1K/6-311++G(2d,2p) + PCM(UAHF/MPW1K/6-311++G(2d,2p))		MP2(FC)/6-31+G(2d,p)//MPW1K/6-31G(d) + PCM(UAHF/MPW1K/6-311++G(2d,2p))		
	Chemical shift, ppm (relative to PPh ₃)	E _{tot}	„G“ _{298, gas}	„G“ _{298, CHCl₃}	
22_1*CHCl₃_1	+62.4	-2418.012453	-2417.605115	-2417.588063	
22_1*CHCl₃_2	+65.9	-2418.011455	-2417.603255	-2417.586714	

22_2*CHCl3_1	+52.1	-2418.011107	-2417.603583	-2417.585496
22_2*CHCl3_2	+50.8	-2418.006454	-2417.600627	-2417.584356
22_3*CHCl3_1	+82.7	-2418.010381	-2417.601381	-2417.583835
22_7*CHCl3_2	+98.7	-2418.007090	-2417.599424	-2417.583280
22_3*CHCl3_2	+85.1	-2418.004473	-2417.598363	-2417.582682
22_4*CHCl3_1	+83.4	-2418.006987	-2417.598943	-2417.581206
22_9*CHCl3_1	+76.6	-2418.005694	-2417.598336	-2417.580631
22_6*CHCl3_1	+78.2	-2418.006641	-2417.597699	-2417.580599
22_7*CHCl3_1	+94.5	-2418.006008	-2417.597546	-2417.580399
22_5*CHCl3_1	+78.1	-2418.006719	-2417.598061	-2417.580133
22_5*CHCl3_2	+78.9	-2418.001595	-2417.595216	-2417.579918
22_8*CHCl3_1	+95.3	-2418.006382	-2417.597685	-2417.579869
22_4*CHCl3_2	+84.1	-2418.001342	-2417.595296	-2417.579790
22_6*CHCl3_2	+84.3	-2418.002483	-2417.594869	-2417.579092
22_9*CHCl3_2	+78.7	-2418.000962	-2417.594742	-2417.578966
22_8*CHCl3_2	+101.0	-2418.000476	-2417.593966	-2417.578030
22_10*CHCl3_1	+83.0	-2418.002900	-2417.592096	-2417.575697
22_10*CHCl3_2	+86.3	-2417.998250	-2417.589613	-2417.573932

< δ > = 62.8 ppm

	MPW1K/6-311++G(2d,2p) + PCM/UAHF/MPW1K/6-311++G(2d,2p)	MP2(FC)/6-31+G(2d,p)//MPW1K/6-31G(d) + PCM/UAHF/MPW1K/6-311++G(2d,2p)			
	Chemical shift, (relative to PPh ₃)	ppm	E _{tot}	„G“ _{298, gas}	„G“ _{298, CHCl₃}
23*CHCl3_1	23.4	-2681.904802	-2681.573102	-2681.564004	
23*CHCl3_2	19.3	-2681.905643	-2681.570377	-2681.562681	
23*CHCl3_3	1.9	-2681.896295	-2681.562347	-2681.556866	
23*CHCl3_4	-7.1	-2681.89152	-2681.557191	-2681.552697	
25*CHCl3_1	25.0	-2681.908211	-2681.574543	-2681.559005	
25*CHCl3_2	27.8	-2681.905468	-2681.572147	-2681.558298	
25*CHCl3_3	27.9	-2681.904232	-2681.571595	-2681.557141	
25*CHCl3_4	23.1	-2681.901681	-2681.571295	-2681.556347	
25*CHCl3_5	24.7	-2681.904530	-2681.570387	-2681.555710	
25*CHCl3_6	25.1	-2681.903721	-2681.570711	-2681.555700	
25*CHCl3_7	25.0	-2681.901241	-2681.570337	-2681.555660	
25*CHCl3_8	21.1	-2681.899313	-2681.567559	-2681.554921	
25*CHCl3_9	23.4	-2681.894490	-2681.564595	-2681.554348	
25*CHCl3_10	23.7	-2681.896045	-2681.565111	-2681.554211	
25*CHCl3_11	22.3	-2681.896353	-2681.564101	-2681.550619	
25*CHCl3_12	20.5	-2681.892574	-2681.561828	-2681.549605	
24*CHCl3_1	28.0	-2682.350967	-2682.004392	-2682.027946	
24*CHCl3_2	32.6	-2682.349738	-2682.003189	-2682.026902	
24*CHCl3_3	28.0	-2682.348483	-2682.004226	-2682.026265	
24*CHCl3_4	29.5	-2682.340607	-2681.998288	-2682.025889	

MPW1K/6-311++G(2d,2p) PCM/UAHF/MPW1K/6- 311++G(2d,2p)		+	MP2(FC)/6-31+G(2d,p)/MPW1K/6-31G(d) PCM/UAHF/MPW1K/6-311++G(2d,2p)		+
Chemical shift, ppm (relative to PPh ₃)	E _{tot}		„G“ _{298, gas}	„G“ _{298, CHCl₃}	
24*ArO*CHCl ₃ _1	31.3915	-3192.678599	-3192.239505	-3192.224589	
24*ArO*CHCl ₃ _2	22.7087	-3192.670886	-3192.236324	-3192.223942	
24*ArO*CHCl ₃ _3	18.423	-3192.67204	-3192.234901	-3192.223172	
24*ArO*CHCl ₃ _4	22.4782	-3192.670493	-3192.235328	-3192.223089	
24*ArO*CHCl ₃ _5	21.0232	-3192.665688	-3192.233148	-3192.221356	
24*ArO*CHCl ₃ _6	26.9253	-3192.670591	-3192.236568	-3192.220982	
24*ArO*CHCl ₃ _7	33.9335	-3192.662721	-3192.232324	-3192.220356	
24*ArO*CHCl ₃ _8	30.253	-3192.668728	-3192.231606	-3192.218810	
24*ArO*CHCl ₃ _9	-35.0522	-3192.672189	-3192.234253	-3192.217871	
24*ArO*CHCl ₃ _10	22.3094	-3192.663438	-3192.230808	-3192.217788	
24*ArO*CHCl ₃ _11	29.9289	-3192.663664	-3192.229630	-3192.217598	
24*ArO*CHCl ₃ _12	26.2319	-3192.669796	-3192.232716	-3192.217370	
24*ArO*CHCl ₃ _13	26.4131	-3192.660097	-3192.226807	-3192.214457	
24*ArO*CHCl ₃ _14	-68.8475	-3192.66627	-3192.231177	-3192.214397	
24*ArO*CHCl ₃ _15	21.0137	-3192.655187	-3192.223636	-3192.214186	
24*ArO*CHCl ₃ _16	-63.3754	-3192.665937	-3192.230089	-3192.213595	
24*ArO*CHCl ₃ _17	-49.3724	-3192.663535	-3192.226437	-3192.212524	
24*ArO*CHCl ₃ _18	27.1949	-3192.658977	-3192.223906	-3192.211556	
24*ArO*CHCl ₃ _19	-38.8093	-3192.656937	-3192.223565	-3192.211390	
24*ArO*CHCl ₃ _20	-41.3591	-3192.656076	-3192.223992	-3192.211067	
24*ArO*CHCl ₃ _21	-65.3327	-3192.661775	-3192.226016	-3192.211036	
24*ArO*CHCl ₃ _22	-40.5328	-3192.660825	-3192.224896	-3192.211000	
24*ArO*CHCl ₃ _23	32.7952	-3192.647088	-3192.218017	-3192.209969	
24*ArO*CHCl ₃ _24	32.0927	-3192.645574	-3192.215242	-3192.209298	

MPW1K/6-311++G(2d,2p) PCM/UAHF/MPW1K/6- 311++G(2d,2p)		+	MP2(FC)/6-31+G(2d,p)/MPW1K/6-31G(d) PCM/UAHF/MPW1K/6-311++G(2d,2p)		+
Chemical shift, ppm (relative to PPh ₃)	E _{tot}		„G“ _{298, gas}	„G“ _{298, CHCl₃}	
23*ArOH*CHCl ₃ _1	-13.5311	-3192.674249	-3192.239322	-3192.218701	
23*ArOH*CHCl ₃ _2	10.058	-3192.669981	-3192.235725	-3192.216139	
23*ArOH*CHCl ₃ _3	18.0117	-3192.661357	-3192.229095	-3192.212299	
23*ArOH*CHCl ₃ _4	26.838	-3192.658330	-3192.225378	-3192.210797	
23*ArOH*CHCl ₃ _5	24.848	-3192.658376	-3192.224501	-3192.210589	
23*ArOH*CHCl ₃ _6	24.0445	-3192.656156	-3192.224677	-3192.209649	
23*ArOH*CHCl ₃ _7	24.2368	-3192.652908	-3192.220668	-3192.208429	

MPW1K/6-311++G(2d,2p) PCM/UAHF/MPW1K/6- 311++G(2d,2p)		+	MP2(FC)/6-31+G(2d,p)/MPW1K/6-31G(d) PCM/UAHF/MPW1K/6-311++G(2d,2p)		+
Chemical shift, ppm (relative to PPh ₃)	E _{tot}		„G“ _{298, gas}	„G“ _{298, CHCl₃}	
25*ArOH*CHCl ₃ _1	34.4015	-3192.648867	-3192.220635	-3192.201989	
25*ArOH*CHCl ₃ _2	33.264	-3192.649169	-3192.218985	-3192.198699	
25*ArOH*CHCl ₃ _3	31.9712	-3192.646273	-3192.215909	-3192.197869	
25*ArOH*CHCl ₃ _4	33.0719	-3192.643498	-3192.214295	-3192.196462	
25*ArOH*CHCl ₃ _5	31.3903	-3192.641135	-3192.211408	-3192.194405	
25*ArOH*CHCl ₃ _6	33.8006	-3192.643229	-3192.212375	-3192.193539	

MPW1K/6-311++G(2d,2p) PCM/UAHF/MPW1K/6-311++G(2d,2p)		+	MP2(FC)/6-31+G(2d,p)/MPW1K/6-31G(d) PCM/UAHF/MPW1K/6-311++G(2d,2p)		+
Chemical shift, ppm (relative to PPh ₃)	E _{tot}		„G“ _{298, gas}	„G“ _{298, CHCl₃}	
33*CHCl ₃ _1	-53.6556	-2681.921210	-2681.584704	-2681.569645	
33*CHCl ₃ _2	-37.0376	-2681.932767	-2681.594346	-2681.578904	

9.3. Calculated Data for Chapter 3

Table 9.3.1. Total energies, enthalpies and free energies (in Hartree) for all stationary points

	MPW1K/6-31+G(d)	MP2(FC)/6-31+G(2d,p)//MPW1K/6-31+G(d)	MP2(FC)/6-31+G(2d,p)//MPW1K/6-31+G(d); PCM/UAHF/RHF/6-31G(d)		
	$E_{\text{tot, gas}}$	$E_{\text{tot, gas}}$	$„H“_{298, \text{gas}}$	$„G“_{298, \text{gas}}$	$„G“_{298, \text{THF}}$
1	-1036.131942	-1033.805540	-1033.506480	-1033.568131	-1033.565437
2_1	-231.167720	-230.606397	-230.507158	-230.542589	-230.544677
2_2	-231.167421	-230.605751	-230.506640	-230.542340	-230.544030
4	-805.080259	-803.679703	-803.567660	-803.608594	-803.611081
7	-511.809352	-510.714225	-510.594103	-510.635796	-510.643207
8_1	-1036.265298	-1034.311952	-1034.096506	-1034.152325	-1034.153201
8_2	-1036.267134	-1034.312233	-1034.096555	-1034.151785	-1034.152470
8_3	-1036.263295	-1034.309681	-1034.094262	-1034.150262	-1034.152031
8_4	-1036.260186	-1034.306915	-1034.091649	-1034.147628	-1034.150050
8_5	-1036.258234	-1034.305992	-1034.090769	-1034.147305	-1034.149042
8_6	-1036.259973	-1034.307365	-1034.092138	-1034.148083	-1034.149023
8_7	-1036.259496	-1034.307123	-1034.091894	-1034.148132	-1034.148610
8_8	-1036.257430	-1034.304837	-1034.089521	-1034.145535	-1034.147941
Int1_1	-2584.215430	-2578.852128	-2578.214936	-2578.355176	-2578.327065
Int1_2	-2584.215840	-2578.847329	-2578.210017	-2578.350488	-2578.324927
TS1_1	-2584.200085	-2578.843830	-2578.207439	-2578.336743	-2578.314114
TS1_2	-2584.205215	-2578.847801	-2578.211146	-2578.339988	-2578.313965
TS1_3	-2584.204044	-2578.843332	-2578.206755	-2578.336928	-2578.313885
TS1_4	-2584.199729	-2578.835118	-2578.198364	-2578.328033	-2578.307348
Inr2_1	-2584.217741	-2578.875320	-2578.237694	-2578.362585	-2578.342617
Inr2_2	-2584.21828	-2578.871384	-2578.233928	-2578.358944	-2578.340968
Inr2_3	-2584.218526	-2578.870152	-2578.233081	-2578.357950	-2578.338221
Inr2_4	-2584.223903	-2578.861221	-2578.223713	-2578.349482	-2578.334216
Inr2_5	-2584.219785	-2578.858677	-2578.221032	-2578.348716	-2578.333975
Inr2_6	-2584.220008	-2578.855318	-2578.217803	-2578.344602	-2578.332395
Inr2_7	-2584.211804	-2578.847834	-2578.209828	-2578.335804	-2578.319836
Inr2_8	-2584.213379	-2578.851163	-2578.213178	-2578.337914	-2578.318185
TS2_RR_1	-2584.202982	-2578.859229	-2578.221933	-2578.341338	-2578.330294
TS2_1	-2584.199683	-2578.858096	-2578.220798	-2578.338465	-2578.329286
TS2_2	-2584.203694	-2578.855060	-2578.218313	-2578.340415	-2578.325722
TS2_3	-2584.199412	-2578.857068	-2578.220201	-2578.337653	-2578.325526
TS2_4	-2584.19381	-2578.849147	-2578.212390	-2578.331134	-2578.325158
TS2_5	-2584.202468	-2578.856862	-2578.219953	-2578.339617	-2578.322788
TS2_RR2	-2584.203608	-2578.853334	-2578.216373	-2578.337525	-2578.322593
TS2_RR3	-2584.204188	-2578.85341	-2578.216498	-2578.336623	-2578.322312
TS2_RR4	-2584.197028	-2578.849769	-2578.212814	-2578.332168	-2578.321538
TS2_6	-2584.190273	-2578.843586	-2578.206993	-2578.327145	-2578.321504
TS2_RR5	-2584.195998	-2578.853388	-2578.216839	-2578.337607	-2578.319201
Int3_RR_1	-2584.239317	-2578.897009	-2578.256597	-2578.372649	-2578.361064
Int3_1	-2584.238027	-2578.886575	-2578.246426	-2578.366543	-2578.357730
Int3_RR_2	-2584.235902	-2578.884997	-2578.244555	-2578.363691	-2578.357030
Int3_2	-2584.237483	-2578.883907	-2578.243639	-2578.363615	-2578.355520
Int3_RR_3	-2584.235185	-2578.883188	-2578.243154	-2578.360648	-2578.353540
Int3_3	-2584.227839	-2578.881450	-2578.241314	-2578.359007	-2578.353031
Int3_4	-2584.200377	-2578.854939	-2578.216293	-2578.335225	-2578.327783

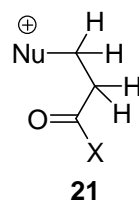
Int3_5	-2584.198700	-2578.854752	-2578.216771	-2578.336468	-2578.327735
Int3_RR_4	-2584.199033	-2578.851587	-2578.213015	-2578.331474	-2578.322756
Int3_RR_5	-2584.194794	-2578.841896	-2578.203488	-2578.324703	-2578.318918
TS3_1	-2584.209886	-2578.870766	-2578.236147	-2578.352731	-2578.340158
TS3_2	-2584.207893	-2578.867938	-2578.232987	-2578.349397	-2578.334879
TS3_RR_1	-2584.201068	-2578.862617	-2578.228150	-2578.345468	-2578.333787
TS3_RR_2	-2584.198690	-2578.863181	-2578.228338	-2578.344709	-2578.331068
TS3_3	-2584.196622	-2578.854615	-2578.219936	-2578.336466	-2578.327478
Int4_1	-2584.230413	-2578.887042	-2578.247213	-2578.368459	-2578.354244
Int4_2	-2584.230746	-2578.886054	-2578.246290	-2578.365320	-2578.349033
Int4_3	-2584.232674	-2578.883119	-2578.243221	-2578.362438	-2578.348765
Int4_4	-2584.221897	-2578.876185	-2578.237275	-2578.354904	-2578.344131
Int4_5	-2584.210045	-2578.867134	-2578.227419	-2578.344892	-2578.329641
Int4_RR_1	-2584.203334	-2578.859764	-2578.220294	-2578.338215	-2578.326040
TS4_1	-2584.207687	-2578.863762	-2578.225395	-2578.348226	-2578.327812
TS4_2	-2584.213606	-2578.863408	-2578.224915	-2578.346703	-2578.326735
TS4_3	-2584.20968	-2578.854178	-2578.215619	-2578.337255	-2578.324491
TS4_4	-2584.205659	-2578.857806	-2578.220668	-2578.341598	-2578.322267
TS4_5	-2584.204769	-2578.855807	-2578.217652	-2578.340580	-2578.321250
TS4_6	-2584.196704	-2578.847007	-2578.208643	-2578.329792	-2578.313346
TS4_7	-2584.192501	-2578.842918	-2578.204797	-2578.326293	-2578.311266
Int5_1	-2584.230383	-2578.869606	-2578.230065	-2578.359714	-2578.340607
Int5_2	-2584.226937	-2578.868684	-2578.229423	-2578.359171	-2578.336415
Int5_3	-2584.218809	-2578.866453	-2578.227392	-2578.360154	-2578.336026
Int5_4	-2584.221443	-2578.866792	-2578.227608	-2578.357456	-2578.335082
Int5_5	-2584.223634	-2578.866095	-2578.227058	-2578.358728	-2578.334760
Int5_6	-2584.220010	-2578.868101	-2578.228992	-2578.359104	-2578.333686
Int5_7	-2584.220932	-2578.856837	-2578.217724	-2578.350554	-2578.332754
Int_p_1	-2584.224672	-2578.875602	-2578.237166	-2578.362055	-2578.345274
Int_p_2	-2584.214979	-2578.866558	-2578.228694	-2578.356694	-2578.344934
Int_p_3	-2584.208080	-2578.866518	-2578.228454	-2578.353307	-2578.341610
Int_p_4	-2584.225338	-2578.872588	-2578.234278	-2578.358419	-2578.341288
Int_y_1	-2584.198207	-2578.845497	-2578.209675	-2578.339980	-2578.322179
Int_y_2	-2584.199932	-2578.850006	-2578.213676	-2578.341421	-2578.321230

9.4. Calculated Data for Chapter 4

Table 9.4.1

	mPW1K/6-31+G(d)	MP2(FC)/G3MP2Large/mPW1K/6-31+G(d)	MP2(FC)/G3MP2Large/mPW1K/6-31+G(d); PCM/UAHF/RHF/6-31G(d)	
	Etot	Etot	„G“ _{298, gas}	„G“ _{298, DMSO}
3_1	-1267.285186	-1265.040105	-1264.713986	-1264.720280
3_2	-1267.283911	-1265.040051	-1264.714916	-1264.719537
3_3	-1267.267871	-1265.025808	-1264.702245	-1264.715614
3_4	-1267.266261	-1265.023474	-1264.700180	-1264.712051
10_1	-1267.742604	-1265.487585	-1265.151836	-1265.195145
10_2	-1267.743910	-1265.492557	-1265.153153	-1265.194358
10_3	-1267.742655	-1265.487773	-1265.151155	-1265.193571
10_4	-1267.741550	-1265.490008	-1265.151181	-1265.192975
11_1	-1267.282487	-1265.041058	-1264.718256	-1264.716504
11_2	-1267.284987	-1265.045608	-1264.721128	-1264.716459
11_3	-1267.279783	-1265.042477	-1264.719432	-1264.715273
11_4	-1267.283702	-1265.042730	-1264.718835	-1264.714852
11_5	-1267.282746	-1265.040994	-1264.717595	-1264.713882
11_6	-1267.278959	-1265.037474	-1264.715508	-1264.713819
12_1	-1075.841650	-1073.908482	-1073.631537	-1073.674750
12B_1	-1075.379886	-1073.460403	-1073.198647	-1073.195110
12B_2	-1075.379391	-1073.459373	-1073.196258	-1073.193581
13_1	-1306.836570	-1304.454521	-1304.100290	-1304.138468
13B_1	-1306.386905	-1304.015186	-1303.675068	-1303.671084
13B_2	-1306.383352	-1304.011318	-1303.670585	-1303.667987
3*DMSO	-1820.449146	-1817.480720	-1817.083034	-1817.077394
11*DMSO	-1820.440582	-1817.481688	-1817.084430	-1817.071779
10*DMSO	-1820.913203	-1817.940245	-1817.531076	-1817.555343
12B*DMSO	-1628.53667	-1625.895606	-1625.564188	-1625.554580
12*DMSO	-1629.014316	-1626.356616	-1626.009847	-1626.036919

Table 9.4.2

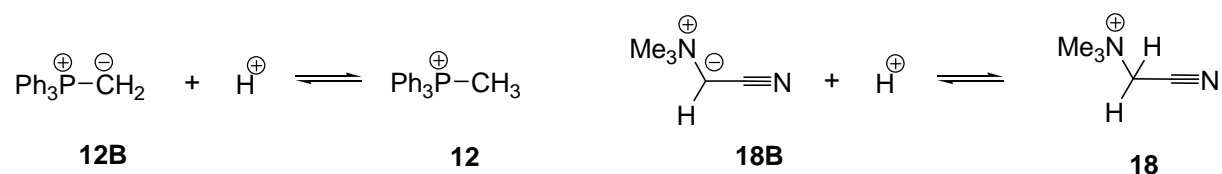


Nu	X	Species	mPW1K/6-31+G(d)		PCM(DMSO)	MP2(FC)/G3MP2large//mPW1K/6-31+G(d)		
			E _{tot} , a.u.	“G” corr., a.u.	/UAHF/RHF /6-31G(d) G solv., a.u.	E _{tot} , a.u.	“G” _{298(gas)} , a.u.	“G” _{298(DMSO)}} , a.u.
PMe ₃	Me	Op.int_1	-692.238432	0.173039	-0.010404882	-691.086387	-690.913348	-690.923753
		Ilide_1	-692.227323	0.170212	-0.002310426	-691.076102	-690.905890	-690.908201
		Ilide_2	-692.233400	0.171997	0.001290652	-691.083515	-690.911518	-690.910227
		Ilide_3	-692.232637	0.171024	0.000892302	-691.082595	-690.911571	-690.910679
		Ilide_4	-692.235027	0.17282	0.000637359	-691.085718	-690.912898	-690.912261
		Proton_1	-692.685413	0.186611	-0.058716678	-691.523306	-691.336695	-691.395411
		Proton_2	-692.681813	0.184654	-0.061967208	-691.518753	-691.334099	-691.396066
	Proton_3	-692.689251	0.188218	-0.057983715	-691.526789	-691.338571	-691.396554	
	OMe	Op.int_1	-767.429628	0.177766	-0.014324639	-766.200864	-766.023098	-766.037423
		Op.int_2	-767.435797	0.17648	-0.010564222	-766.205155	-766.028675	-766.039240
		Ilide_1	-767.428206	0.176021	-0.001386255	-766.202837	-766.026816	-766.028202
		Ilide_2	-767.440400	0.177448	0.001226916	-766.214072	-766.036624	-766.035397
		Proton_1	-767.881646	0.193443	-0.060230405	-766.644016	-766.450573	-766.510804
		Proton_2	-767.891485	0.191764	-0.057282621	-766.653068	-766.461304	-766.518587
Proton_3		-767.895044	0.193093	-0.05651779	-766.656334	-766.463241	-766.519759	
OPh	Op.int_1	-959.129029	0.224913	-0.010309278	-957.528486	-957.303573	-957.313883	
	Op.int_2	-959.125082	0.225384	-0.012412562	-957.527175	-957.301791	-957.314203	
	Op.int_3	-959.128035	0.223261	-0.011472458	-957.527425	-957.304164	-957.315637	
	Ilide_1	-959.120021	0.223835	-4.78019E-05	-957.524731	-957.300896	-957.300943	
	Ilide_2	-959.128550	0.225718	0.002023614	-957.532324	-957.306606	-957.304583	
	Ilide_3	-959.128356	0.224826	0.001210982	-957.532576	-957.307750	-957.306539	
	Proton_1	-959.576171	0.241968	-0.054956261	-957.968843	-957.726875	-957.781831	
	Proton_2	-959.578620	0.24049	-0.056135375	-957.970082	-957.729592	-957.785728	
	Proton_3	-959.578552	0.23974	-0.055991969	-957.969835	-957.730095	-957.786087	
	Proton_4	-959.582195	0.241366	-0.054780988	-957.973363	-957.731997	-957.786778	

PPh ₃	Ph	Op.int_1	-1458.976757	0.375679	-0.005465352	-1456.364544	-1455.988865	-1455.994330
		Ilide_1	-1458.972379	0.373966	0.005592823	-1456.362029	-1455.988063	-1455.982470
		Proton_1	-1459.434460	0.3877	-0.038799216	-1456.810625	-1456.422925	-1456.461724
		Proton_2	-1459.436264	0.391163	-0.036711866	-1456.816923	-1456.425760	-1456.462472
	OPh	Op.int_1	-1534.171864	0.377987	-0.005592823	-1531.483585	-1531.105598	-1531.111191
		Op.int_2	-1534.171588	0.375837	-0.005895569	-1531.481371	-1531.105534	-1531.111430
		Op.int_3	-1534.171257	0.37592	-0.006692267	-1531.481659	-1531.105739	-1531.112431
		Ilide_1	-1534.168667	0.37599	0.004270304	-1531.483478	-1531.107488	-1531.103218
		Ilide_2	-1534.176353	0.376714	0.005624691	-1531.488852	-1531.112138	-1531.106513
		Ilide_3	-1534.176397	0.37599	0.005879635	-1531.488886	-1531.112896	-1531.107017
		Proton_1	-1534.628387	0.391219	-0.037460763	-1531.932270	-1531.541051	-1531.578512
		Proton_2	-1534.635402	0.390982	-0.038177791	-1531.936226	-1531.545244	-1531.583422
H	Proton_3	-1534.635015	0.391924	-0.038592074	-1531.938693	-1531.546769	-1531.585361	
	Op.int_1	-1227.970410	0.299452	-0.009002693	-1225.813631	-1225.514179	-1225.523182	
	Ilide_1	-1227.965101	0.297462	0.002724709	-1225.812314	-1225.514852	-1225.512127	
	Proton_1	-1228.421899	0.313644	-0.044248634	-1226.259230	-1225.945586	-1225.989834	
DMAP	Me	Proton_2	-1228.421104	0.310744	-0.045746427	-1226.255689	-1225.944945	-1225.990692
		Op.int_1	-613.312424	0.222678	-0.018770216	-612.171524	-611.948846	-611.967616
		Ilide_1	-613.287124	0.219595	-0.006293918	-612.155562	-611.935967	-611.942261
		Ilide_2	-613.284489	0.218264	-0.007074683	-612.154855	-611.936591	-611.943666
		Ilide_3	-613.289530	0.220371	-0.005815899	-612.158699	-611.938328	-611.944144
	OMe	Proton_1	-613.771401	0.235612	-0.061457321	-612.621003	-612.385391	-612.446848
		Op.int_1	-688.503919	0.227069	-0.022769643	-687.286500	-687.059431	-687.082200
		Op.int_2	-688.509662	0.226074	-0.019184499	-687.291096	-687.065022	-687.084207
		Ilide_1	-688.478006	0.22304	-0.010341146	-687.272519	-687.049479	-687.059820
		Ilide_2	-688.491692	0.222762	-0.006134578	-687.285620	-687.062858	-687.068992
		Proton_1	-688.963395	0.240971	-0.064771587	-687.737834	-687.496863	-687.561634
	CN	Proton_2	-688.977819	0.241247	-0.060086999	-687.751157	-687.509910	-687.569997
		Op.int_1	-666.212064	0.192632	-0.024171832	-665.037182	-664.844550	-664.868722
		Ilide_1	-666.166388	0.188737	-0.005624691	-665.001964	-664.813227	-664.818852
		Ilide_2	-666.166012	0.188027	-0.00610271	-665.002211	-664.814184	-664.820287
		Ilide_3	-666.175923	0.19055	-0.009528514	-665.012286	-664.821736	-664.831264
Proton_1		-666.636607	0.205472	-0.068340796	-665.454337	-665.248865	-665.317206	
DABCO	Me	Proton_2	-666.632430	0.20418	-0.071639127	-665.449327	-665.245147	-665.316787
		Op.int_1	-576.4167272	0.25026	-0.022737775	-575.327344	-575.077084	-575.099822
		Ilide_1	-576.3656588	0.247132	-0.01978999	-575.275739	-575.028607	-575.048397
		Ilide_2	-576.3719287	0.248341	-0.015041667	-575.282941	-575.034600	-575.049642
		Ilide_3	-576.3676314	0.247327	-0.019136698	-575.278026	-575.030699	-575.049835
		Proton_1	-576.8515078	0.26355	-0.076881403	-575.752374	-575.488824	-575.565706

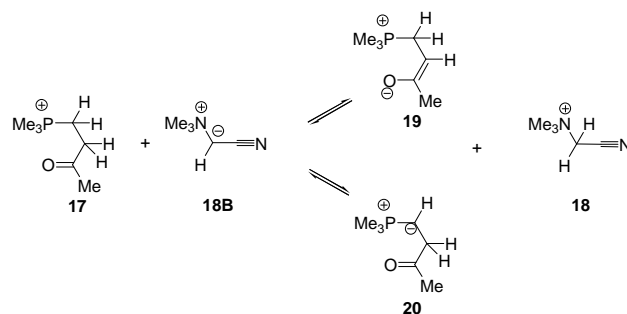
Proton_2	-576.8540916	0.263753	-0.078124253	-575.755208	-575.491455	-575.569579
Proton_3	-576.8519773	0.260958	-0.081709396	-575.752254	-575.491296	-575.573005

Table 9.4.3 Reference acids



Species	mPW1K/6-31+G(d)		PCM(DMSO) /UAHF/RHF /6-31G(d)	MP2(FC)/G3MP2large//mPW1K/6-31+G(d)		
	E_{tot} , a.u.	"G" corr., a.u.	G solv., a.u.	E_{tot} , a.u.	"G" _{298(gas)} , a.u.	"G" _{298(DMSO)} , a.u.
12B	-1075.379886	0.261756	0.003537341	-1073.460403	-1073.198647	-1073.195110
12	-1075.841650	0.276945	-0.043212926	-1073.908482	-1073.631537	-1073.674750
18B	-305.869391	0.122057	-0.016109243	-305.297479	-305.175422	-305.191531
18	-306.291904	0.136256	-0.080976434	-305.715793	-305.579537	-305.660513

Table 9.4.4 Additional calculations to perform G3(MP2)mPW1K(+) scheme and SCS-MP2 calculations



Species	QCISD(T,FC)/6-31G(d)//mPW1K/6-31+G(d)	MP2(FC)/6-31G(d)//mPW1K/6-31+G(d)	G3(MP2)mPW1K(+)	
	Etot, a.u.	Etot, a.u.	"G" _{298(gas)} , a.u.	"G" _{298(DMSO)} , a.u.
19_1	-690.672732	-690.540926	-691.045154	-691.055559
20_1	-690.674752	-690.540696	-691.045628	-691.044735
20_2	-690.677150	-690.543778	-691.046270	-691.045633
20_3	-690.674623	-690.540462	-691.045678	-691.044388
20_4	-690.667217	-690.533193	-691.039914	-691.042224
17_1	-691.132451	-690.995848	-691.473297	-691.532014
17_2	-691.127573	-690.990953	-691.470719	-691.532686
17_3	-691.136907	-691.000159	-691.475318	-691.533302
18B	-305.020670	-304.926716	-305.269376	-305.285486
18	-305.454621	-305.357796	-305.676362	-305.757338

SCS-MP2 calculations

Species	HF/G3MP2large//mPW1K/6-31+G(d)	SCS-MP2(FC)/G3MP2large//mPW1K/6-31+G(d)		
	Etot, a.u.	Etot, a.u.	"G" _{298(gas)} , a.u.	"G" _{298(DMSO)} , a.u.
19_1	-689.501677	-691.076716	-690.903677	-690.914082
20_1	-689.503938	-691.075452	-690.904428	-690.903535
20_2	-689.505464	-691.078285	-690.905465	-690.904827
20_3	-689.503774	-691.076090	-690.904093	-690.902802
20_4	-689.499205	-691.069593	-690.899381	-690.901691
17_1	-689.963590	-691.521051	-691.334440	-691.393157
17_2	-689.960523	-691.516906	-691.332252	-691.394220
17_3	-689.965963	-691.524263	-691.336045	-691.394028
18B	-304.055527	-305.286738	-305.164681	-305.180790
18	-304.488095	-305.710792	-305.574536	-305.655512

9.5. Calculated Data for Chapter 5

9.5.1. Energies of Scan Calculations Performed During Development of MM3 Force Field Parameters For Phosphonium derivatives

Van-der-Waals Parameter

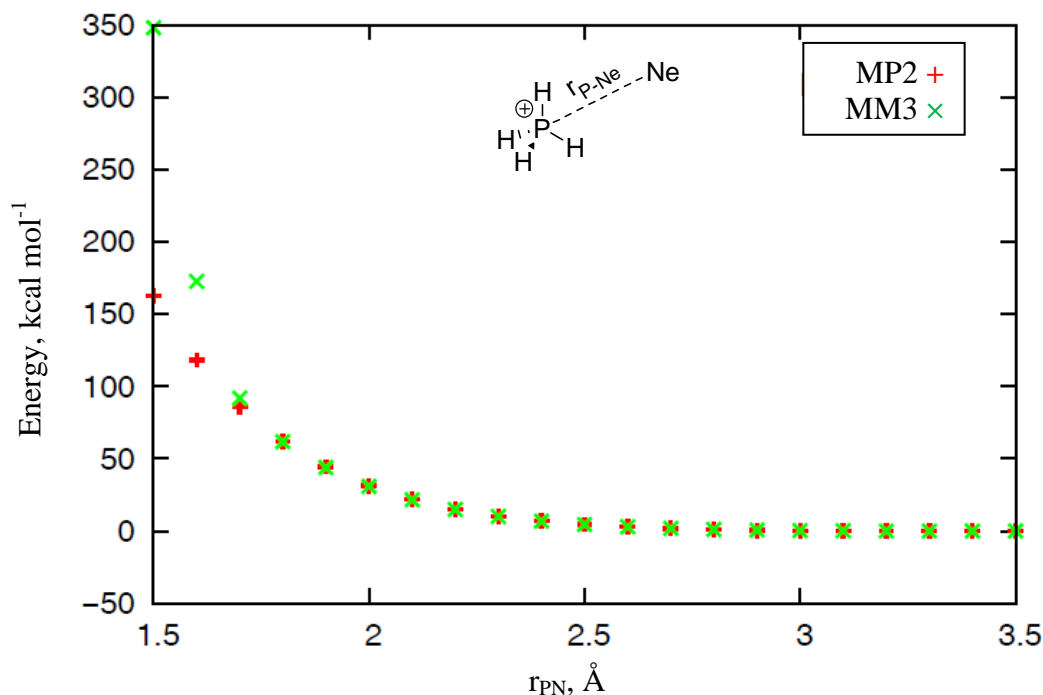


Fig. 9.5.1 Energy comparison between MP2 and MM3 parameters via scan calculation (Ne and PH_4^+).

Parameters with $\text{C}(\text{sp}^3)$

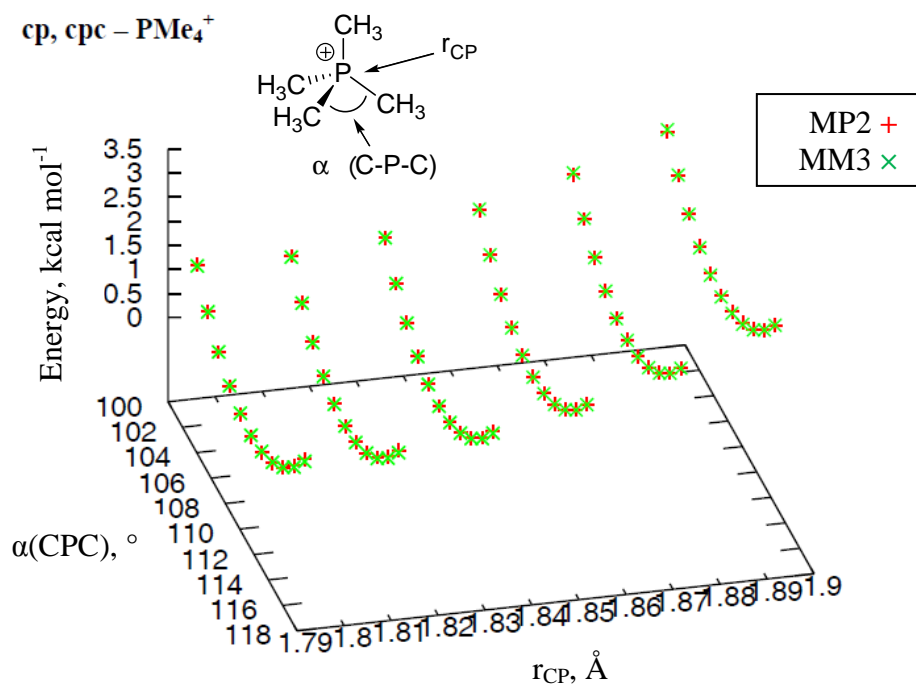
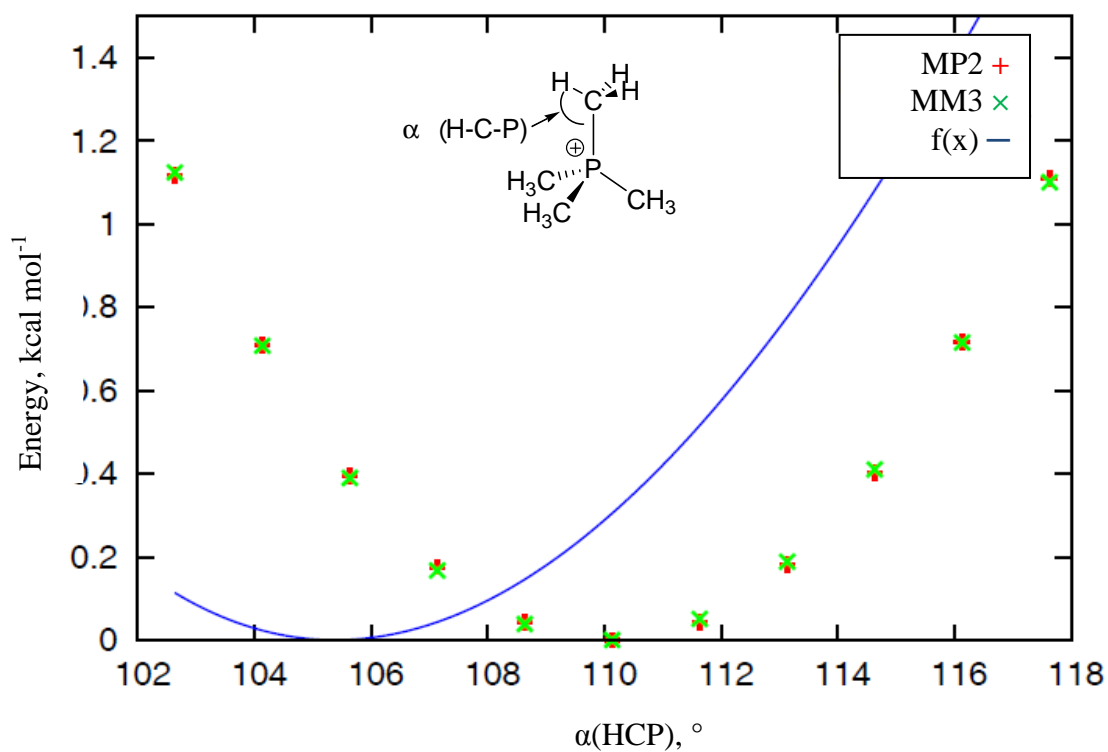


Fig. 9.5.2 Energy comparison of 2D-scans of CP and CPC in PMe_4^+ .



$$f(x)=0.02191418*k*(x-x0)**2*(1-0.014*(x-x0)+5.6*10**-5*(x-x0)**2-7*10**-7*(x-x0)**3+9*10**-10*(x-x0)**4)+z0$$

Fig. 9.5.3 Energy comparison of HCP scans in PMe_4^+ .

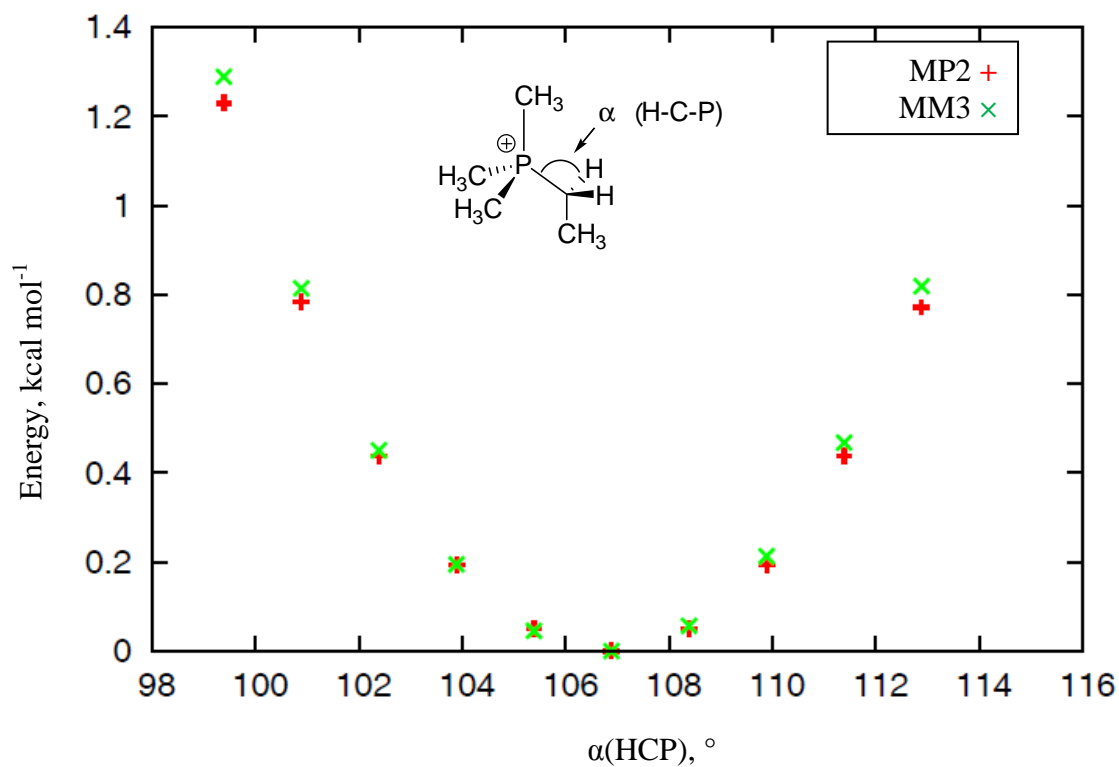


Fig. 9.5.3 Energy comparison of HCP scans in PMe_3Et^+ .

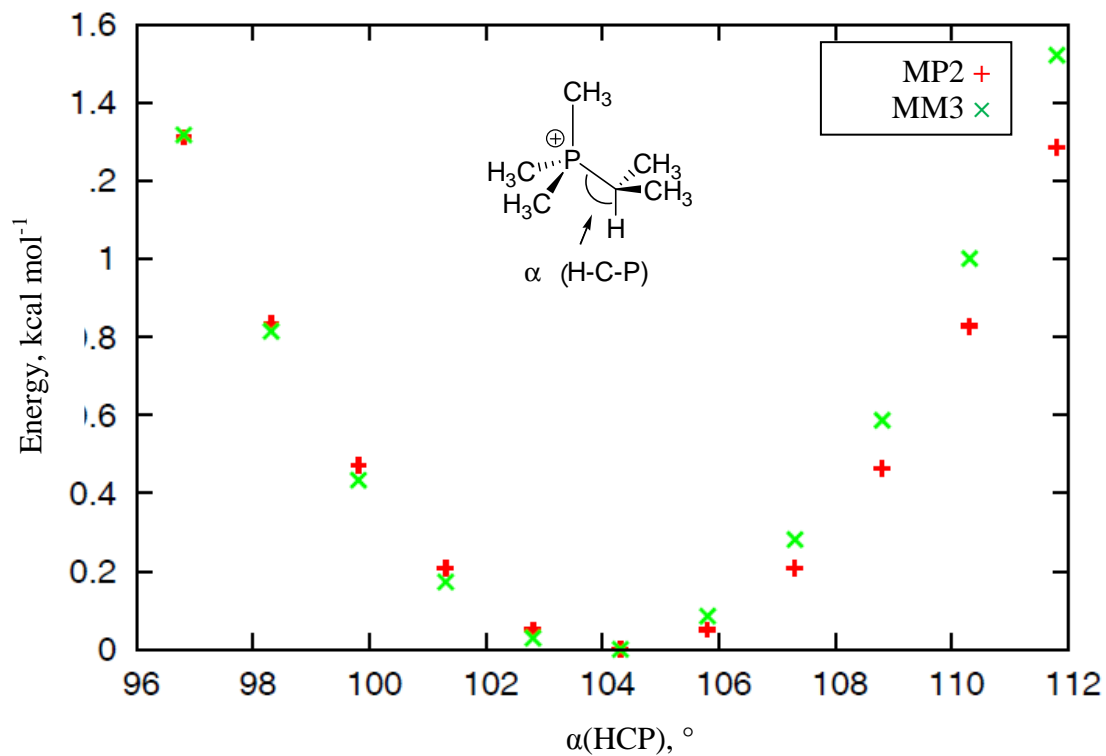


Fig. 9.5.4 Energy comparison of HCP scans in PMe_3iPr^+ .

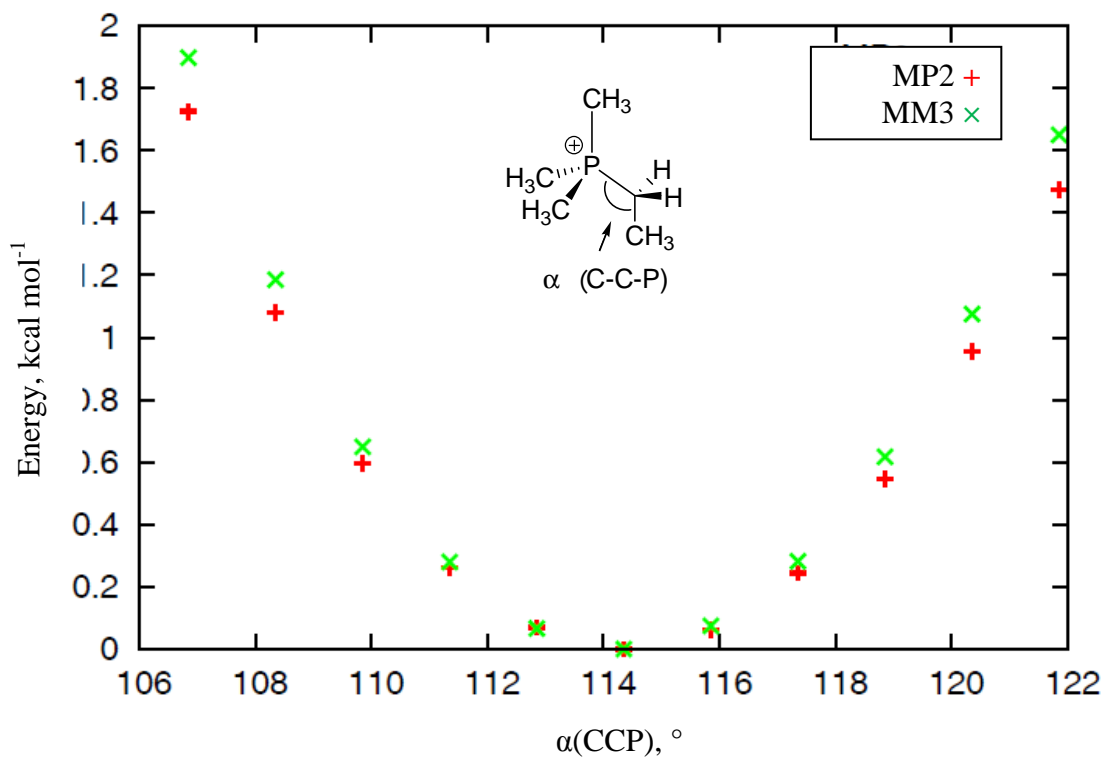
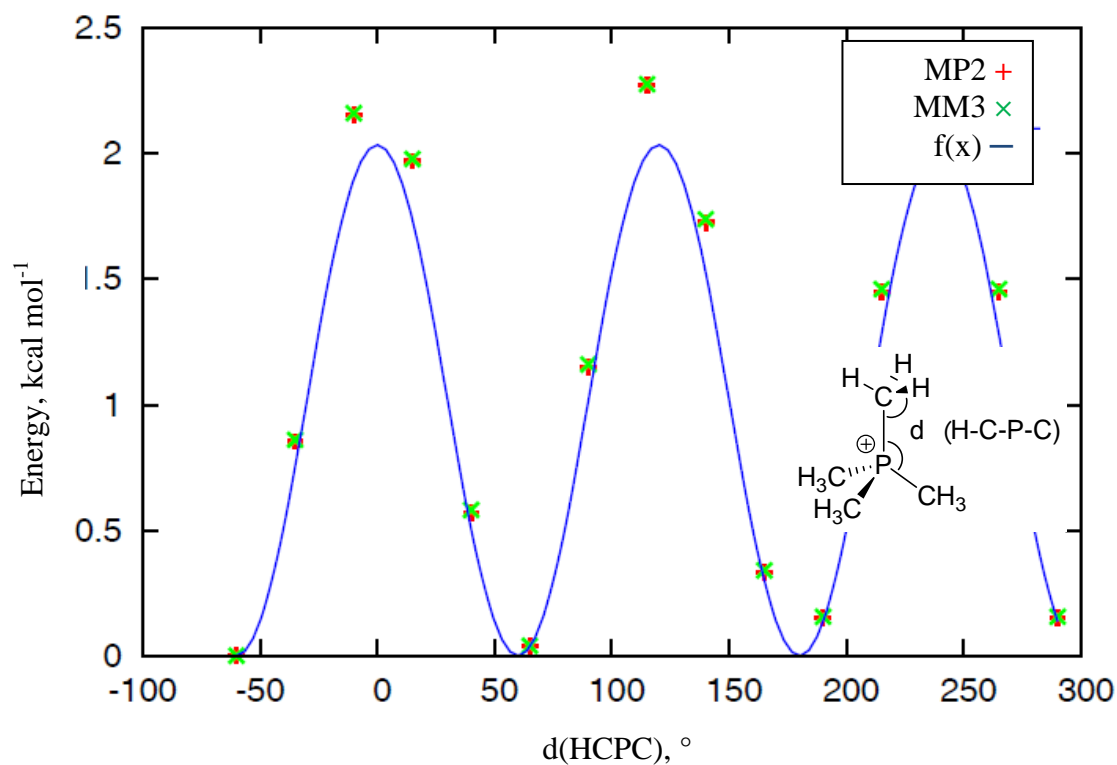


Fig. 9.5.5 Energy comparison of CCP scans in PMe_3Et^+ .



$$f(x)=3*(v1*0.5*(1+\cos(x))+v2*0.5*(1-\cos(2*x))+v3*0.5*(1+\cos(3*x)))+3*(v1*0.5*(1+\cos(x+120))+v2*0.5*(1-\cos(2*(x+120)))+v3*0.5*(1+\cos(3*(x+120))))+3*(v1*0.5*(1+\cos(x-120))+v2*0.5*(1-\cos(2*(x-120)))+v3*0.5*(1+\cos(3*(x-120))))$$

Fig. 9.5.6 Energy comparison of HCPC scans in PMe_4^+ .

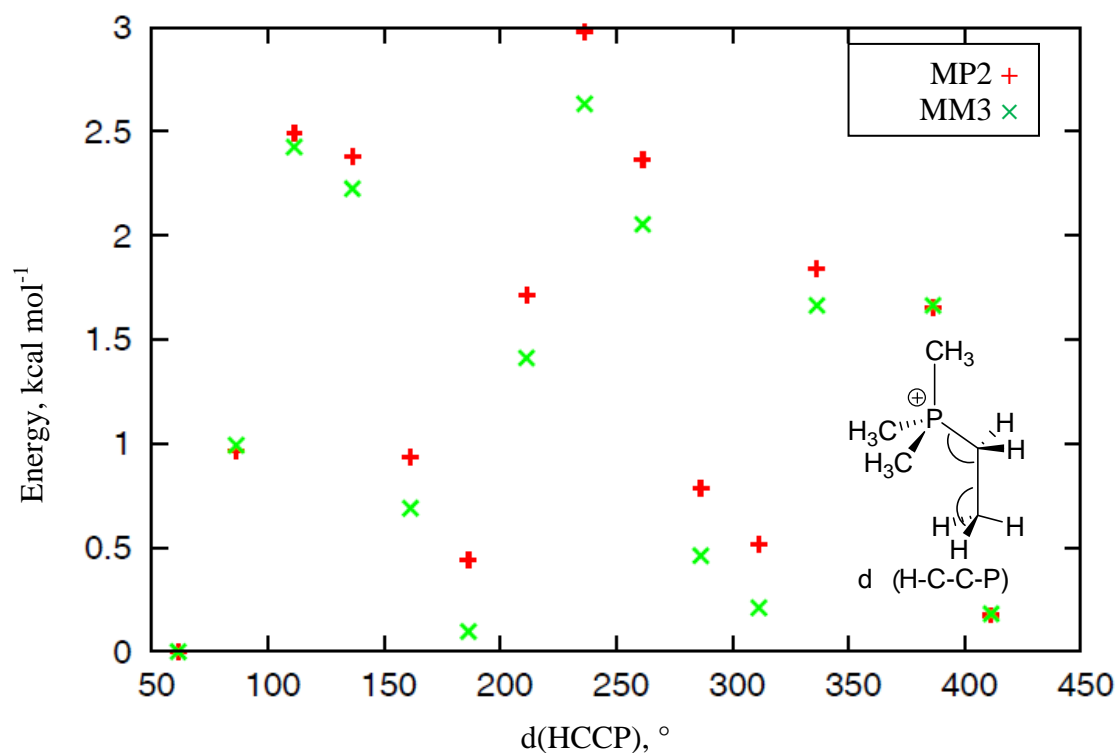


Fig. 9.5.7 Energy comparison of HCCP scans in PMe_3Et^+ .

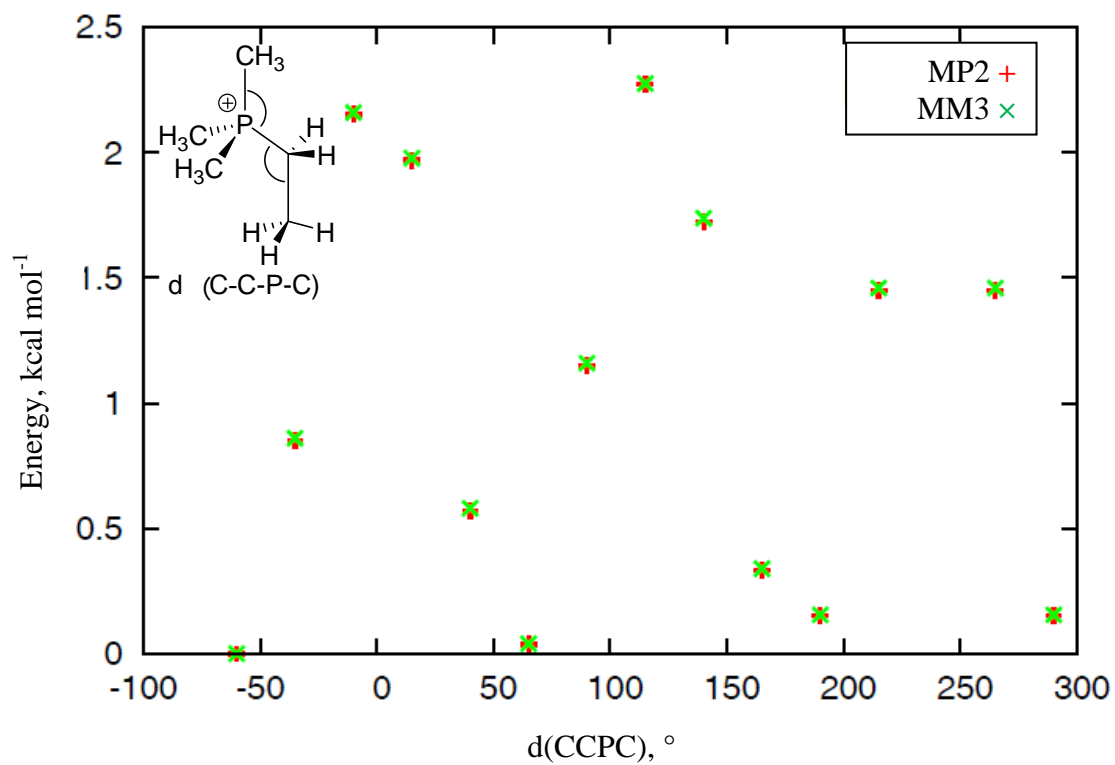


Fig. 9.5.8 Energy comparison of CCPC scans in PMe₃Et⁺.

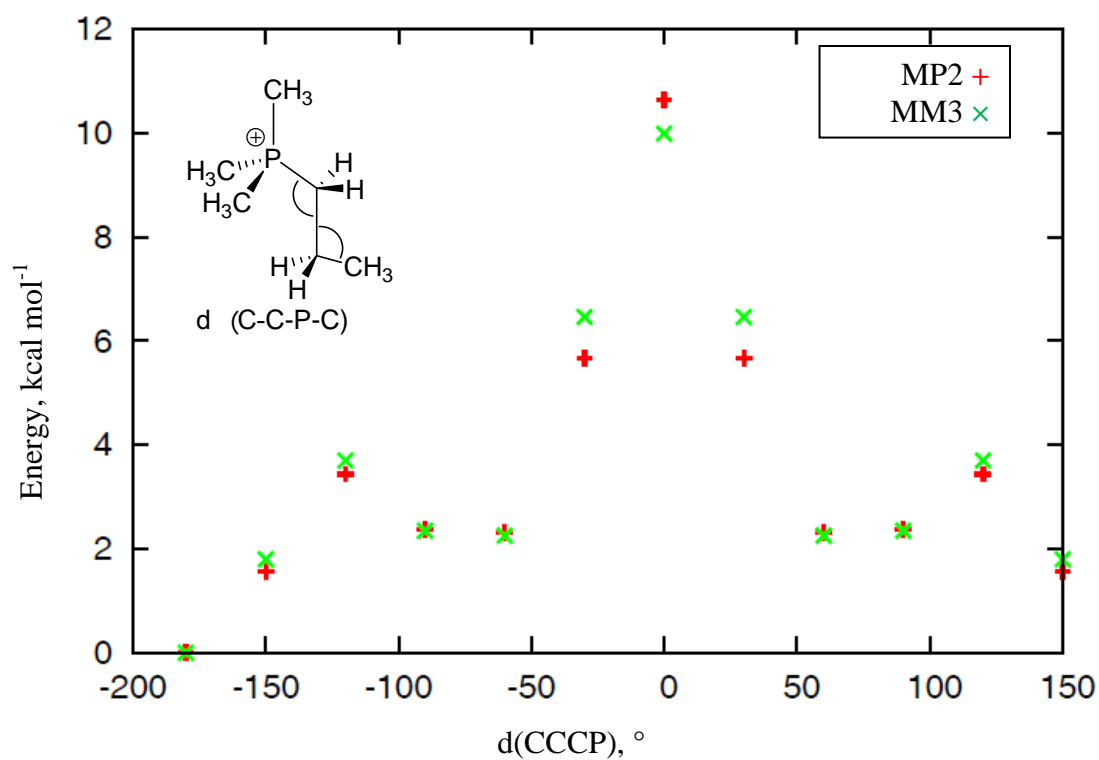


Fig. 9.5.9 Energy comparison of CCCP scans in PMe₃nPr⁺.

Parameters with C(sp²)

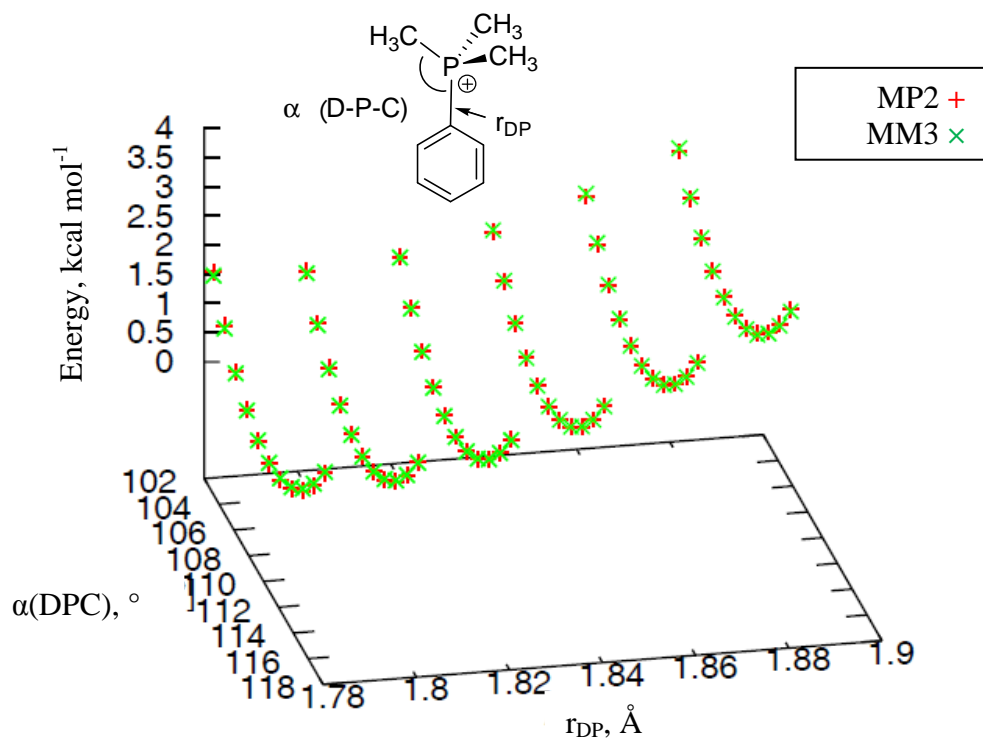


Fig. 9.5.10 Energy comparison of 2D-scans of DP and DPC in PMe₃Ph⁺.

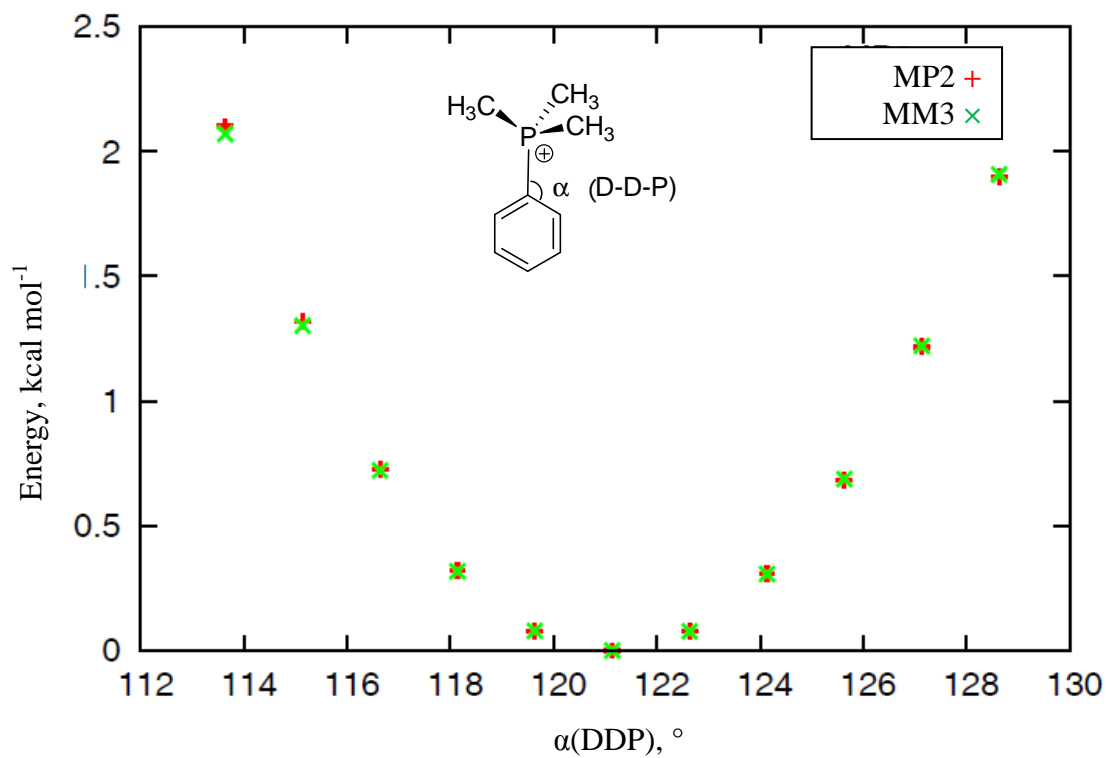


Fig. 9.5.11 Energy comparison of DDP scans in PMe₃Ph⁺.

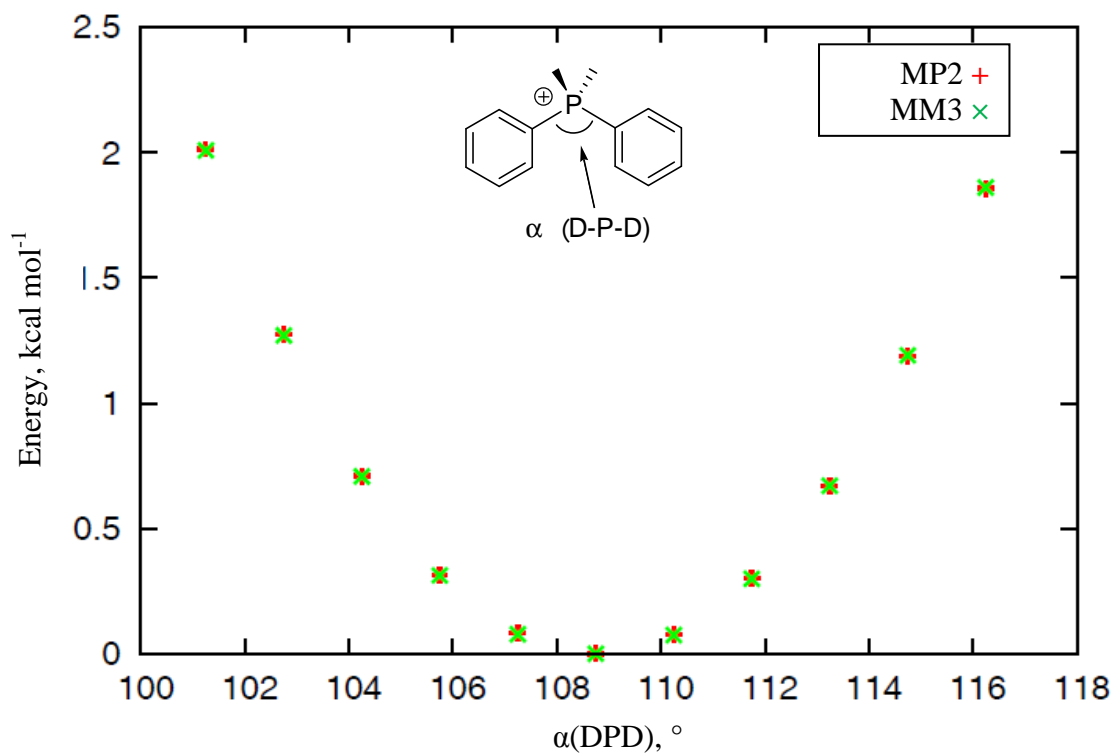


Fig. 9.5.12 Energy comparison of DPD scans in $\text{PMe}_2\text{Ph}_2^+$.

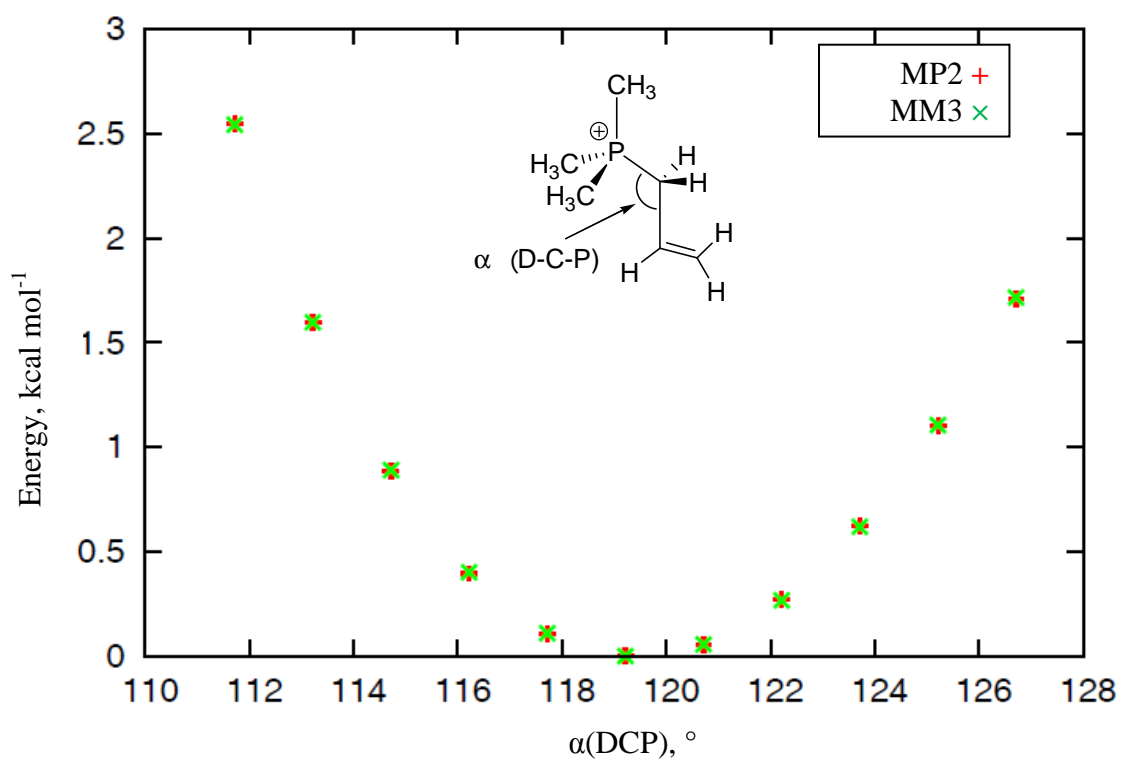


Fig. 9.5.13 Energy comparison of DCP scans in Allyl-PMe_3^+ .

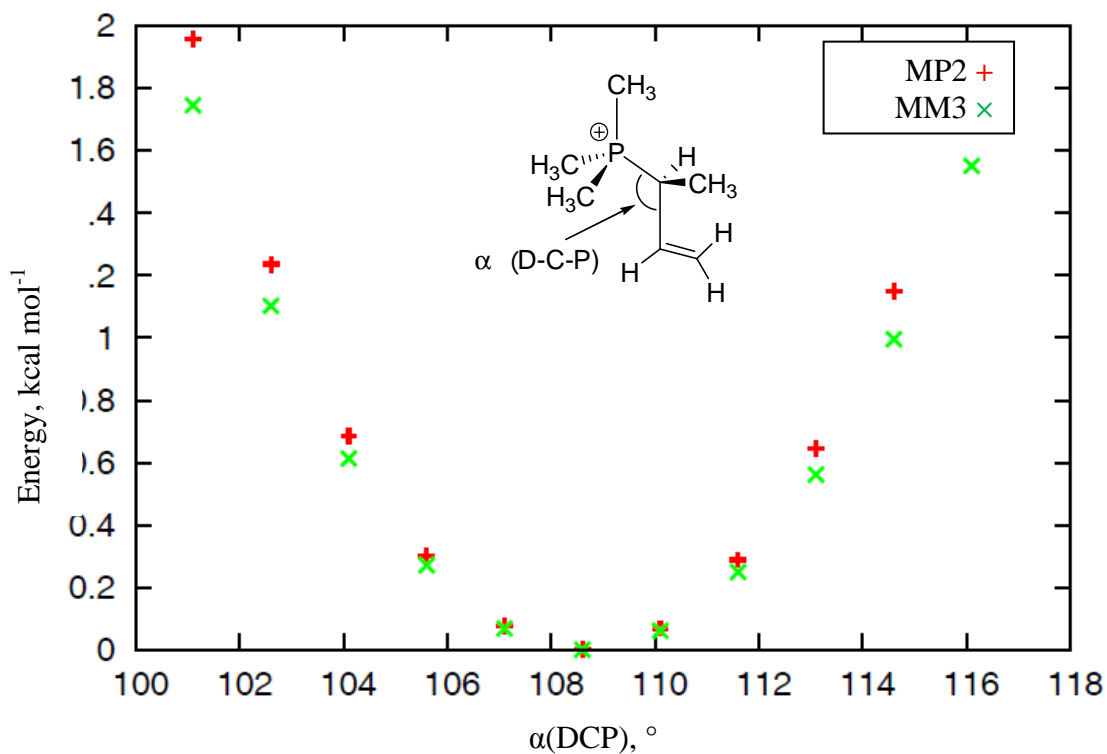


Fig. 9.5.14 Energy comparison of DCP scans in MeAllyl-PMe₃⁺.

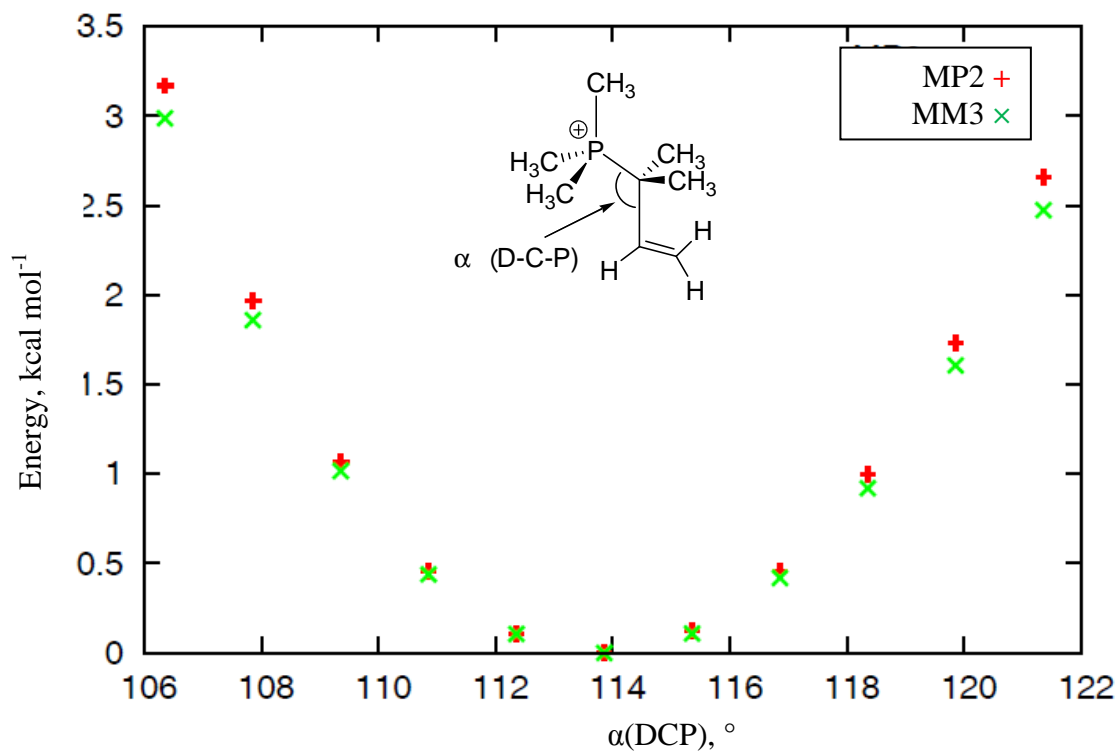


Fig. 9.5.15 Energy comparison of DCP scans in Me₂Allyl-PMe₃⁺.

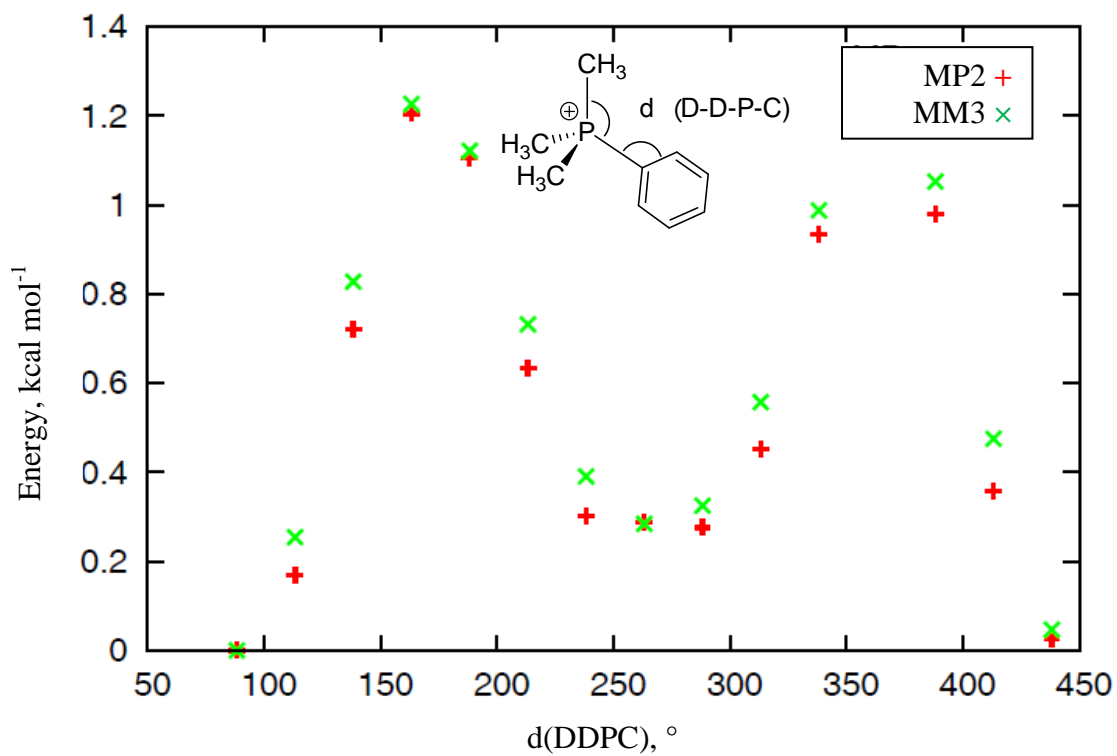


Fig. 9.5.13 Energy comparison of DDPC scans in PH_2MePh^+ .

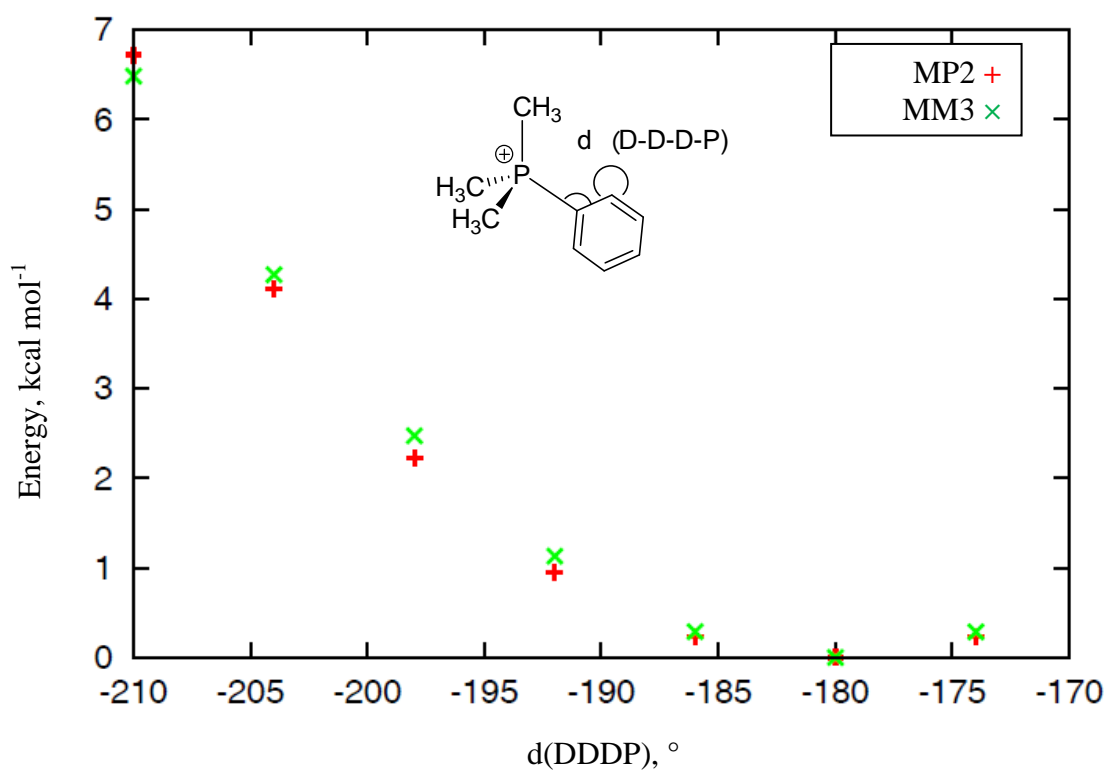


Fig. 9.5.14 Energy comparison of DDDP scans in PMe_3Ph^+ .

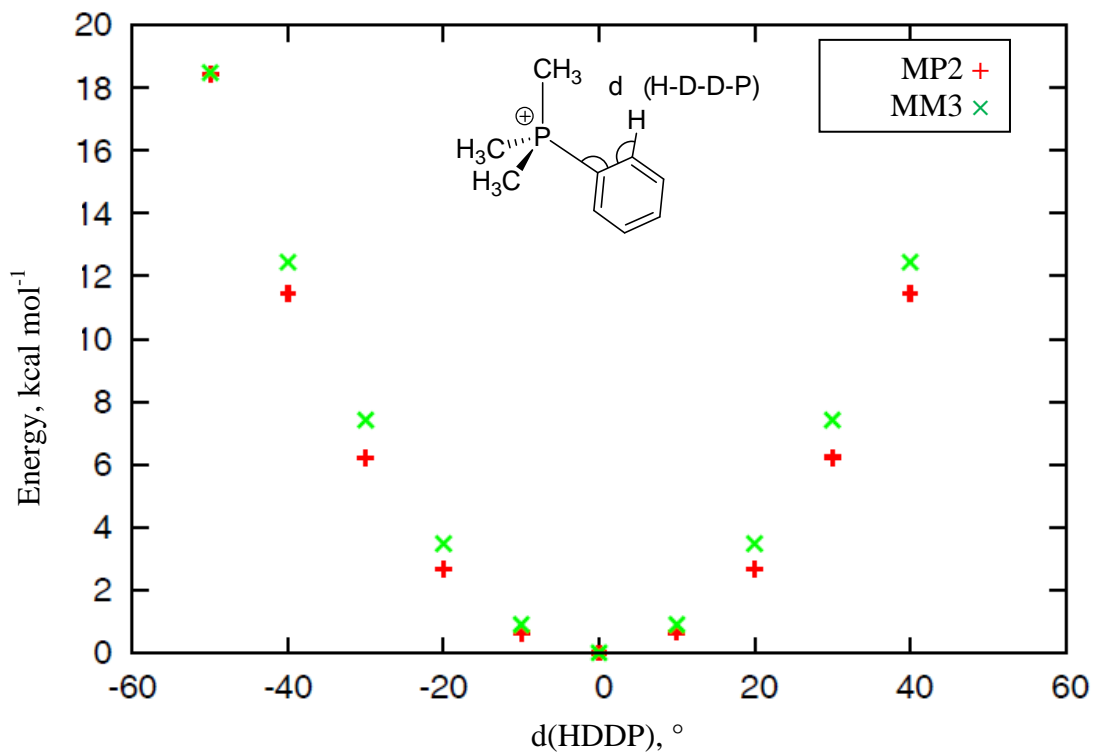


Fig. 9.5.15 Energy comparison of HDDDP scans in PMe_3Ph^+ .

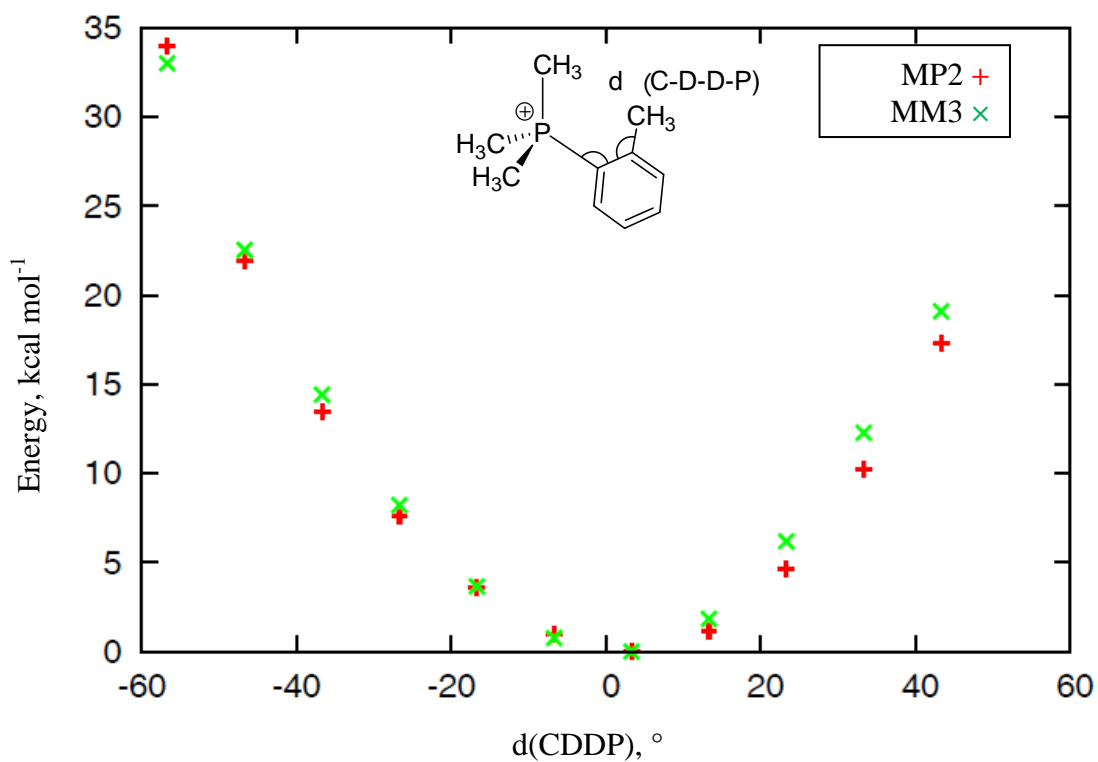


Fig. 9.5.16 Energy comparison of CDDP scans in MePh-PMe_3^+ .

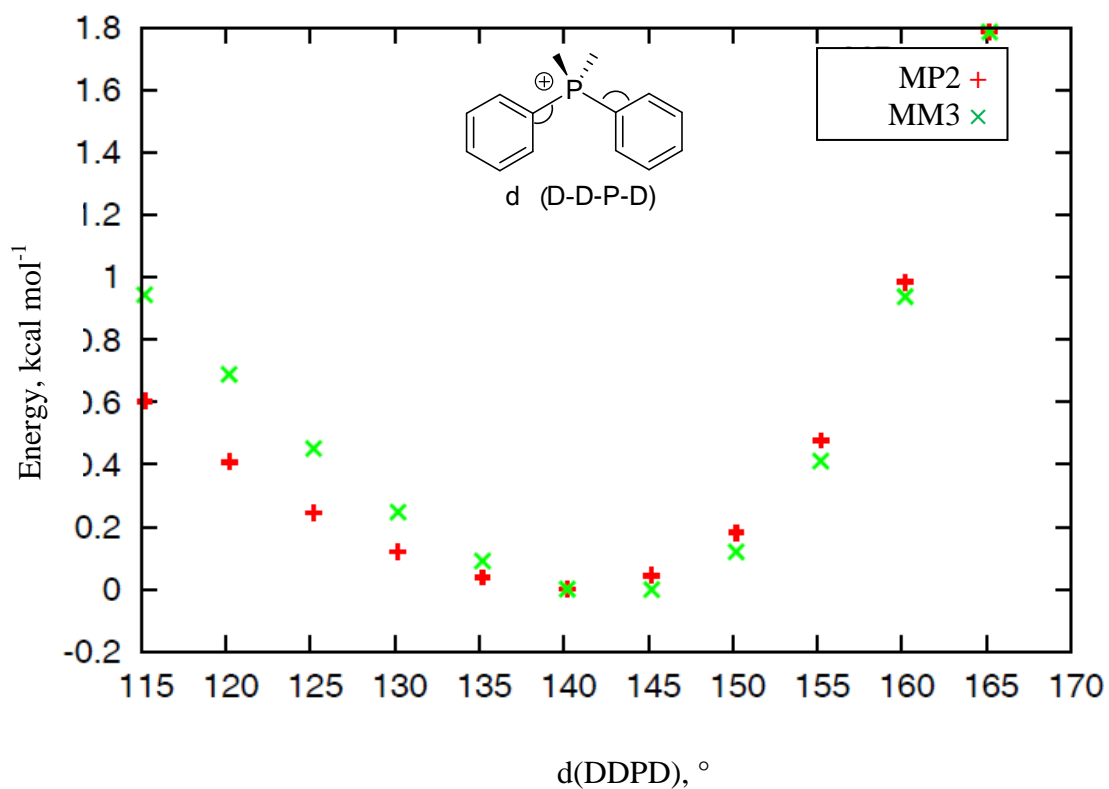


Fig. 9.5.17 Energy comparison of DDPD scans in $\text{PMe}_2\text{Ph}_2^+$.

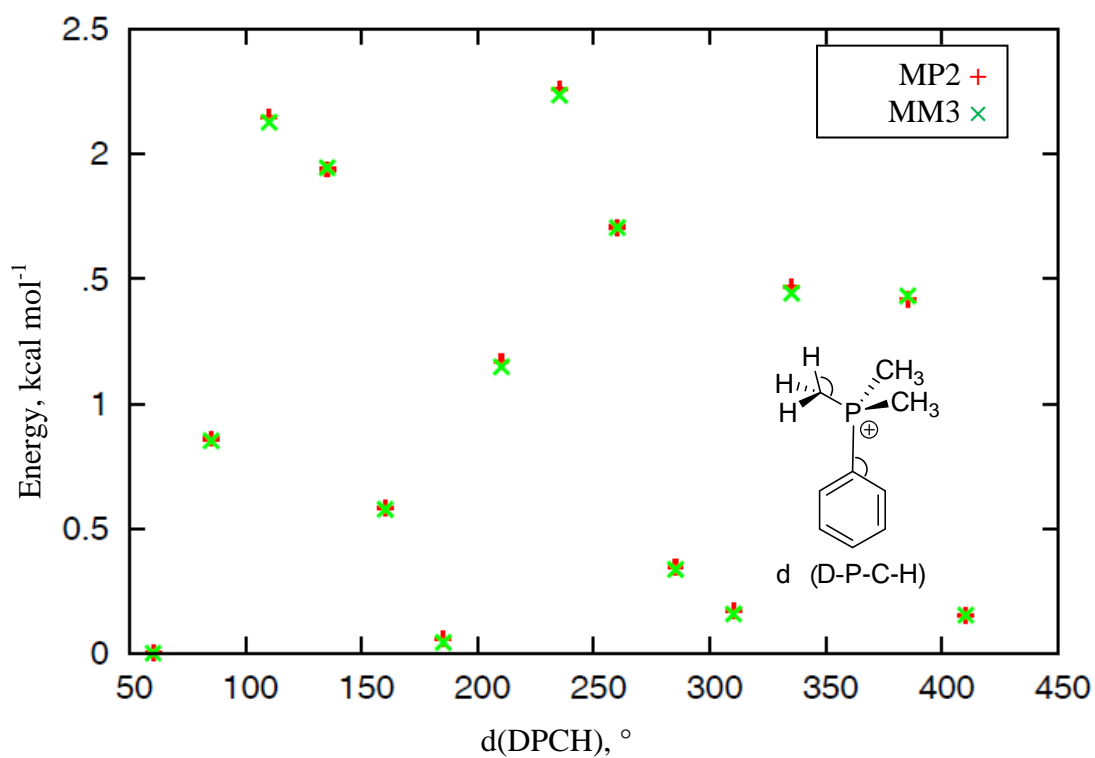


Fig. 9.5.18 Energy comparison of DPCH scans in PMe_3Ph^+ .

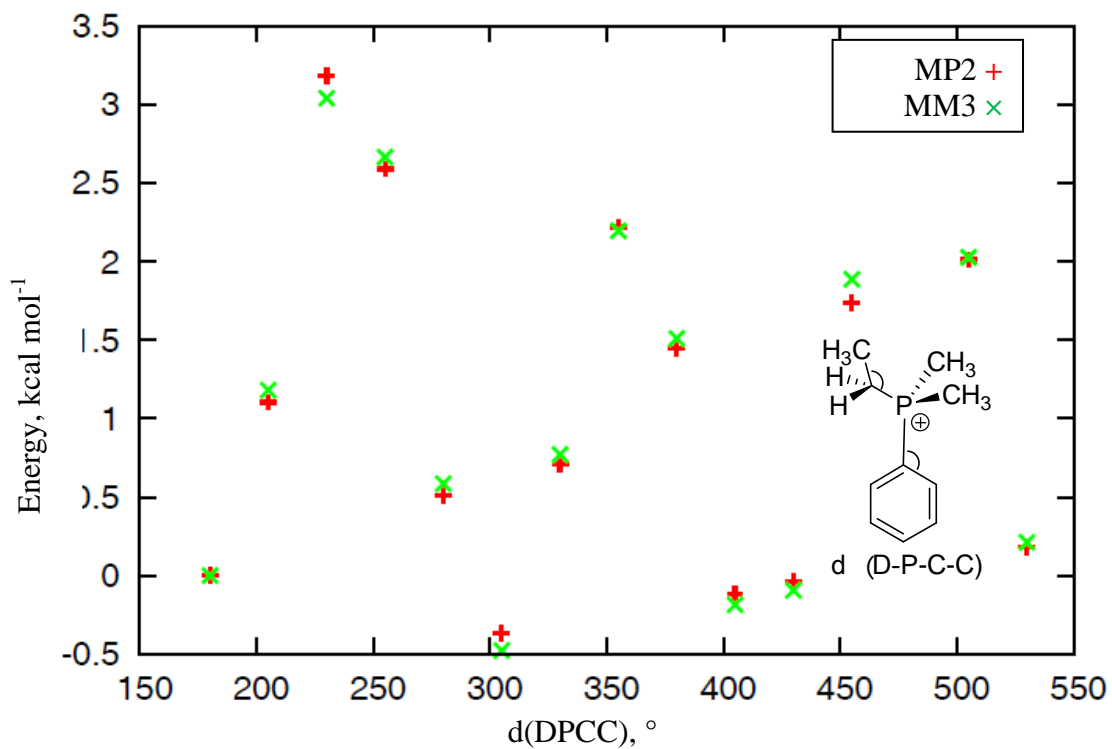


Fig. 9.5.19 Energy comparison of DPCC scans in PMe₂EtPh⁺.

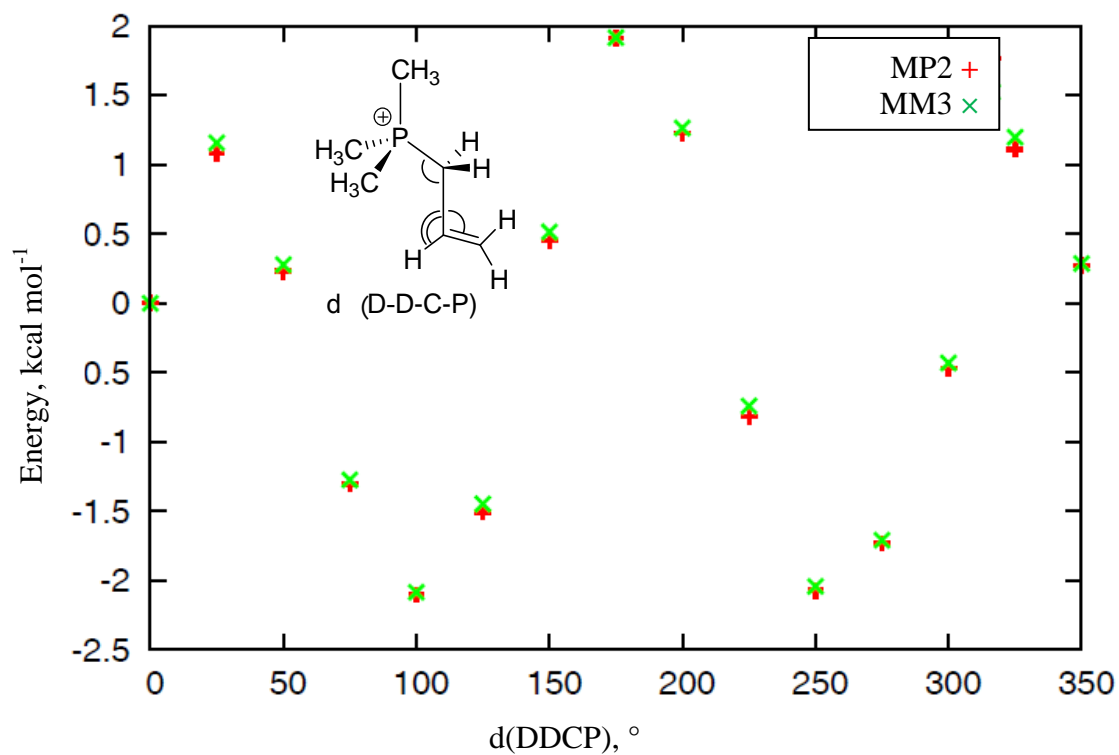
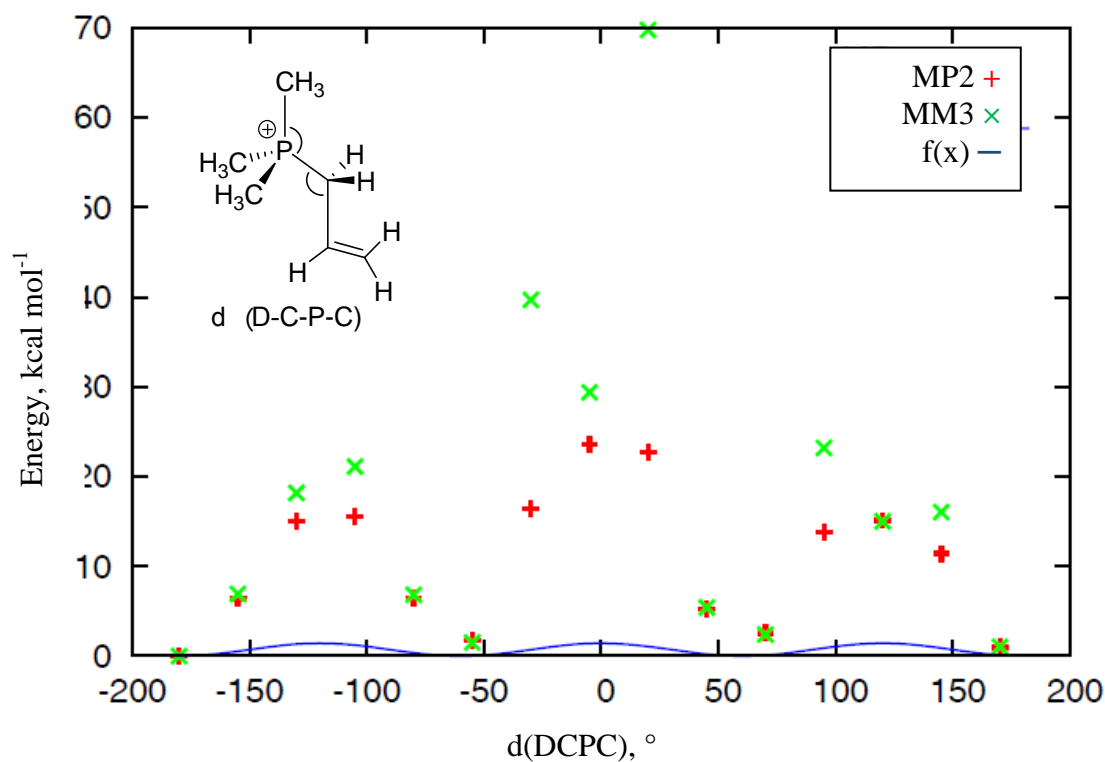
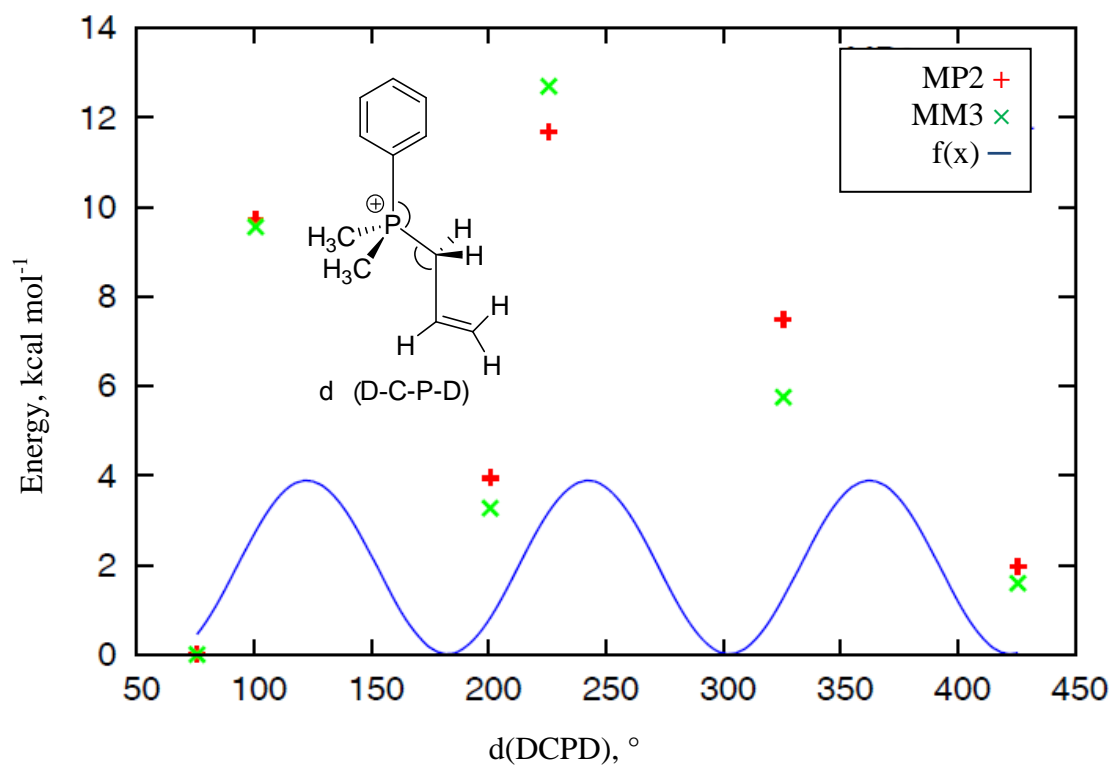


Fig. 9.5.20 Energy comparison of DDCP, HDCP (defined from the same scan) scan in Allyl-PMe₃⁺.



$$f(x)=(v1*0.5*(1+\cos(x))+v2*0.5*(1-\cos(2*x))+v3*0.5*(1+\cos(3*x)))+(v1*0.5*(1+\cos(x+117.909))+v2*0.5*(1-\cos(2*(x+117.909)))+v3*0.5*(1+\cos(3*(x+117.909))))+(v1*0.5*(1+\cos(x-117.91))+v2*0.5*(1-\cos(2*(x-117.91)))+v3*0.5*(1+\cos(3*(x-117.91))))$$

Fig. 9.5.21 Energy comparison of DCPC scans in Allyl-PMe₃⁺.



$$f(x)=(v1*0.5*(1+\cos(x))+v2*0.5*(1-\cos(2*x))+v3*0.5*(1+\cos(3*x)))+(v1*0.5*(1+\cos(x+117.019))+v2*0.5*(1-\cos(2*(x+117.019)))+v3*0.5*(1+\cos(3*(x+117.019))))+(v1*0.5*(1+\cos(x-124.35))+v2*0.5*(1-\cos(2*(x-124.35)))+v3*0.5*(1+\cos(3*(x-124.35))))$$

Fig. 9.5.22 Energy comparison of DCPD scans in Allyl-PMe₂Ph⁺.

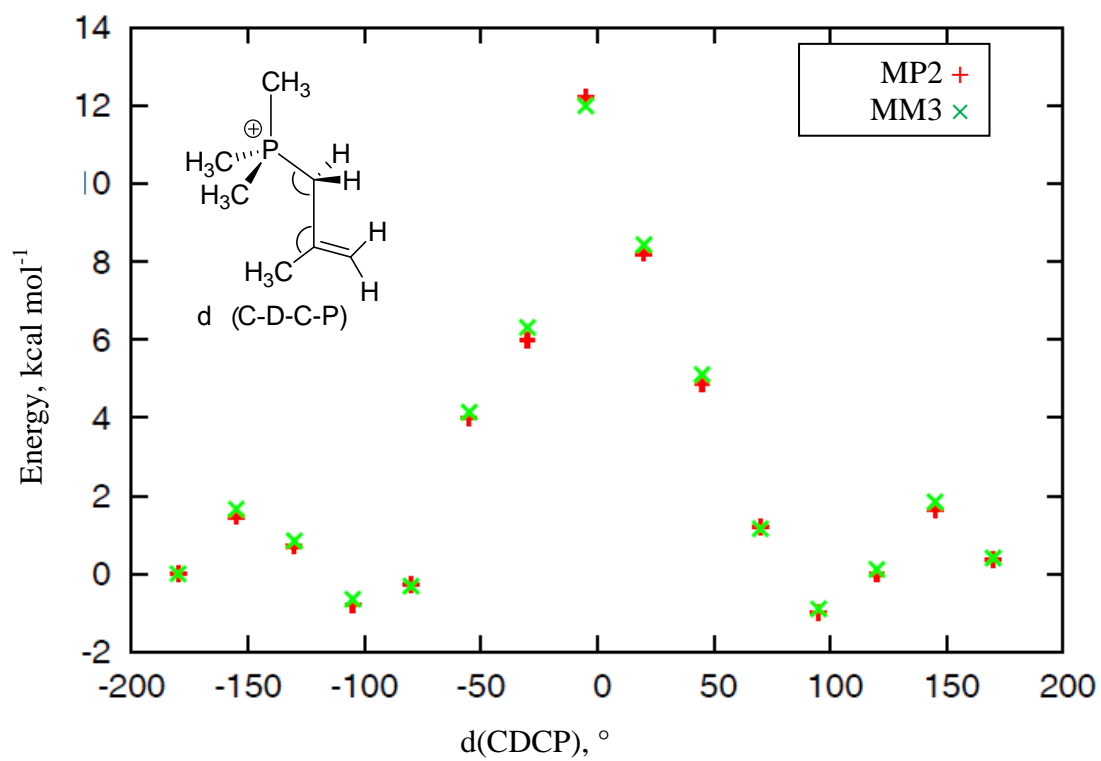


Fig. 9.5.23 Energy comparison of CDCP scans in MeAllyl-PMe₃⁺.

9.5.2. Phosphanes With Unbranched and Branched Acyclic Alkyl Substituents and Cyclic Substituents

Table 9.5.1. Total Energies and Enthalpies (in Hartree) as calculated at the B98/6-31G(d) and MP2(FC)/6-31+G(2d,p)//B98/6-31G(d) level of theory for all systems. If more than one conformer exist at 298.15 K, the single values of each conformer are denoted as well as the Boltzmann-averaged values for H_{298} at MP2(FC)/6-31+G(2d,p)//B98/6-31G(d) level of theory. Only conformers are included with a Boltzmann-weighting of at least 1 % up to a maximum to ten conformers per system.

System	B98/6-31G(d)		MP2(FC)/6-31+G(2d,p)// B98/6-31G(d)	
	E_{tot}	H_{298}	E_{tot}	H_{298}
CH₃⁺	-39.462922	-39.427481	-39.352370	-39.316929
1				-460.069844
1_1	-460.996371	-460.875351	-460.190864	-460.069844
1-Me⁺				-499.616902
1-Me ⁺ _1	-500.690725	-500.527994	-499.779633	-499.616902
2				-499.229506
2_1	-500.291789	-500.140620	-499.380925	-499.229756
2_2	-500.290437	-500.139265	-499.379363	-499.228192
2-Me⁺				-538.778959
2-Me ⁺ _1	-539.988433	-539.795575	-538.971818	-538.778959
3				-538.389368
3_1	-539.587192	-539.405864	-538.570888	-538.389560
3_2	-539.587129	-539.405732	-538.570864	-538.389467
3_3	-539.586011	-539.404407	-538.569936	-538.388332
3_4	-539.585712	-539.404324	-538.569356	-538.387969
3_5	-539.585741	-539.404392	-538.569142	-538.387794
3-Me⁺				-577.940957
3-Me ⁺ _1	-579.286127	-579.063048	-578.164383	-577.941304
3-Me ⁺ _2	-579.285951	-579.062897	-578.163903	-577.940849
3-Me ⁺ _3	-579.285941	-579.062757	-578.163895	-577.940711
3-Me ⁺ _4	-579.284342	-579.061078	-578.162030	-577.938767
4				-577.548752
4_1	-578.882317	-578.670863	-577.760698	-577.549243
4_2	-578.882307	-578.670812	-577.760706	-577.549211
4_3	-578.881414	-578.669729	-577.760384	-577.548699
4_4	-578.881118	-578.669561	-577.759884	-577.548327
4_5	-578.880980	-578.669528	-577.759134	-577.547682
4_6	-578.880980	-578.669524	-577.759129	-577.547673
4_7	-578.880891	-578.669360	-577.758980	-577.547449
4_8	-578.879750	-578.668302	-577.757930	-577.546482
4-Me⁺				-617.102794
4-Me ⁺ _1	-618.583673	-618.330318	-617.356777	-617.103423
4-Me ⁺ _2	-618.583473	-618.329956	-617.356358	-617.102841
4-Me ⁺ _3	-618.583197	-618.329644	-617.355828	-617.102274
4-Me ⁺ _4	-618.583239	-618.329669	-617.355840	-617.102271
4-Me ⁺ _5	-618.581787	-618.328153	-617.354398	-617.100764
4-Me ⁺ _6	-618.581665	-618.328057	-617.354175	-617.100566
4-Me ⁺ _7	-618.581633	-618.328095	-617.354046	-617.100508
5				-538.391333
5_1	-539.589302	-539.408275	-538.572900	-538.391873
5_2	-539.588174	-539.407153	-538.572003	-538.390982
5_3	-539.587825	-539.406637	-538.571340	-538.390152
5_4	-539.587287	-539.406091	-538.571187	-538.389991
5-Me⁺				-577.942235
5-Me ⁺ _1	-579.287376	-579.064571	-578.165220	-577.942415
5-Me ⁺ _2	-579.284837	-579.062040	-578.162866	-577.940069
6				-616.712941

6_1	-618.182248	-617.941090	-616.955068	-616.713910
6_2	-618.182262	-617.941173	-616.954981	-616.713892
6_3	-618.181133	-617.940002	-616.954157	-616.713027
6_4	-618.180839	-617.939626	-616.954237	-616.713024
6_5	-618.181138	-617.940029	-616.954087	-616.712978
6_6	-618.181068	-617.939899	-616.954135	-616.712966
6_7	-618.181010	-617.939943	-616.953560	-616.712493
6_8	-618.180720	-617.939581	-616.953597	-616.712459
6_9	-618.179976	-617.938952	-616.953255	-616.712231
6_10	-618.180221	-617.939058	-616.953333	-616.712170
6-Me⁺				-656.267583
6-Me ⁺ _1	-657.883838	-657.600811	-656.551384	-656.268357
6-Me ⁺ _2	-657.883653	-657.600694	-656.550788	-656.267829
6-Me ⁺ _3	-657.883675	-657.600684	-656.550665	-656.267674
6-Me ⁺ _4	-657.882065	-657.599070	-656.549224	-656.266229
6-Me ⁺ _5	-657.881230	-657.598164	-656.548959	-656.265894
6-Me ⁺ _6	-657.881204	-657.598155	-656.548639	-656.265590
6-Me ⁺ _7	-657.881301	-657.598035	-656.548770	-656.265504
6-Me ⁺ _8	-657.881205	-657.598070	-656.548557	-656.265422
6-Me ⁺ _9	-657.881115	-657.598029	-656.548284	-656.265198
6-Me ⁺ _10	-657.881245	-657.598096	-656.548343	-656.265194
7				-695.034802
7_1	-696.775018	-696.473798	-695.337264	-695.036044
7_2	-696.773868	-696.472765	-695.337118	-695.036016
7_3	-696.773942	-696.472760	-695.336405	-695.035223
7_4	-696.773798	-696.472344	-695.336597	-695.035143
7_5	-696.773832	-696.472713	-695.335952	-695.034834
7_6	-696.772606	-696.471280	-695.336067	-695.034741
7_7	-696.773726	-696.472593	-695.335715	-695.034582
7_8	-696.773083	-696.471843	-695.335677	-695.034438
7_9	-696.772825	-696.471643	-695.335565	-695.034383
7_10	-696.772897	-696.471754	-695.335420	-695.034277
7-Me⁺				-734.593073
7-Me ⁺ _1	-736.479952	-736.136800	-734.937424	-734.594272
7-Me ⁺ _2	-736.479848	-736.136499	-734.936971	-734.593622
7-Me ⁺ _3	-736.479510	-736.136260	-734.936263	-734.593012
7-Me ⁺ _4	-736.478156	-736.134954	-734.935157	-734.591955
7-Me ⁺ _5	-736.477305	-736.133987	-734.934995	-734.591677
7-Me ⁺ _6	-736.478036	-736.134740	-734.934846	-734.591550
7-Me ⁺ _7	-736.477364	-736.134031	-734.934838	-734.591506
7-Me ⁺ _8	-736.478124	-736.134734	-734.934891	-734.591501
7-Me ⁺ _9	-736.477348	-736.133942	-734.934777	-734.591372
7-Me ⁺ _10	-736.477121	-736.133836	-734.934641	-734.591356
8				-577.552930
8_1	-578.886760	-578.675867	-577.764655	-577.553763
8_2	-578.885615	-578.674569	-577.763890	-577.552844
8_3	-578.885623	-578.674542	-577.763890	-577.552809
8_4	-578.885596	-578.674648	-577.763742	-577.552794
8_5	-578.884541	-578.673516	-577.763406	-577.552381
8_6	-578.884756	-578.673738	-577.763157	-577.552138
8_7	-578.885276	-578.674266	-577.763125	-577.552115
8_8	-578.883458	-578.672354	-577.762411	-577.551308
8_9	-578.884029	-578.672918	-577.762227	-577.551116
8-Me⁺				-617.104612
8-Me ⁺ _1	-618.585691	-618.332926	-617.357773	-617.105008
8-Me ⁺ _2	-618.584535	-618.331912	-617.357103	-617.104480
8-Me ⁺ _3	-618.583181	-618.330407	-617.355721	-617.102947
8-Me ⁺ _4	-618.582031	-618.329248	-617.355107	-617.102323
9				-695.036158
9_1	-696.777148	-696.476274	-695.338641	-695.037768
9_2	-696.777175	-696.476313	-695.338476	-695.037614
9_3	-696.775935	-696.475156	-695.337739	-695.036960

9_4	-696.775966	-696.474952	-695.337879	-695.036865
9_5	-696.775941	-696.474913	-695.337859	-695.036831
9_6	-696.776029	-696.475133	-695.337709	-695.036813
9_7	-696.775991	-696.474941	-695.337855	-695.036806
9_8	-696.776020	-696.475044	-695.337765	-695.036790
9_9	-696.775863	-696.474745	-695.337901	-695.036783
9_10	-696.776020	-696.475026	-695.337768	-695.036774
9-Me⁺				-734.592214
9-Me ⁺ _1	-736.480291	-736.137602	-734.936545	-734.593857
9-Me ⁺ _2	-736.479259	-736.136327	-734.936061	-734.593129
9-Me ⁺ _3	-736.480161	-736.137293	-734.935912	-734.593045
9-Me ⁺ _4	-736.479238	-736.136291	-734.935899	-734.592953
9-Me ⁺ _5	-736.480128	-736.137288	-734.935737	-734.592896
9-Me ⁺ _6	-736.478291	-736.135371	-734.935489	-734.592569
9-Me ⁺ _7	-736.478155	-736.135325	-734.935320	-734.592489
9-Me ⁺ _8	-736.479060	-736.136198	-734.935219	-734.592357
9-Me ⁺ _9	-736.479071	-736.136136	-734.935236	-734.592301
9-Me ⁺ _10	-736.479083	-736.136105	-734.935251	-734.592273
10				-812.520264
10_1	-814.666280	-814.275333	-812.912789	-812.521842
10_2	-814.667375	-814.276445	-812.912691	-812.521761
10_3	-814.666120	-814.275086	-812.912277	-812.521243
10_4	-814.665189	-814.274055	-812.912295	-812.521161
10_5	-814.666141	-814.275205	-812.912010	-812.521074
10_6	-814.666247	-814.275380	-812.911927	-812.521059
10_7	-814.665089	-814.274045	-812.912063	-812.521019
10_8	-814.666185	-814.275235	-812.911940	-812.520990
10_9	-814.665077	-814.273919	-812.911925	-812.520767
10_10	-814.664967	-814.273871	-812.911814	-812.520718
10-Me⁺				-852.080761
10-Me ⁺ _1	-854.374538	-853.941503	-852.515266	-852.082231
10-Me ⁺ _2	-854.374190	-853.941393	-852.514736	-852.081940
10-Me ⁺ _3	-854.373488	-853.940383	-852.514723	-852.081618
10-Me ⁺ _4	-854.373538	-853.940333	-852.514725	-852.081520
10-Me ⁺ _5	-854.373439	-853.940354	-852.514587	-852.081501
10-Me ⁺ _6	-854.372400	-853.939482	-852.514139	-852.081221
10-Me ⁺ _7	-854.372327	-853.939451	-852.514043	-852.081167
10-Me ⁺ _8	-854.373274	-853.940189	-852.514213	-852.081127
10-Me ⁺ _9	-854.373179	-853.940210	-852.514058	-852.081088
10-Me ⁺ _10	-854.372322	-853.939355	-852.514046	-852.081079
11				-616.714334
11_1	-618.184164	-617.943271	-616.956247	-616.715354
11_2	-618.182928	-617.942055	-616.955563	-616.714690
11_3	-618.182977	-617.942136	-616.955465	-616.714624
11_4	-618.182943	-617.942011	-616.955532	-616.714599
11_5	-618.182953	-617.942028	-616.955398	-616.714473
11_6	-618.182926	-617.942005	-616.955389	-616.714468
11_7	-618.181892	-617.941003	-616.955143	-616.714254
11_8	-618.181868	-617.940899	-616.955212	-616.714243
11_9	-618.181974	-617.940892	-616.955258	-616.714176
11_10	-618.182118	-617.941320	-616.954865	-616.714067
11-Me⁺				-656.266368
11-Me ⁺ _1	-657.883498	-657.600804	-656.549780	-656.267086
11-Me ⁺ _2	-657.882355	-657.599641	-656.549179	-656.266464
11-Me ⁺ _3	-657.882355	-657.599644	-656.549175	-656.266463
11-Me ⁺ _4	-657.882290	-657.599642	-656.548983	-656.266336
11-Me ⁺ _5	-657.881308	-657.598600	-656.548807	-656.266099
11-Me ⁺ _6	-657.881098	-657.598463	-656.547916	-656.265282
11-Me ⁺ _7	-657.879875	-657.597252	-656.547512	-656.264889
11-Me ⁺ _8	-657.880049	-657.597323	-656.547302	-656.264576
11-Me ⁺ _9	-657.878901	-657.596178	-656.546937	-656.264214
11-Me ⁺ _10	-657.879787	-657.596989	-656.546839	-656.264042

12				-538.393636
12_1	-539.588244	-539.407327	-538.574773	-538.393856
12_2	-539.586615	-539.405739	-538.572794	-538.391918
12-Me⁺				-577.944232
12-Me ⁺ _1	-579.286326	-579.063815	-578.166742	-577.944232
13				-616.715989
13_1	-618.178225	-617.937456	-616.957188	-616.716419
13_2	-618.176618	-617.935883	-616.955395	-616.714660
13_3	-618.176410	-617.935504	-616.955300	-616.714394
13-Me⁺				-656.270876
13-Me ⁺ _1	-657.881357	-657.598580	-656.554033	-656.271256
13-Me ⁺ _2	-657.879374	-657.596685	-656.551872	-656.269183
13-Me ⁺ _3	-657.878696	-657.595912	-656.551172	-656.268388
13-Me ⁺ _4	-657.877891	-657.595206	-656.550362	-656.267677
14				-695.035243
14_1	-696.764415	-696.463812	-695.336484	-695.035881
14_2	-696.763341	-696.462502	-695.335357	-695.034518
14_3	-696.762638	-696.461873	-695.334389	-695.033624
14_4	-696.762440	-696.461212	-695.334289	-695.033061
14_5	-696.762039	-696.461116	-695.333609	-695.032686
14_6	-696.762066	-696.461454	-695.333293	-695.032681
14_7	-696.760293	-696.459351	-695.332179	-695.031238
14-Me⁺				-734.594174
14-Me ⁺ _1	-736.471871	-736.129126	-734.937546	-734.594802
14-Me ⁺ _2	-736.471122	-736.128196	-734.936952	-734.594025
14-Me ⁺ _3	-736.469445	-736.126517	-734.935041	-734.592113
14-Me ⁺ _4	-736.469539	-736.126489	-734.935065	-734.592016
14-Me ⁺ _5	-736.469481	-736.126460	-734.934993	-734.591972
14-Me ⁺ _6	-736.468954	-736.125966	-734.934333	-734.591345
14-Me ⁺ _7	-736.469182	-736.126158	-734.934256	-734.591233
14-Me ⁺ _8	-736.468365	-736.125385	-734.933808	-734.590828
14-Me ⁺ _9	-736.468083	-736.124927	-734.933406	-734.590250
15				-577.556719
15_1	-578.886465	-578.676024	-577.767603	-577.557161
15_2	-578.885522	-578.675023	-577.766660	-577.556161
15_3	-578.884510	-578.673982	-577.765756	-577.555227
15_4	-578.882279	-578.671646	-577.763566	-577.552934
15-Me⁺				-617.106709
15-Me ⁺ _1	-618.583929	-618.331600	-617.359130	-617.106801
15-Me ⁺ _2	-618.581109	-618.328607	-617.355924	-617.103422
16				-695.043972
16_1	-696.776563	-696.476650	-695.344690	-695.044777
16_2	-696.776633	-696.476686	-695.344523	-695.044576
16_3	-696.775424	-696.475499	-695.344040	-695.044115
16_4	-696.775787	-696.475855	-695.343936	-695.044004
16_5	-696.775611	-696.475659	-695.343800	-695.043848
16_6	-696.775546	-696.475518	-695.343603	-695.043576
16_7	-696.774817	-696.474825	-695.343164	-695.043173
16_8	-696.774639	-696.474559	-695.342872	-695.042792
16_9	-696.774720	-696.474593	-695.342910	-695.042784
16_10	-696.774564	-696.474616	-695.342699	-695.042750
16-Me⁺				-734.596465
16-Me ⁺ _1	-736.476703	-736.134674	-734.939499	-734.597470
16-Me ⁺ _2	-736.476635	-736.134466	-734.939039	-734.596870
16-Me ⁺ _3	-736.476555	-736.134548	-734.938738	-734.596731
16-Me ⁺ _4	-736.476433	-736.134376	-734.938769	-734.596712
16-Me ⁺ _5	-736.476517	-736.134645	-734.938568	-734.596695
16-Me ⁺ _6	-736.476409	-736.134380	-734.938617	-734.596588
16-Me ⁺ _7	-736.475762	-736.133699	-734.938612	-734.596549
16-Me ⁺ _8	-736.476114	-736.134160	-734.938435	-734.596481
16-Me ⁺ _9	-736.475926	-736.133960	-734.937814	-734.595848
16-Me ⁺ _10	-736.475745	-736.133708	-734.937754	-734.595717

17				-812.531519
17_1	-814.665707	-814.276335	-812.921906	-812.532534
17_2	-814.665956	-814.276581	-812.921774	-812.532399
17_3	-814.665462	-814.276121	-812.921337	-812.531997
17_4	-814.665061	-814.275638	-812.920948	-812.531524
17_5	-814.664644	-814.275127	-812.921029	-812.531513
17_6	-814.664961	-814.275466	-812.920998	-812.531503
17_7	-814.664958	-814.275423	-812.920993	-812.531458
17_8	-814.664945	-814.275457	-812.920902	-812.531414
17_9	-814.664124	-814.274512	-812.920558	-812.530947
17_10	-814.663582	-814.274153	-812.920194	-812.530764
17-Me⁺				-852.086758
17-Me ⁺ _1	-854.368709	-853.936905	-852.519824	-852.088021
17-Me ⁺ _2	-854.368442	-853.936798	-852.519273	-852.087629
17-Me ⁺ _3	-854.368456	-853.936803	-852.519235	-852.087582
17-Me ⁺ _4	-854.368129	-853.936341	-852.519009	-852.087221
17-Me ⁺ _5	-854.367735	-853.936060	-852.518840	-852.087165
17-Me ⁺ _6	-854.368436	-853.936690	-852.518887	-852.087140
17-Me ⁺ _7	-854.367974	-853.936375	-852.518634	-852.087035
17-Me ⁺ _8	-854.368096	-853.936345	-852.518617	-852.086866
17-Me ⁺ _9	-854.368033	-853.936100	-852.518735	-852.086801
17-Me ⁺ _10	-854.368320	-853.936514	-852.518608	-852.086802
18				-577.559408
18_1	-578.882974	-578.672922	-577.769460	-577.559408
18-Me⁺				-617.112268
18-Me ⁺ _1	-618.584037	-618.332107	-617.364198	-617.112268
19				-695.043102
19_1	-696.762757	-696.463368	-695.342492	-695.043102
19-Me⁺				-734.601912
19-Me ⁺ _1	-736.470129	-736.128730	-734.943311	-734.601912
20				-812.514560
20_1	-814.630252	-814.240491	-812.904321	-812.514560
20-Me⁺				-852.078427
20-Me ⁺ _1	-854.343293	-853.911353	-852.510367	-852.078427
21				-616.724271
21_1	-618.182550	-617.942963	-616.963858	-616.724271
21-Me⁺				-656.272739
21-Me ⁺ _1	-657.879352	-657.597861	-656.554230	-656.272739
22				-773.379503
22_1	-775.368653	-775.010665	-773.737751	-773.379763
22_2	-775.368243	-775.010022	-773.736629	-773.378408
22-Me⁺				-812.927595
22-Me ⁺ _1	-815.066397	-814.665879	-813.328364	-812.927846
22-Me ⁺ _2	-815.065766	-814.665403	-813.327304	-812.926940
23				-930.035898
23_1	-932.554859	-932.077946	-930.512811	-930.035898
23-Me⁺				-969.582606
23-Me ⁺ _1	-972.251943	-971.732487	-970.102493	-969.583038
23-Me ⁺ _2	-972.250674	-971.730952	-970.101315	-969.581593
23-Me ⁺ _3	-972.249772	-971.730229	-970.100256	-969.580713
23-Me ⁺ _4	-972.248294	-971.728588	-970.098738	-969.579032
24				-651.216064
24-Me⁺				-651.216064
25				-1033.516812
25-Me⁺				-1073.069267
26				-537.191893
26_1	-538.345989	-538.188633	-537.349319	-537.191963
26_2	-538.342312	-538.184924	-537.345605	-537.188217
26-Me⁺				-576.740109
26-Me ⁺ _1	-578.042476	-577.843397	-576.939188	-576.740109
27				-614.313661
27_1	-615.695093	-615.501506	-614.507499	-614.313912

27_2	-615.692343	-615.498599	-614.505189	-614.311445
27_3	-615.692047	-615.498273	-614.504346	-614.310572
27-Me⁺				-653.863612
27-Me ⁺ _1	-655.394224	-655.158559	-654.099690	-653.864024
27-Me ⁺ _2	-655.393933	-655.158173	-654.098930	-653.863170
27-Me ⁺ _3	-655.393096	-655.157511	-654.098127	-653.862542
28				-691.435173
28_1	-693.043842	-692.813807	-691.665471	-691.435436
28_2	-693.041564	-692.811529	-691.663637	-691.433602
28_3	-693.038571	-692.808464	-691.661113	-691.431006
28-Me⁺				-730.988661
28-Me ⁺ _1	-732.746080	-732.473852	-731.261227	-730.988999
28-Me ⁺ _2	-732.746007	-732.473804	-731.261194	-730.988991
28-Me ⁺ _3	-732.745680	-732.473451	-731.260386	-730.988156
28-Me ⁺ _4	-732.744884	-732.472684	-731.259551	-730.987351
28-Me ⁺ _5	-732.744521	-732.472362	-731.258799	-730.986640
28-Me ⁺ _6	-732.742665	-732.471431	-731.256499	-730.985264
29				-576.354625
29_1	-577.648530	-577.460788	-576.542706	-576.354964
29_2	-577.647685	-577.460060	-576.542283	-576.354658
29_3	-577.647391	-577.459517	-576.541616	-576.353742
29_4	-577.646116	-577.458234	-576.539961	-576.352079
29-Me⁺				-615.906429
29-Me ⁺ _1	-617.348441	-617.118870	-616.136226	-615.906656
29-Me ⁺ _2	-617.346862	-617.117303	-616.134344	-615.904786
30				-692.639671
30_1	-694.300547	-694.046038	-692.895067	-692.640558
30_2	-694.299433	-694.045029	-692.894530	-692.640127
30_3	-694.299517	-694.045025	-692.894137	-692.639646
30_4	-694.299094	-694.044469	-692.894077	-692.639452
30_5	-694.298681	-694.044150	-692.893776	-692.639245
30_6	-694.297931	-694.043425	-692.892881	-692.638374
30_7	-694.298167	-694.043693	-692.892735	-692.638260
30_8	-694.298163	-694.043566	-692.892847	-692.638250
30_9	-694.297543	-694.042879	-692.892741	-692.638077
30_10	-694.297826	-694.043058	-692.892832	-692.638064
30-Me⁺				-732.196074
30-Me ⁺ _1	-734.005503	-733.708938	-732.493156	-732.196592
30-Me ⁺ _2	-734.004978	-733.708285	-732.492939	-732.196245
30-Me ⁺ _3	-734.005286	-733.708632	-732.492784	-732.196130
30-Me ⁺ _4	-734.003454	-733.706876	-732.491555	-732.194977
30-Me ⁺ _5	-734.003879	-733.707420	-732.491316	-732.194857
30-Me ⁺ _6	-734.003477	-733.706863	-732.490889	-732.194276
30-Me ⁺ _7	-734.002346	-733.705804	-732.489462	-732.192920
31				-808.925527
31_1	-810.952285	-810.630998	-809.247810	-808.926523
31_2	-810.950983	-810.629604	-809.247147	-808.925768
31_3	-810.950852	-810.629411	-809.247009	-808.925568
31_4	-810.949659	-810.628393	-809.246334	-808.925069
31_5	-810.949518	-810.628142	-809.245961	-808.924585
31_6	-810.949138	-810.627765	-809.245826	-808.924453
31_7	-810.949582	-810.628069	-809.245939	-808.924427
31_8	-810.949181	-810.627638	-809.245818	-808.924275
31_9	-810.948110	-810.626634	-809.245078	-808.923602
31_10	-810.948024	-810.626645	-809.244832	-808.923452
31-Me⁺				-848.485656
31-Me ⁺ _1	-850.660901	-850.297246	-848.849889	-848.486233
31-Me ⁺ _2	-850.660825	-850.297065	-848.849980	-848.486220
31-Me ⁺ _3	-850.660927	-850.297213	-848.849546	-848.485833
31-Me ⁺ _4	-850.660715	-850.296892	-848.849535	-848.485712
31-Me ⁺ _5	-850.659964	-850.296287	-848.849114	-848.485438
31-Me ⁺ _6	-850.659263	-850.295624	-848.848703	-848.485065

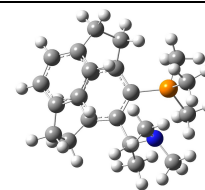
31-Me ⁺ _7	-850.659420	-850.295725	-848.848509	-848.484814
31-Me ⁺ _8	-850.658729	-850.295072	-848.847943	-848.484286
31-Me ⁺ _9	-850.658177	-850.294507	-848.847485	-848.483814
31-Me ⁺ _10	-850.658818	-850.295069	-848.847535	-848.483786
32				-615.548621
32_1	-616.974756	-616.756123	-615.767613	-615.548980
32_2	-616.972323	-616.753756	-615.765989	-615.547422
32_3	-616.972428	-616.753513	-615.764823	-615.545908
32_4	-616.969827	-616.750962	-615.762915	-615.544051
32-Me⁺				-655.101863
32-Me ⁺ _1	-656.675630	-656.415057	-655.362436	-655.101863
33				-771.026414
33_1	-772.951878	-772.635396	-771.343606	-771.027124
33_2	-772.950858	-772.634361	-771.342818	-771.026322
33_3	-772.949058	-772.632482	-771.342119	-771.025543
33_4	-772.949803	-772.633309	-771.341926	-771.025432
33_5	-772.950813	-772.634355	-771.340896	-771.024438
33_6	-772.948254	-772.631658	-771.340896	-771.024300
33_7	-772.946664	-772.630120	-771.340017	-771.023473
33-Me⁺				-810.586007
33-Me ⁺ _1	-812.659316	-812.300771	-810.945189	-810.586644
33-Me ⁺ _2	-812.657985	-812.299400	-810.943854	-810.585269
33-Me ⁺ _3	-812.658201	-812.299520	-810.943661	-810.584980
33-Me ⁺ _4	-812.657911	-812.299181	-810.943708	-810.584977
33-Me ⁺ _5	-812.655693	-812.296909	-810.942139	-810.583355
34				-926.504276
34_1	-928.926292	-928.511862	-926.919497	-926.505067
34_2	-928.926236	-928.511821	-926.919422	-926.505006
34_3	-928.925350	-928.510849	-926.918306	-926.503805
34_4	-928.922901	-928.508590	-926.917255	-926.502943
34_5	-928.924535	-928.510355	-926.917111	-926.502931
34_6	-928.924810	-928.510251	-926.917264	-926.502705
34_7	-928.924830	-928.510287	-926.917230	-926.502686
34_8	-928.924811	-928.510267	-926.917216	-926.502672
34_9	-928.924664	-928.510014	-926.917154	-926.502504
34_10	-928.922635	-928.508092	-926.916522	-926.501979
34-Me⁺				-966.069098
34-Me ⁺ _1	-968.639512	-968.182722	-966.526451	-966.069661
34-Me ⁺ _2	-968.639326	-968.182479	-966.526277	-966.069430
34-Me ⁺ _3	-968.638236	-968.181448	-966.525667	-966.068879
34-Me ⁺ _4	-968.638674	-968.181748	-966.525099	-966.068173
34-Me ⁺ _5	-968.638585	-968.181718	-966.524450	-966.067583
34-Me ⁺ _6	-968.637786	-968.180797	-966.524186	-966.067196
34-Me ⁺ _7	-968.634666	-968.178090	-966.522303	-966.065726
34-Me ⁺ _8	-968.634770	-968.177865	-966.522539	-966.065634
34-Me ⁺ _9	-968.635863	-968.178898	-966.522588	-966.065624
34-Me ⁺ _10	-968.634453	-968.177565	-966.522539	-966.065369
35				-654.719362
35_1	-656.279581	-656.030734	-654.968567	-654.719721
35_2	-656.278069	-656.029107	-654.966692	-654.717730
35_3	-656.276782	-656.027764	-654.966339	-654.717321
35-Me⁺				-694.273148
35-Me ⁺ _1	-695.981191	-695.690430	-694.563909	-694.273148
36				-849.368146
36_1	-851.561080	-851.184125	-849.745811	-849.368856
36_2	-851.559589	-851.182731	-849.744344	-849.367486
36_3	-851.559235	-851.182187	-849.743591	-849.366543
36_4	-851.558011	-851.181065	-849.743344	-849.366397
36_5	-851.556434	-851.179573	-849.741995	-849.365134
36_6	-851.557367	-851.180686	-849.741693	-849.365012
36_7	-851.556992	-851.179918	-849.742018	-849.364944
36_8	-851.557436	-851.180642	-849.741600	-849.364806

36_9	-851.556505	-851.179489	-849.741805	-849.364789
36-Me⁺				-888.929229
36-Me ⁺ _1	-891.270251	-890.851153	-889.348727	-888.929629
36-Me ⁺ _2	-891.268276	-890.849204	-889.346754	-888.927681
36-Me ⁺ _3	-891.267660	-890.848531	-889.345823	-888.926694
36-Me ⁺ _4	-891.266894	-890.847693	-889.345554	-888.926353
37				-1044.015602
37_1	-1046.839178	-1046.334212	-1044.521476	-1044.016511
37_2	-1046.837691	-1046.332564	-1044.519801	-1044.014674
37_3	-1046.837156	-1046.332032	-1044.519312	-1044.014188
37_4	-1046.836104	-1046.331159	-1044.518985	-1044.014040
37_5	-1046.836771	-1046.331715	-1044.518903	-1044.013847
37_6	-1046.836643	-1046.331853	-1044.518182	-1044.013392
37_7	-1046.835104	-1046.330102	-1044.518291	-1044.013289
37_8	-1046.835141	-1046.329905	-1044.518274	-1044.013038
37_9	-1046.834729	-1046.329608	-1044.517996	-1044.012876
37_10	-1046.836320	-1046.331111	-1044.517996	-1044.012787
37-Me⁺				-1083.582284
37-Me ⁺ _1	-1086.554290	-1086.006709	-1084.130727	-1083.583146
37-Me ⁺ _2	-1086.553596	-1086.006194	-1084.130105	-1083.582703
37-Me ⁺ _3	-1086.551723	-1086.004412	-1084.128335	-1083.581025
37-Me ⁺ _4	-1086.551798	-1086.004257	-1084.128346	-1083.580805
37-Me ⁺ _5	-1086.551906	-1086.004324	-1084.128156	-1083.580574
37-Me ⁺ _6	-1086.551905	-1086.004303	-1084.128159	-1083.580557
37-Me ⁺ _7	-1086.551906	-1086.004284	-1084.128172	-1083.580550
37-Me ⁺ _8	-1086.551403	-1086.003945	-1084.127374	-1083.579916
37-Me ⁺ _9	-1086.550794	-1086.003232	-1084.127234	-1083.579671
37-Me ⁺ _10	-1086.550796	-1086.003243	-1084.127223	-1083.579670
38				-693.870295
38_1	-695.565864	-695.286831	-694.150273	-693.871240
38_2	-695.565569	-695.286448	-694.149777	-693.870656
38_3	-695.565119	-695.285994	-694.149430	-693.870305
38_4	-695.565140	-695.285947	-694.149059	-693.869867
38_5	-695.563715	-695.284493	-694.148773	-693.869551
38_6	-695.564706	-695.285578	-694.148555	-693.869427
38_7	-695.564180	-695.285160	-694.147992	-693.868973
38_8	-695.564414	-695.285052	-694.148270	-693.868909
38_9	-695.564010	-695.284734	-694.147778	-693.868502
38_10	-695.563508	-695.284603	-694.147369	-693.868464
38-Me⁺				-733.425226
38-Me ⁺ _1	-735.268597	-734.947693	-733.746676	-733.425772
38-Me ⁺ _2	-735.267731	-734.946821	-733.745726	-733.424816
38-Me ⁺ _3	-735.267503	-734.946515	-733.745522	-733.424534
38-Me ⁺ _4	-735.267672	-734.946690	-733.745341	-733.424358
PH₂Me	-382.386627	-382.326983	-381.789464	-381.729819
PH₂Me₂⁺	-422.046080	-421.944312	-421.343927	-421.242159
PHMe₂	-421.690601	-421.600096	-420.988339	-420.897834
PHMe₃⁺	-431.369348	-461.236987	-460.562018	-460.429657

9.5.3. Cyclophane-substituted Phosphanes
Table 9.5.2

	B98/6-31G(d)		MP2(FC)/6-31+G(2d,p)// B98/6-31G(d)	
	Etot	H298	Etot	H298
39R_1	-1252.027087	-1251.530889	-1249.315520	-1248.819322
39R_2	-1252.022562	-1251.526895	-1249.311943	-1248.816276
39R_3	-1252.022114	-1251.526258	-1249.311392	-1248.815536
39R_4	-1252.020381	-1251.523976	-1249.308756	-1248.812351
39R_5	-1252.018877	-1251.522316	-1249.307067	-1248.810506
39R_6	-1252.017360	-1251.520819	-1249.306582	-1248.810041
39R_7	-1252.005718	-1251.509452	-1249.294125	-1248.797859
39R_8	-1252.005243	-1251.508887	-1249.293315	-1248.796959
39S_1	-1252.024828	-1251.528552	-1249.314207	-1248.817931
39S_2	-1252.022231	-1251.526230	-1249.311826	-1248.815825
39S_3	-1252.020194	-1251.523971	-1249.309504	-1248.813281
39S_4	-1252.020523	-1251.524494	-1249.308901	-1248.812873
39S_5	-1252.020274	-1251.523981	-1249.308455	-1248.812162
39S_6	-1252.019302	-1251.522886	-1249.307165	-1248.810749
39S_7	-1252.018808	-1251.522932	-1249.305855	-1248.809979
39S_8	-1252.012270	-1251.515854	-1249.300921	-1248.804505
40R_1	-1252.045199	-1251.548897	-1249.331805	-1248.835502
40R_2	-1252.039542	-1251.543407	-1249.325600	-1248.829466
40R_3	-1252.037006	-1251.540854	-1249.324624	-1248.828472
40R_4	-1252.032578	-1251.536349	-1249.319323	-1248.823094
40S_1	-1252.040646	-1251.544494	-1249.327996	-1248.831844
40S_2	-1252.035733	-1251.539723	-1249.325600	-1248.829590
40S_3	-1252.039019	-1251.542564	-1249.325809	-1248.829355
40S_4	-1252.034656	-1251.538717	-1249.321104	-1248.825165
41_1	-1190.926607	-1190.548768	-1188.432654	-1188.054815
45_1	-806.232164	-806.005150	-804.609743	-804.382729
45_2	-806.231360	-806.004349	-804.609094	-804.382084
45_3	-806.231066	-806.004074	-804.608748	-804.381756
43_1	-1039.545644	-1039.186464	-1037.356364	-1036.997183
43_2	-1039.539604	-1039.180331	-1037.349044	-1036.989771
44_1	-731.250368	-731.013907	-729.785867	-729.549406

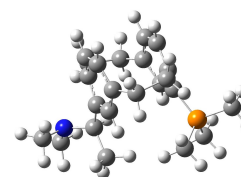




39R_Me+_1	-1291.734557	-1291.195702	-1288.919449	-1288.380594
39R_Me+_2	-1291.734558	-1291.195696	-1288.919441	-1288.380579
39R_Me+_3	-1291.728966	-1291.190884	-1288.909995	-1288.371913
39R_Me+_4	-1291.727849	-1291.189409	-1288.908330	-1288.369890
39R_Me+_5	-1291.725449	-1291.186512	-1288.905414	-1288.366478
39R_Me+_6	-1291.710568	-1291.171518	-1288.892786	-1288.353736
39R_Me+_7	-1291.710568	-1291.171518	-1288.892783	-1288.353733
39R_Me+_8	-1291.708227	-1291.169332	-1288.890636	-1288.351741

39S_Me+_1	-1291.728781	-1291.190260	-1288.909837	-1288.371316
39S_Me+_2	-1291.725532	-1291.186154	-1288.910647	-1288.371269
39S_Me+_3	-1291.726811	-1291.188559	-1288.909095	-1288.370843
39S_Me+_4	-1291.725167	-1291.186790	-1288.907960	-1288.369583
39S_Me+_5	-1291.724655	-1291.186160	-1288.906406	-1288.367911
39S_Me+_6	-1291.723348	-1291.184589	-1288.906193	-1288.367434
39S_Me+_7	-1291.717558	-1291.179387	-1288.898425	-1288.360255

39SN_Me+_1	-1291.716994	-1291.176087	-1288.898728	-1288.357822
39SN_Me+_2	-1291.708348	-1291.167545	-1288.892433	-1288.351630
39SN_Me+_3	-1291.705083	-1291.164392	-1288.885615	-1288.344924
39SN_Me+_4	-1291.700807	-1291.159693	-1288.881613	-1288.340498
39SN_Me+_5	-1291.682159	-1291.140915	-1288.863869	-1288.322626
39SN_Me+_6	-1291.680004	-1291.139054	-1288.861100	-1288.320150



40R_Me+_1	-1291.747962	-1291.210253	-1288.926170	-1288.388461
40R_Me+_2	-1291.741981	-1291.204054	-1288.921288	-1288.383361

40S_Me+_1	-1291.744499	-1291.206580	-1288.923228	-1288.385309
40S_Me+_2	-1291.744295	-1291.206393	-1288.922774	-1288.384872

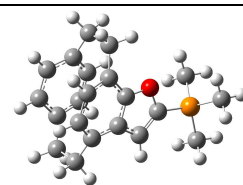
40SN_Me+_1	-1291.733531	-1291.192548	-1288.912870	-1288.371886
40SN_Me+_2	-1291.727813	-1291.187020	-1288.906671	-1288.365878
40SN_Me+_3	-1291.718765	-1291.177603	-1288.898199	-1288.357037
40SN_Me+_4	-1291.714826	-1291.174208	-1288.893876	-1288.353259

41_Me+_1

-1230.620488

-1230.201184

-1228.016255



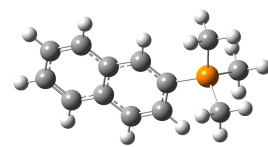
-1227.596950

45_Me+_1

-845.932988

-845.664347

-844.202728



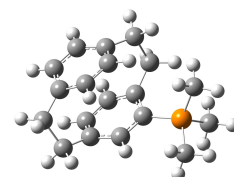
-843.934087

43_Me+_1

-1079.246809

-1078.845968

-1076.948806



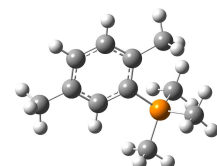
-1076.547966

44_Me+_1

-770.950712

-770.672225

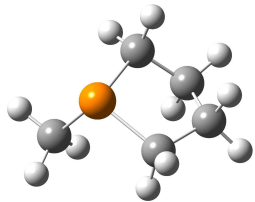
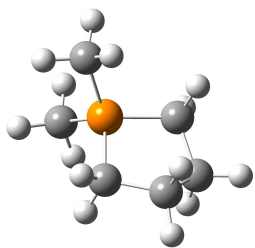
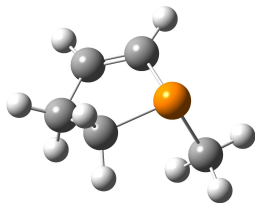
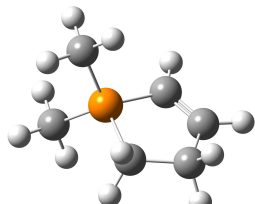
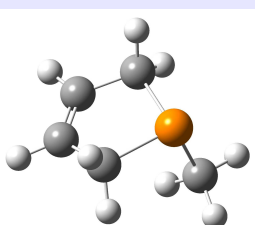
-769.378789

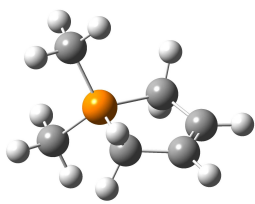
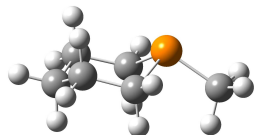
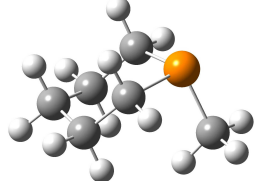
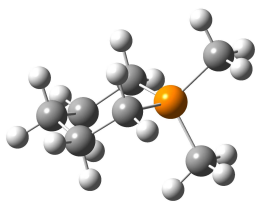
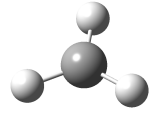


-769.100302

9.5.4. Cyclic Phosphanes

Table 9.5.3

	B98/6-31G(d)		MP2(FC)/6-31+G(2p,d)//B98/6-31G(d)	
	E_{tot}	H_{298}	E_{tot}	H_{298}
49	-538.383378	-538.223939	-537.384337	-537.224898
				
49-Me+	-578.078258	-577.877210	-576.972147	-576.771099
				
47	-537.152608	-537.017432	-536.171106	-536.035930
				
47-Me+	-576.847722	-576.670772	-575.757304	-575.580354
				
46	-537.154551	-537.019731	-536.173303	-536.038483
				

46-Me+				
	-576.843873	-576.667442	-575.754277	-575.577846
48	-615.760012	-615.563078	-614.574756	-614.377822
48-Me+	-655.453918	-655.215172	-654.161473	 -653.922727
50_1				
	-577.683936	-577.494343	-576.580136	-576.390543
50_2				
	-577.683137	-577.493444	-576.579239	-576.389546
50_1-Me+				
	-617.383371	-617.151985	-616.173516	-615.942130
	-39.462922	-39.427481	-39.352370	
CH3+				 -39.316929

9.5.5. MVKA of Recently Synthesized Bifunctional Phosphane Catalysts

Table 9.5.4

	MPW1K/6-31G(d)		MP2(FC)/6-31+G(2p,d)//MPW1K/6-31G(d)	
	E _{tot}	H ₂₉₈	E _{tot}	H ₂₉₈
BPC0	-1036.114027	-1035.814555	-1033.804862	-1033.50539
BPC0_MVK_1	-1267.258099	-1266.856987	-1264.404191	-1264.003079
BPC0_MVK_2	-1267.256318	-1266.855328	-1264.404304	-1264.003314
BPC0_MVKc_1	-1267.276995	-1266.875316	-1264.429498	-1264.027819
BPC0_MVKc_2	-1267.27414	-1266.872154	-1264.424462	-1264.022476
BPC1_1	-1361.983768	-1361.531129	-1358.899958	-1358.447319
BPC1_2	-1361.983093	-1361.530261	-1358.898938	-1358.446106
BPC1_3	-1361.986658	-1361.53389	-1358.896227	-1358.443459
BPC1_4	-1361.972644	-1361.520477	-1358.888954	-1358.436787
BPC1_5	-1361.986498	-1361.5339	-1358.895868	-1358.44327
BPC1_6	-1361.97081	-1361.518601	-1358.886489	-1358.43428
BPC1_MVK_1	-1593.146131	-1592.592497	-1589.519060	-1588.965426
BPC1_MVK_2	-1593.125401	-1592.571426	-	-
BPC1_MVK_3	-1593.112709	-1592.558842	-	-
BPC1_MVKc_1	-1593.151884	-1592.596886	-1589.530341	-1588.975343
BPC1_MVKc_2	-1593.142835	-1592.588074	-1589.522197	-1588.967436
BPC1_MVKc_3	-1593.14225	-1592.587464	-1589.521205	-1588.966419
BPC1_MVKc_4	-1593.136187	-1592.581593	-1589.516613	-1588.962019
BPC2_1	-1244.065312	-1243.70416	-1241.314136	-1240.952984
BPC2_2	-1244.066917	-1243.705722	-1241.311467	-1240.950272
BPC2_3	-1244.06122	-1243.700461	-1241.310238	-1240.949479
BPC2_4	-1244.061207	-1243.700389	-1241.310259	-1240.949441
BPC2_5	-1244.058096	-1243.697221	-1241.308677	-1240.947802
BPC2_MVK_1	-1475.225494	-1474.763687	-1471.932111	-1471.470304
BPC2_MVK_2	-1475.212619	-1474.750888	-1471.922388	-1471.460657
BPC2_MVK_3	-1475.212612	-1474.750879	-1471.922347	-1471.460614
BPC2_MVK_4	-1475.202344	-1474.740257	-1471.915818	-1471.453731
BPC2_MVK_5	-1475.202477	-1474.740031	-1471.915233	-1471.452787
BPC2_MVK_6	-1475.204925	-1474.743841	-1471.913593	-1471.452509
BPC2_MVK_7	-1475.184977	-1474.723414	-1471.901214	-1471.439651
BPC2_MVK_8	-1475.181687	-1474.720097	-1471.895989	-1471.434399
BPC2_MVK_9	-1475.218044	-1474.755754	-1471.923266	-1471.460976
BPC2_MVK_10	-1475.206447	-1474.744000	-	-
BPC2_MVK_11	-1475.202258	-1474.739914	-	-
BPC2_MVK_12	-1475.199379	-1474.737197	-	-
BPC2_MVK_13	-1475.202483	-1474.739957	-	-
BPC2_MVK_14	-1475.195929	-1474.733727	-	-
BPC2_MVK_15	-1475.198949	-1474.736536	-	-
BPC2_MVK_16	-1475.203483	-1474.740833	-	-
BPC2_MVK_17	-1475.20050	-1474.738118	-	-
BPC2_MVKc_1	-1475.2335	-1474.77003	-1471.945570	-1471.482100
BPC2_MVKc_2	-1475.222305	-1474.759184	-1471.937555	-1471.474434
BPC2_MVKc_3	-1475.221689	-1474.758301	-1471.936354	-1471.472966
BPC2_MVKc_4	-1475.222305	-1474.758845	-1471.931963	-1471.468503
BPC2_MVKc_5	-1475.221356	-1474.757818	-1471.930994	-1471.467456
BPC3_1	-1435.748984	-1435.329663	-1432.521852	-1432.102531
BPC3_2	-1435.751621	-1435.332309	-1432.516831	-1432.097519
BPC3_3	-1435.744103	-1435.325301	-1432.515923	-1432.097121
BPC3_4	-1435.751304	-1435.332013	-1432.515872	-1432.096581
BPC3_5	-1435.743703	-1435.32491	-1432.515307	-1432.096514
BPC3_MVK_1	-1666.912331	-1666.392005	-1663.139561	-1662.619235
BPC3_MVK_2	-1666.9006	-1666.37997	-1663.132163	-1662.611533
BPC3_MVK_3	-1666.89456	-1666.374883	-1663.128780	-1662.609103
BPC3_MVKc_1	-1666.918535	-1666.39703	-1663.153699	-1662.632194
BPC3_MVKc_2	-1666.903605	-1666.382057	-1663.140942	-1662.619394
BPC3_MVKc_3	-1666.898913	-1666.377472	-1663.140373	-1662.618932

BPC3_MVKc_4	-1666.906384	-1666.384622	-1663.139415	-1662.617653
BPC3_MVKc_5	-1666.904075	-1666.382734	-1663.137268	-1662.615927
BPC4_1	-1550.235872	-1549.780106	-1546.765679	-1546.309913
BPC4_2	-1550.236117	-1549.780258	-1546.765747	-1546.309888
BPC4_3	-1550.238693	-1549.782855	-1546.760397	-1546.304559
BPC4_4	-1550.231185	-1549.775843	-1546.759602	-1546.304260
BPC4_5	-1550.230802	-1549.775469	-1546.759539	-1546.304206
BPC4_6	-1550.238467	-1549.782662	-1546.759520	-1546.303715
BPC4_MVK_1	-1781.399819	-1780.842889	-1777.383399	-1776.826469
BPC4_MVK_2	-1781.399259	-1780.842329	-1777.383213	-1776.826283
BPC4_MVK_3	-1781.387464	-1780.830362	-1777.375975	-1776.818873
BPC4_MVK_4	-1781.381509	-1780.825289	-1777.372681	-1776.816461
BPC4_MVKc_1	-1781.40561	-1780.847595	-1777.397606	-1776.839591
BPC4_MVKc_2	-1781.405478	-1780.847342	-1777.397562	-1776.839426
BPC4_MVKc_3	-1781.391744	-1780.833901	-1777.386320	-1776.828477
BPC4_MVKc_4	-1781.390668	-1780.832606	-1777.384803	-1776.826741
BPC4_MVKc_5	-1781.393476	-1780.835232	-1777.383076	-1776.824832
BPC4_MVKc_6	-1781.391214	-1780.833196	-1777.380894	-1776.822876
BPC5_1	-1527.952275	-1527.53262	-1524.550409	-1524.130751
BPC5_2	-1527.947385	-1527.52816	-1524.544616	-1524.125393
BPC5_3	-1527.947733	-1527.52855	-1524.544533	-1524.125352
BPC5_4	-1527.954588	-1527.53489	-1524.544730	-1524.125033
BPC5_5	-1527.954241	-1527.5346	-1524.543626	-1524.123985
BPC5_MVK_1	-1759.11781	-1758.59726	-1755.169826	-1754.64928
BPC5_MVKc_1	-1759.122806	-1758.60082	-1755.183011	-1754.661023
BPC6_1	-1111.307321	-1111.002214	-1108.878307	-1108.573200
BPC6_2	-1111.308552	-1111.00331	-1108.877854	-1108.572612
BPC6_3	-1111.303574	-1110.998603	-1108.875100	-1108.570129
BPC6_4	-1111.300896	-1110.995876	-1108.871808	-1108.566788
BPC6_MVK_1	-1342.489651	-1342.082027	-1339.512691	-1339.105067
BPC6_MVK_2	-1342.448667	-1342.041973	-1339.475072	-1339.068378
BPC6_MVK_3	-1342.448564	-1342.04189	-1339.474682	-1339.068008
BPC6_MVK_4	-1342.448385	-1342.041713	-1339.474165	-1339.067493
BPC6_MVK_5	-1342.447283	-1342.040574	-1339.472674	-1339.065965
BPC6_MVK_6	-1342.447385	-1342.0407	-1339.472473	-1339.065788
BPC6_MVK_7	-1342.446127	-1342.039467	-1339.471929	-1339.065269
BPC6_MVK_8	-1342.442506	-1342.03588	-1339.470265	-1339.063639
BPC6_MVK_9	-1342.443237	-1342.036636	-1339.468467	-1339.061866
BPC6_MVK_10	-1342.441427	-1342.034814	-1339.467623	-1339.061010
BPC6_MVKc_1	-1342.477093	-1342.069288	-1339.506135	-1339.098330
BPC6_MVKc_2	-1342.464689	-1342.056977	-1339.497503	-1339.089791
BPC6_MVKc_3	-1342.463235	-1342.055764	-1339.496542	-1339.089071
BPC6_MVKc_4	-1342.46273	-1342.055381	-1339.495967	-1339.088618
BPC6_MVKc_5	-1342.465132	-1342.057547	-1339.495858	-1339.088273
BPC6_MVKc_6	-1342.460755	-1342.053414	-1339.492857	-1339.085516

9.5.6. XKA of Triphenylphosphane and Pyridine-derived Lewis Base Catalysts Using Three Different Michael Acceptors

Table 9.5.5

	MP2(FC)/6-31+G(2d,p)//MPW1K/6-31+G(d) + PCM(UAHF)/RHF/6-31G(d)//MPW1K/6-31+G(d)				
	E_{tot}	H_{298}	E_0	G_{298}	G_{298, CHCl_3}
Ph ₃ P	-1033.805540	-1033.506480	-1033.522956	-1033.568131	-1033.565374
MA1_1	-230.606397	-230.507158	-230.513803	-230.542589	-230.544310
MA1_2	-230.605751	-230.506640	-230.513355	-230.542340	-230.543695
MA2_1	-305.682590	-305.576236	-305.583669	-305.613895	-305.614708
MA2_2	-305.681653	-305.575258	-305.582690	-305.612964	-305.613856
MA2_3	-305.667879	-305.561711	-305.569199	-305.600247	-305.604104
MA2_4	-305.662507	-305.556425	-305.564152	-305.595291	-305.599434
MA3_1	-307.813098	-307.674404	-307.681301	-307.711115	-307.716708
Ph ₃ P*1_1	-1264.404815	-1264.004430	-1264.026959	-1264.079680	-1264.083154
Ph ₃ P*1_2	-1264.404793	-1264.004283	-1264.026708	-1264.078674	-1264.081814
Ph ₃ P*1_3	-1264.391293	-1263.991325	-1264.014236	-1264.067730	-1264.076192
Ph ₃ P*1_4	-1264.389128	-1263.988845	-1264.011828	-1264.065834	-1264.073116
Ph ₃ P*2_1	-1339.467080	-1339.060242	-1339.084122	-1339.139373	-1339.144377
Ph ₃ P*2_2	-1339.470621	-1339.063517	-1339.087132	-1339.141415	-1339.143901
Ph ₃ P*2_3	-1339.470264	-1339.063181	-1339.086794	-1339.140879	-1339.143795
Ph ₃ P*2_4	-1339.465007	-1339.057932	-1339.081352	-1339.136098	-1339.141867
Ph ₃ P*2_5	-1339.464749	-1339.057654	-1339.081023	-1339.134864	-1339.140378
Ph ₃ P*2_6	-1339.463818	-1339.056751	-1339.080432	-1339.134661	-1339.140191
Ph ₃ P*3_1	-1341.588874	-1341.149366	-1341.172643	-1341.225978	-1341.235747
PDLB2_1	-747.576237	-747.180888	-747.197756	-747.240774	-747.244328
PDLB2_2	-747.575744	-747.180467	-747.197267	-747.239662	-747.243360
PDLB2*1_1	-978.181725	-977.683257	-977.706032	-977.756636	-977.764047
PDLB2*1_2	-978.180971	-977.682502	-977.705257	-977.756038	-977.763416
PDLB2*1_3	-978.178939	-977.680804	-977.703669	-977.754319	-977.762510
PDLB2*1_4	-978.178764	-977.680510	-977.703345	-977.754090	-977.761628
PDLB2*1_5	-978.172688	-977.674222	-977.696992	-977.747852	-977.759422
PDLB2*1_6	-978.172993	-977.674444	-977.697175	-977.747848	-977.758812
PDLB2*1_7	-978.171366	-977.672989	-977.695750	-977.746462	-977.757968
PDLB2*1_8	-978.171491	-977.673243	-977.695999	-977.746718	-977.757953
PDLB2*1_9	-978.166473	-977.669194	-977.692714	-977.745261	-977.756496
PDLB2*1_10	-978.165121	-977.667628	-977.691107	-977.744339	-977.756435
PDLB2*1_11	-978.160297	-977.662758	-977.686222	-977.738999	-977.754616
PDLB2*1_12	-978.160229	-977.662637	-977.686059	-977.738828	-977.754222
PDLB2*2_1	-1053.246864	-1052.741815	-1052.765715	-1052.818432	-1052.826352
PDLB2*2_2	-1053.246078	-1052.741080	-1052.765014	-1052.817974	-1052.825798
PDLB2*2_3	-1053.244315	-1052.739584	-1052.763566	-1052.816306	-1052.825007
PDLB2*2_4	-1053.242605	-1052.738150	-1052.762217	-1052.815397	-1052.824736
PDLB2*2_5	-1053.241669	-1052.737363	-1052.761551	-1052.815413	-1052.824719
PDLB2*2_6	-1053.240567	-1052.736544	-1052.760769	-1052.814237	-1052.824181
PDLB2*2_7	-1053.244028	-1052.739206	-1052.763177	-1052.815886	-1052.823823
PDLB2*2_8	-1053.239942	-1052.735868	-1052.760121	-1052.813780	-1052.823134
PDLB2*2_9	-1053.236992	-1052.732622	-1052.756820	-1052.810563	-1052.823073
PDLB2*2_10	-1053.238859	-1052.733921	-1052.757868	-1052.811009	-1052.822770
PDLB2*2_11	-1053.237233	-1052.732746	-1052.756844	-1052.810045	-1052.822157
PDLB2*2_12	-1053.239224	-1052.734170	-1052.758062	-1052.810853	-1052.821880

PDLB2*2_13	-1053.237668	-1052.732995	-1052.756999	-1052.810278	-1052.821736
PDLB2*2_14	-1053.235755	-1052.731511	-1052.755671	-1052.808878	-1052.821340
PDLB2*2_15	-1053.235722	-1052.731516	-1052.755676	-1052.808873	-1052.821272
PDLB2*2_16	-1053.237615	-1052.732789	-1052.756713	-1052.809675	-1052.821229
PDLB2*3R_1	-1055.368669	-1054.832124	-1054.855742	-1054.908215	-1054.922844
PDLB2*3R_2	-1055.366930	-1054.830536	-1054.854215	-1054.906427	-1054.921375
PDLB2*3R_3	-1055.364135	-1054.827469	-1054.851052	-1054.903211	-1054.921139
PDLB2*3R_4	-1055.362519	-1054.826120	-1054.849773	-1054.901800	-1054.919664
PDLB2*3S_1	-1055.368862	-1054.832421	-1054.856091	-1054.908757	-1054.923338
PDLB2*3S_2	-1055.364162	-1054.827528	-1054.851184	-1054.903843	-1054.921500
PDLB2*3S_3	-1055.366851	-1054.830493	-1054.854184	-1054.906424	-1054.921452
PDLB2*3S_4	-1055.362763	-1054.826397	-1054.850078	-1054.902445	-1054.920325

9.6. Calculated Data for Chapter 6

Table 9.6.1

B3LYP/6-31G(d)		
System	E_{tot}	H₂₉₈
PH ₃ BH ₃	-369.786524	-369.723822
PMe ₃ BH ₃	-487.765856	-487.611052
PH ₃ BMe ₃	-487.745307	-487.592404
PMe ₃ BMe ₃	-605.720325	-605.474670
PH ₃ BF ₃ (r(P-B)) = ~2 Å	NM	NM
PH ₃ BF ₃ (r(P-B)) = ~3 Å	-667.697792	-667.650757
PMe ₃ BF ₃	-785.670391	-785.535380
PMe ₃	-461.098424	-460.981668
BF ₃	-324.5532218	-324.536667
PH ₃	-343.140281	-343.112204
PMe ₃	-461.098424	-460.981668
BH ₃	-26.613000	-26.582694
BMe ₃	-144.609064	-144.487552
B98/6-31G(d)		
System	E_{tot}	H₂₉₈
PH ₃ BH ₃	-369.718551	-369.655750
PMe ₃ BH ₃	-487.651276	-487.496507
PH ₃ BMe ₃	-487.631269	-487.478375
PMe ₃ BMe ₃	-605.560363	-605.314973
PH ₃ BF ₃ (r(P-B)) = ~2 Å	NM	NM
PH ₃ BF ₃ (r(P-B)) = ~3 Å	-667.535840	-667.488677
PMe ₃ BF ₃	-785.462977	-785.323189
PMe ₃	-460.996371	-460.875348
BF ₃	-324.446133	-324.429085
PH ₃	-343.084654	-343.056507
PMe ₃	-460.996371	-460.875348
BH ₃	-26.597091	-26.566768
BMe ₃	-144.545972	-144.424571
MPW1K/6-31G(d)		
System	E_{tot}	H₂₉₈
PH ₃ BH ₃	-369.776645231	-369.712404
PMe ₃ BH ₃	-487.737032504	-487.578602
PH ₃ BMe ₃	-487.714502244	-487.557365
PMe ₃ BMe ₃	-605.671022814	-605.419220
PH ₃ BF ₃ (r(P-B)) = ~2 Å	NM	
PH ₃ BF ₃ (r(P-B)) = ~3 Å	-667.589438315	-667.541147
PMe ₃ BF ₃	-785.547413812	-785.404112
PMe ₃	-461.073024	-460.948757
BF ₃	-324.449146	-324.431791
PH ₃	-343.135431	-343.106440
PMe ₃	-461.073024	-460.948757
BH ₃	-26.599714	-26.568938
BMe ₃	-144.574531	-144.450018
MPW1K/6-31+G(d)		
System	E_{tot}	H₂₉₈
PH ₃ BH ₃	-369.778690631	-369.714608
PMe ₃ BH ₃	-487.741224670	-487.583194
PH ₃ BMe ₃	-487.719529272	-487.562842
PMe ₃ BMe ₃	-605.677765317	-605.426586
PH ₃ BF ₃ (r(P-B)) = ~2 Å	-667.608370150	-667.560421
PH ₃ BF ₃ (r(P-B)) = ~3 Å	-667.608309	-667.560305
PMe ₃ BF ₃	-785.571958037	-785.429144
PMe ₃	-461.076331	-460.952348
BF ₃	-324.467095	-324.449957
PH ₃	-343.136347	-343.107383

PMe ₃	-461.076331	-460.952348
BH ₃	-26.600665	-26.569954
BMe ₃	-144.578092	-144.453944
MP2(FC)/aug-cc-pVDZ		
System	E_{tot}	H₂₉₈
PH ₃ BH ₃	-369.137632	-369.074803
PMe ₃ BH ₃	-486.738005	-486.584109
PH ₃ BMe ₃	-486.728547	-486.575984
PMe ₃ BMe ₃	-604.331133	-604.087161
PH ₃ BF ₃ (r(P-B)) = ~2 Å	-666.525834	-666.479384
PH ₃ BF ₃ (r(P-B)) = ~3 Å	-666.527230	-666.480661
PMe ₃ BF ₃	-784.128944	-783.990424
PMe ₃	-460.189797	-460.069553
BF ₃	-323.906698	-323.890230
PH ₃	-342.614054	-342.585805
PMe ₃	-460.189797	-460.069553
BH ₃	-26.486730	-26.456379
BMe ₃	-144.102628	-143.981589
MP2(FULL)/aug-cc-pVDZ		
System	E_{tot}	H₂₉₈
PH ₃ BH ₃	-369.150468	-369.087468
PMe ₃ BH ₃	-486.761139	-486.607085
PH ₃ BMe ₃	-486.751586	-486.598772
PMe ₃ BMe ₃	-604.364852	-604.120624
PH ₃ BF ₃ (r(P-B)) = ~2 Å	-666.546518	-666.499922
PH ₃ BF ₃ (r(P-B)) = ~3 Å	-666.547534	-666.500830
PMe ₃ BF ₃	-784.160213	-784.021573
PMe ₃	-460.208873	-460.088541
BF ₃	-323.917155	-323.900677
PH ₃	-342.623224	-342.594858
PMe ₃	-460.208873	-460.088541
BH ₃	-26.488898	-26.458497
BMe ₃	-144.114590	-143.993392
B97-D/6-31G(d)		
System	E_{tot}	H₂₉₈
PH ₃ BH ₃	-369.751301	-369.689491
PMe ₃ BH ₃	-487.642330	-487.491187
PH ₃ BMe ₃	-487.623811	-487.474472
PMe ₃ BMe ₃	-605.515312	-605.275967
PH ₃ BF ₃ (r(P-B)) = ~2 Å	NM	NM
PH ₃ BF ₃ (r(P-B)) = ~3 Å	-667.515075	-667.479532
PMe ₃ BF ₃	-785.398256	-785.261914
PMe ₃	-460.992961	-460.874981
BF ₃	-324.383827	-324.367224
PH ₃	-343.125102	-343.097206
PMe ₃	-460.992961	-460.874981
BH ₃	-26.592362	-26.562380
BMe ₃	-144.497521	-144.379234

Table 9.6.1

MP2(FC)/6-31+G(2d,p)//MPW1K/6-31G(d)		
System	E_{tot}	„H₂₉₈“
PH ₃ BMe ₃	-369.124253	-369.060011
PMe ₃ BH ₃	-486.745156	-486.586725
PH ₃ BH ₃	-486.728344	-486.571207
PMe ₃ BMe ₃	-604.349004	-604.097202
PH ₃ BF ₃ (r(P-B)) = ~2 Å	NM	NM
PH ₃ BF ₃ (r(P-B)) = ~3 Å	-666.513876	-666.465585
PMe ₃ BF ₃	-784.131666	-783.988364

PMe ₃	-460.191191	-460.066924
BF ₃	-323.913387	-323.896032
MP2(FC)/6-31+G(2d,p)//MPW1K/6-31+G(d)		
System	E_{tot}	„H₂₉₈“
PH ₃ BMe ₃	-369.124253	-369.060011
PMe ₃ BH ₃	-486.745142	-486.586711
PH ₃ BH ₃	-486.728393	-486.571256
PMe ₃ BMe ₃	-604.349009	-604.097206
PH ₃ BF ₃ (r(P-B)) = ~2 Å	-666.510958	-666.462666
PMe ₃ BF ₃	-784.132119	-783.988817
PMe ₃	-460.191189	-460.067206
BF ₃	-323.913551	-323.896413
MP2(FC)/6-31+G(2d,p)//B98/6-31G(d)		
System	E_{tot}	„H₂₉₈“
PH ₃ BMe ₃	-369.123947	-369.061146
PMe ₃ BH ₃	-486.744586	-486.589817
PH ₃ BH ₃	-486.727320	-486.574426
PMe ₃ BMe ₃	-604.347891	-604.102501
PH ₃ BF ₃ (r(P-B)) = ~2 Å	NM	NM
PH ₃ BF ₃ (r(P-B)) = ~3 Å	-666.514157	-666.466994
PMe ₃ BF ₃	-784.131501	-783.991713
PMe ₃	-460.190872	-460.069849
BF ₃	-323.913963	-323.896915
MP2(FC)/6-31+G(2d,p)//B97-D/6-31G(d)		
System	E_{tot}	„H₂₉₈“
PH ₃ BMe ₃	-486.726200	-486.576861
PMe ₃ BH ₃	-486.743317	-486.592174
PH ₃ BH ₃	-369.123204	-369.061394
PMe ₃ BMe ₃	-604.346589	-604.107244
PH ₃ BF ₃ (r(P-B)) = ~2 Å	-666.513315	-666.468771
PMe ₃ BF ₃	-784.130774	-783.994432
PMe ₃	-460.189776	-460.071797
BF ₃	-323.913767	-323.897164
B2K-PLYP/G3MP2large//MPW1K/6-31+g(d)		
System	E_{tot}	„H₂₉₈“
PH ₃ BMe ₃	-487.506633	-487.349945
PMe ₃ BH ₃	-487.526692	-487.368661
PH ₃ BH ₃	-369.634727	-369.570645
PMe ₃ BMe ₃	-605.396907	-605.145727
PH ₃ BF ₃ (r(P-B)) = ~2 Å	-667.480776	-667.432827
PMe ₃ BF ₃	-785.372639	-785.229825
PMe ₃	-460.888810	-460.764827
BF ₃	-324.459070	-324.441932
G3B3		
System	E_{tot}-DE(HLC)	H₂₉₈-DE(HLC)
PH ₃ BMe ₃	-487.451698	-487.304234
PMe ₃ BH ₃	-487.471302	-487.322035
PH ₃ BH ₃	-369.588053	-369.527538
PMe ₃ BMe ₃	-605.334963	-605.098134
PH ₃ BF ₃ (r(P-B)) = ~2 Å	-667.349191	-667.303565
PMe ₃ BF ₃	-785.226929	-785.091918
PMe ₃	-460.833707	-460.716951
BF ₃	-324.366774	-324.350219
G3MPW1K(+)		
System	E_{tot}-DE(HLC)	H₂₉₈-DE(HLC)
PH ₃ BMe ₃	-487.452942	-487.296256
PMe ₃ BH ₃	-487.472665	-487.314635
PH ₃ BH ₃	-369.588492	-369.524414
PMe ₃ BMe ₃	-605.336882	-605.085707
PH ₃ BF ₃ (r(P-B)) = ~2 Å	-667.344435	-667.296486
PH ₃ BF ₃ (r(P-B)) = ~3 Å	-667.349132	-667.301164

PMe ₃ BF ₃	-785.228423	-785.085612
PMe ₃	-324.367051	-324.349913
BF ₃	-460.834714	-460.710731
B2-PLYP-FLP(c=0.65)/G3MP2large//MPW1K/6-31+G(d)		
System	E_{tot}	H₂₉₈
PH ₃ BMe ₃	-487.777598	-487.620910
PMe ₃ BH ₃	-487.797683	-487.639652
PH ₃ BH ₃	-369.756484	-369.692402
PMe ₃ BMe ₃	-605.818522	-605.567342
PH ₃ BF ₃ (r(P-B)) = ~2 Å	-667.796788	-667.748839
PMe ₃ BF ₃	-785.838372	-785.695558
PMe ₃	-461.120389	-460.9964063
BF ₃	-324.689336	-324.6721984
MP2(FC)/G3MP2large//MPW1K/6-31+G(d)		
System	E_{tot}	H₂₉₈
PH ₃ BMe ₃	-486.880996	-486.724308
PMe ₃ BH ₃	-486.900462	-486.742431
PH ₃ BH ₃	-369.199392	-369.135310
PMe ₃ BMe ₃	-604.582384	-604.331204
PH ₃ BF ₃ (r(P-B)) = ~2 Å	-666.798363	-666.750414
PMe ₃ BF ₃	-784.499268	-784.356454
PMe ₃	-460.325413	-460.201430
BF ₃	-324.147569	-324.130431
MP2(FC)/G3large//MPW1K/6-31+G(d)		
System	E_{tot}	H₂₉₈
PH ₃ BMe ₃	-486.883046	-486.726358
PMe ₃ BH ₃	-486.902753	-486.744722
PH ₃ BH ₃	-369.200273	-369.136191
PMe ₃ BMe ₃	-604.585829	-604.334649
PH ₃ BF ₃ (r(P-B)) = ~2 Å	-666.806339	-666.758390
PMe ₃ BF ₃	-784.508652	-784.365838
PMe ₃	-460.327276	-460.203293
BF ₃	-324.155066	-324.137928

9.7. Calculated data for chapter 7

Table 9.7.1

stationary point	E_{tot} (B3LYP/6- 31G(d))	H_{298} (B3LYP/6- 31G(d))	E_{tot} (B3LYP/6- 311G+G(d,p)// B3LYP/6-31G(d))	ΔE_{tot} (kJ/mol)	" H_{298} " (B3LYP/6- 311G+G(d,p)// B3LYP/6-31G(d))	" ΔH_{298} " (kJ/mol)
4	-765.208202	-764.987441	-765.414457	-	-765.193696	-
3	-346.767634	-346.626227	-346.873971	-	-346.732564	-
9_1	-420.810576	-420.686904	-420.947989	0.0	-420.824317	0.0
9_2	-420.822149	-420.698179	-420.937123	28.5	-420.813153	29.3
8_1	-691.181036	-690.941536	-691.366462	0.0	-691.126962	0.0
8_2	-691.181714	-690.941963	-691.366105	0.9	-691.126354	1.6
3_c	-386.085563	-	-386.201349	-	-	-
8_1_c	-730.499302	-	-730.694220	-	-	-
8_2_c	-730.499931	-	-730.693862	-	-	-
3_n	-551.270605	-	-551.438550	-	-	-
8_1_n	-895.681710	-	-895.928746	-	-	-
8_2_n	-895.682849	-	-895.928853	-	-	-
background reaction						
4+3	-1111.975836	-1111.613668	-1112.288428	0.0	-1111.926260	0.0
8_2+9_2	-1112.003863	-1111.640142	-1112.303228	-38.9	-1111.939507	-34.8
8_1+9_2	-1112.003185	-1111.639715	-1112.303585	-39.8	-1111.940115	-36.4
8_2+9_1	-1111.992290	-1111.628867	-1112.314094	-67.4	-1111.950671	-64.1
8_1+9_1	-1111.991612	-1111.628440	-1112.314451	-68.3	-1111.951279	-65.7
4+3_c	-1151.293765	-	-1151.615806	0.0	-	-
8_2_c+9_2	-1151.321451	-	-1151.630985	-39.9	-	-
8_1_c+9_2	-1151.322080	-	-1151.631343	-40.8	-	-
8_2_c+9_1	-1151.310507	-	-1151.641851	-68.4	-	-
8_1_c+9_1	-1151.309878	-	-1151.642209	-69.3	-	-
4+3_n	-1316.478807	-	-1316.853007	0.0	-	-
8_1_n+9_2	-1316.503859	-	-1316.865869	-33.8	-	-
8_2_n+9_2	-1316.504998	-	-1316.865976	-34.1	-	-
8_1_n+9_1	-1316.492286	-	-1316.876735	-62.3	-	-
8_2_n+9_1	-1316.493425	-	-1316.876842	-62.6	-	-
6_4	-1111.949452	-1111.588633	-1112.256434	84.0	-1111.895615	80.5
6_3	-1111.955584	-1111.594277	-1112.260703	72.8	-1111.899396	70.5
6_2	-1111.956002	-1111.593935	-1112.261888	69.7	-1111.899821	69.4
6_1	-1111.956269	-1111.594587	-1112.262093	69.1	-1111.900411	67.9
6_2_c	-1151.274254	-	-1151.589635	68.7	-	-
6_1_c	-1151.274500	-	-1151.589836	68.2	-	-
6_2_n	-1316.456738	-	-1316.824179	75.7	-	-
6_1_n	-1316.457535	-	-1316.824884	73.8	-	-
5	-1111.988713	-1111.624188	-1112.297079	-22.7	-1111.932554	-16.5

7	-1112.016330	-1111.650274	-1112.322183	-88.6	-1111.956127	-78.4
---	--------------	--------------	--------------	--------------	--------------	--------------

Table 9.7.2

stationary point	E _{tot} (B3LYP/6-31G(d))	H ₂₉₈ (B3LYP/6-31G(d))	E _{tot} (B3LYP/6-311G+G(d,p)//B3LYP/6-31G(d))	ΔE _{tot} (kJ/mol)	"H ₂₉₈ " (B3LYP/6-311G+G(d,p)//B3LYP/6-31G(d))	"ΔH ₂₉₈ " (kJ/mol)
catalyzed reaction						
10	-382.257304	-382.085088	-382.359977	-	-382.187761	-
10+4+3	-1494.233140	-1493.698756	-1494.648405	0.0	-1494.114021	0.0
10+8_2+9_2	-1494.261167	-1493.725230	-1494.663205	-38.9	-1494.127268	-34.8
10+8_1+9_2	-1494.260489	-1493.724803	-1494.663562	-39.8	-1494.127876	-36.4
10+8_2+9_1	-1494.249594	-1493.713955	-1494.674071	-67.4	-1494.138432	-64.1
10+8_1+9_1	-1494.248916	-1493.713528	-1494.674428	-68.3	-1494.139040	-65.7
10+4+3_c	-1533.551069	-	-1533.975783	0.0	-	-
10+8_2_c+9_2	-1533.578755	-	-1533.990962	-39.9	-	-
10+8_1_c+9_2	-1533.579384	-	-1533.991320	-40.8	-	-
10+8_2_c+9_1	-1533.567811	-	-1534.001828	-68.4	-	-
10+8_1_c+9_1	-1151.309878	-	-1151.642209	-69.3	-	-
10+4+3_n	-1698.736111	-	-1699.212984	0.0	-	-
10+8_1_n+9_2	-1698.761163	-	-1699.225846	-33.8	-	-
10+8_2_n+9_2	-1698.762302	-	-1699.225953	-34.1	-	-
10+8_1_n+9_1	-1698.749590	-	-1699.236712	-62.3	-	-
10+8_2_n+9_1	-1698.750729	-	-1699.236819	-62.6	-	-
11_5	-1494.252853	-1493.713883	-1494.660274	-31.2	-1494.121304	-19.1
11_4	-1494.254332	-1493.714941	-1494.661444	-34.2	-1494.122053	-21.1
11_3	-1494.255363	-1493.716317	-1494.663513	-39.7	-1494.124467	-27.4
11_2	-1494.261937	-1493.722665	-1494.669193	-54.6	-1494.129921	-41.7
11_1	-1494.261846	-1493.722684	-1494.669262	-54.8	-1494.130100	-42.2
12_8	-1494.227689	-1493.689361	-1494.633683	38.7	-1494.095355	49.0
12_7	-1494.229267	-1493.691054	-1494.635002	35.2	-1494.096789	45.2
12_6	-1494.228093	-1493.690129	-1494.635301	34.4	-1494.097337	43.8
12_5	-1494.228811	-1493.690866	-1494.635303	34.4	-1494.097358	43.7
12_4	-1494.229440	-1493.691130	-1494.636110	32.3	-1494.097800	42.6
12_3	-1494.225674	-1493.687836	-1494.635742	33.2	-1494.097904	42.3
12_2	-1494.227422	-1493.689389	-1494.636299	31.8	-1494.098266	41.4
12_1	-1494.227638	-1493.689213	-1494.639594	23.1	-1494.101169	33.7
12_7_c	-1533.547255	-	-1533.962389	35.2	-	-
12_4_c	-1533.547152	-	-1533.963301	32.8	-	-
12_2_c	-1533.545247	-	-1533.963593	32.0	-	-
12_1_c	-1533.545367	-	-1533.966665	23.9	-	-
12_7_n	-1698.731621	-	-1699.199446	35.5	-	-
12_2_n	-1698.731419	-	-1699.202023	28.8	-	-
12_4_n	-1698.734083	-	-1699.202284	28.1	-	-

12_1_n	-1698.733822	-	-1699.207541	14.3	-	-
13_3	-1494.232601	-1493.693260	-1494.646218	5.7	-1494.106877	18.8
13_2	-1494.240012	-1493.699842	-1494.649963	-4.1	-1494.109793	11.1
13_1	-1494.239909	-1493.700181	-1494.650886	-6.5	-1494.111158	7.5
14_9	-1494.217766	-1493.683185	-1494.628463	52.4	-1494.093882	52.9
14_8	-1494.222172	-1493.686546	-1494.631284	45.0	-1494.095658	48.2
14_7	-1494.226104	-1493.691145	-1494.635132	34.8	-1494.100173	36.4
14_6	-1494.226413	-1493.691763	-1494.635370	34.2	-1494.100720	34.9
14_5	-1494.227315	-1493.692554	-1494.636160	32.1	-1494.101399	33.1
14_4	-1494.225535	-1493.691768	-1494.635801	33.1	-1494.102034	31.5
14_3	-1494.228769	-1493.693907	-1494.637954	27.4	-1494.103092	28.7
14_2	-1494.226506	-1493.692334	-1494.637294	29.2	-1494.103122	28.6
14_1	-1494.229028	-1493.695178	-1494.640219	21.5	-1494.106369	20.1
14_3_c	-1533.546501	-	-1533.965085	28.1	-	-
14_1_c	-1533.546633	-	-1533.967008	23.0	-	-
14_3_n	-1698.734081	-	-1699.205124	20.6	-	-
14_1_n	-1698.735846	-	-1699.208489	11.8	-	-
15_2	-1494.279504	-1493.739901	-1494.686359	-99.6	-1494.146756	-85.9
15_1	-1494.290465	-1493.750686	-1494.697227	-128.2	-1494.157448	-114.0
16_6	-1494.220951	-1493.685626	-1494.625500	60.1	-1494.090175	62.6
16_5	-1494.222632	-1493.687000	-1494.627133	55.8	-1494.091501	59.1
16_4	-1494.219925	-1493.684868	-1494.626990	56.2	-1494.091933	58.0
16_3	-1494.221830	-1493.687183	-1494.628466	52.3	-1494.093819	53.0
16_2	-1494.227839	-1493.691662	-1494.632397	42.0	-1494.096220	46.7
16_1	-1494.229513	-1493.693828	-1494.634956	35.3	-1494.099271	38.7
16_6_c	-1533.538698	-	-1533.952693	60.6	-	-
16_5_c	-1533.540258	-	-1533.954094	56.9	-	-
16_2_c	-1533.545585	-	-1533.959464	42.8	-	-
16_1_c	-1533.547130	-	-1533.961950	36.3	-	-
16_6_n	-1698.726649	-	-1699.192932	52.6	-	-
16_5_n	-1698.728152	-	-1699.194385	48.8	-	-
16_2_n	-1698.732820	-	-1699.199275	36.0	-	-
16_1_n	-1698.734321	-	-1699.201274	30.7	-	-

Curriculum Vitae

Name: Boris Maryasin
Date of birth: 30th, January, 1984
Place of birth: Nizhny Novgorod, Russian Federation
Nationality: Russian Federation
Marital status: Single

Education

Ludwig-Maximilians-Universitaet Muenchen, Germany Ph.D Program in Chemistry in the group of Prof. Hendrik Zipse	July 2007 – June 2011
Visiting Ph.D student in the group of Prof. Shi Min, SIOC, Shanghai, China	Oktober – December 2009
Visiting student in the group of Prof. Yitzhak Apeloig, Department of Chemistry, Technion-Israel Institute of Technology, Haifa, Israel	August – October 2005
Department of Chemistry, University of Nizhny Novgorod, Nizhny Novgorod, Russian Federation Master of Science in Chemistry, diploma with distinction	September 2005 – July 2007
Department of Chemistry, University of Nizhny Novgorod, Nizhny Novgorod, Russian Federation Bachelor of Science in Chemistry, diploma with distinction	September 2001 – July 2005

Work Experience

Ludwig-Maximilians-Universitaet Muenchen, Germany Chemistry and Biochemistry Department Teaching Assistant (T.A.)	July 2007 – now
---	-----------------

Computer and Computational Experience

1. System administrator activity in AK Zipse (LMU), responsible for hardware and software installation and configuration, experience in Linux/Unix and in various scripting languages under UNIX (Bourne Shell, Perl).
2. Operating of various theoretical programs for calculation and modeling of organic molecules: Gaussian, Molpro, Gamess, Tinker, BOSS, Macromodel, Molden, Gaussview

Publications

1. Protonation/Deprotonation Equilibria in the Morita-Baylis-Hillman Reaction
B. Maryasin, Y. Liu, K. Karaghiosoff and H. Zipse, in preparation
2. Theoretical Studies of ³¹P NMR Spectral Properties of Phosphanes and Related Compounds in Solution
B. Maryasin and H. Zipse,
Phys. Chem. Chem. Phys., **2011**, 13, 5150-5158
3. Methyl cation affinity (MCA) values for phosphanes
C. Lindner, B. Maryasin, F. Richter and H. Zipse,
J. Phys. Org. Chem., **2010**, 23, 1036-1042

- The Performance of Computational Techniques in Locating the Charge Separated Intermediates in Organocatalytic Transformations
Y. Wei, B. Sateesh, B. Maryasin, G. N. Sastry, H. Zipse,
J. Comput. Chem., **2009**, Vol. 30, No. 16, 2617-2624
- Titanium Tetra-*tert*-butoxide-*tert*-Butyl Hydroperoxide Oxidizing System: Physicochemical and Chemical Aspects
L. P. Stepovik, M. V. Gulenova, I. M. Martynova, B. Maryasin and V. K. Cherkasov,
Russ. J. General Chem., **2008**, Vol. 78, No. 2., 266-276
- Use of 2-(methoxycarbonyl)phenyllead triacetate in lactone synthesis
B. Maryasin, A. S. Shavyrin, J.-P. Finet and A. Yu. Fedorov,
Russ. Chem. Bull., **2006**, Vol. 55, No. 9, 1612-1616

Presentation in Conference

- B. Maryasin, C. Lindner, H. Zipse, Cation Affinity Numbers in Organocatalysis Research//”A Molecular Graphics and Modelling Society (MGMS) International Meeting”, Germany, Erlangen, 2009
- B. Maryasin, H. Zipse, Theoretical Studies of ³¹P NMR Spectral Properties of Potential Intermediates of the Morita-Baylis-Hillman Reaction./International Conference “The XIIth European Symposium on Organic Reactivity (ESOR XII)”, Israel, Haifa, 2009
- B. Maryasin, A.Y. Fedorov, S.V. Zelentsov, J.-P. Finet, Theoretical study of C-arylation with participation of non-symmetrical triarylbismuth dichlorides./proceedings of the IVTN-2006, 2006
- B. Maryasin, M. Karni, Y. Apeloig, Vinyl Silicene Cation: Substituent effects on the Potential Energy Surface./proceedings of the IVTN-2006, 2006
- B. Maryasin, A.Y. Fedorov, S.V. Zelentsov, S. Combes, J.-P. Finet, Synthesis, structure and reactivity of pentavalent (2-methoxymethylphenyl)bismuth derivatives./International Conference “Organic chemistry since Butlerov and Beilstein until present”, 2006
- B. Maryasin, A.S. Shavyrin, J.-P. Finet, A.Y. Fedorov, Reductive coupling of organolead arylating reagents in the synthesis of lactones./International Conference “Organic chemistry since Butlerov and Beilstein until present”, 2006
- B. Maryasin, A.Y. Fedorov, S.V. Zelentsov, Quantum-chemical study of C-arylation with participation of non-symmetrical triarylbismuth dichlorides./proceedings of the IVTN-2005, 2005

Languages

Russian – Native language

English – Fluent writing, reading speaking

German – Fluent writing, reading, speaking

Honors and Awards

- Prize for successful participation, International Innocentive Chemistry Olympiad for Students
- 1st prize, Oblast Students Chemistry Contest, Nizhny Novgorod, Russia
- 2nd prize, University Students Chemistry Contest, Nizhny Novgorod, Russia
- 2nd prize Oblast Students Chemistry Contest, Nizhny Novgorod, Russia
- 2nd prize Oblast Students Chemistry Contest, Nizhny Novgorod, Russia
- 2nd prize, University Students Chemistry Contest, Nizhny Novgorod, Russia

7. 1st prize, Young Scientist Chemistry Conference, Nizhny Novgorod, Russia
8. 3rd prize, Russian State Chemistry Contest
9. Prize for successful participation, 5th Soros Olympiad in Chemistry
and others (in total about 25 diplomas)